



HAL
open science

Interaction through programmable soft materials

Zhuzhi Fan

► **To cite this version:**

Zhuzhi Fan. Interaction through programmable soft materials. Human-Computer Interaction [cs.HC]. Université Grenoble Alpes, 2024. English. NNT: . tel-04726630

HAL Id: tel-04726630

<https://theses.hal.science/tel-04726630v1>

Submitted on 8 Oct 2024

HAL is a multi-disciplinary open access archive for the deposit and dissemination of scientific research documents, whether they are published or not. The documents may come from teaching and research institutions in France or abroad, or from public or private research centers.

L'archive ouverte pluridisciplinaire **HAL**, est destinée au dépôt et à la diffusion de documents scientifiques de niveau recherche, publiés ou non, émanant des établissements d'enseignement et de recherche français ou étrangers, des laboratoires publics ou privés.



Distributed under a Creative Commons Attribution - NonCommercial - NoDerivatives 4.0 International License

THÈSE

Pour obtenir le grade de

DOCTEUR DE L'UNIVERSITÉ GRENOBLE ALPES

École doctorale : MSTII - Mathématiques, Sciences et technologies de l'information, Informatique

Spécialité : Informatique

Unité de recherche : Laboratoire d'Informatique de Grenoble

Interaction via des matériaux mous et programmables

Interaction through programmable soft materials

Présentée par :

Zhuzhi FAN

Direction de thèse :

Céline COUTRIX

CHARGÉE DE RECHERCHE HDR, CNRS DELEGATION ALPES

Directrice de thèse

Benoît ROMAN

DIRECTEUR DE RECHERCHE, CNRS DELEGATION PARIS CENTRE

Co-directeur de thèse

Rapporteurs :

ANNE ROUDAUT

FULL PROFESSOR, UNIVERSITY OF BRISTOL

JAN BORCHERS

FULL PROFESSOR, RHEINISCH-WESTFALISCHE TECH. HOCH. AA

Thèse soutenue publiquement le **7 mai 2024**, devant le jury composé de :

LAURENCE NIGAY,

PROFESSEURE DES UNIVERSITÉS, UNIVERSITÉ GRENOBLE ALPES

Présidente

CELINE COUTRIX,

CHARGÉE DE RECHERCHE HDR, CNRS DELEGATION ALPES

Directrice de thèse

BENOÎT ROMAN,

DIRECTEUR DE RECHERCHE, CNRS DELEGATION PARIS CENTRE

Co-directeur de thèse

ANNE ROUDAUT,

FULL PROFESSOR, UNIVERSITY OF BRISTOL

Rapporteuse

JAN BORCHERS,

FULL PROFESSOR, RHEINISCH-WESTFALISCHE TECH. HOCH. AA

Rapporteur

MAUD MARCHAL,

PROFESSEURE DES UNIVERSITÉS, INSA RENNES

Examinatrice

KENING ZHU,

ASSOCIATE PROFESSOR, CITY UNIVERSITY OF HONG KONG

Examineur



ACKNOWLEDGEMENT

I want to express my sincere appreciation to my supervisor, Céline Coutrix. Working with her has been an incredible journey. During my PhD interview with Céline, I was drawn to the thesis subject's highly multidisciplinary nature and broad application potential. When I started my PhD, I was excited to plan to dive directly into the project, tackle concrete technical problems, and develop some fancy technologies. However, I quickly realized I knew little about Human-Computer Interaction (HCI) or research. Céline taught me with patience and guided me to understand that research is not only about technology. From her, I learned that research involves first identifying meaningful questions and then solving the corresponding technological problems. I also learned that HCI research focuses primarily on humans, followed by the technology that serves them. Throughout my PhD, Céline consistently provided wise advice and timely support, shaping my research style profoundly. If I have begun to develop my own research style, it has been fundamentally influenced by Céline's guidance. I also want to extend my gratitude to my co-supervisor, Benoît Roman. The new material, Baromorph, developed by his team, forms the technological foundation of my thesis. Benoît always provided detailed and timely answers to my questions with patience, even those that seemed trivial in hindsight. Many times, when I needed help advancing my thesis, Benoît invited me to prototype and conduct physical measurements in his lab, offering valuable advice from both theoretical and practical perspectives. He also warmly facilitated my contact with his friends, colleagues, and current or former PhD students for many times, ensuring I received the most appropriate help. Thanks to Céline and Benoît, I now have confidence and look forward to my academic future.

I also want to thank my thesis reviewers, Anne Roudaut and Jan Borchers, for agreeing to read and evaluate my thesis and providing invaluable suggestions for its improvement. I am grateful to my thesis examiners, Laurence Nigay, Maud Marchal, and Kening Zhu, for agreeing to join my viva jury. I am honored to have these five esteemed individuals and my two supervisors participate in this important phase of my academic journey. Their questions and comments during my viva provided great inspiration and deep reflection for my current and future research. Moreover, Anne and Maud have respectively agreed

twice and once to be external experts for my PhD registration; their expertise and insights have significantly contributed to my thesis advancement. Laurence, the team leader of IIHM, where I spent more than four years. Her efforts in creating a friendly, creative, and inclusive team atmosphere, which was particularly challenging during COVID-19, were indispensable for my PhD experience.

I also want to thank my three internship students, Thomas, Alexis, Fouad, and my friend Tian, for their help in developing prototypes and conducting experiments during my PhD. My gratitude extends to the entire IIHM team, whose warmth and camaraderie made my time with them unforgettable. Thanks to all my friends during my PhD—Adrien, Alix, Anna, Aurélien, Charles, Chaymae, Elliott, François, Gauthier, Hyunyoung, Jérémy, Lei, Michael, Mina, Ophélie, Pu, Renaud, Tom, Vincent, Vittoria, Xiaowen, Yidong and Zhaofeng—for their help, support, and the fun times we shared. A special thanks to my PhD sister, Laura. We started around the same time, shared Céline as our supervisor, and had similar research topics. Our discussions spanned not only research but many other aspects, and I consider myself lucky to have shared this journey with her.

I also want to thank my whole family for their support throughout these years. With all my heart, I want to thank my fiancé, Junkai. We have been together since November 15th, 2019, just a month and a half after I started my PhD. During these years, I learned to conduct research, and I also learned to love. Without your companionship and support, I do not know how I could have happily spent these years, particularly how I could have endured the pandemic. Luckily, I had you, I have you, and I will always have you.

I also want to thank the support of my research from CNRS (80 Prime MeMorI) and the French National Research Agency (ANR-21-CE33-0018).

To my fiancé, Junkai.

ABSTRACT

Shape-changing user interfaces (SCIs) are gaining attention in human-computer interaction (HCI) for their adaptability to data, tasks, environments, and users. SCIs can also change their shapes for various purposes, including information communication, user augmentation, object simulation, and hedonic or symbolic purposes. The advent of programmable soft materials has given HCI researchers the tools to design highly flexible SCIs. Soft materials like silicone particularly attract HCI researchers' interest due to their compatibility with the human body for wearable applications and their significant shape-morphing capabilities. However, there needs to be more understanding of how users perceive the shapes of SCIs made from soft materials and the impact of these materials' softness on users' shape perception abilities. Additionally, the possibilities and challenges of constructing SCIs in soft materials remain largely unexplored.

This Ph.D. thesis addresses three main research questions: (1) How do users perceive SCIs made from soft materials? (2) What types of SCIs can be developed using soft materials, and what are the associated challenges? (3) What are the potential applications for SCIs made from soft materials? To answer these questions, a psychophysical experiment is conducted to investigate users' shape perception abilities with surfaces of different softness. Next, the potential and challenges of creating SCIs with programmable soft materials are explored, and a new technology that enables the construction of soft SCIs with adjustable strength is also developed. Finally, an HCI application featuring novel SCIs made from programmable soft materials is presented, demonstrating how surfaces on the back of a smartwatch can change the shapes for notification applications.

RÉSUMÉ

Les interfaces utilisateur (IU) à forme variable sont de plus en plus étudiées en interaction humain-machine (IHM) en raison de leur capacité à adapter l'interface en fonction des données, des tâches, de l'environnement et des utilisateurs. Les IUs peuvent également changer de forme à des objectifs diverses, notamment la communication d'informations, l'augmentation d'utilisateurs, la simulation d'objets et des objectifs hédoniques ou symboliques. L'émergence de matériaux souples programmables a permis aux chercheurs en IHM de concevoir des IU souples avec une plus grande flexibilité. Les matériaux souples comme le silicone ont suscité l'intérêt des chercheurs en IHM en raison de leur compatibilité avec le corps humain pour les applications portables et de leur remarquable capacité à changer de forme. Cependant, on sait actuellement peu de choses sur la capacité des utilisateurs à percevoir la forme des IU à forme variable et sur l'impact de la souplesse des IU sur la capacité des utilisateurs à percevoir cette forme. En outre, les possibilités et les défis liés à la construction d'IU à forme variable en matériaux souples ont été peu abordés.

Cette thèse de doctorat aborde trois questions de recherche principales : (1) Comment les utilisateurs perçoivent-ils les IUs à changement de forme en matériaux souples? (2) Quelles IUs souple à changement de forme en matériaux souples peuvent être développées et quels sont les défis à relever ? et (3) À quoi peuvent servir les IUs à changement de forme en matériaux souples? Tout d'abord, une expérience psychophysique est menée pour étudier la capacité des utilisateurs à percevoir la forme de surfaces plus ou moins molles. Deuxièmement, les possibilités et les défis liés à la construction d'interfaces à changement de forme à l'aide de matériaux souples sont explorés. Notamment, la thèse propose une nouvelle technologie pour le développement d'interfaces utilisateur souples à changement de forme qui peuvent aussi changer de dureté. Troisièmement, une application d'IHM comportant de nouvelles IUs à changement de forme en matériaux souples est développée, démontrant comment les surfaces à l'arrière d'une montre connectée peuvent changer les formes pour des applications de notification.

TABLE OF CONTENTS

1	Introduction	27
1.1	Scientific context	32
1.1.1	Programmable soft materials	32
1.1.2	Shape-changing interfaces (SCIs)	34
1.2	Research questions	37
1.2.1	Problem I: Lack of understanding of users' shape perception abilities of SCIs	38
1.2.2	Problem II: Lack of SCIs development toolkit and existence of the stretchability-strength trade-off of programmable soft materials . .	39
1.2.3	Problem III: Lack of HCI applications with SCIs in novel program- mable soft materials	40
1.3	Methodology	40
1.4	Thesis contributions	42
1.5	Structure of the thesis	43
2	Background: programmable soft materials and SCIs	47
2.1	SCIs using soft materials	48
2.1.1	Size	48
2.1.2	Curvature	51
2.1.3	Amplitude	59
2.1.4	Porosity	60
2.1.5	Zero-crossing	60
2.1.6	Closure	63
2.1.7	Strength	65
2.1.8	Stretchability	68
2.1.9	Granularity	69
2.1.10	Modularity	72
2.1.11	Speed	78
2.2	Relations among different shape-changing features	80

I	User behavior	83
3	Human capabilities	85
3.1	Introduction	85
3.2	Related work	87
3.2.1	Perception of curvature	87
3.2.2	Perception of softness	89
3.3	Experiment	90
3.3.1	Experimental parameters	92
3.3.2	Participants	92
3.3.3	Stimuli	93
3.3.4	Experimental setup and procedure	93
3.3.5	Experimental design	95
3.4	Data pre-processing and analysis	96
3.4.1	Just-noticeable difference (JND) and Point of subjective equality (PSE)	96
3.4.2	Analysis	98
3.5	Results	98
3.5.1	Just noticeable difference (JND)	98
3.5.2	Point of Subjective Equality (PSE)	100
3.5.3	Exploration time	101
3.5.4	Difficulty estimation	103
3.6	Discussion	105
3.6.1	Partial replication of prior work	105
3.6.2	Impact of softness on precision (JND)	107
3.6.3	Similar accuracy with different softness	109
3.6.4	Slower exploration and higher difficulty with softer material	111
3.6.5	Different measures of softness	112
3.6.6	Linearity of curvature and softness	115
3.7	Guidelines for soft curvy devices	116
3.8	Applications: Building precise and accurate interactive devices	117
3.8.1	Augmented daily objects	117
3.8.2	Devices with custom softness and shape	119
3.8.3	Devices with changing softness and shape	119

3.9	Conclusion	121
II Technological explorations		123
4	SoftMorphees: High shape resolution soft shape-changing modules	125
4.1	Introduction	125
4.2	Related work	126
4.3	SoftMorphees	127
4.3.1	Fabrication	128
4.3.2	Size	130
4.3.3	Curvature	132
4.3.4	Amplitude	136
4.3.5	Porosity	139
4.3.6	Closure	143
4.3.7	Zero-crossing	145
4.4	Discussion	147
4.4.1	Toolkit for programming SCIs with novel programmable soft materials	147
4.4.2	User's perception precision and shape controlling precision on soft UIs with different shape features	148
4.4.3	Rigid materials involved in connecting pneumatically actuated soft shape-changing modules	150
4.4.4	Strength/Stretchability changing technologies involving rigid mate- rials	151
4.4.5	Limitations of building Size-changing UIs using solely soft materials	152
4.5	Conclusion	153
5	Jamming Origami Endoskeleton: Shape-strength controlling technology	155
5.1	Introduction	155
5.2	Related work	157
5.3	Design Space and technical evaluation	161
5.3.1	Thickness difference ($\Delta_{\text{Thickness}}$)	165
5.3.2	Angle difference (Δ_{Angle})	165
5.3.3	Thickness ($\mathbf{h}_{\text{Prism}}$)	165
5.3.4	Thickness of membrane ($\mathbf{h}_{\text{Membrane}}$)	167

TABLE OF CONTENTS

5.3.5	Vacuum level ($\mathbf{P}_{\text{Vacuum}}$)	167
5.3.6	Whether having origami jamming sheets	167
5.3.7	Multiple linear regression on different design parameters	169
5.4	Supplementary strength measurement	169
5.4.1	Origami jamming sheets layers ($\mathbf{N}_{\text{JammingLayers}}$)	171
5.4.2	Vacuum level ($\mathbf{P}_{\text{Vacuum}}$)	171
5.5	Fabrication	172
5.6	Examples applications	174
5.6.1	Tuning the range of shape and stiffness of shape-changing physical buttons at the design stage	174
5.6.2	Tunable strength of wearable haptic device for notifications	175
5.6.3	Wearable sitting posture guidance	176
5.7	Discussion and future work	177
5.7.1	Setup for strength measurement	177
5.7.2	Shape and strength controlling mechanism	179
5.7.3	Design parameters and design tools	181
5.7.4	Force reverse during compression test	181
5.7.5	Shape-changing capability	182
5.8	Conclusion	184

III SCIs design 185

6 Shape morphing watch 187

6.1	Introduction	187
6.2	Related work	188
6.2.1	Noticeability on the wrist	189
6.2.2	Shape-change on the wrist	189
6.2.3	Perception of shape-change	191
6.2.4	Touch, curvature, and softness	192
6.3	Watch design	194
6.4	Watch fabrication	197
6.5	Absolute detection threshold	198
6.5.1	Experimental design	199
6.5.2	Apparatus	200

6.5.3	Participants	200
6.5.4	Procedure	201
6.5.5	Data analysis	203
6.5.6	Results	204
6.6	Discussion	207
6.7	Conclusion	210
7	Conclusion	213
7.1	Thesis Contributions	213
7.2	Short-term Future Work	216
7.2.1	Users' shape perception ability for UIs dynamically changing shapes	216
7.2.2	Design tools for SCIs	217
7.2.3	Extending User study with our novel SCIs	218
7.3	Perspectives for Future SCIs	219
7.3.1	Lower technical barriers for customized SCIs	220
7.3.2	SCIs as standalone everyday objects	221
7.3.3	Wearable SCIs	222
7.3.4	SCIs in Metaverse	224
	Bibliography	227
A	Appendix	305
A.1	Stimuli curvature measurements	307
A.2	Stimulus height change computation	309
A.3	SoftMorphees shape measurements	311
A.4	Details of design parameters of prototypes	317
A.5	Force-displacement curves with different design parameters	321
A.6	Curvature measurements for Morphing watch	327

LIST OF FIGURES

1.1	SCIs adapting shapes to fit different usage contexts, i.e., (a) tasks [509], (b) environment [161], and (c) users [510].	28
1.2	SCIs change the shape for different purposes, e.g., (a) communicating information [326], (b) augmenting users [429], (c) simulating objects [435] and (d) purely hedonic or symbolic purposes [498].	29
1.3	(a) A Baromorph [402] morphs from a plate into a mask (Top left), and (b) its respective shape pattern of air channels (Top right). (c) Examples of Baromorphes with other different shapes (Bottom).	30
1.4	Research methodology of this thesis.	41
1.5	Structure of the thesis.	44
2.1	Different shape-changing features in the taxonomy of Morphees+ [226]. . .	47
2.2	Different technologies for creating <i>Size</i> changing UIs.	49
2.3	Curved surfaces with different types of Gaussian <i>Curvatures</i>	52
2.4	Illustration of technologies of bi-layer structure forming curved surfaces with different Gaussian curvatures.	53
2.5	Bi-layer structures with different materials for making cylindrical <i>Curvature</i> changing UIs.	54
2.6	<i>Curvature</i> changing UIs other than cylindrical shapes.	57
2.7	UIs with changing <i>Amplitude</i>	59
2.8	UIs with changing <i>Porosity</i>	61
2.9	UIs with changing <i>Zero-crossing</i>	62
2.10	UIs with changing <i>Closure</i>	64
2.11	UIs with changing <i>Strength</i> using jamming technology.	66
2.12	UIs with changing <i>Strength</i> using low phase/glass transition temperature materials and magneto-rheological (MR) fluids.	67
2.13	Matrix of actuated pin displays. Their maximum <i>Granularity</i> depends on pins density. Grouping pins and actuating them as one results in lower <i>Granularity</i>	69

2.14	A matrix of <i>Amplitude</i> -changing units in soft materials. Their <i>Granularity</i> is infinite according to Morphees+ [226] definition, while depends on the density of these actuated <i>Amplitude</i> -changing units as Morphees [376] definition.	70
2.15	Modular SCIs actuated with motors	72
2.16	Modular pneumatic SCIs and a toolkit of pumps and solenoid valves used for connecting multiple pneumatic shape-changing modules.	73
2.17	Electronic-free components used for connecting multiple pneumatic shape-changing modules.	74
2.18	Modular SCIs actuated by SMA wires and dielectric elastomers.	75
2.19	UIs with different shape-changing <i>Speed</i>	77
2.20	Figure illustrating relations between different primitive geometric shape-changing features realized with programmable soft materials. Figures in blue arrows connecting different shape-changing features illustrate how one shape-changing feature can be realized with another shape-change. In the case of developing shape-changing UIs with programmable soft materials, the <i>Granularity</i> is infinite according to Morphees+ definition [226]. Changing <i>Modularity</i> , <i>Strength</i> and <i>Stretchability</i> usually need to incorporate rigid materials to realize it, they are thus not presented in this figure and will be further discussed in Chapter 4.	80
3.1	(Top) Example materials and objects and (center) their approximate Young's modulus [438] and respective Shore hardness [437]. (Bottom) Types of silicone and resin used in our experiment: Shore 00-10, Shore 00-50, Shore A-30, and Rigid.	86
3.2	(a) Experimental setup, (b) 3D model of a very curved stimulus, (c) photograph of two stimuli (from the group of softness Shore 00-50) used in our experiment, and (d) pressure sensor and schematics of the circuit for sensor reading (as in [117]).	91
3.3	Experimental procedure with the first repetition illustrated: this participant first experienced the middle curvature ($R_{\text{ref}}= 20$ mm). Every pair in the illustrated repetition indicates the radii of the curved surfaces successively presented in one trial. In every pair, one of the radii is of the reference stimulus ($R_{\text{ref}}=20$ mm).	94
3.4	Just noticeable difference computation and results.	97

3.5	Accuracy (i.e., distance between PSE and reference curvature).	100
3.6	Exploration time.	102
3.7	Subjective discrimination difficulty.	104
3.8	Perception bias (i.e., signed difference PSE - R_{ref}).	109
3.9	Measurements of the softness of our stimuli.	113
3.10	(Left) Force displacement curves resulting from (right) compression tests with a 3D printed spherical indenter as in [418]. Colored lines show our results on a specimen with the same dimensions as the stimuli used in our experiment. Gray lines show prior results [418] from compression test on a jamming layer. The level of vacuum are expressed in inches of mercury (inHg). The larger the value, the higher the vacuum and the stiffer the UI.	120
4.1	An example Baromorph with its air channels pattern and mold.	129
4.2	<i>Length</i> changing prototype. Dashed white circles show that the prototype starts curving when inner pressure reaches 5.0 Psi.	131
4.3	<i>Area</i> changing prototype under different air pressures.	133
4.4	<i>Curvature</i> changing prototypes under different air pressures.	134
4.5	Photos of <i>Curvature</i> changing prototype under different air pressures. . . .	135
4.6	<i>Amplitude</i> changing prototypes with different Wall-AirChannels thickness ratios under different air pressures.	137
4.7	Photos of <i>Amplitude</i> changing prototype (Wall-AirChannels width ratio of 2) under different air pressures	138
4.8	<i>Porosity</i> changing via curving flaps prototype.	141
4.9	<i>Porosity</i> changing via length change prototype under different air pressures.	142
4.10	<i>Closure</i> changing prototype under different air pressures.	144
4.11	Air channel pattern and photos of <i>Closure</i> changing flowers	145
4.12	<i>Zero-crossing</i> changing prototype under different air pressures.	146

4.13 *Curvature* measurements of our *Curvature* changing prototypes (Figure 4.4) and users’ *Curvature* perception precision measured in Chapter 3. Data points present the *Curvature* of our prototypes; we present them using their radius ($1/\text{Curvature}$) to keep consistent with Chapter 3 and improve the legibility. Bars in different colors present users’ perception precision range in different softness conditions. Bars’ center locates at the height of the respective reference *Curvature* value, i.e., 10 mm, 20 mm and 40 mm with their tops at the respective value of $\text{Curvature}_{\text{Reference}} + \text{Curvature}_{\text{JND}}$ and bottoms at $\text{Curvature}_{\text{Reference}} - \text{Curvature}_{\text{JND}}$. One example is indicated with text and arrows in red colors with users’ *Curvature* JND in rigid and 40 mm reference condition measured as 4.32 mm (Chapter 3). The widths of the bars are chosen to cover points in their ranges (if any) and to avoid complete overlaps among bars for better legibility. 149

5.1 Our curvature+stiffness actuation mechanism: (A) origami jamming sheets sandwiched between elastomer structures. (B) When air is vacuumed out of the airtight skin, the structure deforms to reach its maximum curvature and stiffness progressively. 156

5.2 Different technologies for creating geometric shape and strength changing UIs. 158

5.3 A thin prototype made using our technology 161

5.4 Design parameters of our prototypes. To differentiate the two layers of gears, we call the thicker one “*Prism*” and the thinner one “*Tooth*”. Our current design parameters include the thickness and angle difference between “*Prism*” and “*Tooth*” ($\Delta_{\text{Thickness}}$ and Δ_{Angle}), thickness of “*Prism*” (h_{Prism}) and thickness of membrane (h_{Membrane}). We also study the impact of vacuum level P_{Vacuum} on our prototypes’ curvature and strength. 162

5.5	Curvature and strength measurement setup. (a) Curvature measurement. Top left: a prototype before vacuuming our air; Bottom left: a prototype with air vacuuming out; Top right: A prototype with edge detected, bolded and highlighted in red color for visualization; Bottom right: a vernier scale fixed on the support facilitating the conversion of pixels to millimeters. White circles in the left two figures show the buckling [336] of the elastomer membrane connecting elastomer structures and the TPU enveloping membrane. (b) Strength measurement setup. The measurement is done by the compression test with a 3D printed spherical indenter as in [418] and in Chapter 3. The red circle shows the form of "gear", which takes shape when vacuuming prototypes.	163
5.6	Curvature (left) and strength (right) measurement under different thickness differences between "Prism" and "Tooth".	165
5.7	Curvature (left) and strength (right) measurement under different angle differences between "Prism" and "Tooth".	166
5.8	Curvature (left) and strength (right) measurement under different thicknesses of "Prism".	166
5.9	Curvature (left) and strength (right) measurement under different thicknesses of membranes.	167
5.10	Curvature (left) and strength (right) measurement under different vacuum levels.	168
5.11	Curvature (left) and strength (right) measurement under conditions of whether having origami jamming sheets between two layers of gears. . . .	168
5.12	Supplementary strength measurement with two extremities fixed.	170
5.13	Strength measurement in conditions of different layers of origami jamming sheets. (a) Strength (b) Force-displacement curves	171
5.14	Strength measurement under different vacuum levels.	172
5.15	Fabrication process. (a) Molding Elastomer structures. (b) Laser cutting origami jamming sheets. (c) Enveloping elastomer structures and origami jamming sheets together.	173
5.16	A flat button can change shape into a curved button with higher strength.	174

5.17 A bracelet can change its shape to give wearer haptic feedback by contacting with wearers. With our technology’s capability of strength controllability, we can tune the strength of the UI according to the wearing site, i.e., UI tuned to have higher strength for the body site where sensitivity is poorer. 175

5.18 A wearable posture guidance can change shape to alert users of their poor postures and increase movement resistance to correct them. 177

5.19 Setup for strength measurement with two extremities fixed on the slider. With this setup, the two extremities of the prototype are fixed on the slider before the measurement. It can freely change its shape when vacuuming, releasing the vacuum, and compressing during the strength measurement. 178

5.20 Theoretical shape-change of the prototype presented in Figure 5.5(a). After the air has been vacuumed out, the neighbor inclined surfaces of the “Prisms” and “Teeth” should come into parallel and perfect contact with the jamming sheets (line in purple colors) between them. 179

5.21 Two shape status of a popper toy: convex (Left) and concave (Right). It can suddenly turn from a convex to a concave shape and vice versa when a user continuously pushes on it [427]. 181

5.22 This Figure [147] presents CurveUps, the technology of 3D printing spaced prisms on pre-stretched latex membrane to create 3D shapes when releasing the fixation around the membrane and some examples of 3D objects created with this technology. Top left: a flat latex membrane with 3D-printed spaced prisms on it, with the membrane’s boundary fixed on the support plate. Top center: This demonstrates what happens as a local shape changes when the membrane’s fixation is released. Top right: the flat surface turns into the shape of a cow when the fixation is released. Bottom: Some other exemplary 3D objects were created with CurveUps technology. From left to right: Half-Sphere, Hyperboloid, Lilium, Turtle, Bump Cap and Mask. 183

6.1 We present a novel haptic notification mechanism for soft watches, through the change of curvature and contact area of its back surface. The second picture (watch side) shows a loosely tied bracelet for illustration purpose, unlike our experiment. 188

6.2	Positioning to prior wrist-worn feedback: we explore curvature change, while prior work explored different types of feedback.	190
6.3	Positioning to prior curvature-changing wrist-worn devices: PneuHaptic’s airbag deforms in the same way in all directions (isotropic deformation), making the curvature linked to the diameter of the airbag. In addition, it is always in contact with the users’ wrist [160]. RetroShape provides low curvature resolution through its discrete 4×4 surface and its surface is made of hard material [181]. The eyes-free haptic wristwatch relies on a membrane that is always in contact with the user’s wrist, requires high voltage (up to 160V compared to our 12V) and provides limited maximum amplitude (a few mm compared to our $>15\text{mm}$) [329].	190
6.4	Design space of the maximum curvature.	194
6.5	Location design space, on the watch (left) and on the wrist (right).	196
6.6	Design of the molds for the surface we compare, and corresponding shape-changing watch upside down, showing the inside shape at different pressures and the corresponding measured curvatures. The molds are then 3D printed, the shape-changing surfaces are molded in silicone, and the bracelet is 3D printed using elastic resin (see section 6.4).	199
6.7	Experimental setup.	201
6.8	Analysis of the absolute detection thresholds. Error bars indicate bootstrapped 95% confidence intervals.	204
6.9	AttrakDiff scores. Error bars indicate bootstrapped 95% confidence intervals.	205
A.1	Validation of the curvature of our stimuli.	307
A.2	Parameters of the profile of the experimental apparatus (stimulus). The gray dotted line presents a semicircle. The larger black solid line presents the part of the semicircle that makes the stimulus.	309
A.3	SoftMorphees shape measurements setup	311
A.4	<i>Length</i> changing <i>SoftMorphees</i> Measurement. The dashed white circle indicates the supplementary part for inserting the needle, which is not included in <i>Length</i> measurement.	312
A.5	<i>Area</i> changing <i>SoftMorphees</i> Measurement.	313

LIST OF FIGURES

A.6 A R20 *Curvature* changing *SoftMorphees* under the pressure of 4.8 psi. The red curved line indicated the circular fitting edge using the circle-fit 0.1.3 [214] python package. 313

A.7 An *Amplitude* changing *SoftMorphees* with a Wall-AirChannels width ratio of 1 under the pressure of 8 psi. 314

A.8 A *Porosity* changing via length-changing *SoftMorphees* under the pressure of 6.0 psi. 314

A.9 A *Closure* changing *SoftMorphees* under the pressure of 3.4 psi. 315

A.10 Force-displacement curves in conditions of different thickness between two gear layers 321

A.11 Force-displacement curves in conditions of different angles between two gear layers 322

A.12 Force-displacement curves in conditions of different thickness of the thicker gears 323

A.13 Force-displacement curves in conditions of different thickness of membranes connecting gears 324

A.14 Force-displacement curves in conditions of different vacuum levels 325

A.15 Force-displacement curves in conditions of whether having origami layers between gears 326

A.16 curvature measurement setup and results. 327

LIST OF TABLES

3.1	Correspondence table for designers of novel soft and curvy devices.	118
A.1	Parameters of prototypes for curvature and strength measurement	318
A.2	Parameters of prototypes for supplementary strength measurement	319

INTRODUCTION

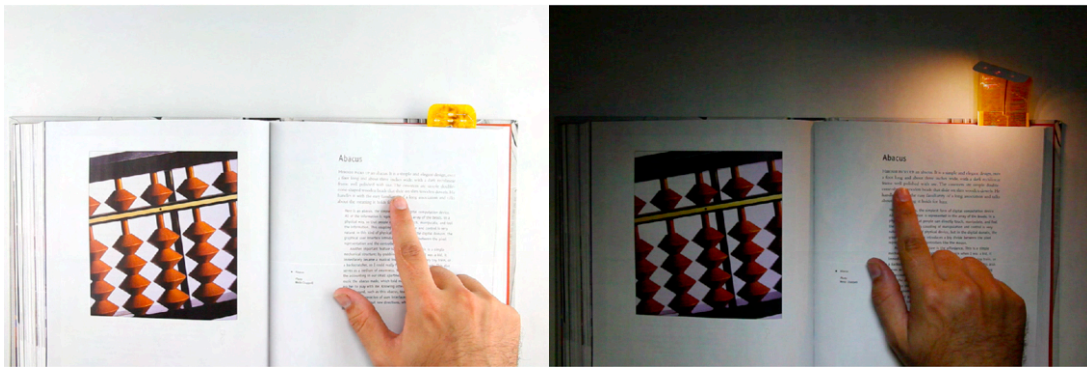
With advancements in flexible display [281, 421], soft sensors [40, 414], actuating technologies [73, 248], and smart materials [358, 270], human-computer interfaces (HCIs) are no longer limited to planar, rigid, and static surfaces such as Liquid-crystal display (LCD) screens. These technological advancements propel HCI researchers toward a revolutionary change in UI design, where UIs can have curved, deformable shapes and even shapes that transform themselves [168, 169, 363, 376]. This shift extends from small wearable devices (e.g., [150]) to room-scaled furniture (e.g., [381, 426]) and interactive architecture (e.g., [314, 296]). On the user side, individuals can now directly interact with everyday objects (e.g., [144]), surfaces (e.g., [483]), and spaces (e.g., [426]) that may have flexible shapes and dynamically change their physical form (e.g., [519, 510]). The research field of Shape-changing interfaces (SCIs) is emerging and providing users with benefits for different purposes [10]. For instance, they can change their shapes to fit tasks, environments, and users (Figure 1.1). They can also be used for communicating information, augmenting users, simulating objects, and purely hedonic or symbolic purposes [10] (Figure 1.2).

Shape-changing interfaces (SCIs) research is naturally cross-disciplinary, engaging with both new technologies and challenges from diverse research fields such as material science [358], robotics [353], psychology [335], and haptics [76]. As an emerging new research field, SCIs face diverse challenges to overcome before emerging into users' everyday lives. Deriving from a workshop with experts from different research areas, Alexander et al. recently identified different grand challenges [10] for SCIs research. These challenges can be classified into four major categories [10]:

1. **User behavior challenges:** challenges related to users' understanding, interaction, and behavior with SCIs. For example, to isolate different factors involved in SCIs and explore their manifold outcomes.
2. **Technological challenges:** challenges related to developing SCIs, such as toolkit building, interface miniaturization, creating high-resolution SCIs, integrating shape-changes with other I/O modalities, and non-functional requirements, such as in-



(a) A phone adapting its shape to different tasks. For example, it can transform into a wristband (right) to be worn [509].

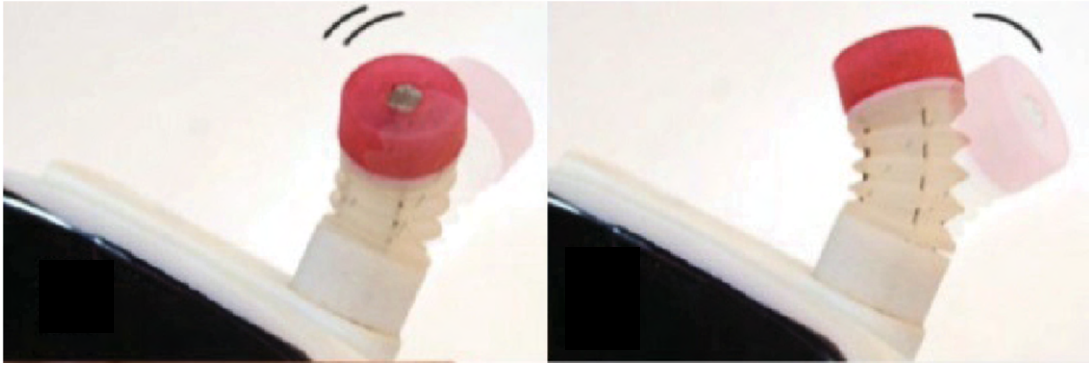


(b) A bookmark responsive to the environment, specifically the lightness of a reading room [161]. On the left, the bookmark is under bright lighting, but upon detecting darkness, it activates a light source and curls up (right) to facilitate continued reading.

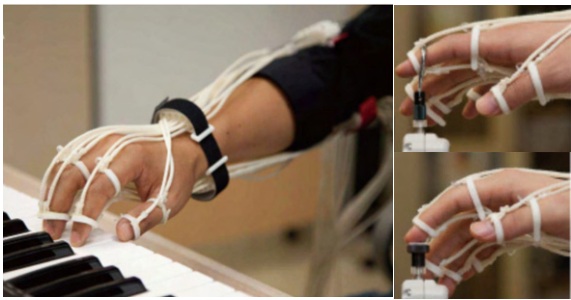


(c) A garment adapting its shape to the wearer [510]. Before exercise, the dress features flat ventilation flaps (left). After the wearer sweats, the ventilation flaps curve to enhance ventilation.

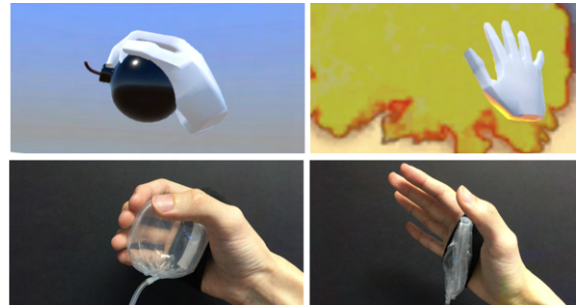
Figure 1.1 – SCIs adapting shapes to fit different usage contexts, i.e., (a) tasks [509], (b) environment [161], and (c) users [510].



(a) Communicating information: A mobile phone's peripheral responsively changes its shape to communicate a message received [326]. For instance, it exhibits forward and backward motion (Left) when receiving messages of 'Yes' and side-to-side motion (Right) when receiving messages of 'No.'



(b) Augmenting users: A soft exoskeleton worn on a user's hand can guide the user to improve their piano performance. For instance, (Top right) the exoskeleton guides the user to extend the index by reducing the length of the partial exoskeleton at the dorsal side, and (Bottom right) guides the user to flex the index by reducing the length of the partial exoskeleton at the palmar side. [429].

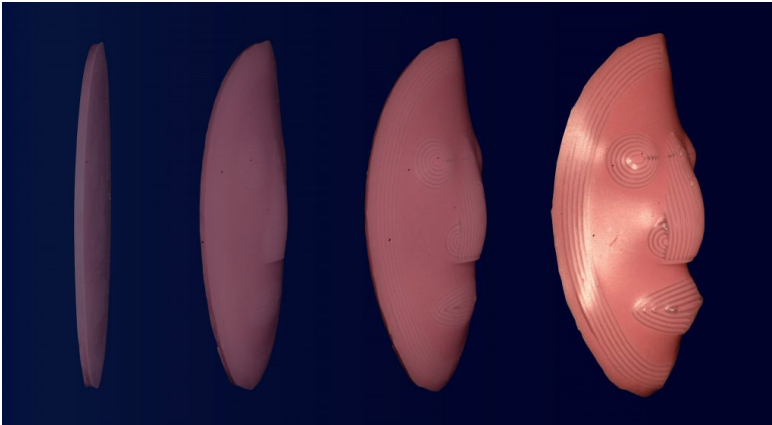


(c) Simulating objects: An airbag can inflate to a ball shape (Left) to simulate a bomb grasped by users in a VR game, and it can be deflated to a flat shape to eliminate contact with the user's fingers to simulate the bomb being thrown [435].

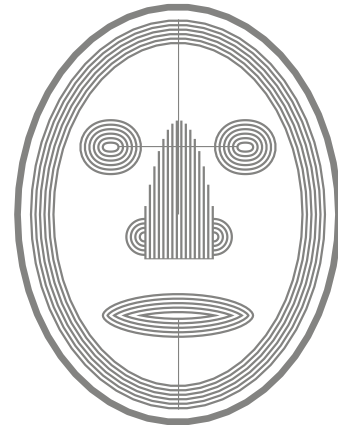


(d) Hedonic and symbolic purposes: A dress can expand (Left to Right) to protect the wearer and signal others to maintain a distance when a proximity sensor detects intrusion into personal space [498].

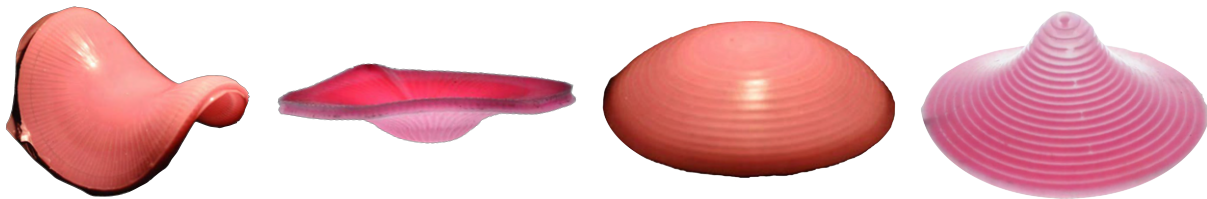
Figure 1.2 – SCIs change the shape for different purposes, e.g., (a) communicating information [326], (b) augmenting users [429], (c) simulating objects [435] and (d) purely hedonic or symbolic purposes [498].



(a) Baromorphs demonstrate remarkable shape-morphing capabilities. Various shape changes can be achieved by constructing Baromorphs with respective shapes of air channels embedded in an elastomer plate. In this figure, the translucent parts represent air channels. A Baromorph can transform dramatically by pressurizing these channels, morphing from a plate into a mask.



(b) The shape pattern of air channels of the mask-morphing Baromorph.



(c) Baromorphes morph from plates to different shapes.

Figure 1.3 – (a) A Baromorph [402] morphs from a plate into a mask (Top left), and (b) its respective shape pattern of air channels (Top right). (c) Examples of Baromorphes with other different shapes (Bottom).

terfaces compliance for safety.

3. **Design challenges:** challenges related to design research, e.g., developing design methodologies adapting to dynamic qualities of SCIs and designing SCIs integrating artifacts and interaction with applications for end-users.
4. **Societal challenges:** challenges related to the regulatory, ethical, and sustainability implications of developing SCIS during their evolution and long-term adoption.

In this thesis, I dedicate my research to improving SCI development by addressing various research challenges. More specifically, my research currently focuses on the challenges of user behavior, technological and design aspects.

Recent advances in material science and the transdisciplinarity between material sci-

ence and HCI [358] offer new opportunities to overcome SCIs research challenges, particularly from technological aspect [10]. Soft materials like silicone (e.g., [509]) are naturally flexible due to their high deformability, making them easily change shape when subjected to applied stress, such as when pressed or stretched by users. Their soft nature ensures high compliance and safety [377], particularly when users wear them on the body [112]. Recent advancements in sensing technologies based on soft materials [40, 414] have significantly lowered the threshold for integrating input abilities into UIs built with soft materials. For example, they are already capable of sensing various user input [451] like touch (e.g., [484, 480]), pressure (e.g., [517, 441]), bending (e.g., [366]), stretching (e.g., [225]), twisting (e.g., [299]), pinching (e.g., [481]). At the same time, advancements in programmable soft materials [358] make it possible to develop SCIs with various shape-changing abilities [226, 376, 363]. Programmable soft materials are responsive soft materials whose shape can react to external stimuli (e.g., air pressure [402, 393] and voltage [308]), potentially achieving shapes predefined by designers [270]. Unlike rigid materials such as motorized pins used in inFORM [108], creating discrete shapes with resolution limited by the size of motors, soft materials like elastomers create a surface with continuous shapes having infinite resolution [226]. Novel programmable soft materials, such as Baromorphs [402] (see Figure 1.3(a)), have paved the way on the material science front for constructing SCIs with high-resolution shape-change abilities. With their high potential of programmable soft materials in SCIs development, the advancement in programmable soft materials lays the technological basis of my research in SCIs in this thesis.

However, technological challenges still exist when using programmable soft materials to construct SCIs. For instance, gaps still need to be bridged as HCI designers need toolkits to integrate emerging programmable soft materials into their UI design [358]. Besides, a significant drawback of using soft materials like elastomers for SCIs is the trade-off between stretchability and strength [358], i.e., their high stretchability leads to their high deformability; thus, high shape-change potential, while low strength. Meanwhile, the strength of UIs can be necessary for HCI applications, for example, supporting users' fingers when pressing on UIs to provide users with haptic feedback [107]. Furthermore, challenges also exist in the aspect of user behavior. One key user behavior challenge is to isolate and study the impact of different factors of SCIs when users interact with them. However, when constructing SCIs using programmable soft materials, new factors that might impact users' experience will be further imported, e.g., softness [223, 505, 328].

The impact of new factors on users' behavior should be explored promptly when using these novel materials in SCIs development. As for design challenges, when constructing SCIs with emerging programmable soft materials, they can manifest as design questions, such as how to integrate artifacts and interaction with applications for end-users into SCIs using these novel materials. To address this question, applications for users with novel SCIs should be developed, accompanied by necessary user evaluations of these interfaces.

This thesis aims to address SCIs research challenges [10] from user behavior, technological and design aspects and unfold them in three steps. First, studying the impact of softness, i.e., one crucial new factor imported as using programmable soft materials for developing SCIs, on users' experience. Second, conducting technological explorations of programmable soft materials to facilitate HCI designers' use of them to create SCIs with various shape-changing abilities and developing new technologies addressing programmable soft materials' stretchability-strength trade-off. They help lay the technological foundation for developing toolkits HCI researchers need when they build their SCIs using these novel materials. Third, design novel SCIs for end-users, shape-morphing watches for notification applications with programmable soft materials and evaluate users' interaction experience. Overall, this thesis aims to understand users' experience with programmable soft materials, provide technological exploration to bridge the gaps between programmable soft materials and HCI, develop new technologies to address drawbacks of current programmable soft materials and develop novel SCIs providing insights into how programmable soft materials can be integrated into SCIs design.

1.1 Scientific context

1.1.1 Programmable soft materials

Programmable soft materials have emerged as a cutting-edge field of research that intersects increasingly with HCI [358]. These materials exhibit remarkable shape-changing abilities in response to various external stimuli, including pressure, e.g., pneumatic (e.g., [503, 509]) or hydraulic (e.g., [395, 151]), voltage (e.g., [258, 113]), magnetic fields (e.g., [19, 205]), and humidity (e.g., [355, 510]). Additionally, shape-memory alloys (SMAs) [280] are utilized to create programmable soft materials, as SMA wires can change their shape when heated based on their "remembered" shape¹. Although SMAs are inherently rigid,

1. SMAs are a kind of alloys that can be treated to acquire a specific shape, i.e., shape remembered. After undergoing a physical deformation (e.g., bent or twisted by users), an SMA wire can be heated

researchers have integrated SMA wires into soft materials such as fabric (e.g., [236, 291]) and elastomers (e.g., [150, 54]) to actuate these materials and induce shape changes upon heating the integrated SMA wires, enabling these materials to be actuated and change their shapes when the integrated SMA wires are heated. The remarkable shape-changing abilities of programmable soft materials have been demonstrated in various examples. For instance, the pneumatically actuated programmable soft material called Baromorph [402] can morph from a plate to a mask by pressurizing air channels embedded in the silicone plate (see Figure 1.3(a)). The shape after pressurization is defined, or programmed, by the shape and density of the air channels. For example, Figure 1.3(b) presents the shape patterns of air channels for the mask-morphing Baromorph. It is like the contour lines on the map, i.e., the air channels are denser where the surface is steeper. Figure 1.3(c) presents some other examples of Baromorphes with different shapes morphing from a plate. Similar strategies can be applied to other materials like dielectric elastomers [258], which change their shapes when high voltage is applied [148].

Emerging SCIs constructed with programmable soft materials have recently been developed for various applications, including haptic devices (e.g., [81, 411, 67]), usage-context adaptable user interfaces (e.g., [326, 509, 161, 510] in Figure 1.1), data physicalization (e.g., [119]), shape-changing displays (e.g., [419]), user assistive technology (e.g., exoskeletons [429]), and adaptive furniture and environment (e.g., [381]). However, current HCI studies usually develop UIs with one or a few shape-change abilities as proof-of-concept prototypes in their specific applications. It lacks a systematical exploration of using soft programmable materials for different shape-change features and respective toolkits [358]. For instance, pneumatically actuated programmable soft materials are commonly used in these applications, often involving the inflation of an air-proof silicone bladder in an isotropic manner² similar to inflating a balloon (e.g., [81, 411, 67, 119]). Recent interfaces like PneuUI [509] incorporate additional anisotropic types of shape-changing, such as bending, twisting, and linearly increasing length, by embedding origami structures into air-proof silicone bladders to restrict the shape-changing along specific directions as air pressure increases. In other words, when origami structures are integrated into air-proof silicone bladders to create interfaces, they can only change their shapes according to the direction of the origami's creases. Similar to matrixes of actu-

through resistive heating to its final transformation temperature and regain its remembered shape.

2. Isotropic inflation refers to the uniform expansion of a material in all directions. When an elastomer bladder is inflated, the pressure exerted on its inner surface causes the material to expand isotropically, stretching equally in all directions and forming a spherical shape.

ated pins (e.g., inForm [108]), systems composed of a matrix of elastomer bladders [419] can form some complex shape transformations like transitioning from a planar surface to the shape of a Stanford bunny [495]. However, their system involves numerous independently controlled elastomer bladders, increasing control complexity and resulting in bulkier systems with multiple valves and pumps. In addition to pneumatically actuated programmable soft materials, other types have also been employed in HCI. However, most of them focus solely on limited shape changes like bending (e.g., [510, 113]) or isotropic inflation (e.g., [151]). Overall, the full potential of shape-changing abilities offered by programmable soft materials still needs to be explored in terms of their utilization in HCI. Besides, various technologies were developed to control UIs' strength [38] like jamming [107] and phase-changing materials [276]. However, the question of combining them with soft programmable materials while addressing the stretchability-strength trade-off of soft materials is still to be answered.

1.1.2 Shape-changing interfaces (SCIs)

Users' perceptual space of SCIs

Rooted in Tangible User Interfaces (TUIs) [199], SCIs permit users to interact directly with physical objects. Compared to GUIs confined behind the glass of a screen [45, 199], SCIs allow users to interact by leveraging their existing human dexterity acquired through everyday object interactions [370, 187, 33]. When users interact with physical objects, they skillfully perceive and assimilate rich information through haptic perception, which includes softness (e.g. [107, 276]), temperature (e.g., [151, 254]), texture (e.g., [448, 86]), shape (e.g., [389, 23]), weight (e.g., [213, 307]) and many other factors [239]. Haptic perception [240], which occurs when we touch and manipulate physical objects [239], forms the basis of our human dexterity [486, 2]. When a haptic perception is impaired, it significantly impacts our interaction with physical objects. For instance, in an experiment by Roland Johansson [502], a participant with three anesthetized fingers (thumb, index, and middle) could not complete the simple task of striking a match. Therefore, understanding users' haptic perception of SCIs is crucial for developing SCIs. Numerous psychophysical experiments have been conducted to investigate users' haptic perception, covering aspects such as softness (e.g. [31, 231]), temperature (e.g., [210]), texture (e.g., [311]), shape (e.g., [89, 458]) and weight (e.g., [455]). However, aside from experiments on users' perception of softness, these studies have primarily focused on users' perception abilities

with rigid objects. Benefiting from the high shape-changing abilities of programmable soft materials [402], SCIs are not limited to rigid UIs; they can be soft and deformed by users (e.g., [509]). Therefore, previous studies on users' haptic perception abilities may not directly apply to SCIs design when using programmable soft materials. For example, when SCIs are constructed with soft materials (e.g., silicone elastomers [509]), user interactions (e.g., pressing with a finger [117]) can cause shape deformations in both the SCIs and fingers. These deformations may impact users' perception of the shape (e.g., curvature) of the SCIs. Studies in neuroscience also suggest that the softness of SCIs may affect users' shape perception (e.g., curvature) since both hard and curvy objects elicit high response frequencies in the same type of cutaneous mechanoreceptive afferent neurons [75, 1]. Considering the potential variations in users' haptic perception abilities due to the use of soft materials in SCIs development, it is essential to conduct further psychophysical experiments that specifically account for the softness of SCIs to gain a better understanding of users' haptic perception abilities in the context of SCIs.

Beyond the aforementioned discriminative touch, i.e., with touch, we perceive and discriminate objects' physical properties like curvature; the touch of objects can also be associated with affective sensations, referred to as affective touch [271]. For instance, when applying objects with different softness on users' fingers, they associate softer objects with more pleasant emotions [328]. When touching objects with different softness, users also tend to associate softer objects with lighter colors and rounded objects and less soft objects with darker colors and less curved objects [420]. An experiment also found that participants performed better in memorization tasks when sitting in a rigid chair and creative tasks when sitting in a soft chair [505]. With these experiments, we know that integrating SCIs built with soft materials into our world needs a better understanding of users' perception of them, including their physical properties and affective sensations, such as emotional impact. Notably, the new factor imported is softness, when programmable soft materials are widely imported into SCIs' design. This is vital to help researchers understand what affordance SCIs provide to users [10], which is critical to developing SCIs with appropriate shapes or appropriate changes of shapes to give the users better affordance. In this thesis, we will start addressing this question from one primary point of view: how the softness of SCIs impacts users' discrimination of objects' physical properties, such as curvature.

Design space of SCIs

The advancement of sensing technologies based on soft materials [40, 414] has made significant progress in integrating input abilities into SCIs. As mentioned earlier, sensors made of soft materials are capable of sensing various user inputs [451], including touch (e.g., [484, 480]), pressure (e.g., [517, 441]), bending (e.g., [366]), stretching (e.g., [225]), twisting (e.g., [299]), pinching (e.g., [481]), etc. However, challenges still exist in realizing the output of SCIs with shape-changing abilities [10]. Rasmussen et al. developed a design space for shape-changing interfaces based on recent advancements in shape-changing interfaces [363]. This design space encompasses different shape changes but does not explicitly discuss the technological approaches to realize each type of shape change. Building upon this work, Roudaut et al. proposed the taxonomy of Morphees [376], which considers the resolution of shape-changing interfaces. Their study [376] also developed a few shape-changing prototypes using different actuating technologies, including motors, SMA wires, and Dielectric Electro Active Polymer (DEAP)³. They compared the resolution of these prototypes; however, their prototypes mainly consisted of rigid interfaces like wood and plastic, and they did not explore the realization of all types of shape-changing in their taxonomy. Coelho and Zigelbaum reviewed various shape-changing materials (e.g., SMA and DEAP) for realizing shape-changing interfaces [73], focusing on properties such as activation speed and power. However, they also needed to explore the realization of different types of shape-changing using these materials. Based on [363, 376], the two widely cited Shape-changing interfaces taxonomies, Kim, Coutrix, and Roudaut developed the taxonomy of Morphees+ [226] and used it to classify everyday objects that can be reconfigured in shape [186].

These systematic reviews can inspire other researchers to develop their SCIs with shape-changing abilities based on previous research [363, 376, 73] and daily objects [226]. However, it lacks toolkits for users to develop SCIs with different shape-changing abilities, which is one key barrier to addressing the challenge of building UIs with shape-changing abilities [10]. Following Morphees+ [226], Kim et al. proposed a toolkit, MorpheesPlug [227], to address this challenge. It provides users with a series of different modules to realize a large range of shape-changing features of Morphees+ [226], including Size, Porosity, Amplitude, Curvature, Closure and Zero-crossing. However, their technology faces miniaturization challenges, as their structures have little shape change when the

3. A DEAP membrane can change its shapes when applied high voltage on it [113]. For example, the DEAP membrane used in Morphees [376] bends when applied voltages between 1000-2500V on it.

thickness is less than 2 cm, and part of their shape-changing features, like Zero-crossing, necessitates a few actuators, which can further prevent miniaturization. For this reason, we proposed a series of soft shape-changing modules in this thesis to provide thinner solutions, i.e., 5 mm, which can be even thinner (approximately 3 mm) to realize all 6 shape-changing features of MorpheesPlug [227] using only one actuator.

Stretchability and Strength are other important shape-changing features [226, 376] when developing SCIs with shape-changing abilities. Meanwhile, the Stretchability-Strength trade-off is an important drawback [358] that soft materials like elastomers need to be addressed when using them to construct SCIs with shape-changing abilities. I.e., the high stretchability of soft materials ensures their high deformability for shape changes, which reversely leads to their low strength. To address this trade-off, it needs to combine technologies controlling UIs' strength [38] with technologies controlling UIs' shapes [363, 376, 73] to strengthen them while keeping their high shape-changing abilities. Current technologies addressing this problem often face drawbacks like needing multiple actuators, causing bulkiness [418]; needing heating to control systems' strength, thus slow transition between hard/soft status because of the intrinsically slow thermal conduction and not allowing fine strength tuning [520, 184]; needing extra thickness for adding strength controlling functions thus bulky [471]. For this reason, we developed a novel technology in this thesis to control both UIs' shapes and strength with only one actuator and not add extra thickness to the shape-changing systems.

1.2 Research questions

As demonstrated in previous studies, programmable soft materials hold significant potential for addressing the challenges associated with shape-changing abilities in the design of SCIs. However, current SCIs in programmable soft materials exhibit limited shape-changing capabilities. We believe that this limitation can be attributed to three main challenges [10] that need to be addressed:

1. **Understanding the user experience of SCIs (User behavior challenges):** In the users' perceptual space, it is crucial to understand better how effectively users can perceive the shape of SCIs and what users' sensation of SCIs' shapes and shape-changes is, particularly considering the softness factor into consideration.
2. **Technological barriers to SCIs development using programable soft materials (Technological challenges):** It lacks toolkits that enable researchers to

design SCIs with various shape-changing abilities using programmable soft materials. It also lacks technology addressing the stretchability-strength trade-off of programmable soft materials.

3. **Design and implementation of SCIs application using programable soft materials (Design challenges):** It lacks HCI applications with SCIs in novel programable soft materials with high shape-changing abilities.

1.2.1 Problem I: Lack of understanding of users' shape perception abilities of SCIs

There needs to be more clarity regarding how users interact with SCIs, specifically in terms of their perception of the shape of SCIs. The shape of UIs plays a crucial role in providing users with haptic feedback for various purposes [509, 23, 364, 419, 103]. Extensive prior research has been conducted on users' shape perception abilities with rigid objects, revealing that people exhibit high precision and accuracy when touching and exploring shapes of rigid surfaces [89, 458, 136, 138]. However, programmable soft materials used in SCIs development are non longer rigid, and their shape can change when users touch and interact with them; further exploration is required to understand users' shape perception abilities on SCIs, particularly considering the softness of the materials used. One challenge in understanding the user experience of SCIs is to isolate different factors, such as visual effects [333] and haptic effects [107]. Implementing SCIs with shape-changing abilities in soft programmable materials will bring new factors, such as softness, which previous experiments usually do not address [89, 458, 136, 138]. Moreover, users' experience with UIs' shapes and softness is also multifaceted, including both the discrimination of UIs' physical properties like roughness [61] and association with multiple affective sensations like emotion [105, 328], colors [250, 420], and smells [275]. Facing this challenge involving various factors, we start from one primary point of how effectively (precisely and accurately) users can perceive the shape of SCIs under different softness conditions. More specifically, we have identified in this thesis two research objectives that need to be addressed:

1. **Objective 1:** Understand users' shape perception abilities on SCIs under different levels of softness.

-
2. **Objective 2:** Provide design guidelines for developers when designing SCIs using materials with different levels of softness.

1.2.2 Problem II: Lack of SCIs development toolkit and existence of the stretchability-strength trade-off of programmable soft materials

Due to their remarkable shape-morphing abilities, programmable soft materials exhibit great potential in addressing the shape-changing challenges in developing SCIs. While novel programmable soft materials [248] are emerging, their integration into HCI still needs to be improved [358], especially when creating UIs with complex shape-changing abilities. Previous design spaces, such as [376, 363, 73, 226], have provided researchers with valuable inspiration in terms of shape-changing taxonomies [376, 363, 226] and comparisons of a few shape-changing materials [73]. The current design space of SCIs [376, 363, 73] is vast, encompassing numerous different shape features, yet the challenges of developing SCIs using programmable soft materials remain unaddressed. For instance, gaps exist between material science and HCI [358], led by high technological barriers for HCI researchers to use novel programmable soft materials in their SCIs development. A few toolkits [227, 518, 266, 78, 509, 225] were also developed recently to lower the technological barrier of developing SCIs with shape-changing abilities. However, they usually use non-stretchable materials [518] or blend soft materials like elastomers and non-stretchable materials [509, 225], which might prevent realizing soft materials' high stretch abilities.

Furthermore, the thickness of modules in the current toolkit [227] or the necessity of combining a few actuators to actuate a few modules to realize shape change [78, 266] often leads to the whole system's bulkiness. Besides, programmable soft materials like elastomers' [402] stretchability-strength trade-off must also be addressed to widen their integration into SCIs design.

From these perspectives, we have identified two research objectives that need to be addressed:

1. **Objective 1:** Conducted a technological exploration of programmable soft materials to realize different shape-changing features in purely soft materials using a single actuator.
2. **Objective 2:** Develop new shape-changing technologies to address the stretchability-

strength trade-off of programmable soft materials.

Our technological exploration of programmable soft materials and the development of new technologies can establish the technological base for further developing toolkits so that HCI researchers can better integrate novel materials into their SCIs development.

1.2.3 Problem III: Lack of HCI applications with SCIs in novel programable soft materials

Novel programmable soft materials [402, 148] have already shown high shape-changing abilities. For example, a Baromorph [402] elastomer plate can morph into a saddle, a semi-sphere, a bowl, a cone, and even a human mask shape (Figure 1.3). Despite the remarkable illustrations of these novel materials' shape-change potential, they lack HCI applications that integrate these novel materials into SCIs. Meanwhile, when designing SCIs using these novel materials, design questions need to be answered, such as what shape changes we should apply and what applications we should build. Respective HCI applications of SCIs with different shape changes should be developed and evaluated by users. Furthermore, technique problems must be overcome when using these novel materials in HCI applications. For example, the thickness of Baromorph plated can be improved to bring users better wearability [112], and the high voltage needed by dielectric elastomers [148] must be anticipated for safety reasons. From these perspectives, we have identified three research objectives that need to be addressed:

1. **Objective 1:** Designing HCI applications with SCIs using novel programmable soft materials with high shape-changing abilities.
2. **Objective 2:** Improving current programmable soft materials for better meeting HCI application requirements.
3. **Objective 3:** Evaluating users' experience interacting with SCIs with different shape-changes.

1.3 Methodology

Our research aims to address challenges [10] in SCIs research, particularly in user behavior, technological and design challenges. Traditional methods to actuate SCIs often

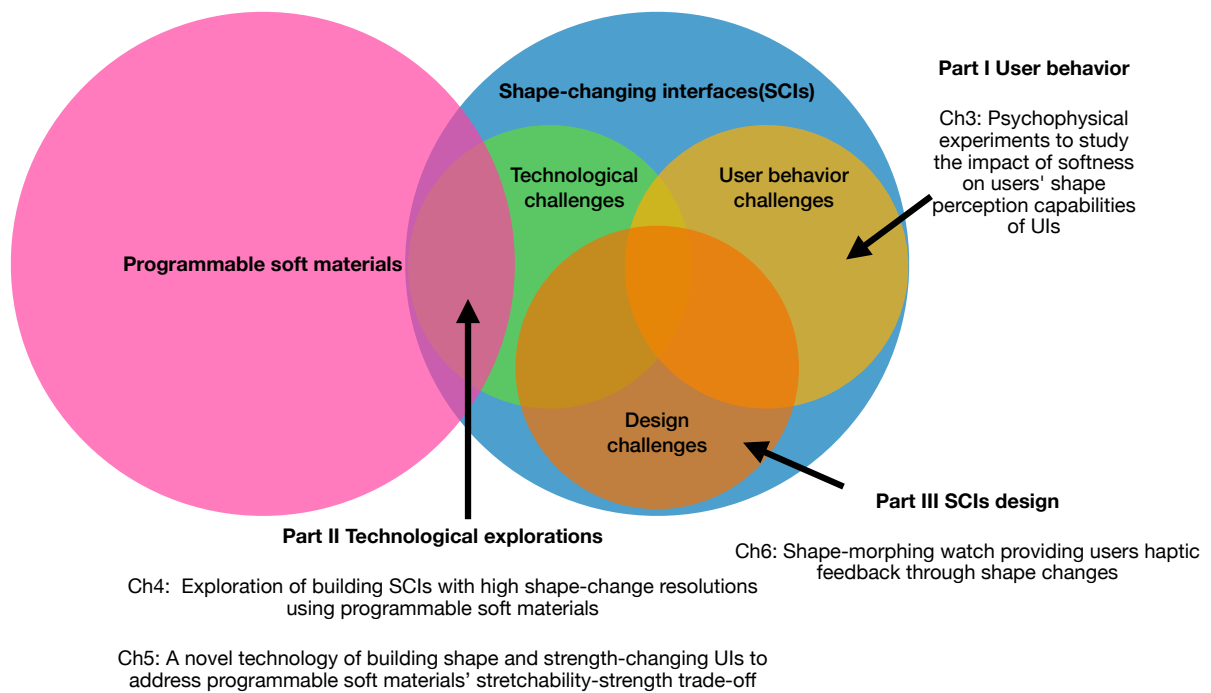


Figure 1.4 – Research methodology of this thesis.

involve bulky systems with many rigid components like motors and gears [246], which limits SCIs's applications, particularly for wearable applications [112]. Emerging programmable soft materials [358] broadly open the potential for building SCIs with the advantages of soft, lightweight, and high shape-changing abilities. However, challenges in building SCIs with programmable soft materials come from user behavior, technological and design aspects [10]. Figure 1.4 presents our research methodology in this thesis, addressing challenges in these three aspects.

Addressing user behavior challenges in building SCIs requires researchers to understand better users' experience with UIs' shape changes, including their discrimination of UIs' shape and associated affective sensations. One key point to address these challenges is to isolate factors involved in users' experience with SCIs. In particular, adopting programmable soft materials into SCIs design imports a novel factor, i.e., the softness. In this thesis, we will partially address these challenges by conducting psychophysical experiments to study the impact of softness on users' shape perception capabilities of SCIs.

One timeless need to address technological challenges in building shape-changing SCIs is providing toolkits for researchers to lower the barrier of constructing SCIs. Appropriate

toolkits are also essential bridges for the gap between emerging programmable materials and soaring demand for shape-changing technologies in the HCI area [358]. Another critical difficulty in addressing technological challenges is miniaturizing SCIs' size and developing high-resolution shape-changing SCIs. To address these challenges, we conducted technological explorations of novel programmable soft materials to construct SCIs with different shape-change features [226, 376]. More specifically, we will provide a series of shape-changing modules covering various shape-changing features [226] based on one recent programmable material, Baromorph [402], to facilitate the development of shape-changing SCIs. These modules are in soft materials (elastomers), have a thin thickness (≈ 5 mm), and can continuously control different shape-changing features using only one actuator, which can thus also help to meet the challenge of SCIs' miniaturization and high resolution. The adaptation of programmable soft materials faces another drawback in technological aspects: their stretchability-strength trade-off [358]. We thus develop a new technology capable of controlling both UIs' shape and strength to address this trade-off. Our explorations in novel programmable soft materials and the development of new shape-strength control technology will pave the way and reduce the technological barriers for HCI researchers to develop SCI toolkits using programmable soft materials.

The final step addresses the design challenges by developing HCI applications with SCIs using programmable soft materials and evaluating users' interaction experience. For this purpose, we improved one novel programmable soft material, Baromorph [402], to develop very thin SCIs (≈ 3 mm) worn on users' wrists in the shape of watches to give wearers haptic feedback through different shape changes. We also conducted psychophysical experiments to study users' perception performance with these novel watches and users' qualitative feedback with these novel SCIs.

1.4 Thesis contributions

The thesis presents three contributions to HCI, addressing respectively SCIs research challenges [10] from three aspects:

1. **User behavior challenges: Study on user's shape perception ability of SCIs** (Chapter 3)
 - (a) We conducted a psychophysical experiment to examine users' shape perception ability, focusing on curvature on surfaces under four softness conditions and three different curvature conditions.

- (b) Based on the results of our experiments, we provide guidelines for designing future SCIs with different levels of softness and shape, with a specific emphasis on curvature.

This chapter leads to a publication in the CHI'23 conference [100].

2. Technological challenges: Conduct technological exploration on programmable soft materials and propose new technology to lower SCIs development barrier (Chapter 4 & 5)

- (a) We introduced *SoftMorphee*, a series of shape-changing modules capable of realizing a large range of SCIs' shape-changing features using programmable soft materials, i.e., *Size*, *Curvature*, *Amplitude*, *Porosity*, *Closure* and *Zero-crossing*. We also discussed the challenges of constructing SCIs with tunable *Modularity*, *Stretchability*, and *Strength* using only soft materials (Chapter 4).

This chapter will be submitted to the CHI'25 conference.

- (b) We developed a new technology called *Jamming Origami Endoskeleton* to address the trade-off between soft materials' high shape-change potential and low *Strength* [358]. This new technology enables UIs to have both high shape-change ability (in particular *Curvature* change) and tunable *Strength* (Chapter 5).

This chapter will lead to a future submission.

3. Design challenges: Implementation of SCIs (Chapter 6)

- (a) We improved a new programmable soft material [402] and developed a wearable shape-changing watch that gives users haptic feedback with changing shapes.
- (b) We conducted a psychophysical experiment to study users' interaction experience with this novel device.

This chapter leads to a publication in the IHM'24 conference [101] and a publication in MobileHCI'24 [102].

1.5 Structure of the thesis

Figure 1.5 presents the outline of the thesis structure. First, we present our research background in Chapter 2 by reviewing different HCI research using programmable soft materials used to construct SCIs. It can also serve as a takeaway chapter for HCI researchers to get an overview of new materials adopted in SCIs development. We then present the work conducted in this thesis. As this thesis addresses SCI research challenges from three

aspects, we articulate the presentation of our work in three parts. Part I presents our study on users’ soft SCIs shape perception abilities for addressing user behavior challenges (Chapter 3). Part II presents our technological exploration of programmable soft materials for constructing SCIs (Chapter 4) and the development of a new technology to overcome soft materials’ stretchability-strength trade-off, which addresses technological challenges (Chapter 5). Part III presents our design of the HCI application of SCIs using programmable soft materials with respective user studies for addressing design challenges (Chapter 6). To conclude this manuscript, Chapter 7 presents this thesis’s limitations and future work, as well as the perspectives we envision for future SCIs.

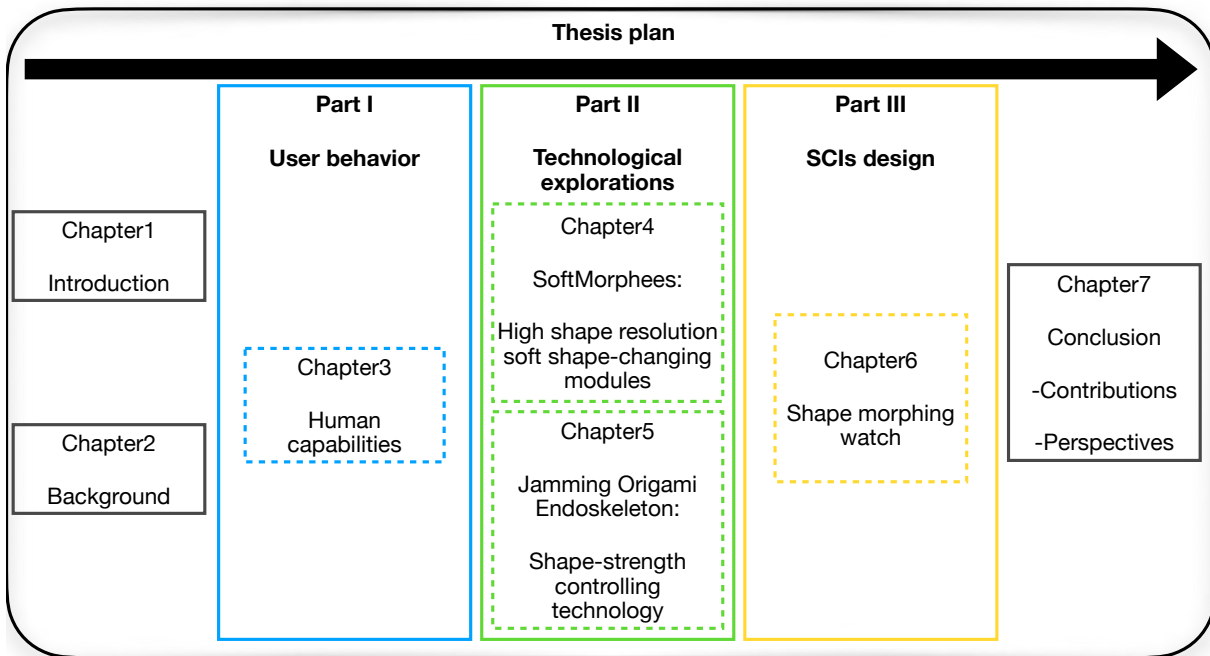


Figure 1.5 – Structure of the thesis.

Chapter 4 and 6 present work from the supervision of two internship students, Alexis SANSON and Thomas RAMES, who Céline and I supervised. I supervised them to develop together the pressure-controlling system, which we used to pressurize our shape-changing modules in these two chapters. I also supervised Alexi’s development of the experiment software and Baromorph prototypes in Chapter 6. Céline and I supervised the design and performance of the study by Alexis in Chapter 6.

The novel shape-changing technology presented in Chapter 5 is a collaboration between us, Tian GAO, Benoît ROMAN, and José BICO from the Laboratory for the Physics and

Mechanics of Heterogeneous Media (PMMH) of Sorbonne University.

BACKGROUND: PROGRAMMABLE SOFT MATERIALS AND SCIs

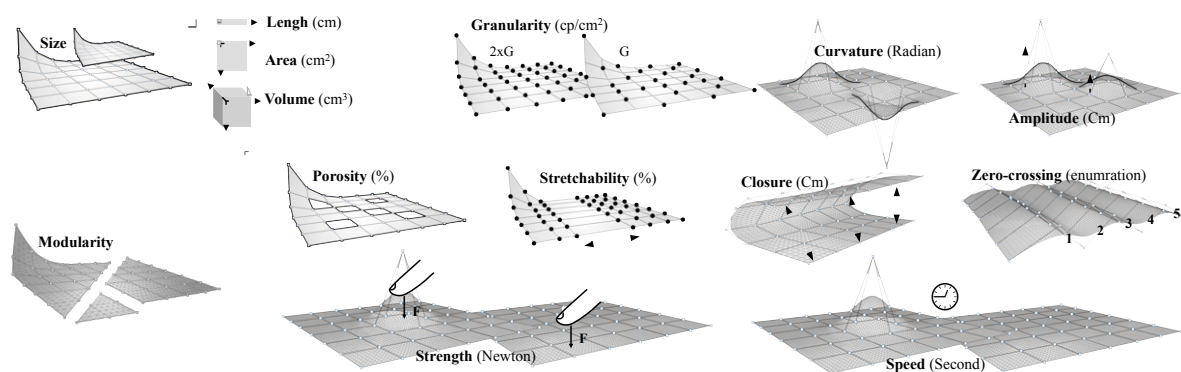


Figure 2.1 – Different shape-changing features in the taxonomy of Morphees+ [226].

In this chapter, we review literature related to different technologies for constructing shape-changing interfaces (SCIs) employing programmable soft materials with various shape features [226] according to Morphees+ taxonomy [226] (Figure 2.1). We choose the Morphees+ taxonomy [226] because it combines and improves upon two of the most impactful taxonomies in the HCI field, namely Rasmussen et al.’s [363] and Roudaut et al.’s [376]. We emphasize that actively shape-changing UIs, referred to as SCIs [10]. In contrast, UIs that can only passively change shape through user input [341] or input-only interfaces (e.g., [425, 517]) are excluded from our discussion. Previous reviews, such as [40, 414], have already thoroughly explored passively shape-changing or input-only interfaces.

2.1 SCIs using soft materials

2.1.1 Size

The *Size* features are categorized into three subtypes: *Length*, *Area*, and *Volume*, which often exhibit correlations. For instance, Yao et al. [509] developed a height-controllable building model (Figure 2.2(c)), illustrating that changes in the building’s height (*Length category*) result in concurrent alterations in its *Volume* and lateral surface *Area*. Rigid actuators, such as linear motors, enable direct control of object *Length* along the motor axis, as demonstrated in actuated matrix displays with controlled pin heights [246, 297, 244, 108, 245]. However, many of these actuators are typically bulky, completely rigid, form a discrete surface, or must be covered by a piece of fabric to form a continuous surface [245].

Due to their high stretchability and airtight properties, elastomers are commonly employed in creating inflatable UIs, as seen in works like [282]. In the context of elastomer bladders, an increase in inner air pressure leads to inflation, increasing *Volume* and, consequently, surface *Area*. Chen et al. [62] designed a shape-changing spoon incorporating an elastomer air bladder to control its food-carrying *Volume*. In this design, inflating the air bladder reduces free space on the spoon head, limiting its food-carrying capacity. Inflating an elastomer bladder uniformly, as achieved with homogeneous material and thickness, leads to isotropic inflation¹ similar to inflating a balloon (Figure 2.2(a)) [119]. The versatility of elastomers is evident in their customizable shapes, facilitated by 3D printing for mold creation and the use of commercial silicone elastomers for molding [282]. Inflatable elastomer bladders find widespread application in developing SCIs across various domains, as demonstrated in works such as [282]. Liquids like water are occasionally employed instead of air, as shown in [151]. Conversely, when bladders are composed of non-stretchable materials, such as the non-stretchable fabrics in *aeroMorph* [318] or PET film in *milliMorph* [256], an increase in inner pressure causes flat bladders to inflate into a spherical shape, resembling a balloon. The lack of stretchability results in increased thickness after inflation, leading to the shrinkage of the airbag’s silhouette and, consequently, a change in *Length* (Figure 2.2(b)).

Diverging from the previously mentioned balloon-like isotropic inflation scenarios,

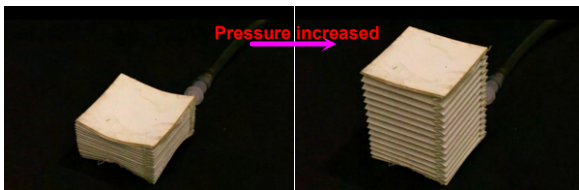
1. Isotropic inflation refers to the uniform expansion of a material in all directions. When an elastomer bladder is inflated, the pressure exerted on its inner surface causes the material to expand isotropically, meaning that it stretches equally in all directions, forming a spherical shape.



(a) Elastomer bladders can inflate into spherical balloon-like shapes with their *Volume* increasing [119].



(b) Bladders in non-stretchable materials can inflate with the shrinkage of silhouette, leading to their *Length* decreasing [306].



(c) Elastomer bladders with bellows-like origami structures embedded inside can inflate to increase their *Length* [509].



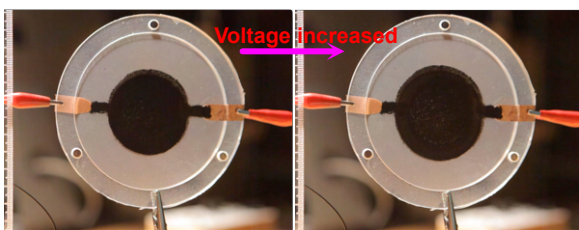
(d) Elastomer bladders molded into bellows-like shape can inflate to increase their *Length* [300].



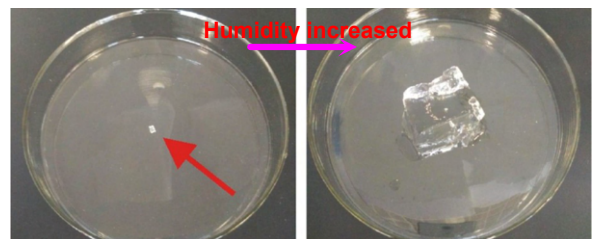
(e) Elastomer tubes sewn into fabric with limited radial expansion can inflate to increase their *Length* [530].



(f) Elastomer tubes with non-stretchable filaments braided around to limit its radial expansion can inflate to decrease (Middle) or increase (Right) their *Length* respectively to different braiding angles (Left) [225].



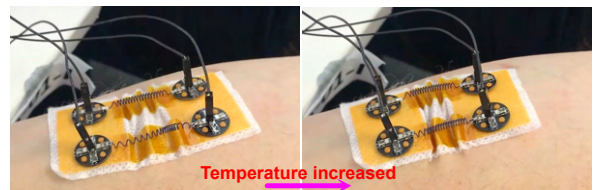
(g) Dielectric elastomer membranes can increase their *Area* when high voltage applied on them [113].



(h) Hydrogels can absorb water and swell in *Volume* [260].



(i) Auxetic structures can be inflated to expand the *Area* [142, 227].



(j) SMA springs can be heated to return to their “remembered” shape, e.g., with a shorter *Length* [274].

Figure 2.2 – Different technologies for creating *Size* changing UIs.

which exhibit varying *Volume* with changes in inner air pressure, embedding origami structures into elastomer bladders [264] confines the bladder’s shape change to specific directions. The shape transforms according to the orientation of the origami’s creases as air pressure increases. For instance, Figure 2.2(c) illustrates the integration of bellows-like origami structures into elastomer bladders. When the inner air pressure is increased, the bladder expands vertically—increasing its *Length*—instead of isotropically expanding in all directions. This directional constraint imposed by the origami structure makes it easier for the bladder to deform vertically. Similarly, molding the elastomer into a bellows-like shape [300] (Figure 2.2(d)) facilitates deformation along the vertical direction, enabling an increase in length when internal pressure rises. The same effect can be achieved by printing a similar structure on stretchable plastic [227], such as TPU. These structures can also be actuated to decrease in length when reducing inner pressure (e.g., [59]).

An alternative technique to constrain the isotropic inflation of an elastomer bladder in a specific direction for creating *Length*-changing UIs is to sew the bladder into fabrics. The stitches around the bladder serve as inflation constraints [530]. For instance, Figure 2.2(e) depicts an elastomer tube sewn into a piece of fabric [531]. The stitches restrict radial expansion, while fabric pleats enable axial extension. Consequently, increasing the inner air pressure leads to tube inflation and a corresponding increase in *Length*. When the air pressure is released, the tube shortens due to the release of stored elastic energy from its stretched state. Drawing inspiration from the technology of McKibben muscles [446], widely used as linear actuators in robotic research (e.g., [445]), recent HCI researchers have explored incorporating a braided sheath around an elastomer bladder to restrict inflation in specific directions for *Length* control. Figure 2.2(f) illustrates the work of Kilic Afsar et al. [225], where elastomer tubes are inserted into nylon monofilament braiding sheaths fixed at two extremities. The braiding angle of the sheaths (Figure 2.2(f) left) determines the direction of length change [253] when inner pressure increases. A braiding angle smaller than 54.4° results in tube contraction (Figure 2.2(f) middle), while an angle larger than 54.4° leads to extension (Figure 2.2(f) right).

In addition to pneumatic inflation and deflation, voltage, and humidity change can also trigger the *Size* change of UIs. For instance, dielectric elastomers [308] can expand their *Area* under high voltage (Figure 2.2(g)) [113]. Certain food materials (e.g., gelatin and starch [476]), biological materials (e.g., natto cell [510]), and hydrogel [260] (Figure 2.2(h)) swell when absorbing water. In contrast to material expansion/shrinkage, auxetic structures [142] can also be employed to develop size-changing UIs. Auxetic structures typically

consist of an arrangement of connected hinge-like cells; the rotation of these cells leads to the expansion/shrinkage of *Area* when stretched/compressed (Figure 2.2(i) left). They are commonly used for constructing UIs that are passively stretched/compressed by users (e.g., [196, 143]). Kim et al. [227] provided an example of printing auxetic structures in TPU, with cells capable of being inflated pneumatically. The inflation of each cell when pressurized pushes them to rotate, resulting in the entire structure expanding the *Area* (Figure 2.2(i) middle to right).

Another frequently used technology is shape-memory alloys (SMAs) [280]. SMA wires can change their shape when heated to return to their “remembered” shape ². This can lead to *Length* changes; for example, an SMA spring can be heated to contract its *Length* (Figure 2.2(j)) [274]. Although SMAs are inherently rigid, researchers have integrated SMA wires into soft materials such as fabric (e.g., [236, 291]) and elastomers (e.g., [150, 54]) to actuate these materials and induce shape changes upon heating the integrated SMA wires.

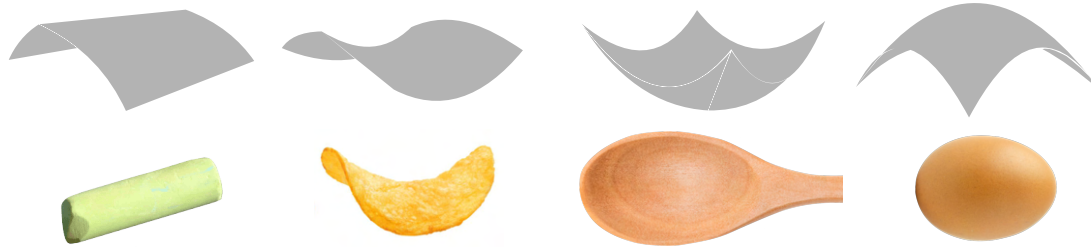
Based on these fundamental physical phenomena of *Size* change under specific stimuli (e.g., voltage, heat, humidity, and pressurization), other types of SCIs can be created (e.g., *Curvature*-changing UIs [150]). These will be further discussed in the following section.

2.1.2 Curvature

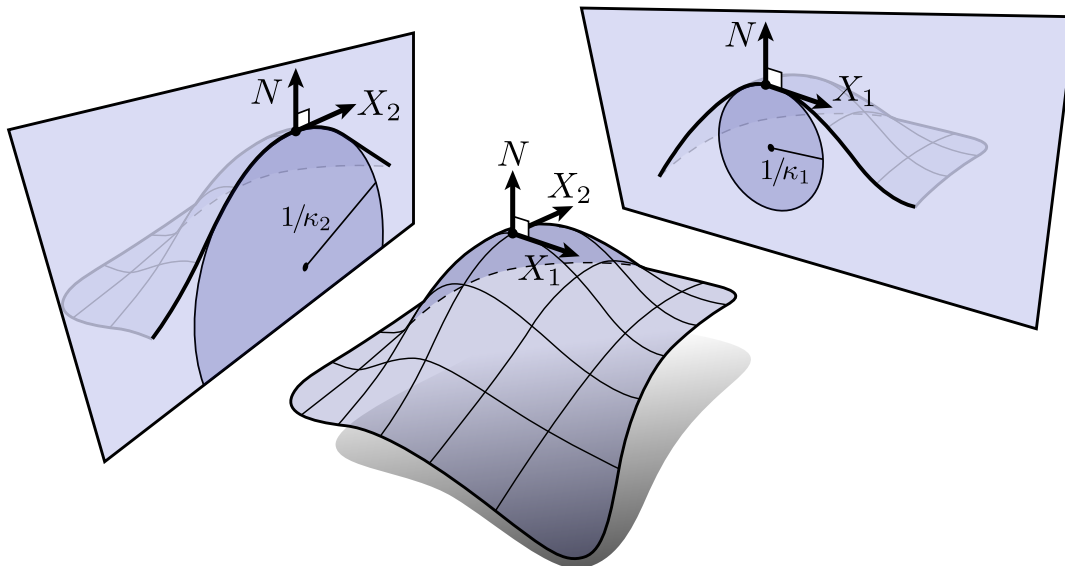
Three distinct curved surfaces, arising from the morphing of a planar surface, are commonly observed in everyday objects: cylindrical surfaces, saddle shapes, and dome surfaces (concave and convex) (Figure 2.3(a)). These three fundamental types of curved surfaces [73, 350] exhibit different Gaussian *Curvatures* [30, 532] (Figure 2.3(b)). Specifically, a cylindrical surface has zero Gaussian *Curvature*, a saddle surface has negative Gaussian *Curvature*, and a dome surface has positive Gaussian *Curvature*.

Numerous UIs for *Curvature* changing (e.g., [509, 345, 523, 524, 225, 295, 476]) achieve *Curvature* changes by bending a planar surface to form a cylindrical surface. Most of these interfaces are based on bilayer structures [337, 365], wherein two layers of materials are composited together and can be independently controlled for extension/contraction. As depicted in Figure 2.4(a), when both layers are composited and change their *Length* in a parallel direction, with one layer extending/contracting more than the other, the surface

2. SMAs are a kind of alloy that can be treated to acquire a specific shape, i.e., shape remembered. After undergoing a physical deformation (e.g., bent or twisted by users), an SMA wire can be heated through resistive heating to its final transformation temperature and regain its remembered shape.



(a) Three types of curved surfaces [532] with respective everyday objects below having this type of curved surface. From left to right are a cylindrical surface with Zero Gaussian *Curvature*, a saddle surface with negative Gaussian *Curvature*, and a concave and convex dome surface with positive Gaussian *Curvature*.

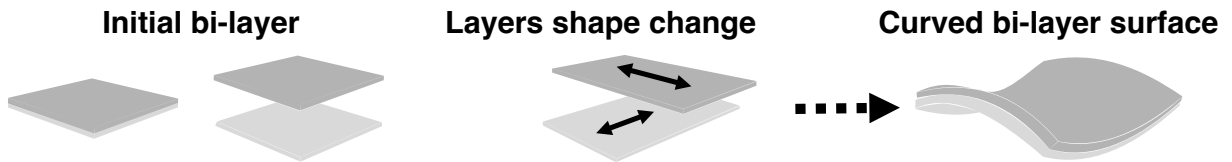


(b) Illustration of Gaussian *Curvature* [222] with a dome shape as example. Gaussian *Curvature* at one point (e.g., the top point of the curved surface in this figure) on a surface is defined as the product of the two principal *Curvatures* in this point, i.e., the maximum and minimum *Curvature* values (i.e., k_1 and k_2) at this point in respective normal plane perpendicularly cutting this surface (i.e., the two planes containing the two circles under the curved surface). For a cylindrical surface, the principal *Curvature* in the normal plane parallel to the cylinder's axial direction is 0; it thus has a Gaussian curvature of 0. For a saddle surface, the two principal *Curvatures*' respective normal directions (i.e., the two \mathbf{N} vectors's directions) are opposite; thus, it has a negative Gaussian curvature. The two normal directions are the same for a dome surface, whether concave or convex (as shown in this Figure), thus having a positive Gaussian *Curvature*.

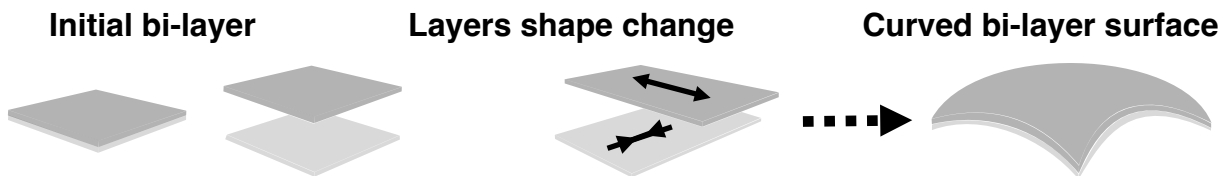
Figure 2.3 – Curved surfaces with different types of Gaussian *Curvatures*.



(a) Bi-layer cylindrical surface with Zero Gaussian *Curvature*: when two layers change their *Length* in a parallel direction, the bi-layer structure will form a cylindrical surface bending toward the relatively shorter layer. For example, as shown in this Figure, with the upper layer increasing its *Length* and the bottom layer decreasing its *Length*, it will bend toward the bottom layer.

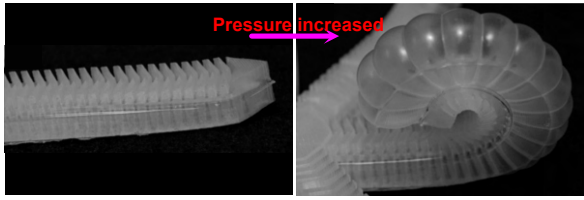


(b) Bi-layer saddle surface with Negative Gaussian *Curvature*: when two layers change their *Length* in an orthogonal direction, with each layer relatively increasing its *Length* in one direction, the bi-layer structure will form a saddle shape. For example, as shown in this Figure, with the upper layer increasing the *Length* in one direction and the bottom layer increasing the *Length* in an orthogonal direction, it curves into a saddle shape.

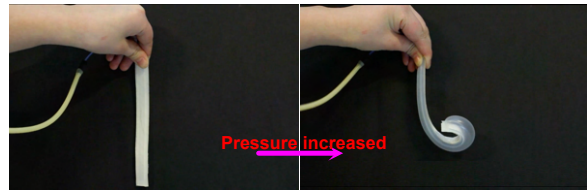


(c) Bi-layer dome surface with Positive Gaussian *Curvature*: when two layers change their *Length* in an orthogonal direction, with one layer relatively increasing its *Length* in both two directions, the bi-layer structure will form a dome shape bending toward the relatively shorter layer. For example, as shown in this Figure, the upper layer increasing the *Length* in one direction and the bottom layer decreasing the *Length* in an orthogonal direction forms a dome surface bending toward the bottom layer.

Figure 2.4 – Illustration of technologies of bi-layer structure forming curved surfaces with different Gaussian curvatures.



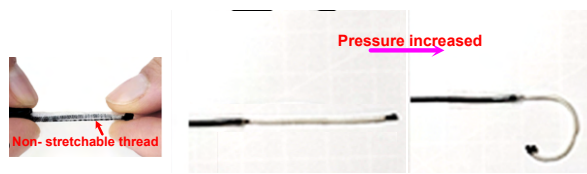
(a) An elastomer bi-layer structure curves to harder elastomer side when inflated [188].



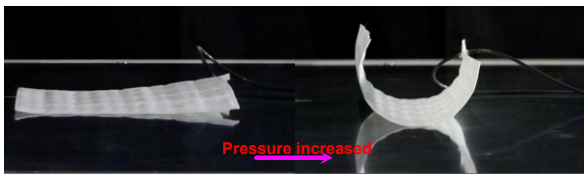
(b) An elastomer and paper bi-layer structure curves to paper side when inflated [509].



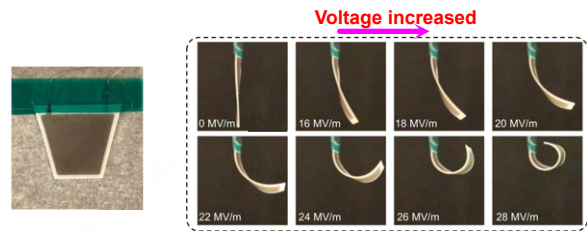
(c) An elastomer tube sewn in fabric and fiberglass bi-layer structure curves to elastomer side when deflated [530].



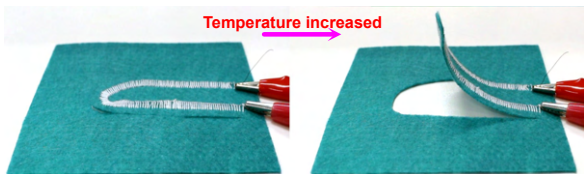
(d) An elastomer tube sewn with sheath and non-stretchable thread bi-layer structure curves to on-stretchable thread side when inflated [225].



(e) A non-stretchable fabric airbag and fabric bi-layer structure curves to airbag side when inflated [318].



(f) A dielectric elastomer and concentrated boron nitride nanosheets bi-layer structure curves to concentrated boron nitride nanosheets side when high voltage is applied [354].



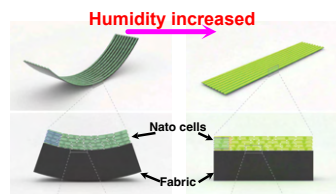
(g) A SMA wire and fabric bi-layer structure curves to SMA wire side when temperature is increased [295].



(h) A gelatin bi-layer structure curves to more porous gelatin side when humidity is increased [476].



(i) An hydrogel and fabric bi-layer structure curves to hydrogel side when humidity is increased [371].



(j) A Nato Cells and fabric bi-layer structure curves to fabric side when humidity is increased [475].

Figure 2.5 – Bi-layer structures with different materials for making cylindrical *Curvature* changing UIs.

bends toward the shorter one, creating a cylindrical surface with zero Gaussian *Curvature*.

The key to achieving cylindrical shape change through bending is realizing different extensions/contractions between the two layers in one direction. One approach is to bond two layers of elastomer with different stretchabilities. For instance, as illustrated in Figure 2.5(a), Ilievski et al. [188] bonded an elastomer layer composed of a series of air bladders made of highly stretchable elastomer Ecoflex 00-30 [192] to another elastomer layer made of less stretchable elastomer Sylgard 184 [55]. When the inner pressure of air chambers increases, the layer of elastomer Ecoflex 00-30 extends more than the layer of Sylgard 184 because of its higher stretchability, leading to the bending of the whole structure toward the less extendable side. This technology is also widely used for actuating soft robots [393, 377]. Asymmetrical extension can also be achieved by constraining the extension of one layer through the embedding of non-stretchable materials into it [509, 345, 523, 524]. For example, Yao et al. [509] embedded a layer of paper on one side of an elastomer air bladder (Figure 2.5(b)), limiting the extension of this side and causing the bending toward the paper side when inflated. The technology of *Length* control by sewing the bladder into fabric (Figure 2.2(e)) [530] and covering a braided sheath around an elastomer bladder (Figure 2.2(f)) [225] can similarly translate into bending by adding a non-stretchable layer on one side to limit the extension of this side. As shown in Figure 2.5(c), removing air pressure from the tube shortens it together with the fabric, while the non-stretchable layer of fiberglass below it constrains the *Length* change of the layer bonding with it, resulting in an upward bending shape-change [530]. Similarly, Kilic Afsar et al. [225] inserted a non-stretchable thread into one side of the braid sheath of the tube to constrain the extension of *Length* on this side when increasing pressure inside, leading to a bending shape-change toward the non-extendable side (Figure 2.5(d)) [225]. Previously mentioned non-stretchable bladders [318, 306], whose *Length* shrinks when inflated, can also be added to a non-stretchable layer to enable bending toward the bladder's side (Figure 2.5(e)).

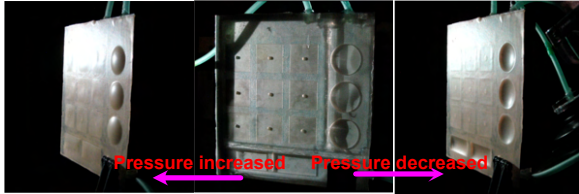
In addition to pneumatic actuation, the previously mentioned technologies for *Length* control can be combined with bilayer structures to achieve bending shape change. For instance, Pu et al. [354] reduced the stretchability of a dielectric membrane on one side by adding a layer of concentrated boron nitride nanosheets, resulting in bending towards the less stretched side when high voltage was applied to the membrane, causing it to expand (Figure 2.5(f)). Nabil et al. [295] induced *Curvature* in a fabric by heating an SMA wire sewn on one side, causing the fabric to curve in that direction as the SMA wire contracted

in *Length* (Figure 2.5(g)). Wang et al. [476] created gelatin films with varying porosity on two sides. Immersing these films in water led to bending towards the more porous side, as the less porous side absorbed more water and swelled more (Figure 2.5(h)). Rivera et al. [371] added a layer of hydrogel to fabrics, resulting in the composite turning towards the fabric side as the hydrogel swelled with increased humidity while the fabric layers did not (Figure 2.5(i)). Similar to the hydrogel-fabric composite [371], Wang et al. [475] fabricated a Nato Cells-fabric composite that bent similarly when humidity changed (Figure 2.5(j)).

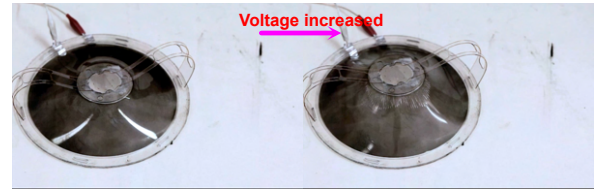
Beyond curving into a cylindrical surface, fixing the periphery of an elastomer membrane over a pressure-controllable chamber can create a convex/concave dome surface (Figure 2.6(a)) by adjusting the air pressure inside the chamber (e.g., [157]). It can also create a convex dome surface (Figure 2.6(b)) [113] by increasing the voltage applied to a dielectric elastomer membrane with its periphery fixed. As shown in Figure 2.4, bilayer structures can also create dome or saddle surfaces beyond cylindrical curved surfaces. For instance, Zhu et al. combined two layers of the aforementioned *Length*-extendable fabric [530] with elastomer tubes sewn into them, allowing extension in orthogonal directions to enable a planar surface to morph into a saddle shape (Figure 2.6(c)). However, creating dome/saddle surfaces with bilayer structures is limited [337]. Specifically, when a flat bilayer structure stretches/shrinks over a certain scale to form a dome/saddle surface, it tends to curve into a cylindrical surface. For example, the condition for a bilayer elastomer membrane with a radius of $R_{Membrane}$ and thickness of $h_{Membrane}$ to stretch/shrink one layer to form a dome (i.e., spherical) surface before curling into a cylindrical surface is $R_{DomeSurface} \gg \frac{R_{Membrane}^2}{h_{Membrane}}$, where $R_{DomeSurface}$ is the radius of the spherical surface [337]. Using the example of the bilayer structure presented in Figure 2.5(f), it can be observed that before curving into a cylindrical surface, the membrane actually stretches to form a dome surface (Figure 2.5(f) second sub-figure on the top right) initially as the voltage progressively increases, while further stretching leads to bending into the cylindrical surface.

To overcome the limitations associated with bilayer structures [337], recent advancements in materials science have facilitated the development of alternative technologies for *Curvature*-change surfaces. Rather than directly addressing the *Curvature* of the surface, Siéfert et al. introduced a novel material called Baromorph [402] to control the local stretch/shrinkage strain³ of elastomer plates, thereby achieving a target shape through

3. Strains indicates the relative deformation. E.g., a string with its original length as L stretching to the length of $L + \Delta L$ or shrinking to the length of $L - \Delta L$ has a strain ϵ as $\frac{\Delta L}{L}$ or $-\frac{\Delta L}{L}$ respectively.



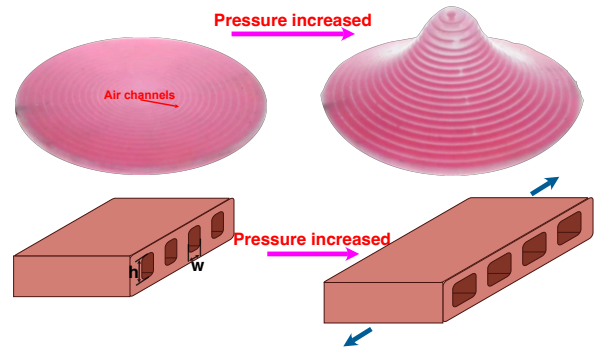
(a) An elastomer membrane with periphery fixed over an air chamber inflates/deflates to a convex/concave dome shape [157].



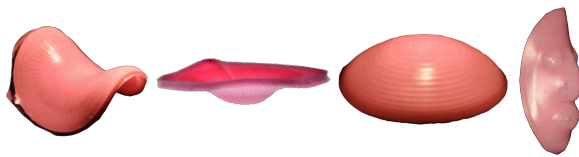
(b) A dielectric elastomer membrane with periphery fixed bulge a convex dome shape when increasing voltage applied on it [113].



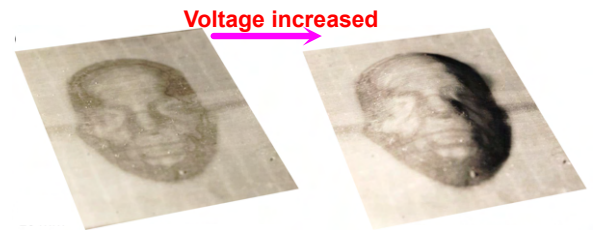
(c) Two orthogonally placed pneumatically extendable elastomer sewn in fabric layers form a saddle shape when two layers inflated together [530].



(d) A Baromorph plate morphs into a cone shape when inflated (Top) with the illustration of its air channels' inflation (Bottom) [402].



(e) Different types of curved surfaces morph form a Baromorph plate [402]. From left to right are a saddle surface (inflated), a concave dome surface (deflated), a convex dome shape (inflated), and a human face shape mask with complex curvature distribution (inflated).



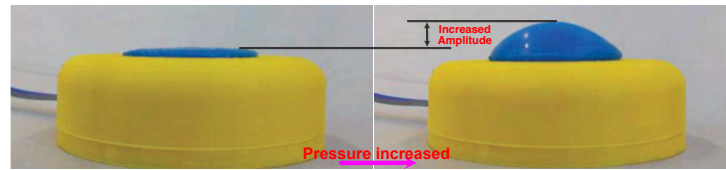
(f) A dielectric elastomer plate morphes in to a human face shape mask when high voltage applied on it [148].

Figure 2.6 – Curvature changing UIs other than cylindrical shapes.

inflation/deflation. In Figure 2.6(d) top, one prototype from [402] demonstrates the transformation into a cone shape from an elastomer plate when air channels embedded in it are pressurized. The height of the air channels in this elastomer plate is designed to be at least twice the width of the channels (denoted as h and w in Figure 2.6(d) bottom). This design choice promotes the in-plane expansion of the channels rather than increasing thickness, as expanding in the in-plane direction is easier. The in-plane expansion of all channels causes the plate to bulge in the center, with the thick external elastomer wall limiting the entire plate’s radial expansion. Siéfert et al.’s strategy for achieving any desired shape involves controlling the local elastomer stretch strain through the density of air channels—higher channel density resulting in larger stretch strain.

In the example of cone morphing, the central part of the cone exhibits a larger slope than the border part, indicating a larger strain in the center compared to the border. Correspondingly, the air channels’ density in the center is larger than in the border, as illustrated in Figure 2.6(d) top. This innovative technology makes it possible to create surfaces with different *Curvature* (Figure 2.6(e)), such as a convex dome surface with positive Gaussian *Curvature*, a concave dome surface with negative Gaussian *Curvature*, and a saddle surface with negative Gaussian *Curvature*. Furthermore, more complex shapes, such as a human face-shaped mask (Figure 2.6(e)), with intricate *Curvature* distribution over the surface, can also be realized using this technology. Similar to Baromorph [402], Hajiesmaili et al. [148] employed a dielectric elastomer membrane, rather than elastomer, to create surfaces with different *Curvature*. The dielectric elastomer membrane expands radially when a voltage is applied. They incorporated 3D-printed plastic nets to limit its expansion under the plastic nets, similar to Baromorph’s walls between air channels. This technology can also generate surfaces with complex *Curvature* distribution (Figure 2.6(f)) by designing the density and shape of the plastic net—higher density results in smaller stretch strain. However, the use of high voltage (≈ 2.5 kV) to actuate the dielectric elastomer membrane may pose safety concerns for HCI applications.

SCIs based on bilayer structures are now widely developed (e.g., [509, 345, 523, 524, 225, 295, 476]). They not only enable UIs to bend for *Curvature* changes, but some features like *Zero-crossing* (e.g., [509]) are also based on them, and these will be further discussed in the following sections. Beyond the aforementioned soft materials, some rigid materials outside our scope, such as thermoplastics that shrink under heat, can also develop bilayer structures for shape change, incorporating layers with different shrinkage strains. These materials are commonly used in technologies like 4D printing (e.g., [473,



(a) An elastomer button can be inflated from flat to convex dome shape with increasing *Amplitude* [132].



(b) An uncovered matrix of actuated pins (Left) can be covered with a piece of fabric (Right) to transform the *Length* change of pins into *Amplitude* change of the fabric surface.

Figure 2.7 – UIs with changing *Amplitude*.

506]). To achieve more complex surface shapes, particularly those with intricate *Curvature* distribution, new materials such as Baromorph [402] provide a significantly improved solution compared to bilayer structures. However, they have yet to see widespread adoption in HCI applications.

2.1.3 Amplitude

As mentioned in Morphees+ [226], the distinction between *Amplitude* and *Length* features are nuanced. The *Length* feature accentuates the extension of an individual object without affecting the neighboring area on a surface. For instance, a radio antenna can adjust the height to enhance signal reception. This feature aptly characterizes height variations in each pin within an actuated matrix of pin displays [246, 297, 244, 108, 245]. In contrast, *Amplitude* underscores the overall shape deformation of a surface. For example, a flat elastomer button [132] can transition from a flat to a convex shape (Figure 2.7(a)). In such cases, the *Amplitude* change effectively describes the surface shape alteration, quantified by the height change of the central point (the highest point post-deformation). Simultaneously, neighboring points around the central point undergo height changes, collectively forming a continuous surface shape. This perspective illustrates that flat surfaces transforming into cylindrical surfaces, as depicted in Figure 2.5(h), contribute to an increase in *Amplitude*. Similarly, the transformation of flat surfaces

into convex or concave dome shapes results in a corresponding increase or decrease in *Amplitude*(Figure 2.6(a)). Actuated matrices of pin displays commonly consist of a few *Length*-controlling units. When a continuous surface, such as a piece of fabric, covers these pins in Relief [245], it transforms discrete *Length* changes into a continuous surface with associated *Amplitude* changes (Figure 2.7(b)).

2.1.4 Porosity

The *Porosity* feature quantifies the percentage of hole surface on a surface [376] and exhibits significant overlap [226] with the *Permeability* feature in Rasmussen et al.’s taxonomy [363]. UIs showcasing dynamic *Porosity* changes are infrequently explored in research due to the non-homeomorphic⁴ nature of such transformations [376]. A noteworthy early instance of a UI incorporating *Porosity* modulation is illustrated by Shutters (Figure 2.8(a)) [72]. Each fabric louver can independently bend to augment the *Porosity*, enabling increased daylight exposure when the SMA wire, positioned behind a louver, heats, causing it to contract and curve. A similar approach was applied in the development of a shape-changing garment (Figure 2.8(b)) designed to enhance ventilation post-exercise [475]. This garment utilized curvature-controlling technology with Nato Cells-fabric composite [475]. Both works [72, 475] share the common goal of curving the cover of an existing hole to increase *Porosity*. In contrast, Hu and Hoffman [177] leveraged the *Volume* expansion of elastomer air bladders, inflated to compress central holes in a surface, resulting in reduced *Porosity* (Figure 2.8(c)). This structure mimics the pore open/close mechanism observed in certain plant tissues [460]. Additionally, the *Surface*-changing UI of auxetic structures (Figure 2.2(i)) increases *Porosity* as the central hole expands during inflation, thereby enlarging the overall structure’s area. Kim et al. employed this design as a window blind for regulating daylight incidence [227].

2.1.5 Zero-crossing

The *Zero-crossing* feature characterizes a shape’s ability to exhibit wave-like forms and is quantified by the count of *Zero-crossing* points [497]. For example, Figure 2.1

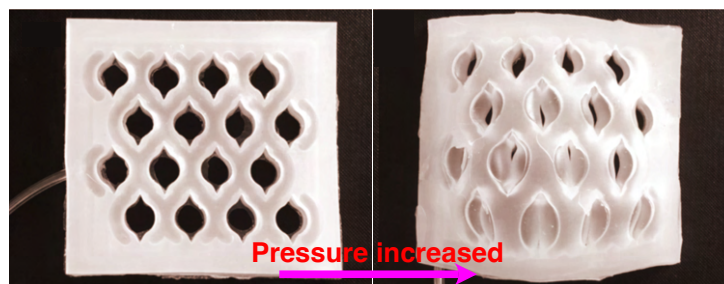
4. Two shapes are homeomorphic means that they are the same from the topological viewpoint, one shape can thus morph into another by stretching and/or shrinking parts of them. For example, the shape of a donut and the shape of a coffee mug are homeomorphic. A donut shape can morph into a coffee mug by shrinking a part of the surface to curve into a dimple and progressively enlarging it, while preserving the donut hole in the mug’s handle (Demonstrated with Figure 8.1.1 in [182]).



(a) SMA wires behind louvers can be heated to curve to open/close them to change the *Porosity* for adjusting daylight incidence [72].



(b) Ventilation flaps at the back of a garment can curve to increase the *Porosity* to enhance ventilation when the humidity increased because the wearer sweats [475].

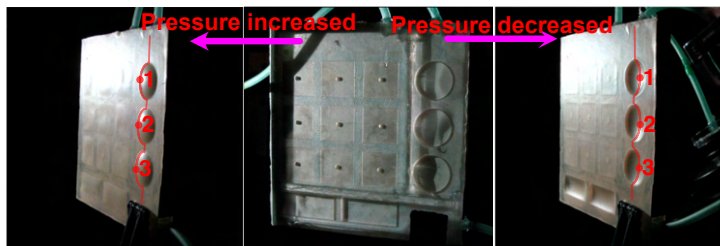


(c) Elastomer bladders's *Volume* expansion under inflation leads to squeezing the central hole thus smaller *Porosity* [177].

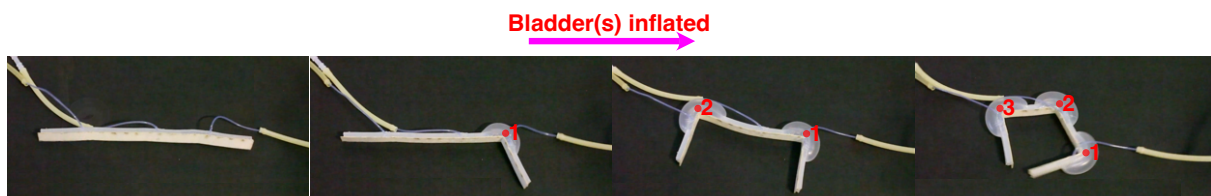
Figure 2.8 – UIs with changing *Porosity*.



(a) Four rigid pieces (white colors in figure) prevent an elastomer tube with sheath's extension underneath them, leading to its curving in 4 parts and increases its *Zero-crossing* points from 0 to 4 [225].



(b) Membrane over a few air chambers can be inflated (deflated) into convex (concave) dome shapes, increases its *Zero-crossing* points from 0 to 3 [157].



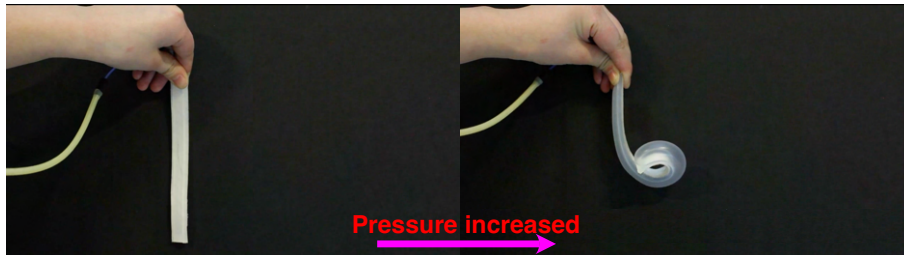
(c) A paper stripe attached with 3 elastomer bladders inflatable to curve it. The bladders are actuated independently with different actuators, which enable the change of the paper stripe's *Zero-crossing* points to multiple values, i.e., 0, 1, 2 and 3. [509].

Figure 2.9 – UIs with changing *Zero-crossing*.

showcases 5 *Zero-crossing* points. Regions of a surface curving to form convex domes or concave domes can generate wave-like patterns, consequently increasing the *Zero-crossing* count. Notably, the *Zero-crossing* feature exhibits significant overlap with the *Curvature* feature [226]. For instance, Kim, Coutrix, and Roudaut systematically collected and categorized 82 distinct shape-changing everyday objects [185] based on their shape-change features, revealing that all 27 instances involving *Zero-crossing* changes also entailed *Curvature* changes. Several UIs that changes *Zero-crossing* (e.g., [509, 225, 318]) were developed using the aforementioned *Curvature*-changing technologies. For instance, Kilic Afsar et al. [225] designed a UI capable of curving in four parts when pressurized (Figure 2.9(a)), leading to an increase in *Zero-crossing* from 0 to 4. Harrison and Hudson [157] enveloped an elastomer membrane over air chambers with pre-defined shapes. By pumping in or vacuuming out air, the membrane assumed a convex/concave dome shape, separated into distinct parts constrained by rigid components of the air chamber, thereby augmenting its *Zero-crossing* (Figure 2.9(b)). However, the majority of *Zero-crossing*-changing UIs exhibit only two states of *Zero-crossing*, transitioning from flat (*Zero-crossing* as 0) to a specified value, e.g., 4 (Figure 2.9(a)). Their *Zero-crossing* values are pre-defined during the fabrication of the UIs. In contrast, UIs with multiple *Zero-crossing* states (more than two) typically require multiple actuators, independently curving a specific UI part. For example, Yao et al. independently inflated three elastomer bladders to bend a paper from 0 *Zero-crossing* points to various values, i.e., 1, 2, and 3 (Figure 2.9(c)).

2.1.6 Closure

The *Closure* feature quantifies the degree of enclosure exhibited by a shape. For instance, a line can be contoured to form a closed circle (Figure 2.10(a)) [509], the faces of a polyhedron can be curved to create a closed polyhedron (Figure 2.10(b)) [318], and flower shapes can unfurl their closed petals to blossom (Figure 2.10(c)) [510]. Instances of structures undergoing *Curvature* alterations to influence *Zero-crossing* can be frequently observed in diverse research [356, 318]. Similar to the *Zero-crossing* feature, *Curvature* control emerges as a fundamental technology in the development of user interfaces that change *Zero-crossing*. This observation aligns with the classification of shape-changing everyday objects [185] in Morphees+ [226]. Specifically, 46 out of 47 objects featuring *Closure* changes also exhibit *Curvature* changes. The sole exception is a drawer (object #127 as enumerated in [185]), where users can slide the drawer box on the drawer slides to open/close it. The actuation of sliding objects often involves rigid motors, a topic



(a) An elastomer and paper bi-layer structure can inflate to be curved, changing its *Closure* from 0% to 100% [509].



(b) A non-stretchable fabric airbags and fabric bi-layer structure in the form of a polyhedron net can inflate to curve, creating a closed polyhedron with *Closure* changing from 0% to 100% [318].



(c) A Nato-cells and fabric bi-layers structure in the form of a flower can bend its petals from curved to flat, leading to the flower's blossoming with decreased *Closure* [510].

Figure 2.10 – UIs with changing *Closure*.

beyond the scope of our study.

2.1.7 Strength

The *Strength* describes the force needed to change the shape of UIs [376], e.g., the force needed to press a dome shape button to flat [416] can vary from 30 N to 40 N with different inner vacuum level (Figure 2.11(b)). One commonly used technology for developing *Strength* changing UIs is jamming [107]. The jamming transition [7] captured the attention of physicists in the 1990s [53]. This transition involves the compression of disconnected media with varying structures, i.e., granular (e.g., ground coffee [8]), fibrous (e.g., nylon fibers [44]) and laminar (e.g., sketch papers [319]), which can initially slide over each other easily. These materials are pressed together and jammed under a pressure gradient, such as a vacuum, causing the system to transition from a soft state to a solid-like rigid state [7], thus increasing its strength (e.g., [8, 107, 269, 406, 405, 319, 277]). Liu and Nagel described jamming transition from a soft state to a solid-like rigid state, in particular with granular jamming media, as a phase change under a pressure gradient just like water phase changes to ice under temperature lowering [252]. Applying jamming in HCI began with the development of an exoskeleton [277] worn around the elbow, designed by Mitsuda et al. It can translate between soft in a non-jammed state and rigid in a jammed state and provide haptic feedback to users when they move their elbows. For example, when wearers play a boxing game in virtual reality (VR), the exoskeleton can give them haptic feedback by becoming rigid to limit their hand movement when their fist kicks a wall in the virtual environment (Figure 2.11(a)). Jamming has then been widely used to construct strength-controllable UIs that provide haptic feedback to users [8, 107, 269, 406, 405] and also to enhance UIs' strength to support heavy loads [319]. For instance, 45 layers of manually bent sketch paper jammed together can withstand a weight of 55 kg [319] (Figure 2.11(c)).

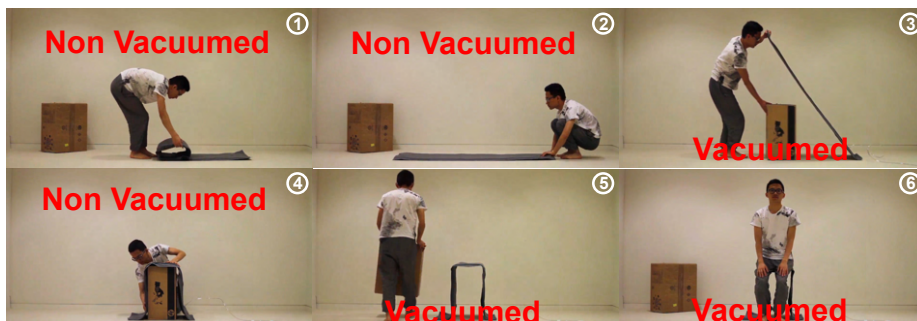
In addition to jamming, designers have also recently started utilizing the phase or glass transition of low melting point metals [385], thermoresponsive hydrogels [276, 217] (Figure 2.12(b)) and thermoplastics (e.g., PLA and ABS used in [64, 520]) (Figure 2.12(a)) to control the strength of UIs. The stiffness of low melting point metals [385] and thermoplastics [64, 520] decreases when heated above their phase or glass transition point (e.g., 105 °C for ABS used in [520]), while the stiffness of thermoresponsive hydrogels increases when heated above their lower critical solution temperature (e.g., 36 °C for the thermoresponsive hydrogel used in [217]). However, using these phase or glass transition



(a) Exoskeleton shown in the white ellipse is Vinyl bags full of foam beads. When jammed by vacuuming the air, its *Strength* will increase, as well as the resistance to wearers' elbow movement [277].

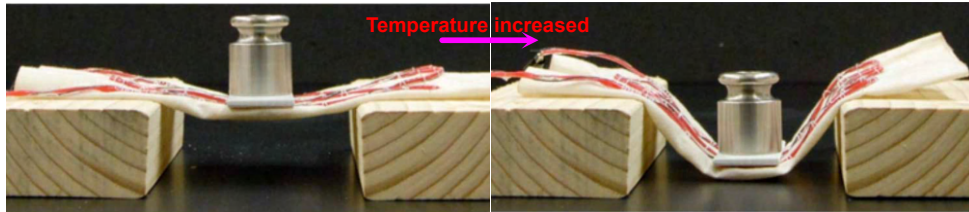


(b) The four pentagonal prisms in this figure are elastomer bladders with ground coffee, whose air inside can be independently vacuumed out (jammed) to increased *Strength* respectively. The cylinder in the white circle (left) is pushed to be a dome shape by the air chamber below it before being jammed and then vacuumed to be jammed (right). The force needed to process it back to flat depends on the vacuum level inside it [416].

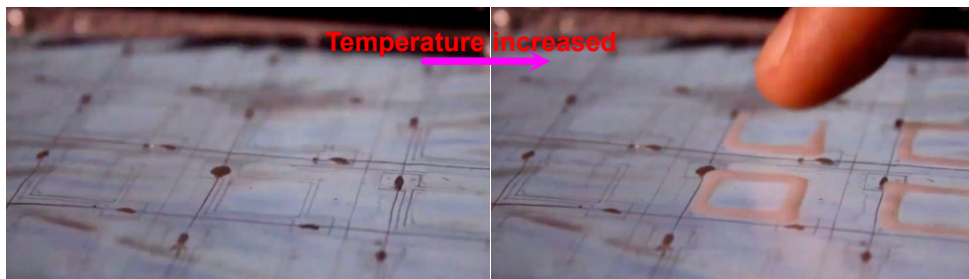


(c) This figure presents 45 layers of 120-gram sketch paper involved in airtight PVC sheets. Before being jammed (sub-figures 1,2, and 4), it has a relatively flexible shape, and users can roll, unroll (sub-figures 1 and 2), and bend it manually (sub-figures 4). After being jammed (sub-figures 3,5 and 6), its *Strength* increases and can keep its shape against gravity (sub-figures 3 and 5) and external load like the users' weight (sub-figure 6) [319].

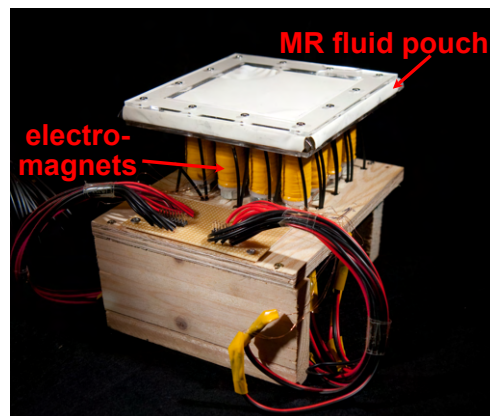
Figure 2.11 – UIs with changing *Strength* using jamming technology.



(a) A metal wire coated with PLA sewn into a piece of fabric. Before heating (Left), the coated PLA is rigid, and it can support a 200 gram mass. After heating (Right), the coated PLA softens and decreases its *Strength* and can no longer support the mass [520].



(b) A layer of hydrogel increases its *Strength* when heated and changes color from transparent (left) to white (right) [205].



(c) A pouch of magneto-rheological (MR) fluids installed over an electro-magnet matrix. When a magnetic field is applied, its *Strength* increases [276].

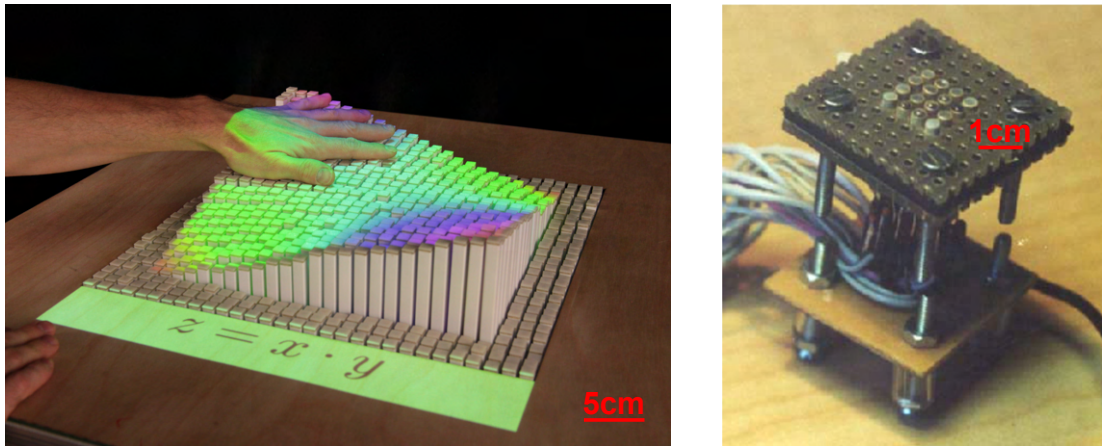
Figure 2.12 – UIs with changing *Strength* using low phase/glass transition temperature materials and magneto-rheological (MR) fluids.

materials typically requires additional heat-insulating structures to prevent harm to the user, especially in wearable devices (e.g., as in [359]) when respective materials' phase or glass transition point is high. Moreover, these materials usually offer only two strength states: rigid when not melted and soft when melted. In contrast, jamming enables more precise strength control by continuously adjusting the vacuum level to tune the strength (e.g., [159]).

Another approach for controlling interface strength is using magneto-rheological (MR) fluids [205, 200] (Figure 2.12(c)). MR fluids consist of magnetizable particles suspended in a carrier oil, such as a mixture of carbonyl iron particles and glycerin [205]. Magnetizable particles can freely move in the carrier oil before applying a magnetic field, while each magnetizable particle becomes a dipole (north and south) and there is a tendency for a chain to be created with neighboring particles when applying a magnetic field [312]. The chains have a mechanical resistance to the fluid flow, thus making it more difficult to move in the carrier oil. For this reason, these fluids exhibit soft behavior (like water) without a magnetic field. At the same time, they become semi-solid (like highly viscous peanut butter) when a magnetic field is applied, and a larger force needs to change their shape. They allow for fine control of the system's strength by adjusting the strength of the magnetic field, resulting in higher strength [200, 433]. Magneto-rheological fluids provide a solution for constructing interfaces with adjustable stiffness and short response times (e.g., < 2 ms [205]). However, the requirement of bulky equipment, particularly large solenoids (e.g., [508]), to generate a strong magnetic field close to the UIs may limit their applications.

2.1.8 Stretchability

The *Stretchability* feature characterizes how much a UI can be stretched or compressed [376]. An essential aspect of employing soft materials, such as elastomers (e.g., [509]), for constructing SCIs is their remarkable *Stretchability*, exemplified by instances where materials can be stretched over 1000% [56]. This exceptional *Stretchability* is pivotal in facilitating substantial shape transformations (e.g., Figure 2.6(e)). In contrast, non-stretchable materials, like sketch paper, exhibit limited shape-change capabilities, primarily confined to curving their corners or edges [170]. The technologies involved in developing *Stretchability*-changing UIs closely align with those associated with enhancing UI *Strength*. For example, utilizing jamming technology [107] results in high *Stretchability* when UIs are in a non-jammed state, as the jamming media within the UIs can move



(a) A matrix of pin actuated by motorized slide potentiometers, with a maximum *Granularity* of 0.62 control points per cm^2 (30×30 pins over 1450 cm^2) [108].

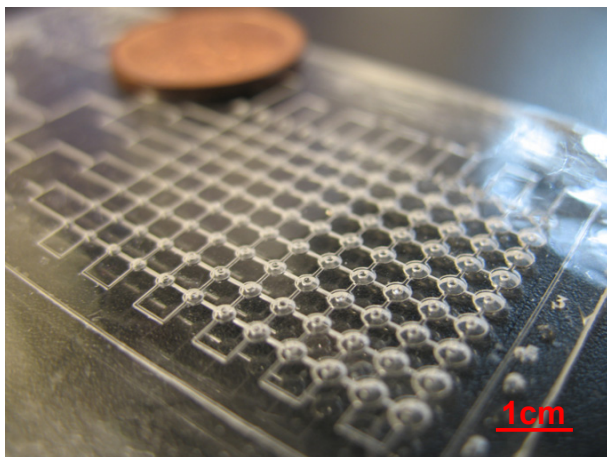
(b) A matrix of pins actuated by thermomechanical actuators, with a maximum *Granularity* of 16 control points per cm^2 (4×4 pins over 1 cm^2) [466].

Figure 2.13 – Matrix of actuated pin displays. Their maximum *Granularity* depends on pins density. Grouping pins and actuating them as one results in lower *Granularity*.

freely during stretching or compression. Conversely, UI *Stretchability* diminishes under jammed conditions due to the friction between jamming media, impeding the stretching or compression of the UI. Similarly, applying a magnetic field to magneto-rheological (MR) fluids [205] decreases UI *Stretchability*. Heating the temperature of thermo-responsive hydrogels [276, 217] above their lower critical solution temperature transitions them to a rigid state, thereby reducing their *Stretchability*. In contrast, heating low-melting-point metals [385] or thermoplastics (e.g., PLA and ABS used in [64, 520]) beyond their phase transition points induces a shift to a softer state, thereby increasing their *Stretchability*.

2.1.9 Granularity

The *Granularity* is defined as the ratio between the number of control points and the area of the object. In Morphees [376] definition, control points refer to points actuated to change an object's shape. For example, each pin in a matrix of actuated pin display is a control point. According to Morphees definition, the change of *Granularity* was only realized with actuated-pin matrix, i.e., grouping pins and actuating them as one results in lower *Granularity*. Later, in Morphees+ [226], the definition of control points is clarified as joints or points capable of shaping an object. For instance, a foldable



(a) A matrix of inflatable PDMS bladders, with a density of 16.6 actuated *Amplitude*-changing units per cm^2 (108 inflatable bladders over 6.5 cm^2) [283].



(b) A matrix of dielectric elastomer membranes, with a density of 3 actuated *Amplitude*-changing units per cm^2 (20 actuated elastomer bladders over 1.54 cm^2) [234].

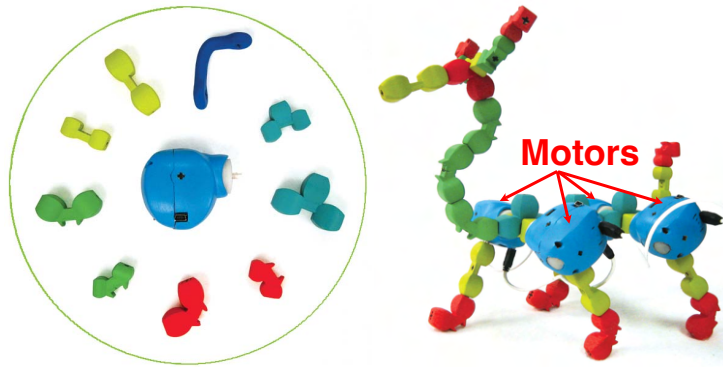


(c) A matrix of inflatable elastomer bladders, with a density of 0.19 actuated *Amplitude*-changing units per cm^2 (16 actuated elastomer bladders over 84 cm^2) [412, 466].

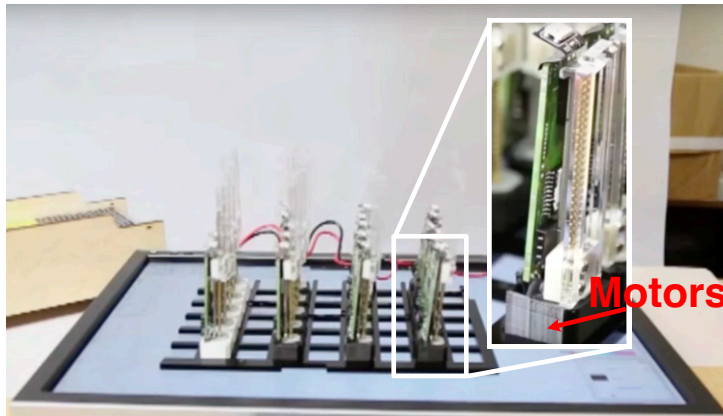
Figure 2.14 – A matrix of *Amplitude*-changing units in soft materials. Their *Granularity* is infinite according to Morphees+ [226] definition, while depends on the density of these actuated *Amplitude*-changing units as Morphees [376] definition.

penknife with a single control point allows its blade to be folded into the handle, even if it is not actuated to change its shape. After clarification, it can also better describe deformable materials like water with which the actuated shape-changing points are hard to determine. According to Morphees+, soft materials such as elastomers and fabric possess infinite control points. For example, when a Baromorph plate in elastomer morphs into a dome surface (Figure 2.13), all points of its surface change their *Curvature*. In this case, the *Granularity* of UIs made of programmable soft materials remain infinite during shape changes.

Similar to matrixes of actuated pin displays (Figure 2.13) with pin independently actuated to change the height, a series of matrixes of *Amplitude*-changing units (Figure 2.14) in soft materials were developed. The density of *Amplitude*-changing units can well fit Morphees' *Granularity* definition of actuated points density. Grouping different *Amplitude*-changing units can lead to *Granularity* decreasing. According to Morphees+ definition, their *Granularity* should be infinit. When using them to provide users with haptic feedback, their *Granularity* must meet the tactile spatial resolution requirements specific to each site [238]. More specifically, Lederman [238] conducted tactile spatial resolution measurements using a 2-point threshold test, revealing an average resolution of approximately 45 mm on forearms and 3.5 mm on fingertip pads. Subsequent researchers built upon Lederman's work to develop matrixes of *Amplitude*-changing units in soft materials, tailoring their designs to meet the tactile spatial resolution requirements of different body sites. For example, Moraes, Sun, and Simmons [283] created a Braille display (Figure 2.14(a)) featuring a matrix of molded micro elastomer (PDMS) inflatable bladders. The *Granularity* of this display is 16.6 actuated *Amplitude*-changing units per cm^2 (108 actuated elastomer bladders over 6.5 cm^2), with a distance of approximately 2.5 mm between each bladder—smaller than the measured fingertip resolution of 3.5 mm [238]. Similarly, Koo et al. [234] developed a Braille display using a matrix of dielectric elastomer membranes (Figure 2.14(b)). When high voltage is applied to it, each membrane can bulge out with *Amplitude* increased. The *Granularity* of this display is 13 actuated *Amplitude*-changing units per cm^2 (20 actuated elastomer bladders over 1.54 cm^2), with a distance of approximately 3 mm between each bladder—again, smaller than the measured fingertip resolution of 3.5 mm [238]. In another application, Sonar et al. [413] devised a matrix of elastomer inflatable bladders (Figure 2.14(c)) to be worn around the forearm, providing haptic feedback by pressurizing bladders to inflate them. The *Granularity* in [413] is 0.19 actuated *Amplitude*-changing units per cm^2 (16 actuated elastomer bladders over



(a) Topobo: a toolkit with motorized modular modules for constructing shape-changing toys [360].



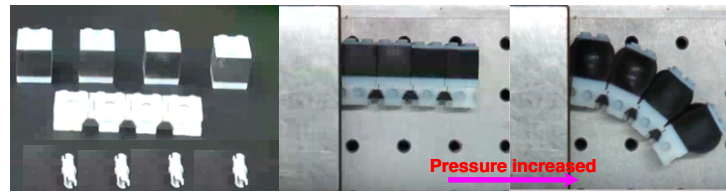
(b) ShapeClip: a toolkit with motorized height changing units for constructing SCIs, e.g., a matrix of actuated pin display as shown in this Figure [155].

Figure 2.15 – Modular SCIs actuated with motors

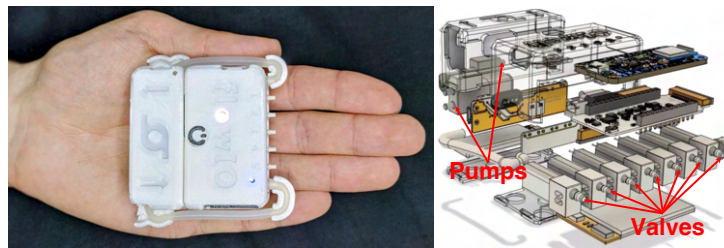
84 cm²), with a distance of approximately 20 mm between each actuator—smaller than the measured forearm resolution of 45 mm [238].

2.1.10 Modularity

The *Modularity* feature refers to the ability to split an object into several parts that can be combined while maintaining its original functionality. *Modular* SCIs, actuated with motors, typically involve multiple motors, with one motor assigned to each shape-changing part. For instance, Raffle, Parkes, and Ishii developed Topobo [360] to enable users, especially children, to connect different modules and build their shape-changing toys. In Topobo, each shape-changing part requires an independent motor for actuation



(a) Soft LEGO: inflatable modules (Left) can be connected in series for sharing one actuator and realizing the desired shape-change, e.g., bending (Right) [243].



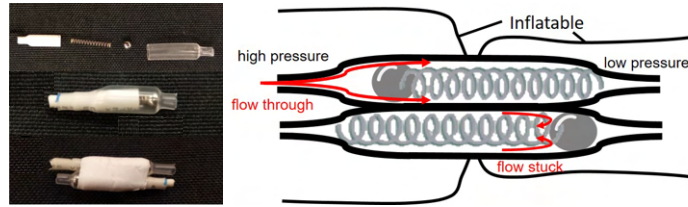
(b) FlowIO: A toolkit composed of 7 solenoid valves and two pumps used for connecting and actuating different pneumatic shape-changing modules [401].

Figure 2.16 – Modular pneumatic SCIs and a toolkit of pumps and solenoid valves used for connecting multiple pneumatic shape-changing modules.

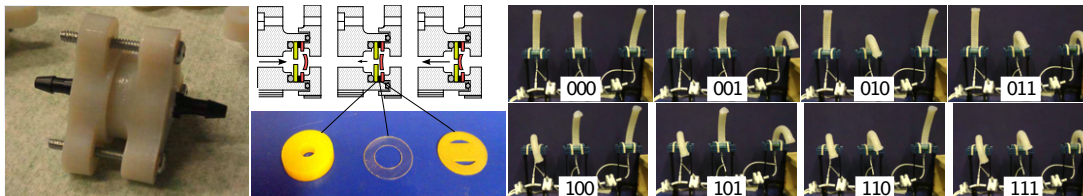
(Figure 2.15(a)). Hardy et al. developed ShapeClip [155], a toolkit for prototyping SCIs with independent shape-change modules. It has high *Modularity*, where each module requires a linear motor for shape-change actuation, increasing bulkiness.

In contrast to motors actuating *Modular* shape-change UIs, pneumatically actuated *Modular* SCIs allow connecting different modules in series to share pumps for inflating and/or vacuuming out air [243, 78, 372]. For instance, Lee et al. developed Soft LEGO [243], enabling users to connect a series of inflatable modules and actuate them with a single pump to achieve the desired shape-change (Figure 2.16(a)). In this example, different modules were inflated with the same pressure and actuated simultaneously. To enable pneumatic actuation of *Modular* SCIs while independently controlling each module and sharing pumps, valves are needed to control the connection of modules to pumps and actuation. For example, Shtarbanov developed FlowIO [401] (Figure 2.16(b)), a toolkit for pneumatically actuating up to five modules independently. It utilizes 7 solenoid valves: 1 connected to a pump for air intake, 1 connected to a pump for air vacuuming, and 5 for independently controlling the pneumatic actuation of modules.

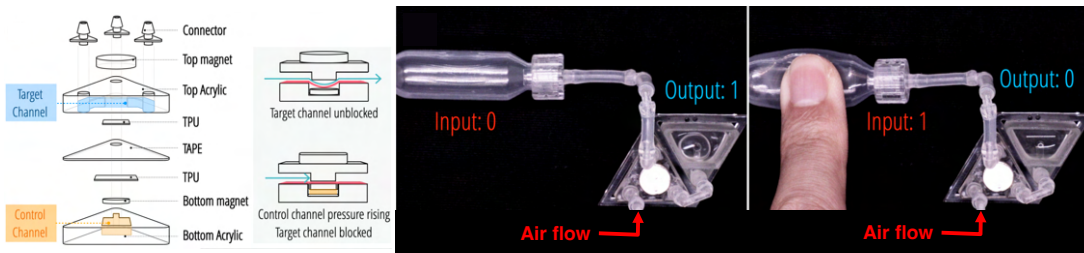
To address certain drawbacks associated with the use of traditional solenoid valves, such as high cost, the presence of numerous rigid electromagnetic components limiting



(a) A check valve without electromagnetic components (Left) unrestricted airflow in one direction(e.g., from left to right in the top valve as shown in the Right Figure), while restricting airflow in the reverse direction (e.g., from left to right in the bottom valve as shown in Right Figure) [59].

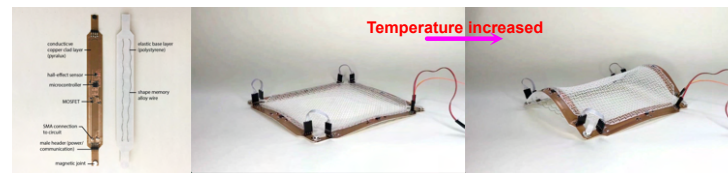


(b) A check valve without electromagnetic components (Left) unrestricted airflow in one direction(e.g., from left to right as shown in Top Middle Figure), while restricting airflow in the reverse direction at low flow rates (e.g., as shown in Top Middle Figure, high rates airflow from right to left cause the block of the valve.) Connecting two such valves in opposite directions forms a band-pass valve, permitting low flow in both directions but shutting off at high flow. Using multiple such band-pass valves allows using a single actuator to inflate serially connected pneumatic modules (Right) separately: 1 means inflated, 0 means non-inflated) [301].

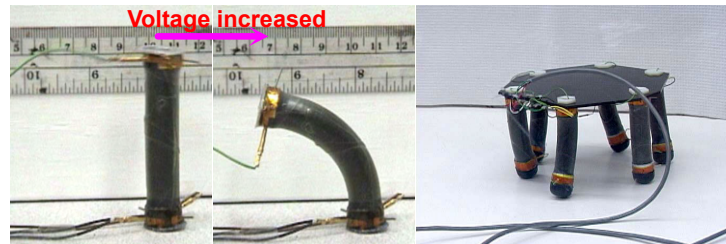


(c) Exploded views of an electronic-free switch component and the working mechanism (Left): when the control channel is not inflated, airflow can freely pass; when the control channel is inflated, airflow is blocked. A NOT logic implemented with such switch component (Right): Airflow is coming from the left bottom. When the control channel is not inflated (status default, input as 0), airflow freely passes to the right side (output as 1); when the control channel is inflated (pressure increased as being pressed by the user, input as 1), airflow is blocked to the right side(output as 0) [257].

Figure 2.17 – Electronic-free components used for connecting multiple pneumatic shape-changing modules.



(a) Modules actuated by SMA wires (Left) connected (Right) with conductive wires sharing the current for heating (actuation) [428].



(b) Modules actuated by dielectric elastomers (Left) connected (Right) with conductive wires sharing the voltage (for actuation) [334].

Figure 2.18 – Modular SCIs actuated by SMA wires and dielectric elastomers.

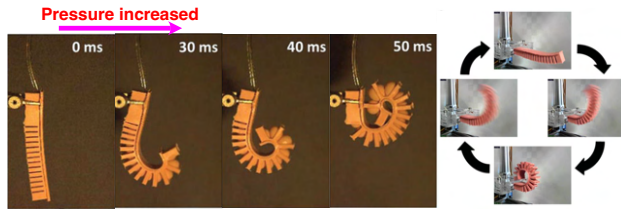
their application in harsh environments, and the need for regular maintenance [12], researchers have begun developing valves for use in pneumatically actuated UIs that do not incorporate electromagnetic components (e.g., [59, 257, 301, 375]). For instance, Napp et al. [301] devised a check valve allowing unrestricted air passage in one direction, while restricting airflow in the reverse direction at low flow rates. This restriction prevents rapid inverse airflow with high pressure from deforming an elastomer valve flap and sealing the flow channel (Figure 2.17(b) top middle). Two such valves, connected in opposite directions, form a band-pass valve, permitting low flow in both directions but shutting off at high flows. They also demonstrated the use of multiple check valves and band-pass valves to enable the arbitrary inflation of specific serially connected pneumatically bending structures from a single pressure source [393] (Figure 2.17(b) right). Chen et al. [59] developed similar systems for controlling serially connected pneumatically actuated shape-change UIs, utilizing a check valve with a ball-spring structure instead of an elastomer valve flap to establish a unique airflow direction (Figure 2.17(a)).

In addition to opening specific valves under predefined actuating pressure from shared pumps [301, 59], recent research has facilitated the electronic-free connection of different pneumatically actuated modules with more complex logic relations [257, 383]. For instance, Lu et al. [257] created an electronic-free kit to emulate the functions of standard

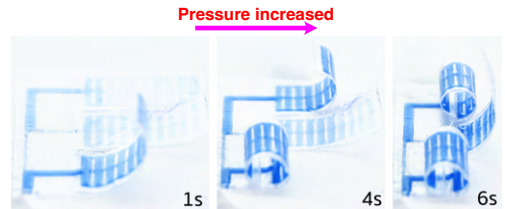
electronic components such as switches, diodes, resistors, and capacitors. They combined these components to realize various logic relations among interconnected modules, such as AND, NOR, NAND, AND, and OR. Figure 2.17(c) illustrates an example of the NOT logic they implemented with a switch component. When the control channel is not inflated (Status "0"), air can pass through the switch, resulting in high pressure in the switch's output (Status "1"). Conversely, when the control channel is inflated (Status "1"), the top membrane of the control channel blocks airflow through the switch, leading to low pressure in the switch's output (Status "0"). Similar technologies have been developed and applied in numerous micro-scale microfluidic systems for connecting different modules with designed logic relations (e.g., [92, 285, 485, 84]).

SMA wires have been employed to develop SCIs, particularly for constructing *Modular* systems. Given that most SMA wire-actuated UIs utilize joule heating to alter the wire's temperature and induce shape changes, connecting different modules with SMA wires through conductive wires to share the current for actuation proves to be a convenient approach. For instance, Tahouni, Qamar, and Mueller [428] introduced a toolkit for prototyping SCIs, with the basic module consisting of a bi-layer SMA wire structure capable of bending towards the SMA wire side when heated. They affixed magnets to the two extremities of each module to facilitate assembly with other modules, connecting them with conductive wires to share the current for actuation and shape-change control (Figure 2.18(a)). Similar approaches were also explored in [327, 511]. Dielectric elastomers, which change shape when a voltage is applied [113], offer another avenue for SCIs, where connecting different modules using conductive wires to share the voltage for actuation is practical. For example, Pei et al. [334] connected six bending modules made of dielectric elastomers to construct a six-legged robot (Figure 2.18(b)).

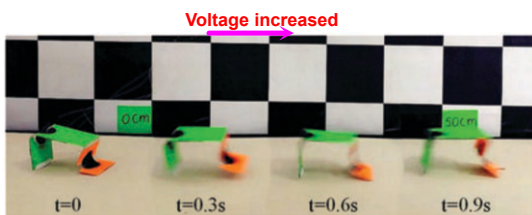
On the other hand, shape-changing technologies employing hydration and swelling materials, such as hydrogel [371], which rely on humidity changes for actuation, are less convenient for *Modular* connections. Typically requiring immersion in water [203] or activation by environmental humidity changes, like rain [259], these methods are not as practical as wire-connected SMA-actuated UIs [428] or tube-connected pneumatically actuated UIs [257] for interconnecting different humidity-driven UIs to share actuation or control.



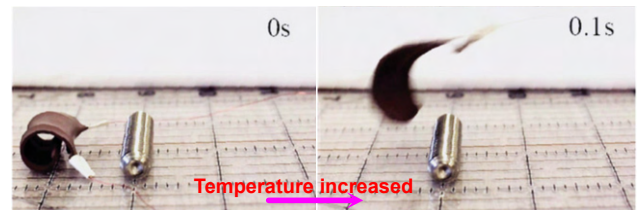
(a) A pneumatic elastomer bending structure fully bending in 50 ms when pressurized at 3.45 bar (Left). A full actuation circle (Right) increases from 1 Hz to 5 Hz with the actuation pressure rising from 0.55 bar to 1.17 bar [286].



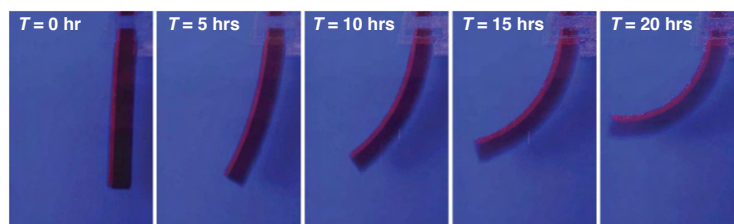
(b) Three hydraulic bending bladders connected with channels in different sizes: the bladder (Middle) connected with the longest and narrowest channel deformed last and the bladder (Front) connected with the shortest and widest channel deformed first [256].



(c) A dielectric elastomers actuated robot can run at 50 cm s^{-1} when applied a voltage of 5.5 kV and 30 cm s^{-1} when applied a voltage of 4.5 kV [525].



(d) A SMA wire actuated structure can bend from a quasi-circular shape to a quasi-linear shape within 0.1 s when heated, while needing more than 3 s to cool down. The current intensity can adjust the heating speed, and the cooling speed is challenging to address [180].



(e) A hydrogel actuated structure requires 20 hours immersed in water to bend 90° and its actuation speed is also challenging to address [521].

Figure 2.19 – UIs with different shape-changing *Speed*.

2.1.11 Speed

Shape-change *Speed* is heavily dependent on the chosen actuation method, such as pneumatically inflating/deflating elastomer chambers (e.g., [509]), applying voltage to dielectric elastomers (e.g., [113]), heating shape-memory alloy (SMA) wires (e.g., [150]), increasing humidity in hydration-swelling materials (e.g., [510]), heating materials with low phase or glass transition points (e.g., [385]), and enhancing the strength of the applied magnetic field on magneto-rheological (MR) fluids (e.g., [205]).

Pneumatic actuation *Speed* is generally high and controllable through the applied air pressure and pump flow rate [401]. Controlled inflation and deflation of air chambers achieve actuation with adjustable *Speed* by regulating airflow. For instance, a pneumatic elastomer bending structure measuring approximately 90 mm × 30 mm × 10 mm can rapidly transition from linear to quasi-circular in 50 ms when pressurized at 3.45 bar [286] (Figure 2.19(a)) with a maximum flow rate of 11 L min⁻¹ from an air compressor. The frequency of a complete actuation cycle (Figure 2.19(a)) increases from 1 Hz to 5 Hz with the actuation pressure rising from 0.55 bar to 1.17 bar. Channel dimensions carrying air/liquid also influence *Speed*, with longer or narrower channels offering more resistance and thus lower *Speed* [257, 256]. Figure 2.19(b) [256] illustrates that when pressurized with dyed blue water, three bladders curved sequentially based on channel resistance, i.e., the bladder connected by the longest and narrowest channel deformed last.

Dielectric elastomers' actuation *Speed* is generally high and adjustable by voltage supply [525]. For example, a bi-layer dielectric elastomer structure measuring roughly 50 mm × 50 mm × 0.5 mm, serving as one leg of a soft robot (orange leg in Figure 2.19(c)), can bend from 80° to 110° within 0.9 s under a 5.5 kV power supply. Coordinating with another bi-layer dielectric elastomer structure (green leg in Figure 2.19(c)), it enables the robot to run at speeds exceeding 50 cm s⁻¹. Adjusting the power supply allows for corresponding changes in actuation *Speed*, with a lower voltage of 4.5 kV resulting in reduced bending *Speed* and a respective lower robot moving speed of 30 cm s⁻¹ [525].

The *Speed* of heating SMA wires to trigger shape-change is also rapid. For instance, heating a \varnothing 0.3 mm SMA wire with a total length of 123 mm embedded in an elastomer sheet measuring roughly 55 mm × 22 mm × 1.5 mm with a 4 A current can bend it from a quasi-circular shape to a quasi-linear shape within 0.1 s (Figure 2.19(d)). However, the cooling time for the SMA wire is more than 3 s [180]. Most SMA actuators use joule heating to change temperature with actuation time controllable by adjusting the current intensity passing through the SMA wire [465]. However, reducing a hot SMA wire's cooling

time often involves other cooling methods [190], potentially complicating UI development or limiting their application scenarios, e.g., immersing SMA wire in oil [330].

In comparison to the three aforementioned actuation methods, increasing the humidity of hydration and swelling materials (e.g., [510]) for shape-change is relatively slow due to the intrinsically low *Speed* of the water diffusion process [521, 154]. For example, a bi-layer hydrogel structure measuring approximately $40\text{ mm} \times 25\text{ mm} \times 15\text{ mm}$ requires 20 hours to immerse in water and bend 90° (Figure 2.19(e)) at room temperature ($\approx 23^\circ\text{C}$) [521]. A very thin bi-layer Nato Cells structure (0.0036 mm thick of Nato cells coated on 0.2 mm thick of latex film) [510] needs more than 10s to bend approximately 70° . Increasing water temperature can enhance water diffusion *Speed* [449, 476], but diffusion *Speed* is proportional to the square of the UI's size made from these materials [521], meaning that Shape-Change *Speed* decreases quadratically with increasing UI size [521].

As for *Strength* and *Stretchability*-changing UIs, pneumatic jamming technologies [107] generally exhibit high *Speed*. For instance, an elastomer bladder measuring approximately $47\text{ mm} \times 27\text{ mm} \times 8\text{ mm}$, filled with coffee particles constituting about half of its volume, can achieve full jamming in 1s using a small pump (0.9 W). The *Speed* can be further enhanced by increasing the volumetric flow rate (i.e., the power) of the pump vacuuming out air [107]. Another method providing a high *Speed* for *Strength* and *Stretchability* change involves applying a magnetic field to MR fluids, typically taking around a few milliseconds (e.g., [205]), as it requires minimal time for magnetizable particles to suspend in their carrier oil [126]. However, using bulky solenoids (e.g., [508]) to generate a strong magnetic field close to the UIs may restrict their applications.

In contrast, the *Speed* of changing UIs' *Strength* and *Stretchability* by heating materials with low phase or glass transition points (e.g., [217]) is generally slow. The same applies to waiting for melted materials to cool down and return to their original *Strength* and *Stretchability* status. For instance, a small thermoresponsive hydrogel (2.5 mL) requires more than 1 min to transition from soft to rigid when heated at 2.5 W and more than 5 min to return to a soft state after heating cessation and cooling down at room temperature ($\approx 22^\circ\text{C}$) [217]. Most UIs for changing *Strength* and/or *Stretchability* employ joule heating, embedding metal wires within them [217, 276, 64, 520]. The heating *Speed* can be increased by elevating the current intensity passing through the wires, although methods to accelerate UIs' cooling *Speed* might impose significant restrictions on their application scenarios or introduce development complexity, such as immersing them in water [179].

2.2 Relations among different shape-changing features

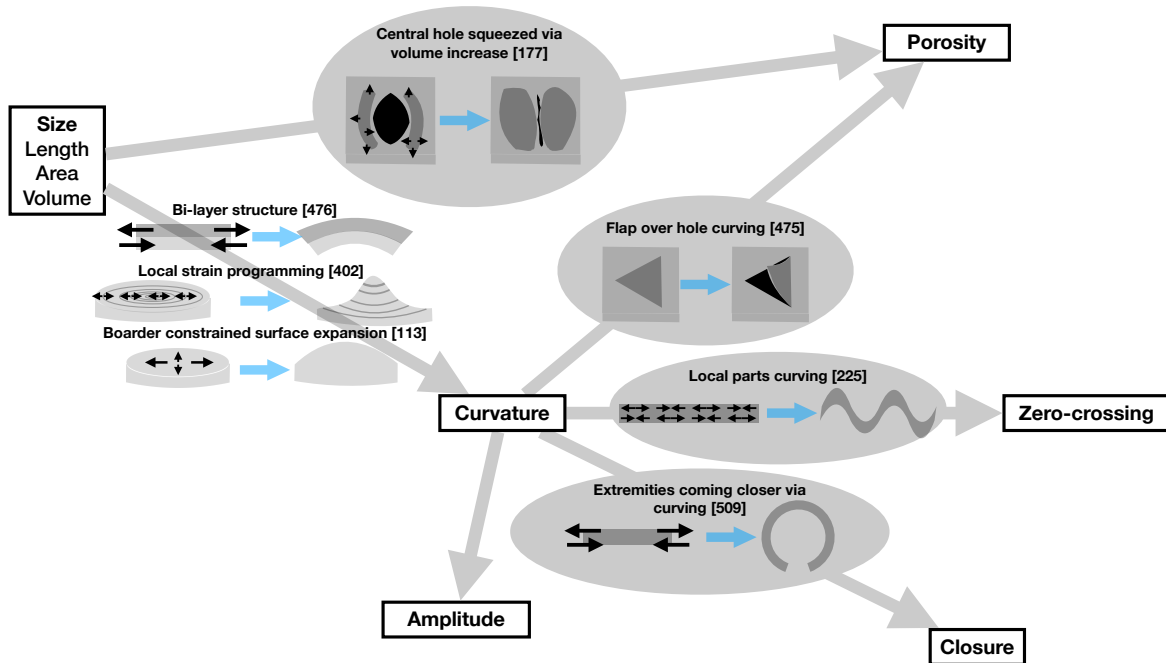


Figure 2.20 – Figure illustrating relations between different primitive geometric shape-changing features realized with programmable soft materials. Figures in blue arrows connecting different shape-changing features illustrate how one shape-changing feature can be realized with another shape-change. In the case of developing shape-changing UIs with programmable soft materials, the *Granularity* is infinite according to Morphees+ definition [226]. Changing *Modularity*, *Strength* and *Stretchability* usually need to incorporate rigid materials to realize it, they are thus not presented in this figure and will be further discussed in Chapter 4.

Building upon extensive research into soft SCIs and material, it becomes evident that *Size* and *Curvature* play pivotal roles in the development of UIs with other shape-changing features, such as *Amplitude*, *Porosity*, *Zero-crossing* and *Closure*. The relationships among various technologies for creating UIs with different shape-changing features using soft materials like elastomers [509] and fabrics [531] are briefly illustrated in Figure 2.20. The *Size* features include three subtypes: *Length* [300], *Area* [113] and *Volume* [260]. The *Size* changing technologies can be the base for constructing *Curvature* changing SCIs via three methods:

1. Building bi-layer structures with different *Size* change of each layer can enable the

Curvature-change [476].

2. Programming local strain via actuation, e.g., air channels' width increase of a Baromorph plate when pressurized, can enable *Curvature-change* [402].
3. Fixing the border of a surface with expanding *Area* will lead to the surface's bulge to a convex dome, thus enabling *Curvature-change* [113].

With these technologies [476, 402, 113] changing *Curvature* will at the same time lead to the *Amplitude* change.

Meanwhile, *Size-changing* technology can also be used to build *Porosity-changing* UIs. For example, *Volume* increase of elastomer bladders around a hole will squeeze the hole and reduce the *Porosity* [177].

Based on *Curvature* changing technologies, we can change *Porosity*, *Zero-crossing* and *Closure*. For instance:

1. A flap curving over a hole will lead to *Porosity* increasing [475].
2. A straight strip with local parts curving will lead to *Zero-crossing* increasing [225].
3. A straight strip curve with its extremities coming closer will lead to *Closure* increasing [509].

Apart from the 6 primitive geometric shape-changing features of *Size*, *Curvature*, *Amplitude*, *Porosity*, *Zero-crossing* and *Closure*, other shape-changing features including *Stretchability*, *Strength*, *Speed*, *Modularity* and *Granularity* orthogonal to them. For instance, *Stretchability* enables these features' change, and the low *Strength* is the trade-off of high *Stretchability* [358]. *Speed* can express how rapidly all these features change and the range of their shape-change rapidity. *Modularity* indicates the connection between different modules. Meanwhile, modules with different shape-changing features can be connected together. As for the *Granularity* feature, it remains infinite according to Morphees+ definition [226] as our study focuses on UIs developed with programmable soft materials in this thesis.

Noteworthy is the incorporation of rigid materials in certain technologies, exemplified by glass beads utilized as jamming media for changing *Strength*. A detailed discussion of these technologies is deferred to Section 4.4 in Chapter 4 where we present our technologies *SoftMorphees* of using only soft materials to realize different shape-changing features also related challenges.

Given our current state of the art, we recognize that *Curvature-changing* UIs play a pivotal role in constructing various types of SCIs (Figure 2.20). Recently, *Curvature-*

changing UIs have also attracted a lot of HCI researchers' interests (e.g., [157, 132, 423, 509, 133]). Moreover, *Curvature* serves as fundamental information for encoding any 3D shapes [378]. Meanwhile, objects with curved surfaces play integral roles in our daily lives, constantly surrounding and engaging our senses (e.g., [492, 224, 169, 362, 491, 494, 88, 5, 309, 82, 233, 467]). Hence, in this thesis, our focus will predominantly be on the *Curvature* features of UIs, with Chapter 3 delving into users' *Curvature* perception ability, particularly under different softness conditions, Chapter 5 developing UIs capable of changing both *Curvature* and *Strength*, and Chapter 6 creating a shape-morphing watch that provides users with haptic feedback by altering *Curvature*.

PART I

User behavior

HUMAN CAPABILITIES

3.1 Introduction

In the Introduction (Chapter 1), we discussed the user behavior challenges in shape-changing interfaces (SCIs) research and we identified the research problem concerning users' ability to perceive shapes of SCIs. Unlike traditional planar rigid UIs, such as planar LCD screens, SCIs can exhibit diverse shapes [363, 376, 226]. When users interact with and explore SCIs through contact and touch, their shapes offer important information, enhancing the interaction experience in multiple aspects, including improved affordance [442], haptic feedback [411], ergonomics [25] and enhanced immersion in applications such as virtual reality (VR) and augmented reality (AR) [435]. Understanding how well users can perceive the shapes of SCIs is thus a pivotal question to address before delving deeper into the development of SCIs with dynamic shape-changing capabilities using programmable soft materials—another research problem discussed in the Introduction (Chapter 1).

Our surroundings are filled with objects boasting curved surfaces [169, 362]. Everyday items also come in various degrees of softness [228], inviting intentional or unintentional tactile exploration of their shapes. Over the past decades in HCI research, a growing focus has been on curved and soft materials [358]. The perception of soft surface curvature becomes crucial in scenarios like VR when users touch surrounding objects for haptic feedback [165], during surgical VR training with a soft organ proxy conveying feedback through local curvature [290], when receiving curvature-based shape notifications from a soft mobile device [509], or when soft physical buttons transition between modes based on their curvature [157]. In these instances, user experience is influenced by the perceived curvature of the soft surface [10, 240].

As outlined in our state-of-the-art review in Chapter 2, emerging technologies enable the actuation of UI curvature (Section 2.1.2) and softness¹ (Section 2.1.7). Ensuring the

1. The *Softness* is related to *Strength* feature in Morphees [376] and Morphees+ [226] taxonomies.

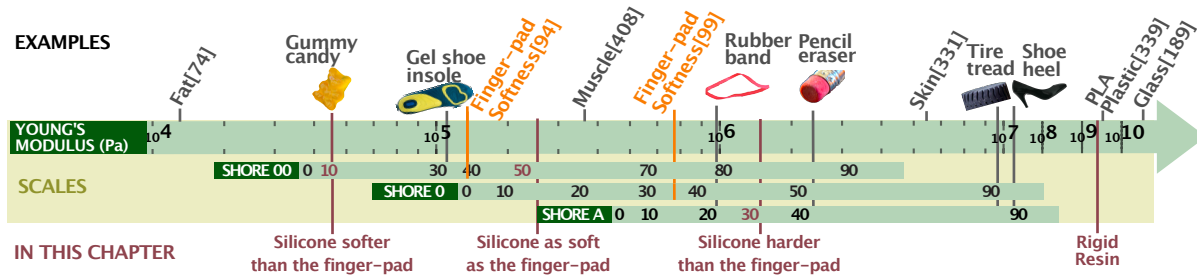


Figure 3.1 – (Top) Example materials and objects and (center) their approximate Young’s modulus [438] and respective Shore hardness [437]. (Bottom) Types of silicone and resin used in our experiment: Shore 00-10, Shore 00-50, Shore A-30, and Rigid.

effectiveness of such haptic feedback requires insight into users’ ability to perceive the curvature of a soft UI. Addressing this issue is of paramount importance and timeliness, as it represents a bottleneck in guaranteeing the efficiency of future interaction techniques [358, 10].

Based on prior work [74, 331, 189, 339, 408, 99, 94], we defined as *soft*² the materials that have a Young’s modulus³ in the order of 10^4 – 10^6 Pa. Figure 3.1 shows that human fat, muscle, skin and silicone elastomer⁴ are soft. Prior work studied the curvature perception of *rigid* objects [138, 351, 171, 456, 459, 457, 255, 136, 137, 470, 346]. However, we do not know yet how well users perceive the curvature of *soft* objects, and whether the softness impacts the perception of the curvature. Yet, softness may have an impact on curvature perception, because both hard and curvy objects lead to a high response frequency of the same type of cutaneous mechanoreceptive afferent neurons [75, 1].

To design efficient haptic feedback with curvy and soft UIs, HCI designers particularly

Higher *Softness* usually corresponds to lower *Strength*.

2. Different measures can be used for describing the *Softness* level, such as Young’s modulus [438], stiffness [31] and Shore hardness [437]. These measures are calculated differently and can convert among each other [278, 439]. We further discussed differences and relationships among these measures in Section 3.6.5.

3. The Young’s modulus is a measure of the rigidity of materials. It is defined by the ratio between the lengthwise tension or compression on a material and its change of length [438]. The larger the modulus, the more rigid the material.

4. Durometer (Shore) hardness test is a commonly used hardness test for elastomeric materials. Durometer measurements assess the material’s resistance to indentation, a higher durometer reading corresponds to a harder material. Different types of durometers have different hardness test ranges. A **Shore 00** durometer is typically used to test the hardness of extremely soft rubber, human and animal tissue; a **Shore 0** durometer is typically used to test the hardness of soft rubber and very soft plastics; a **Shore A** durometer is typically used to test the hardness of harder rubber, e.g., soft vulcanized rubber and natural rubber [437].

need to know users' *precision*, *accuracy* and *speed* when perceiving a change in the curvature of the soft UI. Users' precision is the minimum change in curvature of the soft UI that users can notice (Just Noticeable Difference or JND). Users' accuracy is the distance between the actual and perceived curvature (Point of Subjective Equality or PSE). Users' speed is the time users need to perceive the curvature of the soft UI (exploration time). In this chapter, we are the first to measure the impact of softness on users' precision, accuracy, and speed when perceiving the curvature.

3.2 Related work

Our work builds on top of previous work that studied users' psychophysical perception of curvature and softness.

3.2.1 Perception of curvature

Curvature can be perceived through cutaneous and kinesthetic cues. The cutaneous cues refer to the responses of mechanoreceptors [209] innervating the finger pad skin within and in the neighborhood of the contact area [240, 415]. The kinesthetic cues refer to the sense of position and motion of limbs, along with associated forces, conveyed by the sensory receptors in the skin around the joints, joint capsules, tendons and muscles [240, 415]. During passive touch, users only use cutaneous cues, while active touch [129] involves kinesthetic cues [240].

Passive touch. Goodwin, John, and Marceglia applied surfaces with different curvature as stimuli to participants' passive index finger with controlled force [136, 137]. They found that increasing the contact force (e.g., from 0.196 N to 0.588 N) could lead to participants' judging stimuli slightly less curved [136], and increasing the contact area (e.g., from 19.6 mm^2 to 53.6 mm^2) could slightly decrease participants' discrimination threshold [137]. Meanwhile, they found that both the effect of contact force [136] and contact area [137] were much smaller than the effect of surface curvature itself. They then used microneurography to record responses of tactile mechanoreceptors on participants' finger pads [1] when applying the same stimuli used in [136] to participants' passive index fingers. They found that the SAI afferents could well code the curvature information of stimuli for their steeply monotonically increasing response frequency to the stimuli curvature, whereas their response frequency increased slightly under larger contact force.

In short, with passive touch, which involves only cutaneous cues, participants can well discriminate surface curvature despite some slight bias induced by contact area and contact force.

Active touch. Gordon and Morison found participants' impressive performance when discriminating different curvatures with active touch [129]. They conducted several experiments [139] asking participants to use their index finger to actively explore the curvature of a graded series of surfaces produced using plano-convex lenses (diameter of 60 mm, step edge of 2 mm and base-to-peak height from 0 mm to 9.46 mm). They found participants could, in average, distinguish a lens with base-to-peak height of 0.09 mm from a lens with base-to-peak height of 0 mm (i.e. a flat lens).

Pont, Kappers, and Koenderink found the effective stimulus for participants to discriminate surface curvature was the total height change over the surface (i.e., the ratio between the height and width of stimuli) when they slide a finger over it to explore the curvature [347]. This was confirmed by Louw, Kappers, and Koenderink in their experiment measuring participants' detection thresholds for curvature in a larger range with stimuli having a Gaussian profile whose width (σ) ranges from 0.15 mm to 240 mm [255]. They found the discrimination threshold (i.e., stimulus height) of Gaussian-shaped stimuli increased with a power of 1.3 with increasing stimulus width. These work suggested that kinesthetic cues of participants' finger motion (e.g., the ratio of movement distance in the vertical and horizontal direction) can help participants to discriminate surface curvature.

Frisoli et al. conducted an experiment to confirm the important role of cutaneous cues during curvature perception [116]. Authors asked participants to discriminate the curvature of rendered virtual curved surfaces. These surfaces were rendered by a device providing haptic information (cutaneous and/or kinesthetic cues) at the fingertip. Their participants discriminated the curvature in two different conditions. (A) First, with *only kinesthetic cues*: participants inserted their finger into a thimble supported by a kinesthetic haptic device [70]. This device could provide users with kinesthetic cues by applying to the finger tip a force in the direction perpendicular to the virtual surface rendered. (B) Second, with *both kinesthetic and cutaneous cues*: during the exploration, an additional small mobile plate supported by the same kinesthetic haptic device kept in contact with the finger tip. In addition to the previous kinesthetic cues, the plate could rotate instantaneously along the tangent to the point of contact between the finger and the virtual surface, to provide cutaneous cues informing about the shape geometry at the contact

point. They found that with combined kinesthetic+cutaneous cues (B), participants were more precise: they had a 43% lower threshold for curvature discrimination compared to only kinesthetic cues.

In short, prior work found that users leverage both cutaneous and kinesthetic cues for curvature perception. However, their stimuli were either *rigid* curved objects (e.g., [139, 347, 255, 137, 136]), or rendered virtual curved surfaces with a *rigid* plate varying orientation (e.g., [116]). Consequently, these surfaces did not deform when the users' finger press on them. When touching a soft surface, the surface deformation can provide users with important cutaneous cues [31]. Meanwhile, the deformation will inversely change the local curvature of the surface. We need to further explore how this deformation caused by the surface softness will impact users' perception of the surface curvature. Such an information will ensure reliable haptic feedback to users of soft SCIs.

3.2.2 Perception of softness

Srinivasan and LaMotte [415] studied the impact of cutaneous and kinesthetic cues on participants' perception of softness. They asked participants to discriminate the softness of flat stimuli made of rubber with 5 different levels of softness and in three conditions: (1) actively pressing with their middle finger on the stimuli; (2) actively pressing with their middle finger on the the stimuli with local cutaneous anesthesia; or (3) passively applying the stimuli on their middle finger pad with controlled contact force and speed. In condition 1, both cutaneous and kinesthetic cues were available to participants. In condition 2, only kinesthetic cues were available. In condition 3, only cutaneous cues were available. They found with only kinesthetic cues (2), participants' average discrimination accuracy decreased markedly (e.g., from $\geq 93\%$ to $\leq 55\%$ when discriminating between the softest stimuli and medium-soft stimuli). With only cutaneous cues (3), participants' average discrimination accuracy decreased much more slightly (e.g., from averagely 98% to averagely 93% when discriminating between the softest stimuli and the medium-soft stimuli). Their work revealed the critical role of cutaneous cues in softness discrimination.

According to Hertz's contact theory [207], the contact area of a finger with another soft surface increases as the finger presses deeper into the soft surface. This contact area increases more rapidly with a softer surface. Based on Hertz's contact theory, Bicchi, Scilingo, and De Rossi developed the Contact Area Spread Rate (CASR) device [36, 386] to provide participants with cutaneous information through the contact area between the finger and the device. The device varies its contact area with the user's finger pad,

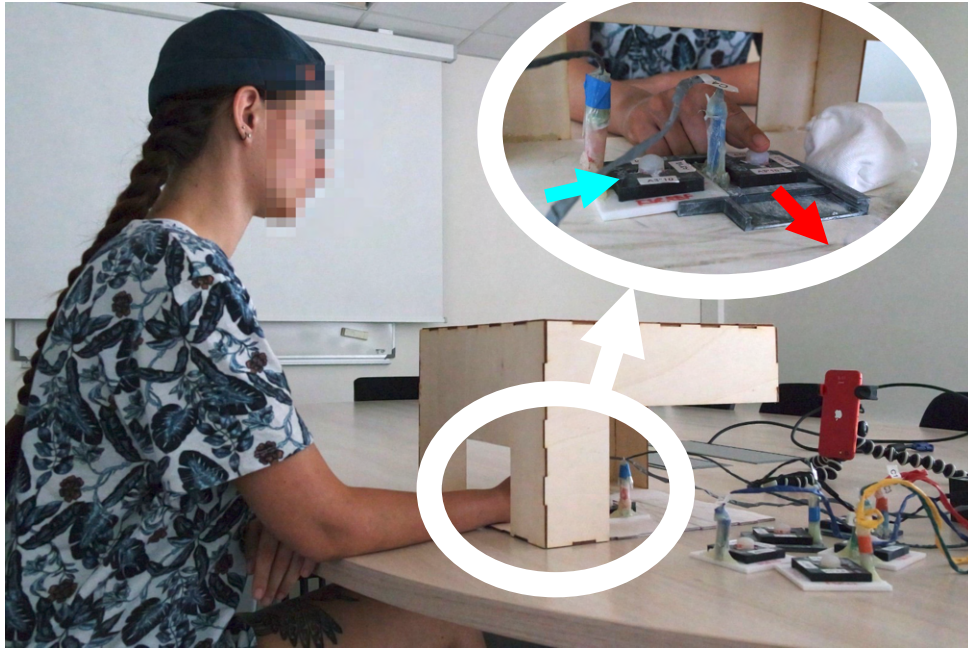
through a set of concentric cylinders of different radii in a telescopic arrangement. As the finger presses at the top of the system, it indents more deeply the cylinders. The finger gets in contact with the larger cylinders, enlarging the contact area. Bicchi, Scilingo, and De Rossi controlled the rate of the enlargement of the contact area according to the softness of the simulated surface: the softer the surface, the more rapidly the contact area increases as the finger presses on it. They found that with the cutaneous information provided by CASR, the participants had a similar success rate for the recognition of softness compared to real objects: 75% on average with CASR vs. 87% on average by directly exploring objects. This experiment further confirmed the important role of cutaneous cues, in particular the contact area, in softness discrimination.

Bergmann Tiest and Kappers conducted several softness estimation experiments using cutaneous and/or kinesthetic cues. They verified the vital contribution of cutaneous cues in softness discrimination (90% on average) and also show the less important contribution of kinesthetic cues (10% on average) [31].

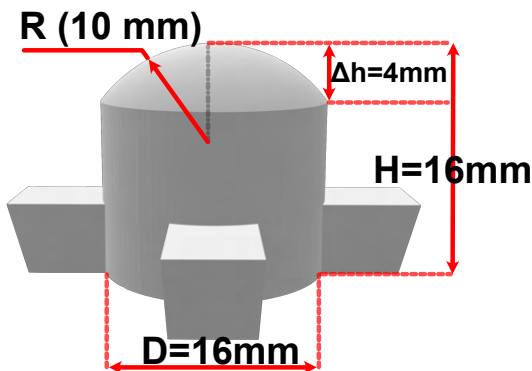
Users take both kinesthetic and cutaneous cues for softness estimation. However, cutaneous cues play a major role in softness perception. Both these cues also took part in participants' curvature perception. When participant touch and explore curved surfaces with different softness, both types of cues can vary based on curvature *and* softness. E.g., both the cutaneous cues of pressure distribution around the contact area and the kinesthetic cues of finger position can be different because of the different surface deformation and/or finger pad deformation. Consequently, there might be an impact of softness on curvature perception. For this reason, we study here the impact of softness on curvature perception.

3.3 Experiment

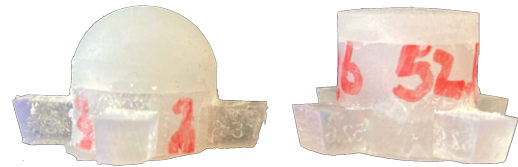
The goal of our experiment is to explore whether the softness impacts participants' ability to discriminate between different surface curvatures. For this, we use a method called *constant stimuli* [351, 352, 450]. This method presents successively to participants two stimuli in a random order in a trial: one with the reference curvature as the stimulus of reference, and another with a different curvature as the stimulus of comparison (Figure 3.2(a) top right). It then assesses if they can discriminate the most curved stimulus. This enables us to measure the just noticeable difference (JND) and the point of subjective equality (PSE) in curvature discrimination with stimuli of different softness. We also



(a) A participant exploring our stimuli. The first stimulus exits following the direction of the red arrow and the second stimulus enters following the blue arrow.



(b) R indicates the radius of the curved surface. The smaller the radius means the more curved the surface. Δh indicates height change over the curved surface ($\Delta h = R - \sqrt{R^2 - D^2/4}$).



(c) Example stimuli: the left one is the most curved ($R = 8.3$ mm), and the right one is the flattest ($R = 52.6$ mm)



(d) (Left) The pressure sensor Interlink FSR406 stuck on the 3D printed support and (middle) a stimulus to install on this support. (Right) The schematics of the circuit for one sensor.

Figure 3.2 – (a) Experimental setup, (b) 3D model of a very curved stimulus, (c) photograph of two stimuli (from the group of softness Shore 00-50) used in our experiment, and (d) pressure sensor and schematics of the circuit for sensor reading (as in [117]).

measure the exploration time participants needed for discrimination.

3.3.1 Experimental parameters

Our independent variables were SOFTNESS and CURVATURE:

Softness: *Shore 00-10*, *Shore 00-50*, *Shore A-30* and *Rigid* (bottom of Figure 3.1). The rigid stimuli served as a baseline and to compare our results to prior work [352]. As users categorize an object as hard or soft based on whether the object is more or less soft than the finger pad [115], we chose the experimental levels of softness based on existing measurements of the index finger pad hardness (\approx Shore 00-50) [99, 94]. The softness of our soft stimuli was designed to be (1) softer (Shore 00-10), (2) as soft as (Shore 00-50), and (3) harder (Shore A-30 \approx Shore 00-80 [278]) than the index finger pad.

Curvature: To investigate perceptual sensitivity over a broad range of UI curvatures, we studied 3 different curvature levels: *very curved*, *middle curved*, and *little curved* as in [352]. Each curvature condition corresponds to a stimulus of reference with radius $R_{\text{ref}}=10, 20$ and 40 mm. Participants were presented with 6 stimuli whose curvature clustered around the comparative stimulus of reference as in [352]:

- Very curved ($R_{\text{ref}}=10$ mm): $R=8.3, 8.8, 9.4, 10.7, 11.5$ and 12.5 mm;
- Middle curved ($R_{\text{ref}}=20$ mm): $R=16.7, 17.6, 18.8, 21.4, 23.1$ and 25 mm;
- Little curved ($R_{\text{ref}}=40$ mm): $R=32.3, 34.5, 37, 43.5, 47.6$ and 52.6 mm.

In each curvature condition, three stimuli of comparison were more curved than the reference stimulus, three were less curved than the reference stimulus, and their curvatures (in m^{-1}) were equally spaced, as explained in [127]. Figure 3.2(c) shows one stimulus with the most curved surface ($R=8.3$ mm) and one with the flattest surface ($R=52.6$ mm) from the group of softness Shore 00-50.

3.3.2 Participants

We recruited 12 participants (6 women, 6 men, $M=26.1$ years old, $SD=4.1$ years) at the local university. One participant was left-handed. Each participant received a voucher worth 50€. We measured the hardness of participants' dominant index finger pad with a BAREISS HP Shore 00 durometer. The measurement followed a standard procedure [99]. The average hardness of participants' finger was Shore 00-38.28 ($SD=Shore\ 00-4.43$).

3.3.3 Stimuli

We used 84 stimuli in total: 4 SOFTNESS \times 3 CURVATURES levels \times 7 stimuli (6 comparison stimuli + 1 reference stimulus). We printed the rigid stimuli with photo-polymer resin (Formlabs standard clear resin) using a stereo-lithography 3d printer (Formlabs Form3). We fabricated the molds for the soft stimuli with the same printer and with the same resin as the one used for the rigid stimuli. We used three types of silicone from *Smooth-On, Inc.* for our soft stimuli: Ecoflex 00-10, Ecoflex 00-50, and Dragon Skin 30 respectively for softness levels Shore 00-10, Shore 00-50, and Shore A-30. We followed instructions from *Smooth-On, Inc.* for molding and unmolding. We verified the actual curvatures of the fabricated stimuli as in [416] and report them in appendix A.1.

All our stimuli had the same height and the same base diameters. This prevents confounding haptic cues from height [348] and contact area [137]. We chose for our stimuli a base-to-peak height of 16 mm and a diameter of 16 mm, as shown in Figure 3.2(b). The width (i.e., diameter) of our stimuli is similar to the a human’s index finger pad [79] and to many existing soft UIs (e.g., [481, 27, 114]). The height of our stimuli allows participants to freely rest their arms and wrists on the table to avoid fatigue during the experiment and is similar to the height used in [255]. The 3D models of the stimuli or their molds are provided in the supplementary material for replication [100].

We used magnesium powder to reduce friction between the skin and the silicone surface as in [138]. We spread the magnesium powder evenly over all stimuli with a chalk ball before each experimental session. During the experiment, participants can freely access the chalk ball to spread the magnesium powder on their fingers when feeling too much friction.

3.3.4 Experimental setup and procedure

Participants first signed an informed consent form and filled out a short demographic questionnaire. As shown in Figure 3.2(a), participants sat at a table while their arms and wrists rested freely on the table to avoid fatigue during the experiment. They freely explored the curvature of the stimuli with the index finger of their dominant hand. A box prevented participants from seeing their fingers and the stimuli. In front of the participants, we installed a camera on a tripod to record participants’ finger movements when exploring our stimuli (Figure 3.2(a)).

Our experiment used a two-alternative forced-choice procedure. In each trial, we



Figure 3.3 – Experimental procedure with the first repetition illustrated: this participant first experienced the middle curvature ($R_{\text{ref}}=20$ mm). Every pair in the illustrated repetition indicates the radii of the curved surfaces successively presented in one trial. In every pair, one of the radii is of the reference stimulus ($R_{\text{ref}}=20$ mm).

presented the pair of stimuli to compare sequentially, as we are interested to know if users can perceive a change in the curvature of a single “widget” –such as a button changing its curvature over time– as many interactive devices do, e.g., [157, 462, 132]. We chose to have an interruption, as small as possible, between the exploration of each stimulus, as this is the most common procedure [232] and users sometimes take their finger off the UI in real situations. We expect this method to measure a safer JND for designers as prior work showed that continuous exploration of both stimuli –i.e., with no interruption in the exploration of both comparison stimuli– resulted in a smaller JND in compliance [232].

We aim at a quick switch between the two stimuli to be compared, to decrease the “time error” due to the memory of the first stimuli fading with time [352, 232]. For this, as shown in Figure 3.2(a), the experimenter places both stimuli to be compared on a 3D printed rail guide. When switching, the support guides the sliding of the first stimulus out of the participant’s reach, and the sliding of the second stimulus precisely below the participant’s finger. The average switching time between two stimuli in our experiment was 2.25 s (SD= 0.21 s), similarly to prior work [351, 136, 137].

A participant had to indicate which of the two presented stimuli (Figure 3.2(a) top right) felt more curved (as in [457]) by saying “first” or “second”. No restrictions were imposed on the exploration time of each stimulus, as in [457, 171, 351].

As the example shown in Figure 3.2(d) (left), we stuck a 39.6×39.6 mm² commercial pressure sensor (*Interlink FSR406* [195]) on each 3D printed support with double-sided tape. This sensor enables the recording of the force that participants applied to our stimuli when exploring our stimuli. Figure 3.2(d) (right) shows the schematics of the trans-impedance circuit that we implemented to ensure a nearly linear output of our sensors, following the guide of the vendor (Interlink Electronics) similar to the circuit implemented in [117]. We used a *Teensy2* to read the sensors’ output.

We developed a software running on macOS using PyQT5 [249] for the experimenter

to quickly and correctly present the stimuli, and to record the exploration time and the exploring force of each stimulus, and the participants' answers. The exploration time of the first stimulus was defined as the duration between the time when the experimenter asked the participants to start exploring the first stimulus, and the time participants signaled the experimenter that they completed their exploration. Then the experimenter switched the stimuli as presented in Figure 3.2(a) and asked participants to explore the second one. The exploration time of the second stimulus was defined as the duration between the time when the experimenter asked the participants to start exploring the second stimulus, and the time participants answered "first" or "second" as the most curved.

3.3.5 Experimental design

Independent variables were `SOFTNESS` and `CURVATURE`. We used a fully-crossed, within-subjects factorial design with repeated measures. Every participant experimented with all softness and curvature conditions.

The first dependent variable was the percentage of times the participants responded that the stimulus of comparison felt more curved than the stimulus of reference. The second dependent variable was the exploration time, for both first and second exploration of a trial of discrimination between two stimuli.

As shown in Figure 3.3, we had in total 3 series of experimental comparisons, one for each curvature level. Participants trained before each series. For this, they compared the two most different pairs of stimuli, i.e., the least and the most curved to the current reference stimulus. The softness of the training stimuli was chosen randomly. As in [348], the experimenter gave feedback on the correctness of the answer during the training, and the experimental series started after participants correctly judged four of these combinations successively. In each series, we had four blocks of experimental comparisons, one block for each softness condition. Each block was repeated three times. In each block of experimental comparisons, we repeated twice each of the 6 possible comparisons to the reference stimulus, in opposite order [352]. This led to 12 trials per block. Figure 3.3 shows an example of 12 trials that one participant experienced. As in [457], the participants did not know that the reference stimulus was presented in all trials. As in [348, 457], participants did not receive feedback on their performance during the experiment.

After finishing all 12 trials of one block, participants were allowed to take a short break until they felt ready for the next block. The order of presentation of the three

series was randomized. The order of presentation of the four blocks was counterbalanced across participants according to a Latin square. The order of presentation of 12 trials in one block was pseudo-randomized. Each series of experimental comparisons took around 75min. Participants completed each series of experimental comparisons on three different half-days to reduce the impact of fatigue. After each series, participants filled a short 5 items Likert-scale questionnaire to evaluate the difficulty of the curvature discrimination in each softness condition from very easy to very difficult. In total, the experiment took 4 hours for each participants.

Following previous work, we draw the following three hypotheses for all curvature conditions:

H1: The softer the surface, the lower participants' curvature perception precision, i.e., the larger the just noticeable difference (JND) in curvature.

H2: The softer the surface, the lower the participants' curvature perception accuracy, i.e., the larger distance between the point of subjective equality (PSE) and the reference curvature.

H3: The softer the surface, the slower participants discriminate the curvature, i.e., they take longer exploration time for the first stimulus, for the second stimulus, and for their average.

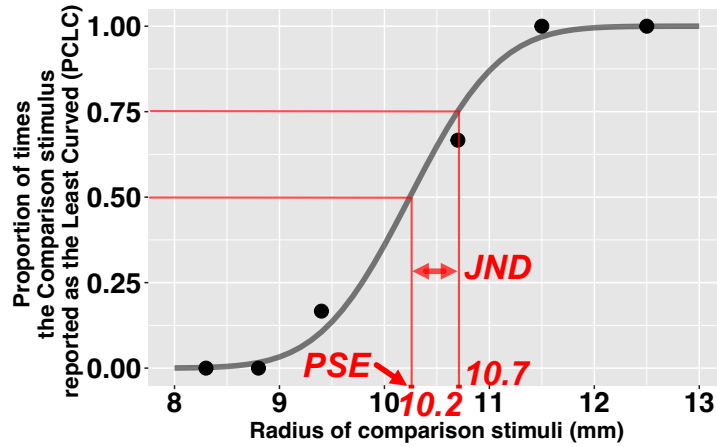
In order to reduce unintentional false positive inflation of results [501], our study was registered before collecting the data⁵.

3.4 Data pre-processing and analysis

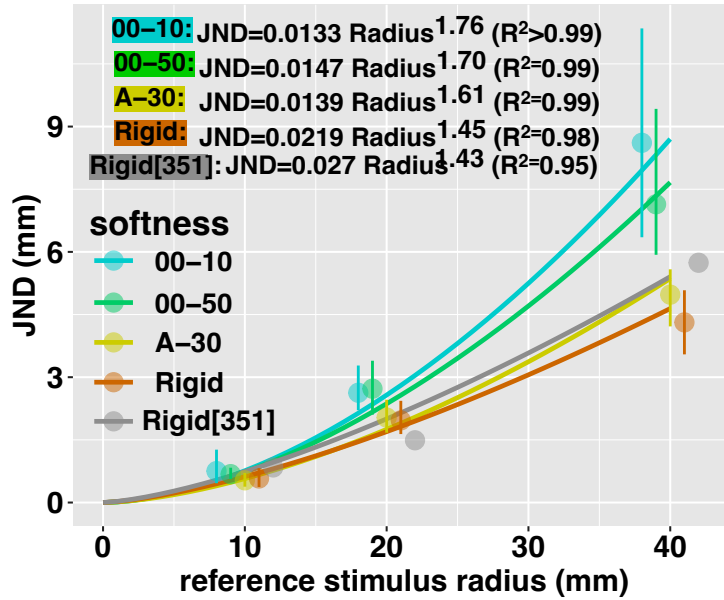
3.4.1 Just-noticeable difference (JND) and Point of subjective equality (PSE)

We computed the JND and PSE values for each participant in each softness \times curvature as in [287]. We first fit the proportion of times participants reported the comparison stimulus as the least curved with a Generalized Linear Model using a probit link function [287] to obtain a psychometric curve based on standard psychophysical protocol [127, 287]. Figure 3.4(a) presents an example of a psychometric curve, resulting from the fitting of participant P2's responses when discriminated stimuli with $R_{\text{ref}}=10\text{mm}$ and $\text{SOFTNESS}=\text{Shore 00-50}$.

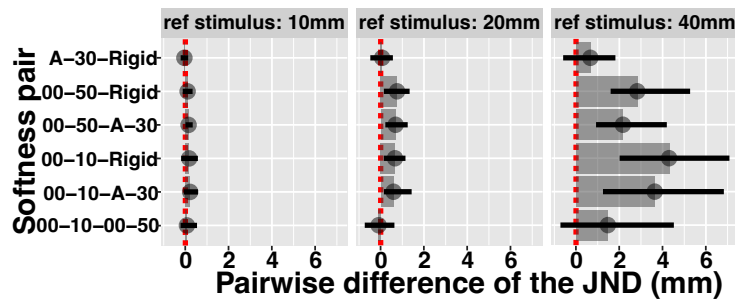
5. Registration of the experiment available at <http://osf.io/scnj9/>



(a) Proportion of times P2 reported the comparison stimulus as less curved than the reference stimulus for *Shore 00-50* and $R_{ref}=10$ mm and its psychometric function fit.



(b) JND results for all CURVATURES and SOFTNESS. The results were fitted by a power curve [422, 351]. Data points were slightly jittered horizontally to avoid overlap. The gray color shows Provancher et al.'s data [351].



(c) JND pairwise differences between each softness pair (Y axis) for each curvature condition, computed for each participant individually and averaged.

Figure 3.4 – Just noticeable difference computation and results.

We then estimate the PSE and JND values based on the psychometric curve obtained with the fit functions based on standard psychophysical protocol [127, 287]. The PSE refers to the 50% point on the psychometric curve, where participants have half chance on average to judge the comparison reference less curved than the reference stimulus (e.g., 10.2 mm in Figure 3.4(a)). The PSE is a measure of participants' perception accuracy [287]. A PSE closer to the reference curvature (e.g., closer to 10 mm in Figure 3.4(a)) means less perception bias, thus better accuracy.

The distance between the 50% point and 75% point on the psychometric curve (e.g., 10.7 mm in Figure 3.4(a)) indicates the JND (e.g., 0.5 mm in Figure 3.4(a)). The JND indicates the threshold of difference in curvature that can be perceived with a probability halfway between a chance response (i.e., 50%) and an always-correct response (i.e., 100%). The JND refers to participants' perception precision: the smaller the JND, the better the precision [287].

3.4.2 Analysis

We use estimation techniques based on means and 95% bootstrapped confidence intervals (CI) as recommended by Dragicevic [91], and pairwise differences to show effect sizes. These methods are recommended by the APA [20] and largely adopted [83, 221, 80, 206, 237, 293]. We opted for this nuanced analysis of the direction and magnitude of the effect. A pairwise difference is an intra-subject measurement that expresses the effect size and is computed between each mean. This allows to quantify the difference per participant.

3.5 Results

3.5.1 Just noticeable difference (JND)

H1 is partially verified: Participants do not have a lower curvature perception precision with a softer surface. I.e., not in all curvature condition, they had a larger JND of curvature in a softer condition.

Figure 3.4(b) shows that **in the most curved condition ($R_{ref}=10$ mm), participants performed with similar perception precision in all four softness conditions** : Shore 00-10 JND= 0.75 mm (CI [0.45, 1.25]), Shore 00-50 JND= 0.68 mm (CI [0.56, 0.83]), Shore A-30 JND= 0.53 mm (CI= [0.38, 0.71]), Rigid JND= 0.58 mm

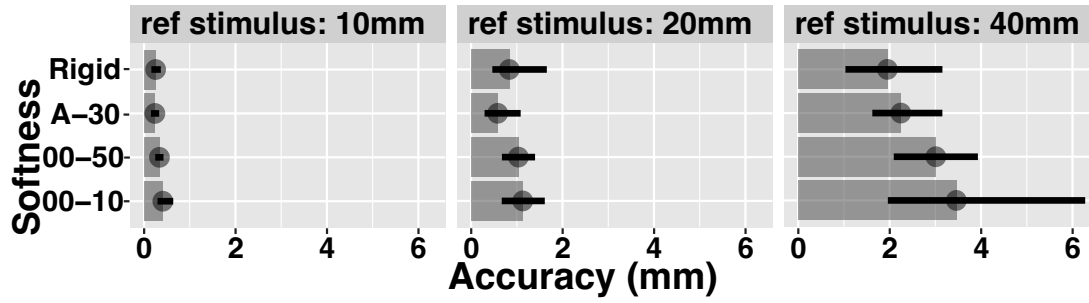
(CI= [0.38, 0.83]). We did not measure an effect of softness. It is consistent with the pairwise difference shown in Figure 3.4(c): the error bars of all softness pairs cross zero in CURVATURE=10 mm condition.

In middle curved condition ($R_{\text{ref}}=20$ mm), participants performed with similar perception precision in the two softest conditions: Shore 00-10 JND=2.63 mm (CI [2.20, 3.28]), Shore 00-50 JND= 2.72 mm (CI [2.09, 3.38]). **Participants also performed with similar perception precision in the two hardest conditions:** Shore A-30 JND=2.03 mm (CI [1.67, 2.46]), Rigid JND=1.97 mm (CI= [1.64, 2.44]). **Participants performed with better perception precision in the two hardest conditions than in the two softest conditions.** It is consistent with the pairwise differences shown in Figure 3.4(c): in $R_{\text{ref}}=20$ mm condition, only the error bars of the pairs *Shore 00-10–Shore 00-50* and *Shore A-30–Rigid* cross zero. This can result from a small difference (see Figure 3.4(b)). What we learn from this experiment is that the curvier, the less the impact of the softness of the curvature perception. $R_{\text{ref}}=20$ mm might lie at the limit of curvature where this happens.

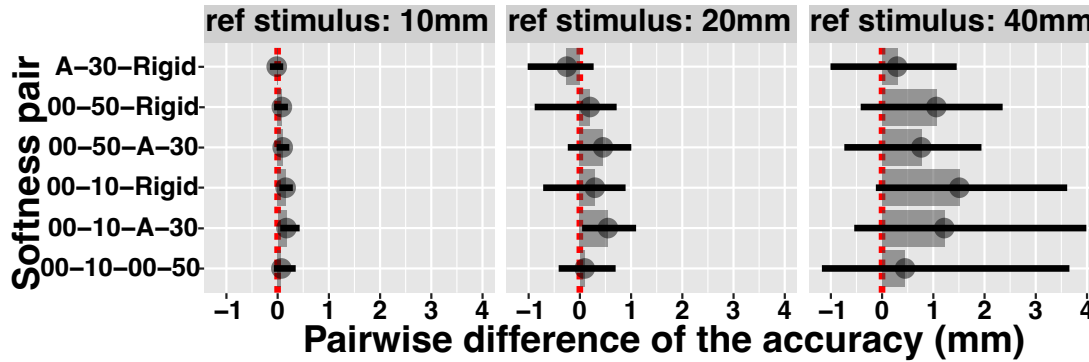
In the flattest condition ($R_{\text{ref}}= 40$ mm), participants performed with better precision in the more rigid conditions (Figure 3.4(b)): Shore 00-10 JND=8.61 mm (CI [6.35,11.36]), Shore 00-50 JND=7.14 mm (CI [5.93,9.38]), Shore A-30 JND=4.93 mm (CI [4.24,5.58]), Rigid JND=4.32 mm (CI [3.53,5.06]). However, in Figure 3.4(c), in $R_{\text{ref}}=40$ mm condition, the error bars of the pairs of *Shore 00-10–Shore 00-50* and *Shore A-30–Rigid* cross zero. This suggests **similar perception precision in the two hardest conditions and also in the two softest conditions, for the flattest curvature.** **Participants performed with better perception precision in the two hardest conditions than in the two softest conditions.** These might be explained by a higher variability among participants, because the error bars are larger in $R_{\text{ref}}=40$ mm in Figures 3.4(b) and 3.4(c).

Figure 3.4(b) shows that participants' JND increased as the stimuli become flatter from $R_{\text{ref}}=10$ mm to 40mm. More precisely, the power-law fit results in Figure 3.4(b) show that the exponent increases from 1.45 to 1.76 as the stimuli become softer from Rigid to Shore 00-10. In addition, all exponents are larger than 1. This suggests that, with a softer material, participants' curvature perception precision may more strongly decrease as the surface becomes flat. In addition, the difference in perception precision between different softness conditions may be larger as the surface becomes flat.

Interestingly, Provancher et al. conducted similar curvature perception experiments



(a) Perception accuracy in each curvature and softness.



(b) Pairwise difference in accuracy between pairs of softness.

Figure 3.5 – Accuracy (i.e., distance between PSE and reference curvature).

with only rigid stimuli [351, 352]. Their results are shown in gray on Figure 3.4(b). Their results are similar to our result with the rigid condition, with a slightly lower JND with $R_{\text{ref}}=20$ mm and a slightly higher JND with $R_{\text{ref}}=40$ mm. We further discuss our replication of their experiment with rigid stimuli in section 3.6.1.

3.5.2 Point of Subjective Equality (PSE)

H2 is not verified: Participants do not have a lower curvature perception accuracy with a softer surface. I.e., there was not a larger distance between the PSE and the reference curvature in softer conditions in each curvature condition.

Figure 3.5(a) shows that participants tended to be less accurate when exploring less curved surfaces. The average distance between PSE and the reference curvature is 0.31 mm (CI=[0.26,0.38]) for $R_{\text{ref}}=10$ mm, 0.90 mm (CI=[0.69,1.15]) for $R_{\text{ref}}=20$ mm, and 2.67 mm (CI=[2.12,3.48]) for $R_{\text{ref}}=40$ mm. **In the most curved condition ($R_{\text{ref}}=10$ mm), participants performed with similar perception accuracy in all four softness conditions.** The distance between the PSE and the reference curvature is 0.41 mm (CI

[0.29, 0.63]) for Shore 00-10, 0.34 mm (CI [0.24, 0.43]) for Shore 00-50, 0.24 mm (CI [0.15, 0.33]) for Shore A-30, and 0.25 mm (CI [0.16, 0.37]) for rigid. We did not measure an effect of softness. It is consistent with the pairwise differences shown in Figure 3.5(b): the error bars of all softness pairs cross zero when $R_{\text{ref}}=10$ mm.

In the middle curved condition ($R_{\text{ref}}=20$ mm), participant performed with the highest perception accuracy in the little rigid condition and the lowest perception accuracy in the softest condition. The distance between the PSE and the reference curvature is 0.58 mm (CI [0.29, 1.09]) in the Shore A-30 condition, and 1.13 mm (CI [0.67, 1.62]) in the Shore 00-10 condition. Participants' perception accuracy with Shore 00-50 and Rigid conditions were similar and located between the accuracy of the previous other two softness conditions. The distance between the PSE and the reference curvature is 1.03 mm (CI [0.67, 1.41]) with Shore 00-50 and 0.83 mm (CI [0.45, 1.65]) with rigid stimuli. All error bars in $R_{\text{ref}}=20$ mm condition (Figure 3.5(b)) cross zero or near it. This suggests that **participants' perception accuracy was similar in all four softness conditions.**

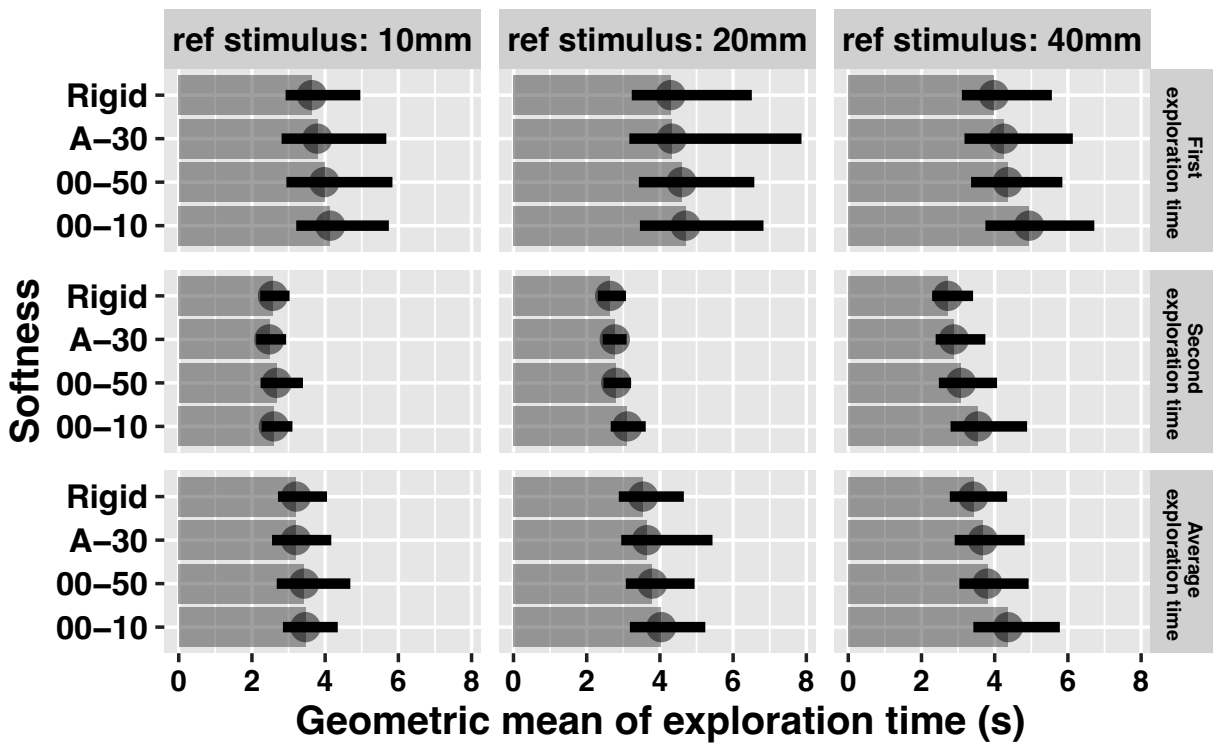
In the flattest condition ($R_{\text{ref}}=40$ mm), participants performed with decreasing perception accuracy with softer conditions (Figure 3.5(a)). The distance between the PSE and the reference curvature is 3.46 mm (CI [1.96, 6.29]) with Shore 00-10, 3.01 mm (CI [2.08, 3.93]) with Shore 00-50, 2.24 mm (CI [1.62, 3.14]) with Shore A-30, and 1.95 mm (CI [1.04, 3.14]) with rigid stimuli. However, Figure 3.5(b) shows that error bars of the pairwise comparisons between all six softness pairs cross zero for $R_{\text{ref}}=40$ mm. This suggests that participants had **similar perception accuracy in all four softness conditions with the flattest curvature.**

3.5.3 Exploration time

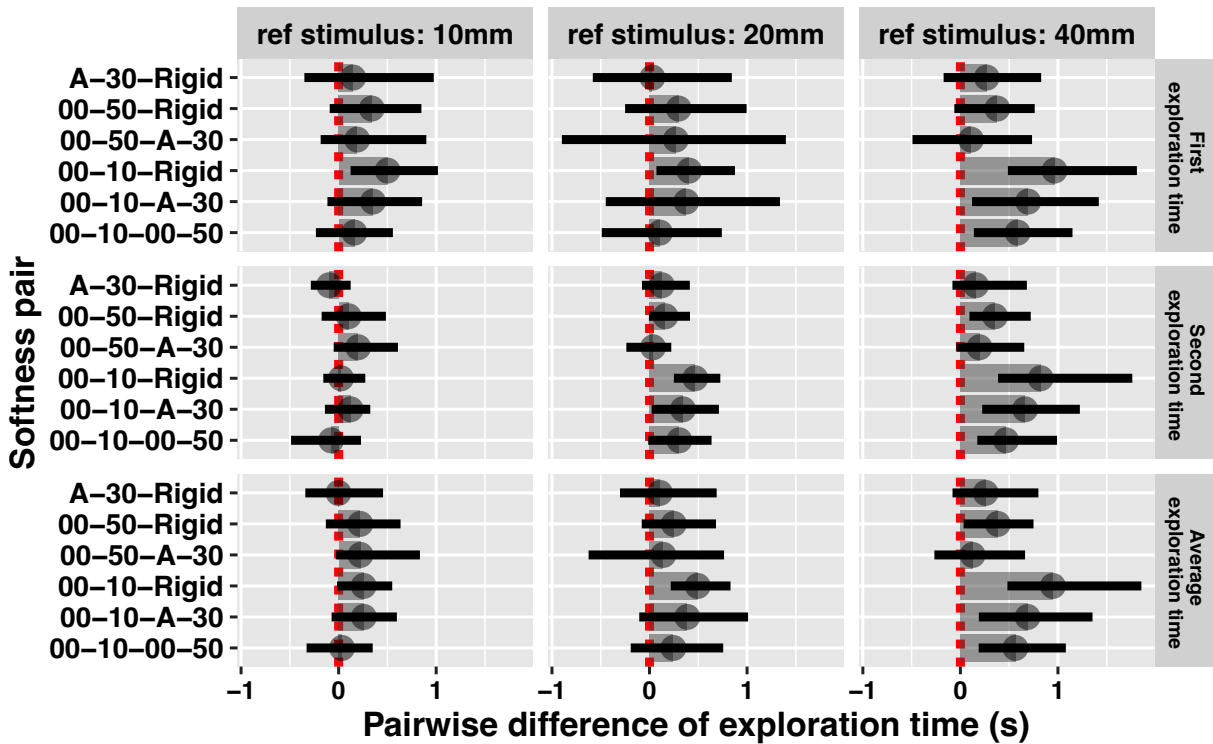
H3 is partially verified: Participants do not discriminate curvature slower with a softer surface. I.e., not in all curvature conditions, participants needed longer exploration time for the first stimulus, for the second stimulus, and for their average in softer conditions.

Figure 3.6(a) shows that participants need much less time to explore the second stimulus in a trial after completing the exploration of the first one. This applies to all reference curvature and softness conditions. After taking the time to memorize the first stimulus, participants make their decision faster with the second stimulus.

In all three curvature conditions, the softer the stimulus, the longer the exploration times (Figure 3.6(a)). For instance, when $R_{\text{ref}}=10$ mm, participants'



(a) Exploration time of the first stimulus of a trial (top), of the second stimulus (middle), and their average (bottom), in each curvature and softness condition.



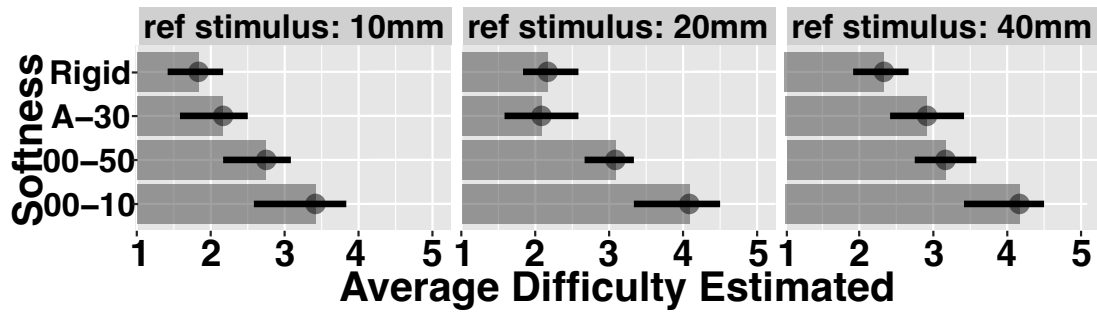
(b) Pairwise difference of the time between pairs of softness for each curvature condition.

Figure 3.6 – Exploration time.

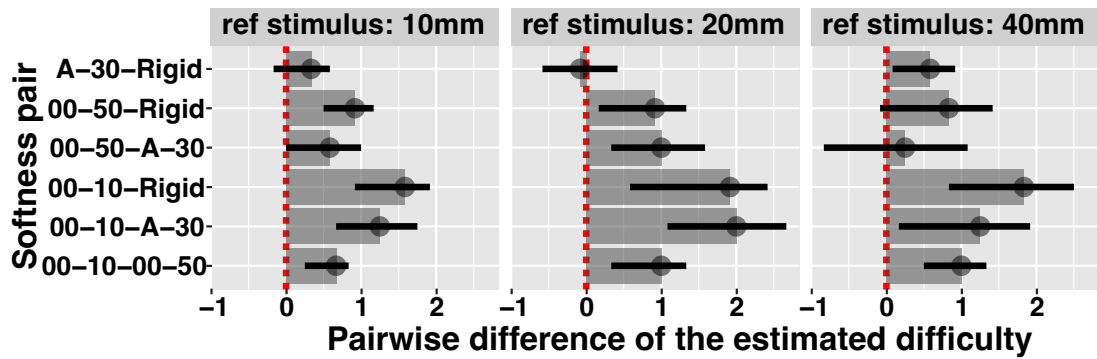
average exploration time increased from 3.21 s (CI [2.70, 4.03]) when exploring the rigid stimuli to 3.46 s (CI [2.85, 4.37]) when exploring the softest stimuli (Shore 00-10). When $R_{\text{ref}}=20$ mm, participants' average exploration time increased from 3.54 s (CI [2.87, 4.64]) to 4.04 s (CI [3.17, 5.24]). When $R_{\text{ref}}=40$ mm, participants' average exploration time increased from 3.98 s (CI [3.11, 5.57]) to 4.37 s (CI [3.42, 5.78]). However, there are large overlaps of error bars in almost all three curvature conditions for all the three exploration times. This indicates the **slow increase of the necessary time to explore the curvatures of softer surfaces**. This is consistent with the pairwise differences of exploration times (Figure 3.6(b)). Seven out of the nine *Shore 00-10-Rigid* pairwise comparisons do not cross zero, showing that there is a major increase of exploration times between the softest and the rigid condition. However, all the error bars of the pairwise difference of exploration time of two neighbor softness pairs cross zero or near it (*Shore 00-10-Shore 00-50*, *Shore 00-50-Shore A-30*, *Shore A-30-Rigid*). The only exception is the pairwise difference of exploration time of *Shore 00-10-Shore 00-50* for $R_{\text{ref}}=40$ mm. In these conditions, the pairwise difference of exploration time is 0.59 s (CI [0.14, 1.15]) for first stimulus, 0.47 s (CI [0.17, 0.99]) for the second stimulus, and 0.56 s (CI [0.18, 1.08]) for their average. This exception suggests that **in the flattest condition ($R_{\text{ref}}=40$ mm), participants need a much longer exploration time (all for the first stimulus, the second stimulus, and their average) when exploring the softest (Shore 00-10) stimuli than other softness conditions** including its neighbor softness condition (Shore 00-50).

3.5.4 Difficulty estimation

In addition to the three measures registered⁵, i.e., JND, PSE, and Exploration time, we also studied participants' subjective difficulty to discriminate the curvatures. Figure 3.7(a) shows that **participants clearly found more difficult to discriminate between curvatures when the material is softer**. E.g. in the most curved condition ($R_{\text{ref}}=10$ mm), participants found it rather easy (M=1.83, CI [1.42, 2.17]) to discriminate the rigid stimuli. However, they found it rather neutral (M=3.42, CI [2.58, 3.83]) to discriminate the softest stimuli. In the middle curved condition ($R_{\text{ref}}=20$ mm), participants found it rather easy (M=2.17, CI [1.83, 2.59]) to discriminate the rigid stimuli. However, they found it rather difficult (M=4.08, CI [3.33, 4.50]) to discriminate the softest stimuli. In the little curved condition ($R_{\text{ref}}=40$ mm), participants found it rather easy (M=2.33, CI [1.92, 2.75]) to discriminate the rigid stimuli. However, they found it rather difficult



(a) The curvature perception difficulty estimated by participants in each curvature and softness condition, from 1 (very easy) to 5 (very difficult).



(b) Pairwise difference in subjective difficulty between two softness for each curvature condition.

Figure 3.7 – Subjective discrimination difficulty.

($M=4.17$, CI [3.42, 4.50]) to discriminate the softest stimuli. These results are consistent with the pairwise differences shown in Figure 3.7(b). All the error bars of the pairwise differences between Shore 00-10 and rigid do not cross zero.

3.6 Discussion

3.6.1 Partial replication of prior work

Our experiment, through the curvature perception of rigid curved surfaces, was a partial replication of previous work [351, 352]. While we shared the same curvature levels of stimuli used in prior work, we extended the scope of Provancher et al.'s experiment to stimuli with different softness. In their experiment, participants rolled their index finger along the circumferential direction of rigid cylinders with different radii to explore their curvature. On the contrary to our stimuli that had spherical surfaces, Provancher et al.'s stimuli were curved only in the direction along the finger (distal-proximal direction), not in the direction across the finger (radial-ulnar direction). The reason for this difference is that one of our objectives was to prepare guidelines for the design of soft curvature-changing UIs, such as buttons [132, 462, 157]. We found that spherical shapes were more widespread than cylindrical shapes in soft curvature-changing UIs. For instance, Pneumatibles [132], Fingertip Softness Tactile display [114], Haptic Jamming [419], and Inflatable Hemispherical Multi-touch Display [423] are soft curvature-changing UIs with spherical shapes.

Another difference with their experiment is the diameter D of the stimuli base cylinder (Figure 3.2(b)). In their experiment, the flatter the stimulus (i.e., the larger the radius of the curved surface), the larger the diameter of the stimulus. In our experiment, as shown in Figure 3.2(b), all of our stimuli had the same base diameter. A reason for this difference is that we wanted to prevent any confounding cues from the contact area [137], because a larger diameter can result in a larger contact area with the participants' finger pads, in addition to larger exploratory movements. Another reason for this difference is that one of our objectives was to prepare guidelines for the design of soft curvature-changing UIs. Curvature and size are two independent dimensions of SCIs [226], and curvature-changing UIs do not necessarily change their size (e.g., [132]). In addition, enlarging a UI might be troublesome because of geometrical constraints from the body or environment [10]. Future work should study the impact of the base diameter.

As shown in Figure 3.4(b), Provancher et al. curvature perception precision (i.e., JND) of rigid surfaces was similar to ours in $R_{\text{ref}}=10$ mm: 0.84 mm [351] vs. 0.58 mm (CI [0.38, 0.83]). For $R_{\text{ref}}=20$ mm, Provancher et al.'s participants were slightly more precise: 1.49 mm [351] vs. 1.97 mm (CI [1.64, 2.44]). For $R_{\text{ref}}=40$ mm, Provancher et al.'s participants were slightly less precise: 5.74 mm [351] vs. 4.31 mm (CI [3.53, 5.06]).

We hypothesize that these differences come from the two types of cues in curvature perception: the kinesthetic and cutaneous cues. Pont, Kappers, and Koenderink [348] found that kinesthetic cues were effective for participants to discriminate surface curvature. In particular, when users slide their finger over the stimulus to explore the curvature, an effective cue is the total height change over the surface. In other words, users discriminate from the ratio between the height and width of stimuli, i.e. the ratio of $\frac{\Delta h}{D}$ in Figure 3.2(b). As a consequence, when two stimuli have the same curvature but are of different base diameters, the larger stimulus has the larger total height change over the surface ($\frac{\Delta h}{D}$), and therefore, this can improve participants' curvature perception precision. When $R_{\text{ref}}=20$ mm, the base diameter of Provancher et al.' cylindrical stimuli was larger than ours (see Figure 4-6 in [352]). For this reason, their participants could get stronger kinesthetic cues from rolling their fingers on the stimuli than our participants. This might explain why they found better precision when $R_{\text{ref}}=20$ mm. However, this cannot not explain why Provancher et al.'s curvature JND was slightly less precise when $R_{\text{ref}}=40$ mm.

Vogels, Kappers, and Koenderink studied participants' curvature discrimination absolute threshold, i.e., the just noticeable difference between a curved surface and a flat surface ($0m^{-1}$), through static touch –which involves only cutaneous cues. They studied stimuli with double curved surfaces (e.g., spherical and elliptical). They found a lower threshold ($0.2 - 0.32m^{-1}$, i.e., corresponding radius $3.125 - 5m$) than the threshold found by Pont, Kappers, and Koenderink in [346] ($0.5 - 0.9m^{-1}$, i.e., corresponding radius $1.11 - 2m$) with cylindrical stimuli. This suggests that double curved surfaces (e.g., spherical surfaces) could provide participants with better cutaneous cues than single curved surfaces (e.g., cylindrical surfaces). In our experiment, participants touched and explored stimuli with spherical surfaces, which should provide them with better cutaneous cues than stimuli with cylindrical surfaces [351, 352]. When exploring stimuli in $R_{\text{ref}}=40$ mm, the kinesthetic cue weakened both in Provancher et al.'s and our experiment because of smaller ratio of $\frac{\Delta h}{D}$ (detailed calculation in appendix A.2). The cutaneous cues might play an more important role in curvature discrimination, while the kinesthetic cue was

weaker. This might explain why the precision we found when $R_{\text{ref}}=40$ mm was better than prior work [351, 352].

We suppose that in nearly flat condition, the kinesthetic cues were so weak that the cutaneous cues played a more important role, while kinesthetic played a more important role when the surface curvatures were more curved ($R_{\text{ref}}=20$ mm). When exploring surfaces very curved ($R_{\text{ref}}=10$ mm), we suppose that both cutaneous and kinesthetic cues were strong, and participants can well combine them. Thus, if one of these cues is weaker, participants' perception precision should not significantly decrease. This may also explain why users had similar perception precision and accuracy with very curved surfaces in different softness conditions.

3.6.2 Impact of softness on precision (JND)

To propose an explanation of the impact of softness on JND as the surface becomes flatter, we use Hertz contact theory [208]. Hertz contact theory provides a model for the contact between two elastic bodies. Even though Hertz contact theory is a rough model of finger pad contact [317], it helps to understand the process when our finger touches soft curved surfaces. Based on Hertz contact theory, we can roughly simplify the contact and deformation between participants' finger pads and our curved surfaces as the contact and deformation between two elastic curved spheres [37, 387] with respectively the radius of $R_{\text{FingerPad}}$ and R_{Stimulus} , and Young's modulus of $E_{\text{FingerPad}}$ and E_{Stimulus} . The contact area between a finger and a curved soft stimulus can be approximated as a circle with the following radius r [37, 387]:

$$r = \left(\frac{3PR}{4E}\right)^{\frac{1}{3}} \quad (3.1)$$

Where P is the pressure that participants applied to the stimulus, R is the the relative radius of curvature, and E is the equivalent modulus. These variables depend on the radius and Young's modulus of participants' finger pad [317] and the stimulus: $E = (0.75(\frac{1}{E_{\text{Stimulus}}} + \frac{1}{E_{\text{FingerPad}}}))^{-1}$ and $R = (\frac{1}{R_{\text{Stimulus}}} + \frac{1}{R_{\text{FingerPad}}})^{-1}$.

To simplify the analysis of the impact of the stimulus curvature R_{Stimulus} and stimulus softness E_{Stimulus} on the deformation, we suppose that:

$$E_{\text{FingerPad}} = a E_{\text{Stimulus}}, \quad R_{\text{FingerPad}} = b R_{\text{Stimulus}} \quad (3.2)$$

Where a and b are participant-dependent constants. Then, the relative radius of cur-

vature R and the equivalent modulus E can be written as: $E = \frac{4a}{3(a+1)} E_{Stimulus}$, $R = \frac{b}{b+1} R_{Stimulus}$. Equation 3.1 can then be simplified as $r = \left(\frac{9b(a+1)}{16a(b+1)}\right)^{\frac{1}{3}} \left(\frac{PR_{Stimulus}}{E_{Stimulus}}\right)^{\frac{1}{3}}$. As $\left(\frac{9b(a+1)}{16a(b+1)}\right)^{\frac{1}{3}}$ is constant for each participant, we can set it as a constant C in the purpose of simplifying the analyze. Equation 3.1 can then be simplified as:

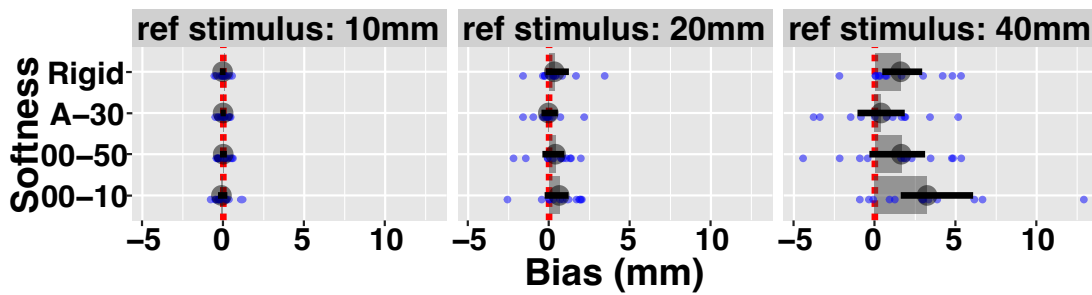
$$r = C \left(\frac{PR_{Stimulus}}{E_{Stimulus}}\right)^{\frac{1}{3}} \quad (3.3)$$

According to equation 3.3, either the increase of stimulus softness (i.e., smaller $E_{Stimulus}$) or the decrease of stimulus curvature (i.e., larger $R_{Stimulus}$) will lead to a larger contact area.

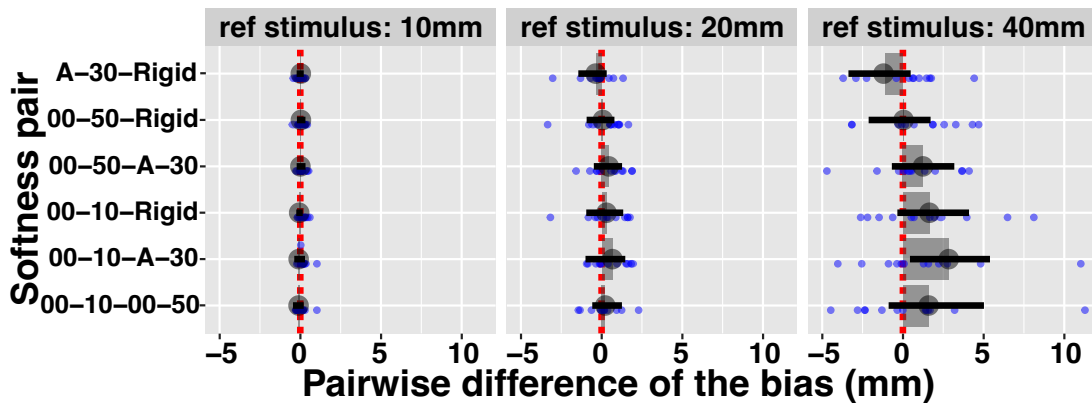
The JND power-law fit on Figure 3.4(b) shows that the softer the stimuli, the larger the exponent. In addition, all exponents were larger than 1. This suggests that, with a softer material, participants' curvature perception precision may more strongly decrease as the surface becomes flat. Also, the difference in perception precision between different softness conditions may be larger as the surface becomes flat. To better understand the impact of surface softness on contact area under different curvature conditions, we can calculate the derivatives of r over $E_{Stimulus}$:

$$\frac{\partial r}{\partial E_{Stimulus}} = -\frac{C}{3} (PR_{Stimulus})^{\frac{1}{3}} E_{Stimulus}^{-\frac{4}{3}} \quad (3.4)$$

According to equation 3.4, with flatter stimuli (i.e., larger $R_{Stimulus}$), the contact area increases more rapidly with softer stimuli (i.e., smaller $E_{Stimulus}$). This is consistent with our JND power-law fit result: Figure 3.4(b) suggests a larger difference in perception precision between different softness conditions as the surface becomes flatter. This might be explained by the surface and/or the finger pad deformation. On the one hand, a larger contact area slightly improves participants' perception precision [137] when passively touching rigid stimuli. On the other hand, the larger contact area means also bigger deformation of the stimulus and the finger pad. This deformation might inversely harm our perception of the shape, e.g., when stimuli are too flat and/or too soft. So far, this did not explain why participants could perform in soft conditions as precisely as in rigid conditions with our most curved stimuli ($R_{ref} = 10$ mm). We suppose the reason is that both cutaneous and kinesthetic cues were strong enough. A slight deformation of the stimulus and/or the finger pad should then not significantly decrease participants' precision.



(a) Perception bias in each CURVATURE and SOFTNESS.



(b) Pairwise difference in bias between two SOFTNESS for each CURVATURE.

Figure 3.8 – Perception bias (i.e., signed difference $PSE - R_{ref}$).

3.6.3 Similar accuracy with different softness

One of our main findings was that participants' perception accuracy did not differ systematically between different softness conditions in all curvature conditions. Yet, when exploring less curved surfaces, participants tended to be less accurate.

Previous work found factors possibly biasing participants' curvature perception accuracy with *rigid* stimuli. Among them, Vogels, Kappers, and Koenderink [470] observed bias from the shape of the surface around participants' fingers: they experimented with stimuli with double curved surfaces (e.g., spherical and elliptical), which can be defined by two principal curvatures. They found that the curvature in the direction perpendicular to participants' finger (radial–ulnar direction) biases participants' perception accuracy of the curvature along their finger (distal–proximal direction). E.g., their participant judged a curvature to be more convex when the perpendicular curvature was convex than when this curvature was concave. The fact that participants tended to be less accurate (i.e., larger absolute values bias) when exploring less curved surfaces in our experiment might

be explained by the bias of the shape of the surface around participants' fingers [470]. The deformation of stimuli and/or finger pads during the exploration may change the curvature distribution around participants' finger pads, as the surface is no longer a sphere. According to Hertz's contact theory [208], when exploring less curved surfaces (larger $R_{Stimulus}$ in equation 3.3), the deformation is larger (larger r in equation 3.3). This may explain the tendency for a lower accuracy.

The PSE indicates the curvature that participants subjectively feel equal to the corresponding reference curvature. To design accurate feedback with softness- and/or curvature-changing UIs, we should compensate for the difference between the real curvature and the curvature we expect participants will subjectively feel. For this reason, it is important to know whether systematic bias exists in any curvature and/or softness condition. Figure 3.8(a) shows the bias (i.e., the difference between PSE and the reference curvature) in each curvature and softness condition⁶. We can see that almost all error bars cross zero, except two in the flattest condition: For $R_{ref}=40$ mm, the bias for the Shore 00-10 material is 3.23 mm (CI [1.60, 6.07]), and the bias of the rigid material is 1.59 mm (CI [0.46, 2.93]). This indicates that, in average, participants overestimated the curvature of rigid and softest stimuli in the flattest condition. I.e. participants felt that a rigid stimuli with an actual radius of 43.23 mm was a radius of 40 mm, and that participants felt that a Shore00-10 stimuli with an actual radius of 41.59 mm was a radius of 40 mm. This suggested that we should shift very soft (Shore 00-10) or rigid UIs' curvature to less curved when developing nearly flat UIs ($R \approx 40mm$).

In our experiment, the loss in accuracy occurred only in two extreme softness conditions (i.e., Shore 00-10 and rigid) when discriminating the lowest curvatures ($R \approx 40mm$). In addition, the participants in average overestimated the curvature under these conditions only. A larger $R_{Stimulus}$ can lead to larger deformation, and thus more bias. Furthermore, in the two extreme softness conditions, the large difference of softness between finger pads and stimulus lead to great deformation of either the stimuli (Shore 00-10 condition) or the finger pad (Rigid condition). This may explain the bias specific to these conditions. To better understand the overestimation of curvature for these conditions, future work can consider techniques for modeling the finger pad deformation when pressing on a rigid surface [145]. In addition, Figure 3.8 show a large variation among participants (blue dots). This may be explained by participant-dependent constants a and b in equation 3.2.

6. Figure 3.5 shows the distance between PSE and the reference curvature, i.e. the absolute value of the difference between PSE and the reference curvature. Figure 3.8 shows the difference, which can be either negative or positive.

Modeling techniques [145] may also help future understanding of the variation among participants.

3.6.4 Slower exploration and higher difficulty with softer material

There is no prior work on the exploration time of soft and curvy surfaces. We found that participants' exploration time in the softest condition was longer than the rigid condition for all curvatures (for the first and second stimulus, and their average). At the same time, the increase of the exploration time was slow when surfaces become softer. We can explain the slow increase in exploration time thanks to prior work. Neurophysiologists found that the SAI afferents play a major role in the cutaneous cues to encode the object shape (i.e., surface curvature in our experiment) [1, 209]. Prior work passively applied surfaces with different curvatures on participants' finger pads with controlled force and recorded the response of SAI afferents [1]. They found that the form of stimulus-response functions (i.e., the number of responses of SAI to different curvature of stimulus) measured over 1s were similar to the responses measured over 0.2s. This suggested our tactile mechanoreceptors are capable of rapidly encoding surface curvature information (within 0.2s). We hypothesize that the rapid shape-encoding capability of our mechanoreceptors might rapidly provide us with important cutaneous cues to estimate the curvature when our finger pads first touches a surface of any softness. On the contrary to passive perception [1], active curvature perception involved both cutaneous and kinesthetic cues [116]. We suppose the poorer kinesthetic cues with softer stimuli (i.e., the larger deformation of stimuli leads to less height change during exploration) may play a major role in the increase of the exploration time. The fact that mechanoreceptors rapidly provide cutaneous cues may explain the slow increase of exploration time.

These two types of cues involved in curvature perception may also explain why participants estimate the discrimination difficulty to be larger in softer conditions. Participants perceived both kinesthetic and cutaneous cues for curvature discrimination. Both are affected by surface deformation and may hinder participants' discrimination. Future work can further study the impact of softness on participants' subjective difficulty to perceive curvature.

3.6.5 Different measures of softness

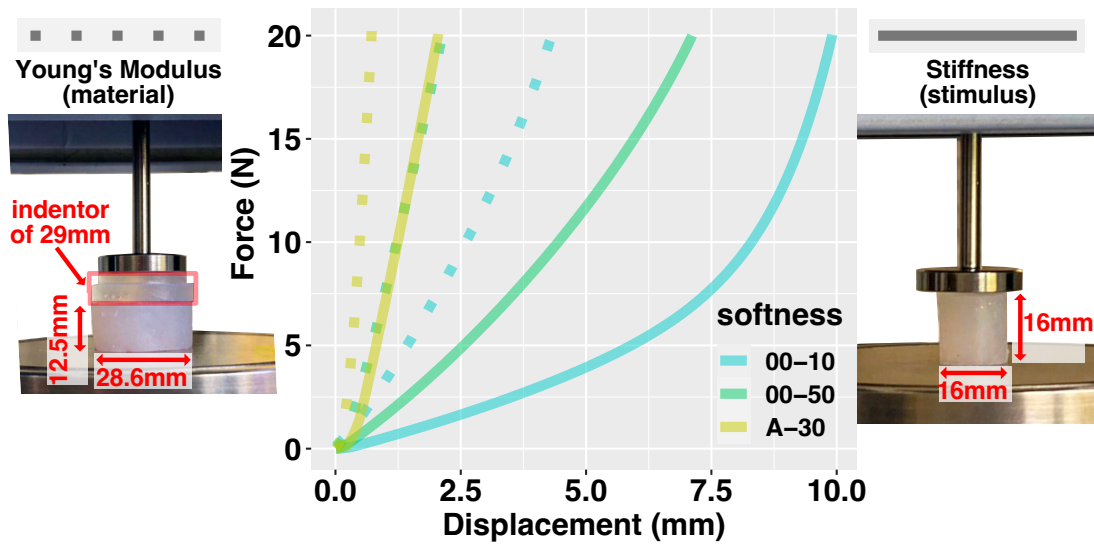
The softness of an object can express different physical quantity. First, the Young's modulus (E) of a material is the ratio between the pressure, i.e., the force per unit area (F/A) applied to the object and the strain, i.e., the relative deformation of the object ($\Delta l/l$): $E = \frac{F/A}{\Delta l/l}$ [438, 439]. The Young's modulus is a property of the material and is independent of the size and shape of the object.

Second, the stiffness (k) of an object is the ratio between the applied force and the deformation: $k = \frac{F}{\Delta l}$. The stiffness is a property of the object and depends on its shape and size. E.g., a silicone cylinder is half stiff as another silicone cylinder of the same material, if it has the same cross-sectional area but half the thickness [31].

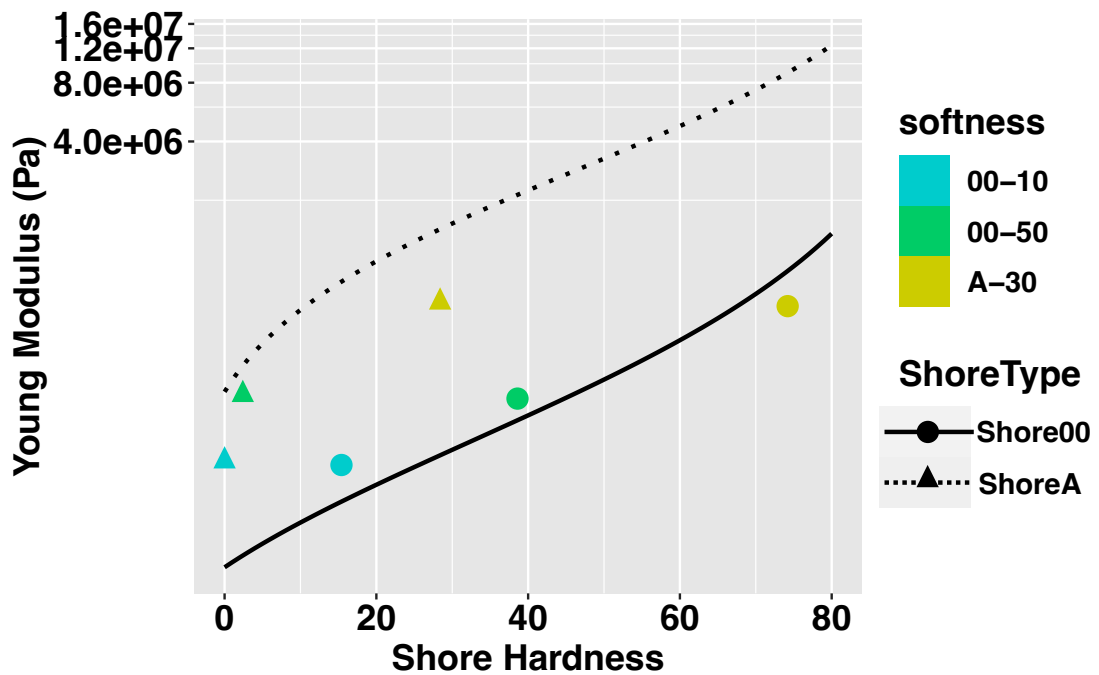
Bergmann Tiest and Kappers compared these two measures of softness [31]: they demonstrate the major contribution of the Young's modulus (E) for softness discrimination (90% on average) and show the less important contribution of stiffness (k) (10% on average).

Both the Young's modulus and the stiffness can be measured through compression tests. Such tests control the force applied and measures the resulting displacement while the material is compressed. We conducted compression tests to measure the stiffness of our stimuli and the Young's modulus of our materials (Figure 3.9(a)). We used a SHIMADZU Autograph AGS-X Precision Universal Tester [398]. We followed the standard procedure with a loading speed of 0.2 mm/s [439]. Figure 3.9(a) presents the force-displacement curves that we measured with test specimens made of the same silicone as our soft stimuli. We used linear least-square regression to determine the slope of these curves (as in [31]). Although we computed the stiffness k as the slope –as in the definition– we notice that this is an approximation: Figure 3.9(a) shows that the stiffness of the Shore 00-10 test specimen is nonlinear, i.e., the slope is not constant during the whole test. However, the R^2 of the linear least-square regression is 0.86 for Shore 00-10, which is acceptable. The regression for all other curves have $R^2 \geq 0.96$. We found the stiffness of the stimuli to be $k_{00-10} = 1.54Nmm^{-1}$, $k_{00-50} = 2.75Nmm^{-1}$, and $k_{A-30} = 10.70Nmm^{-1}$. We found the Young's modulus of each silicone to be $E_{00-10} = 0.088MPa$, $E_{00-50} = 0.193MPa$, and $E_{A-30} = 0.573MPa$.

Third, the Shore hardness is another measure of the softness of a material, similar to the Young's modulus. Shore hardness can be easily measured with a durometer. Compared with a compression test machine, a durometer is portable, cheap and does not need expertise for its operation. A compression test (Figure 3.9(a)) compress the whole test



(a) Compression tests: Young's Modulus (dotted line, left) measured following the standard [439]. The indenter is 3D printed with rigid resin; The stiffness (solid line, right) measured with specimens with the same dimension as the stimuli used in our experiment.



(b) Young's Modulus (predicted [278] and measured) vs. measured Shore 00 and Shore A hardness.

Figure 3.9 – Measurements of the softness of our stimuli.

specimen and measure the deflection of the whole specimen. In contrast, during a hardness test with a durometer, the surface of the indenter of a durometer, in contact with the test specimen, typically has a diameter ranging between 2.8 mm and 3.6 mm⁷[437]. The surface of the indenter of a durometer is smaller than the contact area between the participants' finger and the stimuli during our softness perception experiment. As opposed to the deflection of the whole specimen in a compression test (Figure 3.9(a)), the Shore hardness test measures the local deformation of the surface of the test specimen. There is no prior work studying participants' softness perception performance using Shore hardness as a measure of the softness of the stimuli. As a consequence, we do not know the respective contribution of the local deformation –Shore hardness– and the global deformation –Young's modulus– in users' softness perception. To help the design of soft UIs, designers can convert Young's modulus to Shore hardness and vice-versa [278]. The x axis of Figure 3.9(b) presents our measurements of the Shore hardness, with BAREISS HP Shore 00 and WALFRONT Shore-A durometers, following [439]. The y axis of Figure 3.9(b) presents the Young's modulus of the same object. The points in the graph show the Young's modulus we *measured* as in Figure 3.9(a). The lines in the graph show the Young's modulus we *predicted* using the existing conversion formula [278]. We found the Shore 00 hardness of each silicone to be $ShoreHardness00_{00-10} = 15$, $ShoreHardness00_{00-50} = 39$, and $ShoreHardness00_{A-30} = 74$. We found the ShoreA hardness of each silicone to be $ShoreHardnessA_{00-50} = 2$, and $ShoreHardnessA_{A-30} = 28$. The Shore 00-10 silicone is out range of a ShoreA durometer, which returns 0. Figure 3.9(b) shows that the Shore00 hardness highly correlate with the measured Young's modulus (correlation coefficient $r \geq 0.98$). In contrast, the formulas [278] did not fit well our Shore00 ($R^2=0.31$). The low R^2 might come from the small sampling size, i.e., only three data points [51]. For the measurement of Shore A, we do not study the correlation coefficient (r) and R^2 , as we had only two data points.

The non-linearity of stiffness during the compression (Figure 3.9(a)) impacts participants' perception of softness [340]. For this reason, we provide our whole force-displacement curve in addition to the three direct measurements of softness, i.e., Young's modulus, Stiffness, and Shore Hardness.

7. Different type of durometers have different dimension and form of indenter and used for measuring different scale of hardness. For example, a Shore 00 Durometer has a hemispherical indenter with a diameter of 2.38 mm and is typically used for testing extreme soft rubber, human and animal tissue, etc. A Shore A durometer has a truncated cone indenter with its top surface diameter of 0.79 mm and is typically used for testing harder rubber, leather, etc.

In our experiment, we chose the softness of our three soft stimuli based on the softness of the fingers pad, i.e., softer, as soft as, and harder than the index finger pad. We used the Shore hardness as a measure of softness, as it is convenient to measure on finger pads, contrary to other softness measurements. Meanwhile, there is no prior work on how the different measures of softness may impact our results. We provide different measures of softness, including Young’s modulus, Stiffness, and Shore hardness (both Shore A and Shore 00) with force-displacement curves, which should help other designers to build their devices based on our results.

3.6.6 Linearity of curvature and softness

For each CURVATURE condition, the curvature of comparison stimuli was linearly distributed around the reference curvature, as explained in [127]. The curvature of our reference stimuli was not strictly linear: 100 m^{-1} for $R_{\text{ref}}=10\text{ mm}$, 50 m^{-1} for $R_{\text{ref}}=20\text{ mm}$ and 25 m^{-1} for $R_{\text{ref}}=40\text{ mm}$. Figure 3.4(b) shows that the decrease of participants’ curvature perception precision, i.e., the increase of JND, was exponential and non-linear. This suggests an exponential decrease of curvature perception precision when the stimuli become flatter, consistent with [351, 352, 138, 255]. Besides the three conditions of curvature we studied, i.e., $R_{\text{ref}}=10\text{ mm}$, 20mm , and 40 mm , Provancher et al. also studied the condition with $R_{\text{ref}}=30\text{ mm}$. We did not study the condition of $R_{\text{ref}}=30\text{ mm}$ to reduce the total experiment time (around 4h). We found the exponent in the softness condition of the rigid stimuli was 1.45, which is similar to the exponent of 1.43 in [351, 352]⁸. This suggested that we can use our power fitted curve (Figure 3.4(b)) to predict the JND in curvature condition not studied in our experiment despite the non-linearity of the distribution of the curvature of our stimuli, in particular with rigid stimuli whose curvature range is located between our studied values, i.e., R_{ref} from 10 mm to 40 mm .

In our three soft conditions, the JND also increased exponentially with respective exponent: 1.61 for Shore 00-10, 1.70 for Shore 00-50, and 1.76 for Shore A-30. This suggests a higher non-linear increase of JND with a softer surface: the softer the surface, the more the participants’ curvature perception precision decrease as the surface becomes flat. The respective Young’s modulus of the three soft stimuli were $E_{00-10} = 0.088\text{ MPa}$, $E_{00-50} = 0.193\text{ MPa}$, and $E_{A-30} = 0.573\text{ MPa}$, whose distribution is not linear. We noticed however that the exponents of the three JND curves (1.76 for Shore 00-10, 1.70

8. The exponent is computed with the JND data provided in [351, 352].

for Shore 00-50, 1.61 for Shore A-30) seem linearly distributed according to the three Young's modulus ($R^2=0.92$). However, further experiments are necessary to confirm this through the study of users' curvature perception with additional softness levels.

3.7 Guidelines for soft curvy devices

This experiment provides quantitative data to design precise and accurate haptic feedback with soft curvy UIs. First, users can perceive with high precision and accuracy in the most curved condition ($R \approx 10$ mm) with any softness. Designers can use material of any softness to construct very curved UIs (radius ≈ 10 mm) for the most precise and accurate haptic feedback. In average, users can distinguish the surface curvature with a precision of 0.63 mm (CI=[0.53,0.78]) and an accuracy of 0.31 mm (CI=[0.26,0.38]). On the contrary, when UIs are less curved (radius ≥ 20 mm), designers should avoid using very soft material (softness $<$ Shore 00-50) or dynamically stiffen the UI to reach a softness \geq Shore 00-50. If the UI cannot change its softness, designers should provide a curvature change larger than the JND measured (Figure 3.4(b)) in corresponding softness and curvature condition, to ensure the curvature change is perceived. For example, a UI with a radius ≈ 20 mm should bend or flatten more than 2.72 mm if softer than Shore 00-50, and more than 2.00 mm if softer than Shore A-30.

Second, users can perceive the curvature of a very curved surface more accurately. The average accuracy of participants is 0.31 mm (CI=[0.26,0.38]) in $R_{\text{ref}} = 10$ mm; 0.90 mm (CI=[0.69,1.15]) in $R_{\text{ref}} = 20$ mm; 2.67 mm (CI=[2.13,3.49]) in $R_{\text{ref}} = 40$ mm. As a consequence, for better accuracy of curvature-based haptic feedback, designers should focus on the highest curvatures. At the same time, users can perceive the curvature of a surface with similar accuracy in all softnesses. This suggests that using stiff –or stiffening– material without changing the UI curvature will not improve users accuracy. When designing soft curvature-changing UIs, designers can fully focus on the interaction design and the application context, without worrying about the softness of a specific material: the softness will not have a significant impact on the output accuracy of the UI.

We observed a systematic curvature overestimation of 3.23 mm (CI=[1.60,6.07]) in the softest and flattest curvature. If designers cannot avoid these softness and curvature but still require accurate curvature feedback, they can offset by 3.23 mm the curvature of very soft and flat UIs (e.g., with a radius > 40 mm and softness \approx Shore 00-10). Providing an even flatter surface ($R=43.23$ mm) will be perceived as a curvature of $R= 40$ mm.

Third, users need longer exploration time to perceive the curvature of softer surfaces. Users took in average 3.95s to explore a Shore 00-10 curvature vs. 3.39s to explore a rigid curvature. This suggests that stiffening the UIs [107] will enable more rapid feedback. If UIs cannot change their softness, the time between each refresh of UIs' curvature may need to be longer than the exploration time we measured. For instance, the curvature refresh rate of UIs softer than Shore 00-10 may need to be lower than 0.25 Hz, 0.27 Hz for UIs softer than Shore 00-50, and 0.28 Hz for UIs softer than Shore A-30 respectively. This is an opportunity for *slow* [149] ambient on-body feedback supporting long-term interaction.

3.8 Applications: Building precise and accurate interactive devices

Recent work explored interactive devices where the softness plays an important role [117]. We now show how our measurements of users' precision, accuracy and speed when perceiving the curvature of soft devices, inform the design of efficient haptic display through curvature and softness for such devices.

First, recent work presented technologies to vary participants' perception of softness of objects (e.g., Shore hardness of objects [434]). Recent work also proposed devices with different softness, e.g., different Shore hardness (e.g., [228]), different Young's modulus [340], or different stiffness [418]. We provide the measurements of the Young's modulus (Figures 3.9(a) and 3.9(b)), Shore hardness (Figure 3.9(b)), and stiffness (Figure 3.9(a)) used in our experiment, so that designers can directly apply our results when building their own soft devices. We summarize these findings in Table 3.1 to quickly enable precise and accurate curvature perception of future devices.

Second, we further distinguish three cases for the application of our results to current devices: (1) augmenting daily objects, building devices with (2) customized softness and shape, and (3) with changing softness and shape.

3.8.1 Augmented daily objects

Leveraging daily objects for interaction enable ubiquitous devices [121, 382]. VR systems can now scan users' surroundings to find daily objects with the most similar shape to the object manipulated in VR [165]. This reduces the visual-haptic mismatch,

Table 3.1 – Correspondence table for designers of novel soft and curvy devices.

		SOFTNESS			CURVATURE (radius in mm)	PRECISION (mm)	ACCURACY (mm)	TIME (s)
Shore hardness		Stiffness (N.mm-1)	Young's modulus (MPa)	Jamming vacuum (inHg) [418]				
00-10	N.A.	1.54	0.088	0	10	0.75	0.41	3.46
					20	2.63	1.13	4.04
					40	8.61	3.46	4.37
00-50	A-02	2.75	0.193	0	10	0.68	0.34	3.43
					20	2.72	1.03	3.79
					40	7.14	3.01	3.80
00-74	A-30	10.70	0.573	15	10	0.53	0.24	3.20
					20	2.03	0.58	3.65
					40	4.98	2.24	3.68
Rigid					10	0.58	0.25	3.21
					20	1.97	0.83	3.54
					40	4.31	1.95	3.98

i.e., the mismatch between what users see in VR and what they touch and manipulate physically. Current technology (e.g., [24, 96]) also automatically measures the softness of objects. This can provide VR systems with softness information about surrounding daily objects. Our results help designers to fine-tune their algorithm to better choose soft objects in users' surroundings for haptic feedback in VR. For instance, when choosing a very soft and flat UIs (e.g., with $R > 40$ mm and \sim Shore 00-10), the algorithm can choose an even flatter surface ($R = 43.23$ mm) to provide a curvature perception of $R = 40$ mm.

In addition, prior work proposed a technique changing users' perceived softness of daily objects by controlling the expansion of the finger pad [434]. This device allows to change the perceived hardness \geq Shore A-50 to \approx Shore A-40. This range of softness is within the range of our experiment, i.e., between Shore A-30 and rigid. Their device leaves the center of the finger pad free, which allow users to directly perceive the curvature of the object. Our study informs future work with such devices by allowing the prediction of users' perception of the curvature of objects according to their perceived softness. For instance, when touching an object of curvature $R = 10$ mm with the device, designers can expect 0.53-0.58 mm precision and 0.24-0.25 mm accuracy in curvature perception.

3.8.2 Devices with custom softness and shape

3D printing eases the building of personal interactive devices [289] with complex geometric shape (e.g., [448]) and embedded interactive capabilities (e.g., [198]). 3D printing now also enables the customization of softness [228, 279, 448, 265, 340] to reach the desired haptic properties. Our results allow designers to predict users' accuracy and precision of curvature perception when manipulating 3D printed soft objects. For instance, OmniSoft [228] allows to build devices in the range of Shore A-02 to Shore A-30 –a range included in our experiment. Our results now extend Omnisoft with information about users perception of the object's local curvature depending on its local softness.

Our results can also be readily used together with a new model that converts a softness, e.g., a Young's modulus, into an infill geometry ensuring the same perceived softness [340]. Using our measurements of the Young's modulus (Table 3.1) as an input to the model, our results now extend this prior work with the corresponding users' precision and accuracy in perception of the object's local curvature depending on its local softness.

3.8.3 Devices with changing softness and shape

Prior work enabled devices capable of changing their softness, e.g., through jamming [418, 107]. Adding a jamming layer on top of an existing shape-changing device such as LayerPump [120], dynamically changeable buttons [157, 132], the inflatable hemispherical display [423], PneuUI [509], AirPinch [133], MultiJam [507], Pneumatic Auxetics [93], StringTouch [374], or PneuSeries [59], allows building devices providing haptic feedback through both softness and shape. The jamming layer can follow the shape of the shape-changing device, thanks to its malleability prior to jamming [418, 509]. By controlling the vacuum level in the jamming layer [418, 107], a device can change its softness: the higher the vacuum level, the stiffer the jamming layer.

Our results can be used to refine the design of such devices. We illustrate this on the example of a device that changes its curvature and softness through pneumatic actuation and a jamming layer [418]. Figure 3.10 shows two sets of force-displacement curves: one (in gray) that we reproduce from [418], and the other (in color) that we measured as in [418] with our specimen made of silicone of different softness. To measure the force-displacement, we used the same indenter as in [418], i.e., a printed rigid sphere with a diameter of 9.5 mm (Figure 3.10, right). We can see in Figure 3.10 that the force-displacement measurements of the jamming layer at the 15 inHg level of vacuum overlaps

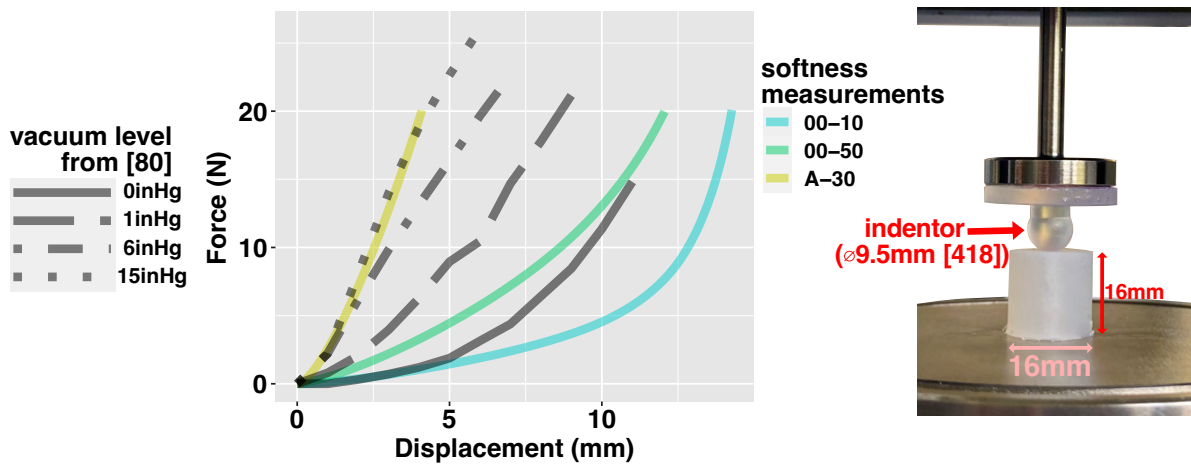


Figure 3.10 – (Left) Force displacement curves resulting from (right) compression tests with a 3D printed spherical indenter as in [418]. Colored lines show our results on a specimen with the same dimensions as the stimuli used in our experiment. Gray lines show prior results [418] from compression test on a jamming layer. The level of vacuum are expressed in inches of mercury (inHg). The larger the value, the higher the vacuum and the stiffer the UI.

with our Shore A-30 specimen measurements. In addition, the 0 inHg level of vacuum partially overlaps with Shore 00-10 specimen measurements when the displacement of the indenter is < 5 mm. We can also see that the measurements of our Shore 00-50 lie between the jamming layer at 0 and 1 inHg. This suggests that a jamming layer with a vacuum level between 0 and 1 inHg might produce force-displacement measurements that overlap or partially overlaps with the measurements of our Shore 00-50. Based on Figure 3.10, we can now predict the precision and accuracy in curvature perception of such a device changing its curvature and softness. For instance, a curved UI with a jamming layer like [418] at 15 inHg of vacuum should provide users with similar curvature perception precision and accuracy as our stimuli in Shore A-30 condition (Table 3.1). When the vacuum level is at 1 inHg, the UI should provide better curvature perception precision than our Shore 00-50 stimuli, in particular when the UI surface is very flat (e.g., with a radius > 40 mm). When the vacuum level is at 0 inHg, the UI should provide similar curvature perception precision and accuracy as our Shore 00-10 stimuli, if users' fingers do not press too deep into the UI (e.g., ≤ 5 mm).

3.9 Conclusion

In this chapter, we addressed user behavior challenges of SCI research by isolating a new factor, softness, imported by programmable soft materials into SCIs development and studying its impact on users' shape perception abilities of UIs. We experimented to assess the accuracy (point of subjective equality), precision (just noticeable difference), and exploration time when perceiving the curvature of UIs across four levels of softness. Our results reveal six new findings.

- Users perceive our curviest surfaces (surface radius $R \approx 10mm$) as precisely (JND ≈ 0.63 mm) in different softness conditions.
- Users perceive our middle curved surfaces ($R \approx 20mm$) 25% more precisely in the two least soft conditions (JND $\approx 2mm$) compared to the two softest conditions (JND $\approx 2.68mm$).
- Users perceive our least curved surfaces ($R \approx 40mm$) in the softest condition (JND= 8.61 mm) with half the precision of the rigid condition (JND= 4.31 mm).
- Users perceive curvier surfaces with better accuracy, from 2.67 mm to 0.31 mm.
- Users perceive surface curvature with similar accuracy in different softness conditions.
- Users perceive 17% slower all curvatures in the softest condition (3.95 s) compared to the rigid condition (3.39 s).

HCI designers can readily use the resulting guidelines to design efficient soft curvature-changing UIs. If feedback precision is crucial, designers should focus on very curved UIs ($R \approx 10mm$), where any softness can provide users with precise haptic curvature information. Alternatively, if designers need a larger range of curvatures, designers should change the stiffness to little rigid material (Shore A-30 in Figure 3.1). If feedback accuracy is crucial, designers should focus on very curved UIs ($R \approx 10mm$). Stiffening the material cannot improve the accuracy. If UIs need a high curvature refresh rate (e.g., $> 0.25Hz$), designers should use materials of softness $> Shore 00-10$ (Figure 3.1), and keep very soft curvature-changing UIs for a slower refresh rate.

As discussed in Chapter 2, the versatility of curvature-changing UIs extends to various other types of SCIs. The HCI community can build upon this work to design SCIs with soft materials, incorporating different soft shape-changing abilities. In the subsequent chapters (Part II), we will address technological challenges in SCIs research. More specifically, we propose a series of shape-changing modules in Chapter 4 to facilitate researchers

developing diverse SCIs using programmable soft materials to create diverse SCIs and introduce a novel technology in Chapter 5 that enables UIs to change both their curvature and softness/strength.

PART II

Technological explorations

SOFTMORPHEES: HIGH SHAPE RESOLUTION SOFT SHAPE-CHANGING MODULES

4.1 Introduction

In Chapter 2, we comprehensively reviewed different technologies using programmable soft materials to realize different shape-changing features of Morphees+ taxonomy [226]. The lack of a toolkit for HCI researchers to realize all or most shape-changing features is one of the technological challenges in HCI. Certain technologies, such as PneuUI [509], enable the creation of more shape-changing features, i.e., *Size*, *Curvature*, *Zero-crossing*, and *Closure* (refer to Figure 2.2(c), 2.5(b), 2.9(c) and 2.10(a)) by combining rigid materials (e.g., paper) and soft materials (e.g., silicone elastomer). However, these approaches rely on the non-stretchable nature of rigid materials, such as paper, to achieve the intended shape-changing features. This reliance could compromise the stretchability and deformability of the UIs themselves. Moreover, isolating factors when conducting experiments with such UIs was recognized as a grand challenge in SCIs research [10]. Current prototypes lack material/technological consistency, making it difficult to avoid confounding factors in experiments can thus suffer from user behavior challenges. Using the same materials and technology for different shape-changing features can help address this challenge as only a single factor remains: the design, with a single material/technology.

Instead of directly developing the SCIs toolkit, we start with a technological exploration of novel materials to answer an essential question: what shape changes can be realized with programmable soft materials? Recent advancements in programmable soft materials like Baromorph [402] provide the possibility to realize various shape changes involving purely soft materials(Figure 2.6(e)). In this chapter, primarily based on Baromorph, we try to develop a technology using only soft materials, i.e., elastomers, to cover

as many Morphees+ features as possible. We currently create *SoftMorphees*, a series of shape-changing modules encompassing six out of the eleven Morphees+ shape-changing features, exclusively utilizing soft materials, i.e., *Size*, *Curvature*, *Amplitude*, *Porosity*, *Closure* and *Zero-crossing*. We also provide their feature measurements under different air pressures with respective regression equations to facilitate other researchers' designs. They can pave the way from a technological aspect to develop further a toolkit for HCI researchers to create their soft SCIs with desired shape changes, which can help lower the barrier to constructing SCIs. Meanwhile, using the same materials and technology for different shape-changing features can help address the challenges of isolating factors when conducting experiments on users' experiences with different SCIs [10]. Additionally, we discussed the challenges associated with existing technologies for developing SCIs using only soft materials.

4.2 Related work

Emerging SCIs with programmable soft materials were created in recent years [376, 363]. However, challenges [10] still exist for developing SCIs, including the need for toolkits for developing different SCIs. As presented in Chapter 2, bi-layer structures, i.e., bonding two layers with different stretchability, are commonly seen in HCI research for creating different shape changes. For example, Yao et al. [509] embedded non-stretchable papers into elastomers bladders to limit their stretches in some designed directions to realize *Size*, *Curvature*, *Zero-crossing* and *Closure* controlling. Similarly, Kilic Afsar et al. [225] braided non-stretchable nylon sheaths around silicone tubes to limit their expansion in some designed directions to realize *Size*, *Curvature*, *Zero-crossing* and *Closure*. However, the bi-layer structures have an intrinsic limit [337] in creating curved surfaces other than cylindrical surfaces 2.6, as discussed in Section 2.1.2. Furthermore, the involvement of non-stretchable materials could compromise the stretchability and deformability of the UIs themselves.

Recently, a series of toolkits [227, 518, 266, 78] for developing SCIs were developed for facilitating the prototyping barrier [10]. Most were built by connecting a few primitive modules with simple shape-changing abilities to realize other shape changes. For example, Martinez Castro et al. [266] glued a few elastomer bending actuators (like Figure 2.5(a)) under fabric to actuate it forms a planar plane to a surface with various *Zero-crossing* values. Cui et al. realize different shape-change UIs by connecting a few

two length-changing elastomer bladders with origami structures embedded inside (like Figure 2.2(c)) together. For example, they bonded two length-changing elastomer bladders to form a bi-layer structure that can bend to one side and change the *Curvature* when the pressure inside one bladder changes. Different from them, Kim et al. developed a toolkit, MorpheesPlug [227], includes six different primitive 3D-printable shape-changing modules, providing designers with more primitive shape-changes. Their modules cover five different Morphees+ shape-changing features, including *Size*, *Curvature*, *Amplitude Closure*, and *Porosity*. *Zero-crossing* is realized by connecting a few primitive modules, i.e., connecting a few *Amplitude* changes modules together and using a few actuators separately inflating them.

Similar to MorpheesPlug [227], we developed a series of primitive shape-changing modules, *SoftMorphees*, to realize different shape-changes, covering six out of the eleven Morphees+ shape-changing features, i.e., *Size*, *Curvature*, *Amplitude*, *Porosity*, *Closure* and *Zero-crossing*. They will serve as the technological foundation to develop a SCIs toolkit with novel programmable soft materials. Different from [227], our module (Figure 4.12(b)) can realize multiple *Zero-crossing* values, i.e., 0,1,2,3,4, with only one actuator, which can help to reduce the bulkiness. Furthermore, we can build thinner prototypes compared with MorpheesPlug [227]. MorpheesPlug [227]’s structures need to be thick, as their structures have little shape-change when the thickness is less than 2 cm. However, the thinness of UI is important, particularly for wearable applications [112]. The modules that we developed in this chapter are approximate 5 mm thin (Figure 4.2(c), 4.3(c), 4.5, 4.7), 4.8(c), 4.9(c), 4.10(c), 4.11 and 4.12(b)). In section 6.4, we further present our instructions to fabricate thinner prototypes with a thickness of 3 mm.

4.3 SoftMorphees

This section presents the technology *SoftMorphees*, mainly based on the new soft material, Baromorph [402]. We developed a group of pneumatically actuated shape-change modules to address 6 among 11 different shape-change features of Morphees+ [226] using only soft materials (elastomers), i.e., *Size*, *Curvature*, *Amplitude*, *Porosity*, *Closure* and *Zero-crossing*. We also developed new technologies to address the *Strength* and *Stretchability* changing features, Jamming Origami Endoskeleton, which concerns using rigid materials (Mylar plastic sheets) as jamming media. We will present it in Chapter 5. As for the *Modularity* changing feature, it is practical to realize it by connecting different

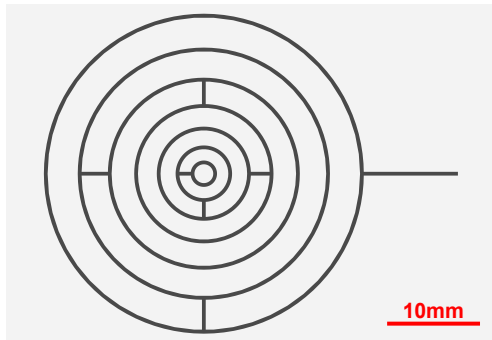
pneumatically actuated modules with tubes, solenoid valves, or other sophisticatedly designed electronic-free modules [257] as previously discussed in section 2.1.10. The *Speed* feature is orthogonal to other shape-changing features [227]. Our prototypes are actuated by pneumatical inflation whose *Speed* depends on air pressure and pumps' flow rate controlling [401] rather than our UIs' design. For this reason, we will not address the *Speed* feature here.

4.3.1 Fabrication

We first briefly introduce the fabrication procedures of our prototypes before presenting different prototypes for different shape-changing features. You can also find a video of the Baromorph fabrication tutorial in [373]. Baromorph's fabrication contains three major steps:

1. **Mold design and printing:** Siéfert et al. suggested that one main factor impacting the shape of a Baromorph [402] plate after pressurization is the density of air channels, i.e., larger channels density lead to larger stretch strain. This is the basic principle of designing a Baromorph's mold. Figure 4.1 presents one Baromorph and its air channels pattern and mold as an example. It has a larger air channel density in the center than in the edge (Figure 4.1(a) and 4.1(c)), leading to larger stretch strain in the center than in the edge when inflated (Figure 4.1(d)).
2. **Elastomer structures molding:** We mold the elastomer structures with the silicone elastomers. We also fabricated a membrane with the same silicone to be sealed with the molded part.
3. **Assembling:** Finally, we glue the membrane and molded part together to make the prototype airproof by spreading a thin film of uncured silicone of the same type.

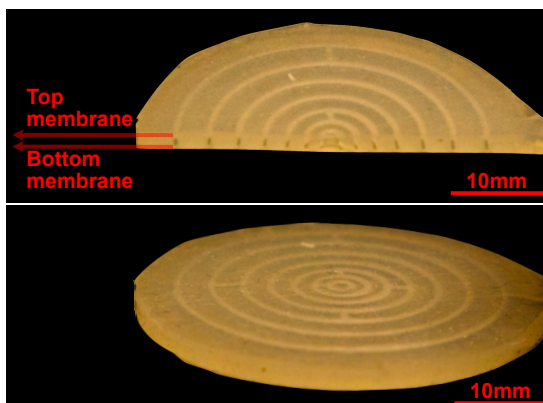
Prototypes presented in this chapter are all molded using DragonSkin10NV [191] as it provided a trade-off between large shape-changing ability and fast curing and fabrication. Their molds are printed with photo-polymer resin (Formlabs standard clear resin [368]) using a stereo-lithography 3d printer (Formlabs Form3 [109]) to ensure the printing precision. To measure the shapes of our prototypes, we use a Panasonic Lumix G Hybrides camera with a LUMIX G VARIO 14-140 lens (Focal length $f=135$ mm, resolution 1096×2160) to take photos of our prototypes with different inner air pressures. Then, we detect



(a) Air channels pattern of a Baromorph whose density of air channels (rings) progressively increases from the edge to the center with the distance between air channels decreasing from 3.2 mm to 1.2 mm. Bars between rings are auxiliary channels connecting them. The far right bar is an auxiliary channel to insert a needle as an air inlet and outlet.



(b) A Baromorph mold 3D printed with a Form3 high precision Stereolithography (SLA) 3D printer [109] in clear resin [368].



(c) Bottom: a Baromorph fabricated with the mold as presented in Figure 4.1(b) using DragonSkin10 NV silicone [191]. Top: A Baromorph cut in the middle. We can see two membranes covering air channels. One is directly molded together with air channels during the molding step. One is glued to the molded part after demolding.



(d) The Baromorph inflates with an inner air pressure of 12 Psi. We can see that the membrane covering air channels stretch in the center more than in the edge. This leads to the inflated Baromorph having a larger slope in the center than in the edge.

Figure 4.1 – An example Baromorph with its air channels pattern and mold.

and analyze their contours with OpenCV [315]. Details of measurement can be seen in appendix A.3.

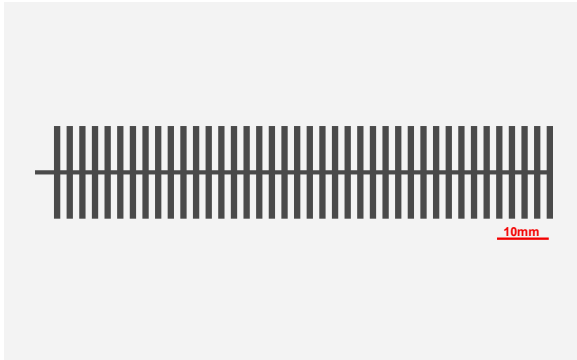
4.3.2 Size

The *Size* features are categorized into three subtypes: Length, Area, and Volume, which often exhibit correlations. In this section, we explicitly present two prototypes, i.e., one majorly increases its size in one direction when pressurized, leading to *Length* increase, and one majorly increases its size in two orthogonal directions in a plan when pressurized, leading to *Area* increase.

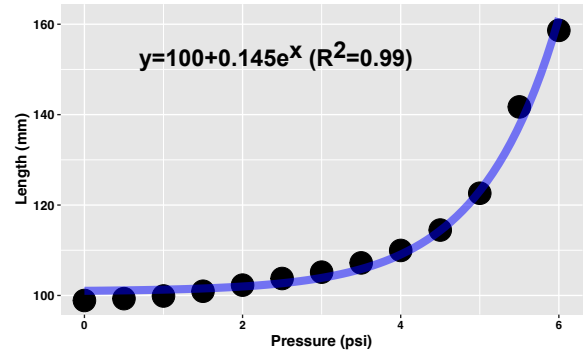
Length

Figure 4.2(a) presents the patterns of air channels in this Baromorph capable of increasing its *Length* as inner air pressure increases. In this prototype, the width of air channels is equal to 1.2 mm, the same as the distance between channels, i.e., the width of the walls between channels. In the original concept of Baromorph [402], Baromorphs usually have thicker an external wall compared with the thickness of walls between channels, for limiting their in-plane expansion when pressurized but bulging out in the perpendicular direction instead. For example, Figure 4.1 presents a prototype with walls thickness ranges from 1.2 mm to 3.2 mm while having the thickness of the external wall as 4 mm. In this *Length* increasing prototype, it needs to have its external silicone walls thin enough to facilitate in-plane expansion. For this reason, we design this prototype with the external wall's thickness to be the same as air channel distance, i.e., 1.2 mm. The thickness of the top and bottom membranes was also designed to have the same thickness of 1.2 mm. Together with the 3 mm thick air channels, the total thickness of this prototype is 5.4 mm. Figure 4.2(b) presents the measurement of this prototype's length under different air pressures, and Figure 4.2(c) presents its photos under different air pressures. When air pressure increases from 0 Psi (Pound per square inch) to 6 Psi, its *Length* increases by 60% from 99 mm to 159 mm. With Figure 4.2(b) and 4.2(c), we can see that its *Length* increases more rapidly as the air pressure becomes larger. Meanwhile, we can see the prototype starts to curve (indicated in dashed white circles in Figure 4.2(c)) from 5.0 Psi. I will further discuss its curving in section 4.4.5.

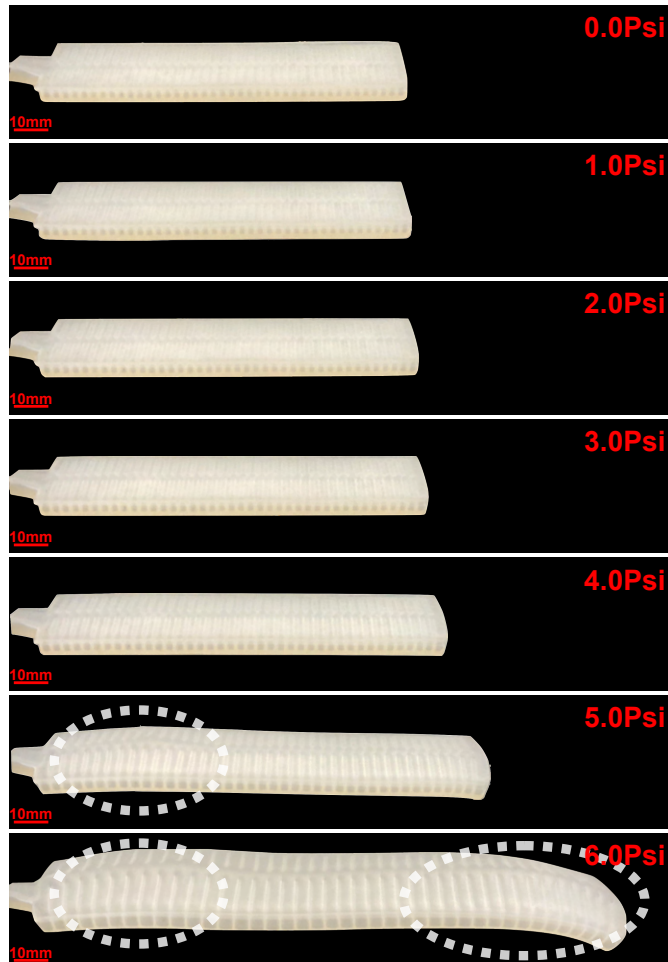
An exponential function can well fit its *Length* increase by air pressure with a R^2



(a) Air channels pattern of our *Length* changing prototype.



(b) Length of *Length* changing prototype under different air pressures and respective regression.



(c) Photos of *Length* changing prototype under different air pressures.

Figure 4.2 – *Length* changing prototype. Dashed white circles show that the prototype starts curving when inner pressure reaches 5.0 Psi.

(Coefficient of determination) equal to 0.99:

$$Length = 100 + 0.145e^{Pressure} (R^2 = 0.99), 0Psi \leq Pressure \leq 6Psi \quad (4.1)$$

Area

Figure 4.3(a) presents the patterns of air channels of a prototype capable of increasing its *Area* as inner air pressure increases. We get inspiration from [125] to design its zig-zag shape air channels for in-plane expansion in two orthogonal directions. Same as *Length* increasing prototype (Figure 4.2), we design this prototype's external wall with a thickness of 1.2 mm, same as its air channel distance. Figure 4.3(b) presents the measurement of this prototype's area under different air pressures, with Figure 4.3(c) presenting respective photos. When its inner pressure increases from 0 Psi to 2.5 Psi, its *Area* increases by 26% from 2044 mm^2 to 2566 mm^2 . In this air pressure range, an exponential function can well fit its *Area* increase by air pressure with a R^2 larger than 0.99:

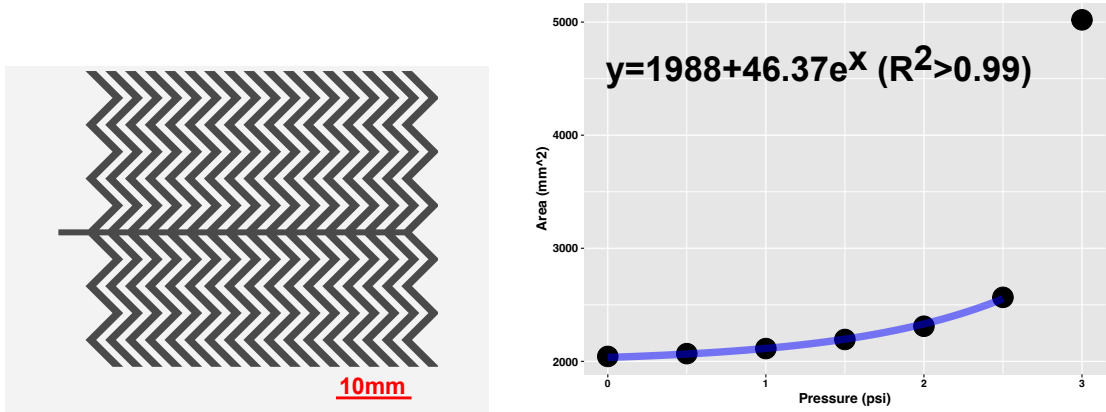
$$Area = 1988 + 46.37e^{Pressure} (R^2 > 0.99), 0Psi \leq Pressure \leq 2.5Psi \quad (4.2)$$

Increasing its inner pressure to 3.0 Psi will lead to approximately doubling its *Area* to 5012 mm^2 and a clear curving up from this plane. I will further discuss its curving in section 4.4.5. Including this data point, an exponential function fits worse the *Area* increase with a R^2 equal to 0.83. Further increasing its inner pressure to larger than 3.0 Psi has led to the prototypes' fragmenting. The 3.0 Psi is thus near the maximum pressure this prototype can support.

Currently, we focus on prototypes with changing *Size* in-plane, i.e, 1D *Length* changing and 2D *Area* changing. *Volume* changing structures with size changing in all three dimensions using soft materials can be achieved by inflating an elastomer bladder like inflating a balloon [119].

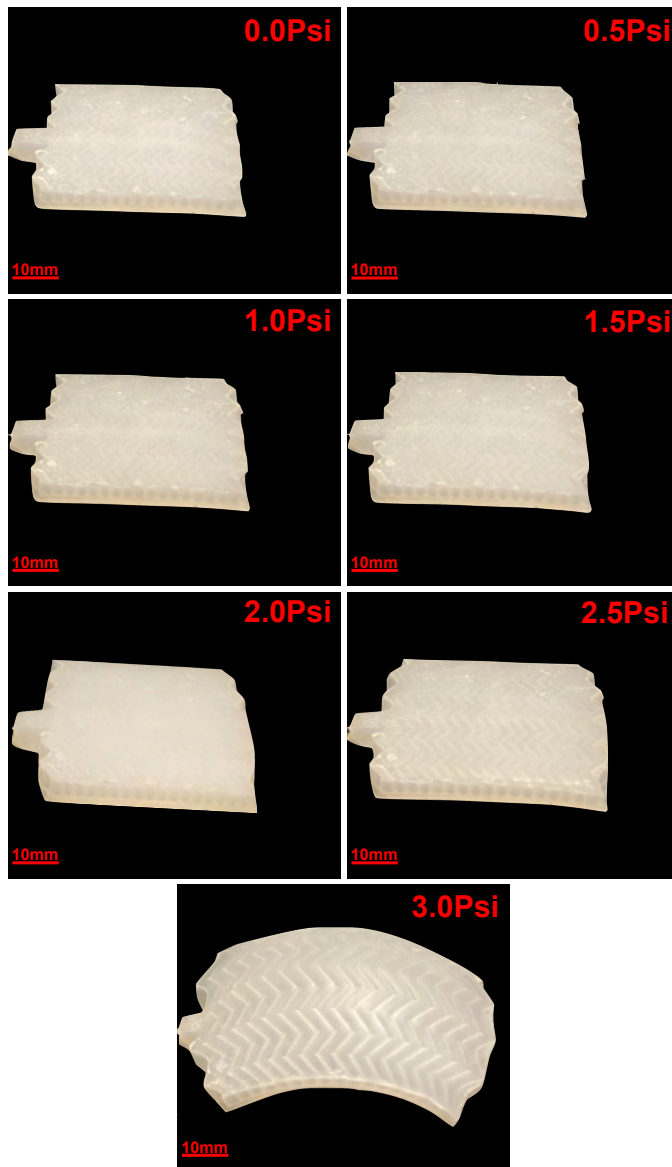
4.3.3 Curvature

As presented in Figure 2.6(e), Baromorph can create both surfaces with positive Gaussian curvature (either concave or convex domed shape) and with negative Gaussian curvature (saddle shape). We developed two prototypes capable of increasing their *Curvatures* from flat shapes (0 curvature) to convex domed shapes (positive curvature). Figure 4.4(a) presents the patterns of air channels of these two prototypes. We create these patterns



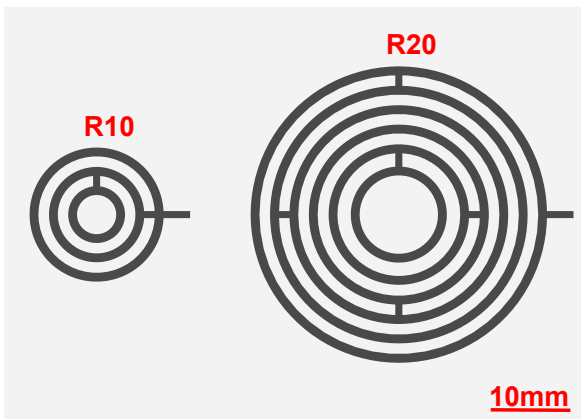
(a) Air channels pattern of Area changing prototype.

(b) Area of Area changing prototype under different air pressures and respective regression.

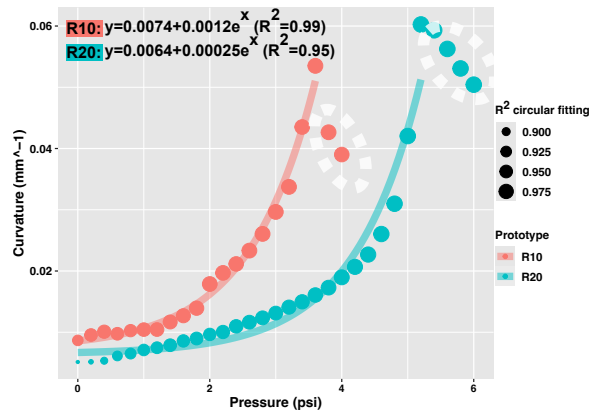


(c) Photos of Area changing prototype under different air pressures.

Figure 4.3 – Area changing prototype under different air pressures.



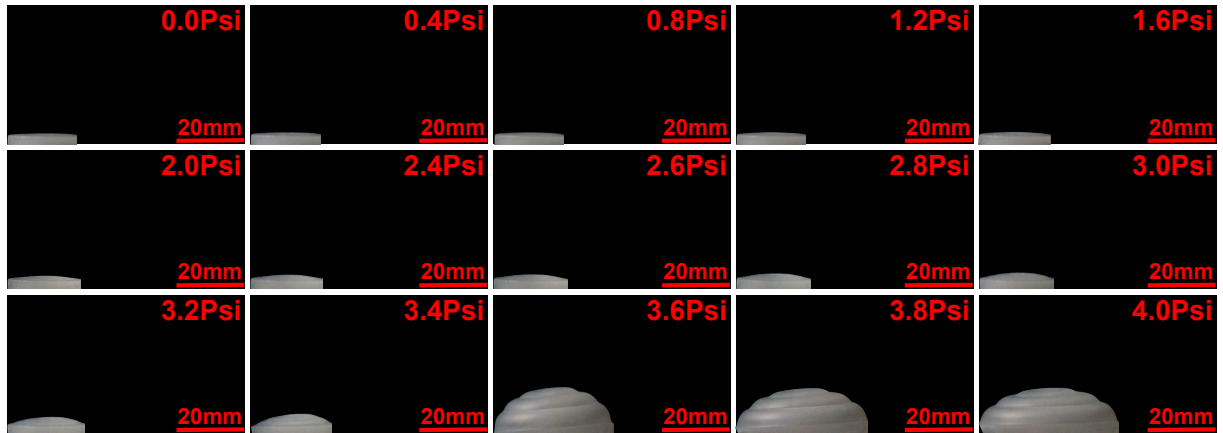
(a) Air channels pattern of *Curvature* changing prototype. The left one (R10) is created based on the contour lines of a demi sphere with a radius of 10 mm, and the right one (R20) is based on the contour lines of a demi sphere with a radius of 20 mm.



(b) Curvature of *Curvature* changing prototypes under different air pressures and respective regression. Points sizes indicate the R^2 values of circular fitting [214] to calculate their *Curvatures*. At the beginning of inflation, prototypes are nearly flat and thus poorly fitted by a circle with respectively small circular fitting R^2 . Points in dashed white circles are excluded from regression fitting. In these points, our prototypes' *Curvature* stop to increase (decrease instead) as pressure increases and result in poor regression fitting.

Figure 4.4 – *Curvature* changing prototypes under different air pressures.

R10 Prototype



R20 Prototype

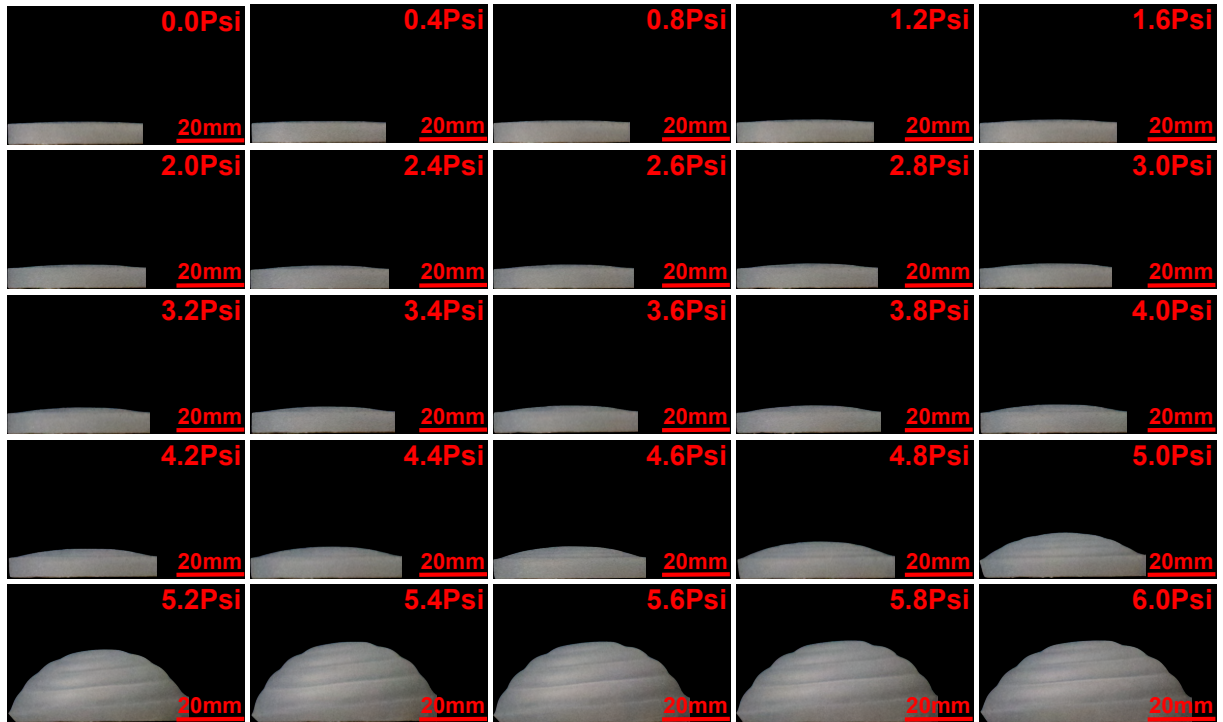


Figure 4.5 – Photos of *Curvature* changing prototype under different air pressures.

by projecting an objective 3D shape on a plane to get its contour lines as the shape of air channels as proposed in [402]. The air channels (R10 Prototype) on the left in Figure 4.4(a) are based on the contour lines of a demi sphere with a radius of 10 mm with

a few auxiliary channels (i.e., bars between rings) connecting them. Figure 4.4(a) right presents air channels (R20 Prototype) based on the contour lines of a demi sphere with a radius of 20 mm . Figure 4.5 presents photos of these two prototypes with different inner air pressures. Figure 4.4(b) presents the *Curvature* measurement of these two prototypes with different inner air pressures. We calculate their curvature by circular fitting [214] the contours of their top surfaces, which is detected using the OpenCV 4.6.0 [315]. Figure 4.5 and 4.4(b) indicates that *Curvature* of these two prototypes increases more rapidly as the air pressure becomes larger before arriving at their maximum *Curvature*. The R10 prototype arrives at its maximum *Curvature* of $0.054mm^{-1}$ (i.e., radius of 18.7 mm) with inner air pressure of 3.6 Psi and the R20 prototype arrives at its maximum *Curvature* of $0.06mm^{-1}$ (i.e., radius of 16.6 mm) with inner air pressure of 5.2 Psi. Before arriving at their maximum values, the following exponential functions can well fit their *Curvature* increase by air pressure.

R10 Prototype:

$$Curvature = 0.0074 + 0.0012e^{Pressure} (R^2 = 0.99), 0Psi \leq Pressure \leq 3.6Psi \quad (4.3)$$

R20 Prototype:

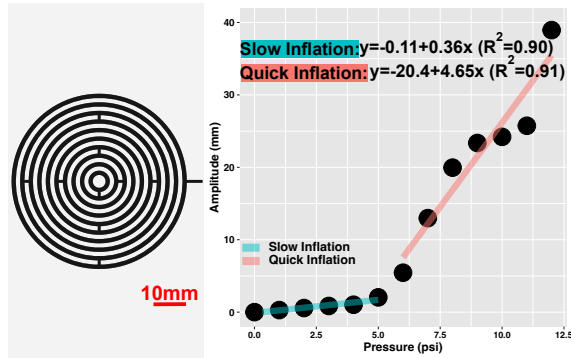
$$Curvature = 0.0064 + 0.00025e^{Pressure} (R^2 = 0.95), 0Psi \leq Pressure \leq 5.2Psi \quad (4.4)$$

When reaching their maximum *Curvature*, further increasing the air pressure will reversely decrease their *Curvature*.

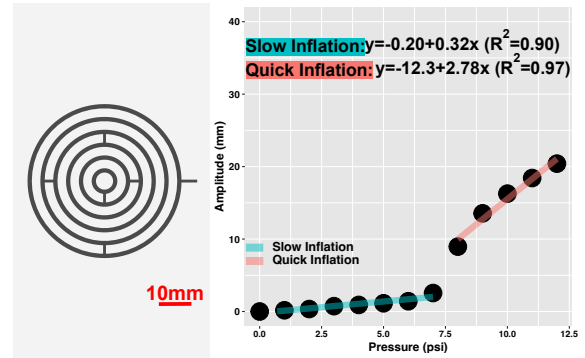
We have currently developed these two flat to convex domed shapes prototypes; we leave for future work prototypes to create other types of curved shapes like concave domed shapes and saddle shapes with precise *Curvature* controlling and prototypes with different *Curvature* distribution over the surface like the one shown in Figure 4.1(d) and 1.3.

4.3.4 Amplitude

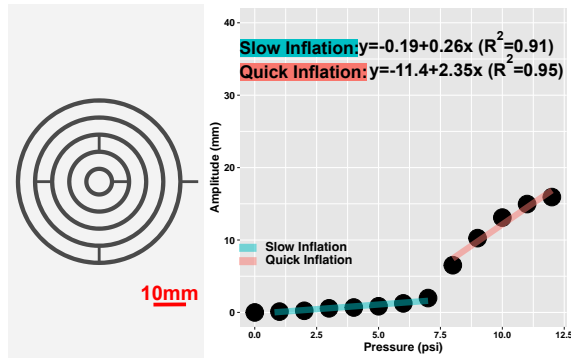
A larger Baromorph's channel density can lead to larger stretch strain [402]. Thus, under the same pressure condition, higher channel density will lead to larger *Amplitude* change when its radial expansion is limited by its external wall [402]. Here, we created a series of 5 prototypes with different channel densities by varying the distance between channels, i.e., the width of the walls between channels. On the left of Fig-



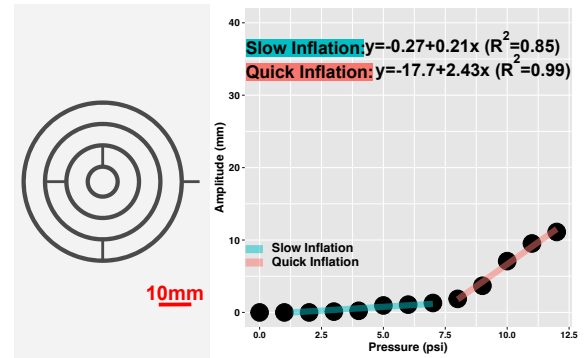
(a) *Amplitude* changing prototype with Wall-AirChannels width ratio of 1. Left: Air channels pattern. Right: *Amplitude* values under different air pressures and respective regression.



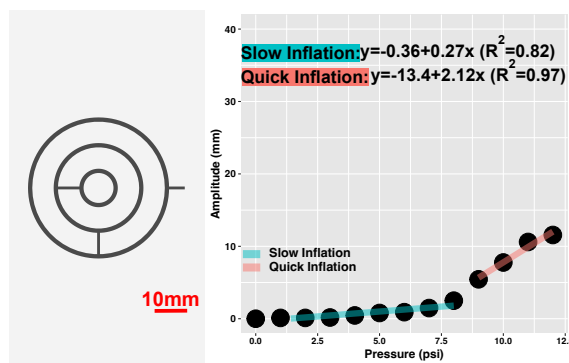
(b) *Amplitude* changing prototype with Wall-AirChannels width ratio of 2. Left: Air channels pattern. Right: *Amplitude* values under different air pressures and respective regression.



(c) *Amplitude* changing prototype with Wall-AirChannels width ratio of 3. Left: Air channels pattern. Right: *Amplitude* values under different air pressures and respective regression.



(d) *Amplitude* changing prototype with Wall-AirChannels width ratio of 4. Left: Air channels pattern. Right: *Amplitude* values under different air pressures and respective regression.



(e) *Amplitude* changing prototype with Wall-AirChannels width ratio of 5. Left: Air channels pattern. Right: *Amplitude* values under different air pressures and respective regression.

Figure 4.6 – *Amplitude* changing prototypes with different Wall-AirChannels thickness ratios under different air pressures.

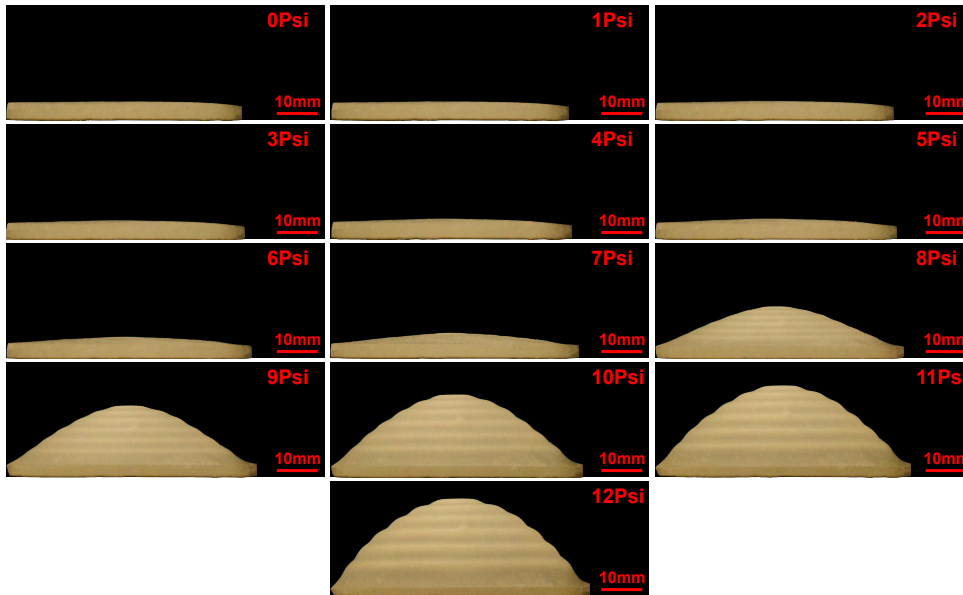


Figure 4.7 – Photos of *Amplitude* changing prototype (Wall-AirChannels width ratio of 2) under different air pressures

ures 4.6(a), 4.6(b), 4.6(c), 4.6(d), 4.6(e), we present air channels shape patterns of these Baromorphs. They all have the same width of air channels as 1.2 mm, and the distance between air channels varies from 1.2 mm to 6 mm with respective Wall-AirChannels width ratio being 1, 2, 3, 4 and 5. On the right of Figures 4.6(a), 4.6(b), 4.6(c), 4.6(d), 4.6(e), we present the measurement these Baromorphs' *Amplitude* with different inner air pressures and respective regression result. In these figures, we can see that our prototypes' *Amplitude* increases more rapidly as the air pressure becomes larger, while exponential functions can not well fit each prototype's *Amplitude* in different air pressure conditions with small R^2 values of around 0.6. In contrast, we can see that there exists a pressure threshold for each prototype, i.e., 5 Psi for Wall-AirChannels width ratio 1 prototype, 7 Psi for ratios 2, 3, and 4 prototypes, and 8 Psi for ratio 5 prototype. Before the threshold, each prototype's *Amplitude* increases slowly, and after the threshold, their *Amplitude* increases quickly. Separately considering these two regions for each Baromorph, linear functions can well fit their *Amplitude* increase by air pressure.

Wall-AirChannels width ratio 1 prototype:

$$Amplitude = \begin{cases} -0.11 + 0.36 \times Pressure (R^2 = 0.90), & 0Psi \leq Pressure \leq 5Psi \\ -20.4 + 4.65 \times Pressure (R^2 = 0.91), & Pressure > 5Psi \end{cases} \quad (4.5)$$

Wall-AirChannels width ratio 2 prototype:

$$Amplitude = \begin{cases} -0.20 + 0.32 \times Pressure (R^2 = 0.90), & 0Psi \leq Pressure \leq 7Psi \\ -12.3 + 2.78 \times Pressure (R^2 = 0.97), & Pressure > 7Psi \end{cases} \quad (4.6)$$

Wall-AirChannels width ratio 3 prototype:

$$Amplitude = \begin{cases} -0.19 + 0.26 \times Pressure (R^2 = 0.91), & 0Psi \leq Pressure \leq 7Psi \\ -11.4 + 2.35 \times Pressure (R^2 = 0.95), & Pressure > 7Psi \end{cases} \quad (4.7)$$

Wall-AirChannels width ratio 4 prototype:

$$Amplitude = \begin{cases} -0.27 + 0.21 \times Pressure (R^2 = 0.85), & 0Psi \leq Pressure \leq 7Psi \\ -17.7 + 2.43 \times Pressure (R^2 = 0.99), & Pressure > 7Psi \end{cases} \quad (4.8)$$

Wall-AirChannels width ratio 5 prototype:

$$Amplitude = \begin{cases} -0.36 + 0.27 \times Pressure (R^2 = 0.82), & 0Psi \leq Pressure \leq 8Psi \\ -13.4 + 2.12 \times Pressure (R^2 = 0.97), & Pressure > 8Psi \end{cases} \quad (4.9)$$

In Figure 4.7, we present the photos of a prototype with the Wall-AirChannels width ratio of 2 under different pressure conditions as an illustration.

4.3.5 Porosity

Here, we present two prototypes capable of changing the *Porosity* when inner air pressures change. One is inspired by the ventilation flaps (Figure 2.8(b)) introduced in [475], which can be curved up over a hole that they covered to increase the *Porosity*. One is based on the *Length* changing prototype that we presented before (Figure 4.2), which can increase their length to cover a hole to decrease the *Porosity*.

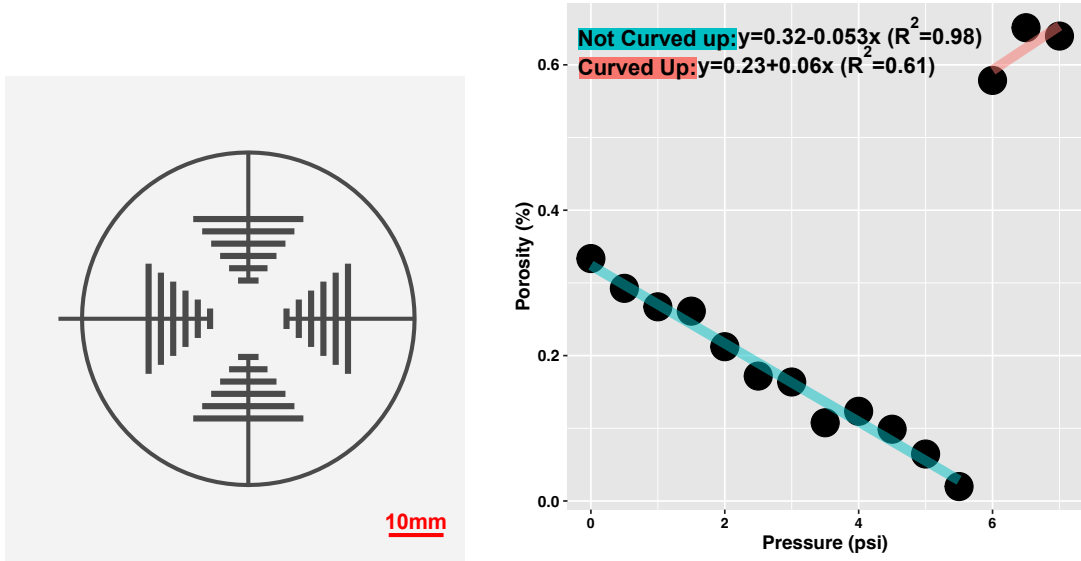
Porosity change via curving flaps

Figure 4.8(a) presents the air channels pattern of the *Porosity* changing via curving flaps prototype. To make sure the flaps bend upward instead of bending downward, this prototype's bottom membrane is designed to be slightly thinner than its top membrane as 1 mm vs. 1.2 mm. Together with air channels' thickness of 3 mm, this prototype's total thickness equal to 5.2 mm. It has four flaps connected. To facilitate the flaps' bending up, we slightly cut off some silicone around each flap, which leaves some spaces around them. This makes it have a small original *Porosity* as 0.3% before increasing inner air pressure (Figure 4.8(b) and 4.8(c)). Figure 4.8(c) presents photos of this prototype with different inner air pressures. In each pressure condition, we present two photos of our prototypes. The top one is taken over the prototype, which is used then for calculating the *Porosity*, and the bottom one is taken from the side of the prototype to visualize the flaps' curving up. Figure 4.8(b) presents the measurement of *Porosity* under different air pressures. From these two figures, we can see that, before flaps bend out of the original plane at 6.0 Psi, flaps inflate as air pressure increases, progressively decreasing its porosity from 0.3% to 0.02%. At 6.0 Psi, flaps' bending out increases porosity to increase to 0.6%. Further increasing the air pressure to 6.5 Psi leads to the porosity increasing to 0.7%, while increasing the air pressure further to 7.0 Psi will reversely lead to its porosity decrease to 0.6% as flaps inflate and cover the hole in the center. Before flaps' bending out at 6.0 Psi, a linear function can well fit the prototypes' *Porosity* change by air pressure with a R^2 as 0.98, while it fits much worse after 6.0 Psi with a R^2 as 0.61:

$$Porosity = \begin{cases} 0.32 - 0.053 \times Pressure (R^2 = 0.98), & 0Psi \leq Pressure < 6Psi \\ 0.23 + 0.06 \times Pressure (R^2 = 0.97), & Pressure \geq 6Psi \end{cases} \quad (4.10)$$

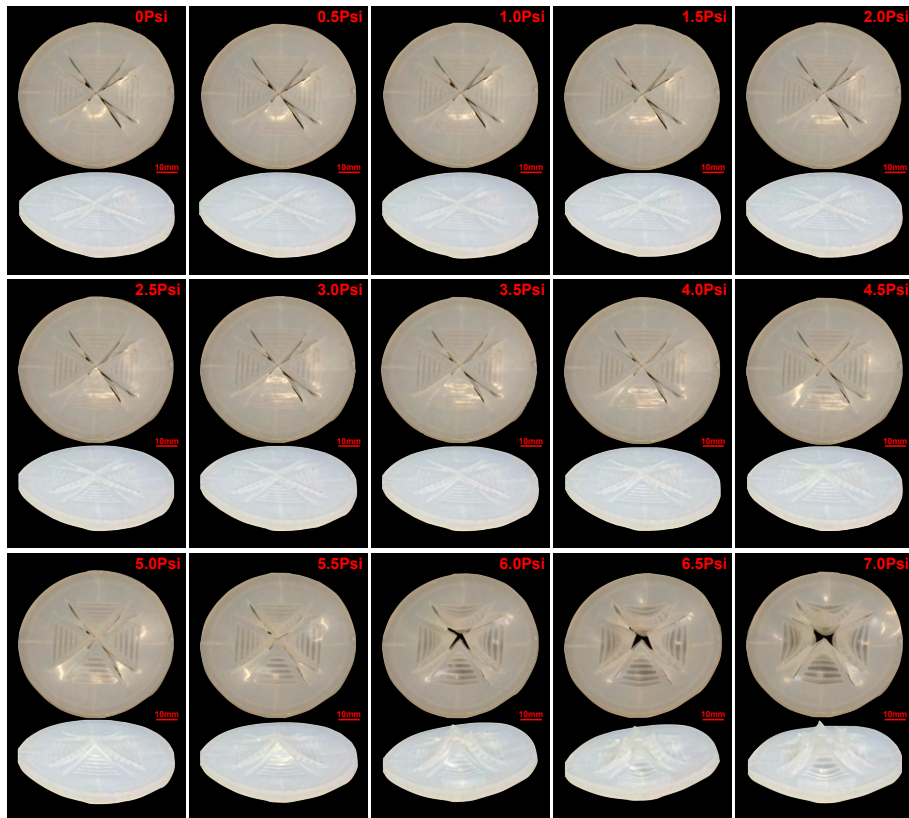
Porosity change via length change

In section 4.3.2, we have already presented the prototype capable of increasing its *Length* as inner pressure increases. We develop a *Porosity* changing prototype with flaps capable of increasing their lengths to fill a hole in the center (Figure 4.9(c)). Figure 4.9(a) presents the air patterns of this prototype. It comprises two flaps capable of increasing their *Length* as pressure increases. Same as earlier presented *Length* increasing prototypes, this prototype's top and bottom membrane thickness is designed to be the same, i.e., 1.2 mm. Together with air channels's thickness of 3 mm, this prototype's total thickness



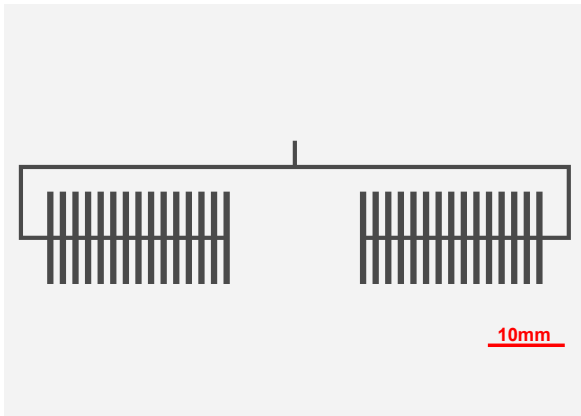
(a) Air channels pattern of *Porosity* changing via curving flaps prototype.

(b) *Porosity* measurements of *Porosity* changing via curving flaps prototype under different air pressures and respective regression.

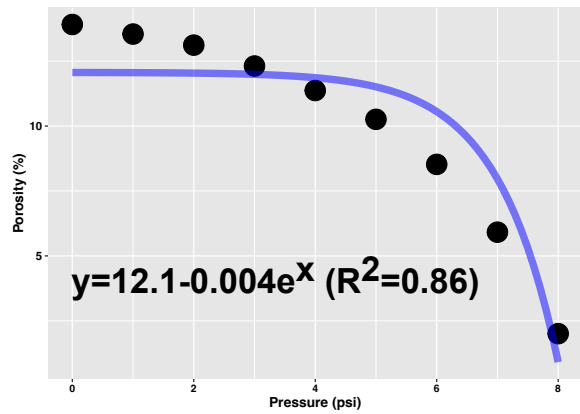


(c) Photos of *Porosity* changing via curvature prototype under different air pressures. In each pressure condition, we present two photos of our prototypes. The top one is taken over the prototype, and the bottom one is taken from the side of the prototype.

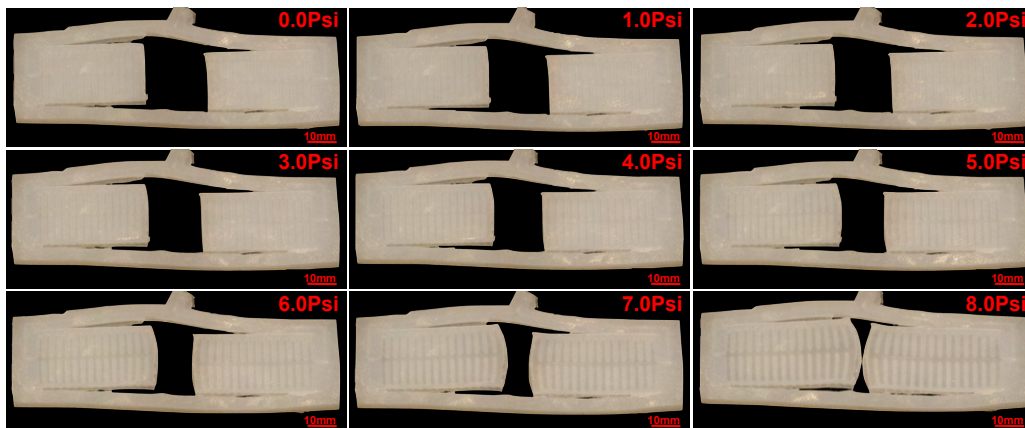
Figure 4.8 – *Porosity* changing via curving flaps prototype.



(a) The shape pattern of air channels of *Porosity* changing via length change prototype.



(b) Porosity of *Porosity* changing via length change prototype under different air pressures and respective regression.



(c) Photos of Porosity of *Porosity* changing via length change prototype under different air pressures.

Figure 4.9 – *Porosity* changing via length change prototype under different air pressures.

equal to 5.4 mm. Figure 4.9(c) presents photos of this prototype with different inner air pressures. Similar to the *Porosity* changing via curving flaps prototype (Figure 4.9(c)), we slightly cut off some silicone around each flap to facilitate their movement. Figure 4.9(b) presents its *Porosity* measurement with different inner air pressures. With pressure increases from 0 Psi to 8 Psi, the *Length* increases of two flaps, making the hole between them smaller, leading its *Porosity* to decrease from 14% to 2%. At 8 Psi, the two flaps start to contact each other, and its *Porosity* thus arrives at the minimum value. Further pressure increase will lead to flaps' tilting as shown in Figure 4.9(c) the prototype with an inner pressure of 9 Psi. Before flaps' tilting, we can roughly use an exponential function to fit its *Porosity* change by air pressure with a R^2 as 0.86:

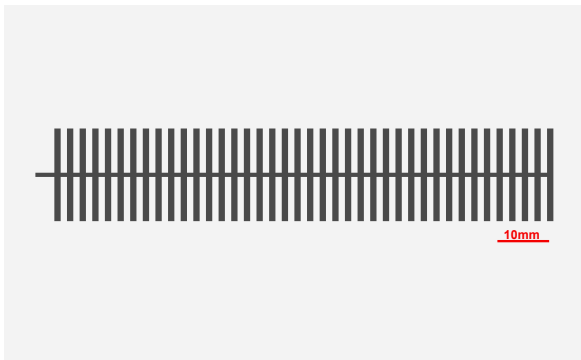
$$Porosity = 12.1 - 0.004e^{Pressure} (R^2 = 0.86), 0Psi \leq Pressure \leq 8Psi \quad (4.11)$$

We choose an exponential function here to fit the *Porosity* as it is based on our technology of *Length* changing (Figure 4.2), which can fit well with an exponential function ($R^2=0.99$). Future work should further study better functions to fit its *Porosity* change.

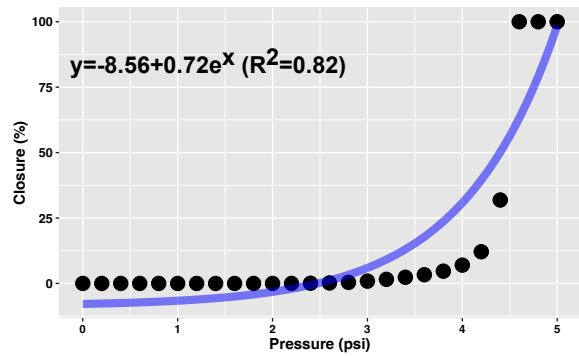
The earlier presented *Porosity* changing via curving flaps prototype (Figure 4.9(c)) is capable of decreasing its *Porosity* from 0.3% to 0.02% before flaps bending out and then increasing the *Porosity* to a maximum value of 0.7% with flaps bending out, which lead to prototypes' thickness increasing approximately 20 mm. Compared with it, this *Porosity* changing via length change prototype presents a larger *Porosity* controlling range from 14% to 2% without increasing the prototype's thickness.

4.3.6 Closure

Figure 4.10(a) presents the air channels pattern of our prototype of *Closure* changing. This is the same as our *Length* changing prototype shown in Figure 4.2(a). We use the same mold to fabricate these two prototypes. The difference between them is that our *Length* changing prototype's top and bottom membranes have the same thickness of 1.2 mm, while the *Closure* changing prototype has different membrane thickness, one of 1.2 mm and one of 1.0 mm, which enable its bending to the thicker membrane side when inner pressure increases. Figure 4.10(c) presents photos of this prototype under different pressure conditions. Figure 4.10(b) presents the measurement of its *Closure* under different pressure conditions. From these two Figures, we can see that before 2.4



(a) The shape pattern of air channels of *Closure* changing prototype.



(b) Closure of *Closure* changing prototype under different air pressures and respective regression.



(c) Photos of *Closure* changing prototype under different air pressures.

Figure 4.10 – *Closure* changing prototype under different air pressures.

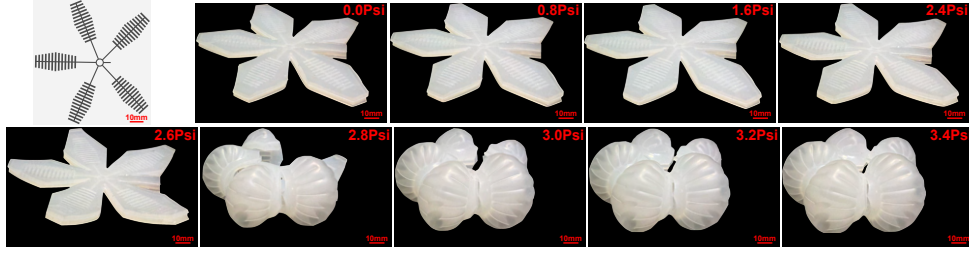


Figure 4.11 – Air channel pattern and photos of *Closure* changing flowers

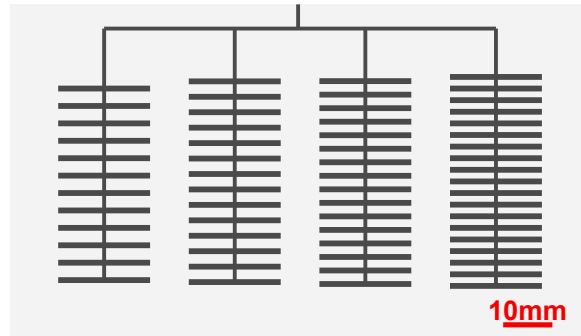
Psi, the prototype barely bends, which leads to its *Closure* staying at 0. It starts to curve at 2.4 Psi, which leads to the increase of *Closure*, and we can see that its *Closure* increases more rapidly as the air pressure increases. When pressure arrives at 4.4 Psi, its *Closure* reaches 30%. Then, further increasing the pressure to 4.6 Psi leads to the two extremities contacting each other, leading to a *Closure* value of 100%. We further discuss the sudden change in its shape in section 4.4.2. We can roughly fit its *Curvature* increase by air pressure using an exponential function with the R^2 as 0.82:

$$Closure = -0.85 + 0.72e^{Pressure} (R^2 = 0.82), 0Psi \leq Pressure \leq 5Psi \quad (4.12)$$

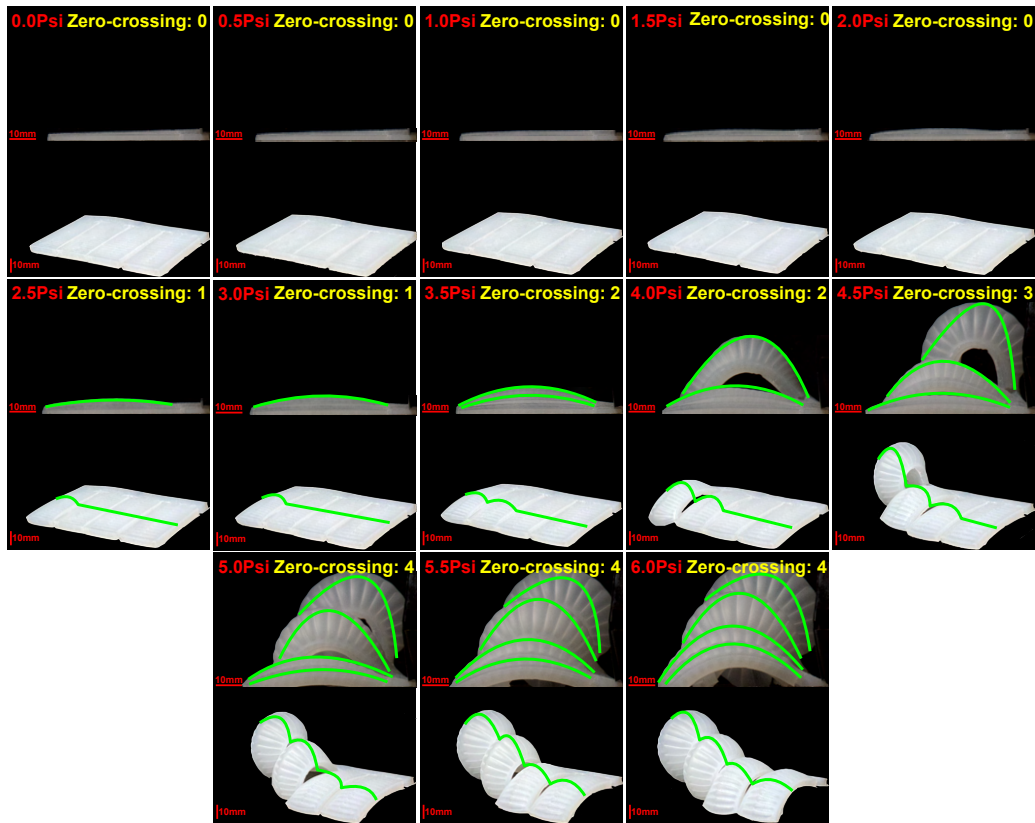
Based on this prototype, we construct a flower with 5 bendable petals (Figure 4.11) to change their *Closure*, which is inspired by [510]. Similar to the prototype shown in Figure 4.11, its *Closure* suddenly increases to nearly 100% when pressure arrives at a certain level, i.e., 2.4 Psi. We will discuss it in section 4.4.2.

4.3.7 Zero-crossing

As shown in Figure 4.10(c), the prototype starts curving until its inner air pressure arrives at a certain level, i.e., 2.4 Psi for this prototype. We also find that varying the Wall-AirChannels width ratio can impact the pressure that a prototype needs to start curving, i.e., a larger Wall-AirChannels width ratio will lead to the need for larger air pressure for bending it. Based on this, we connected four bendable structures similar to the one presented in Figure 4.10 with different Wall-AirChannels width ratios, i.e., 1, 1.33, 1.66, and 2 as four branches. Their air channel widths are all 1.2 mm, while their distances between channels are different, i.e., 1.2 mm, 1.6 mm, 2 mm and 2.4 mm. Figure 4.12(a) presents the air channels pattern of our *Zero-crossing* changing prototype.



(a) The shape pattern of air channels of *Zero-crossing* changing prototype.



(b) Photos of *Zero-crossing* changing prototype under different air pressures. In this pressure condition, we present two photos of the prototype: the top one taken from a side and the bottom one taken above it. Green curves in the side-view photos (Top) indicate the curved surfaces of branches bent after inflation, and green curves in the above-view photos (Bottom) indicate the surface shape with zero-crossing points greater than 0.

Figure 4.12 – *Zero-crossing* changing prototype under different air pressures.

Same as the *Closure* changing prototype, our *Zero-crossing prototype* has different top and bottom membrane thickness, i.e., the top membrane of 1 mm and the bottom membrane of 1.2 mm. Figure 4.12(b) presents photos of our prototypes with different inner air pressures. We present two photos for each pressure condition: the top one taken from a side and the bottom one taken above it. From this figure, we can see that when the pressure arrives at 2.5 Psi, with the Wall-AirChannels width ratio = 1 branch starts to curve up, leading the prototype's *Zero-crossing* increasing from 0 to 1. The ratio = 2 branch curves at 3.5 Psi, leading the prototype's *Zero-crossing* to increase from 1 to 2. The ratio = 3 branch curves at 4.5 Psi, leading the prototype's *Zero-crossing* to increase from 2 to 3. Finally, at 5.0 Psi, all branches curve up, leading to the prototype's *Zero-crossing* increasing from 3 to 4. Compared to previous related work in section 2.1.5, our prototype provides a solution for creating UIs with multiple *Zero-crossing* values needing only a single actuator.

4.4 Discussion

This section discusses existing challenges and future work for developing UIs with different shape-changing features using programmable soft materials.

4.4.1 Toolkit for programming SCIs with novel programmable soft materials

In Figure 2.20, the significance of curvature change is evident, playing a pivotal role in the creation of diverse SCIs, including *Amplitude*, *Porosity*, *Zero-crossing* and *Closure*. Adopting bi-layer structures in SCIs has attracted substantial attention from HCI researchers. Numerous software tools have been developed to facilitate the utilization of these technologies by designers, as demonstrated by previous works [318, 225, 256, 476, 510, 474]. Emerging programmable soft materials, exemplified by Baromorph [402], offer substantial potential for realizing intricate surface shapes, especially with complex curvature distributions, such as the human face mask illustrated in Figure 2.6(e). To achieve objective surface morphing using Baromorph from a planar plate, Siéfert et al. proposed projecting the intended surface shape onto a plane. This process generates contour lines representing the air channels of a Baromorph plate. Notably, the density of contour lines or air channels correlates with the steepness of the slope on the Baromorph

post-inflation. This projection technique is a fundamental principle for designing shape-changing surfaces with Baromorph. However, there is a current absence of toolkits to aid designers in working with such novel materials, particularly lacking software as developed in previous work [409, 318, 225, 256, 476, 510, 474] for designing a Baromorph based on an objective surface shape or simulating surface shape variations under different air pressures. Our SoftMorphees modules developed in this chapter provide a large range of different primitives for shape change. Our measurements of their shapes under different air pressures and respective regression equations can help other researchers develop their UIs. Further study should provide end-users with an SCI toolkit by addressing end-user programming tools for designing customized SCIs, considering different design parameters, such as materials types, pressure, prototype thickness, and air channel width.

4.4.2 User’s perception precision and shape controlling precision on soft UIs with different shape features

In Chapter 3, we delve into users’ *Curvature* perception precision, i.e., *Just Noticeable Difference* (JND), under different softness conditions. Figure 4.13 presents our measurement of users’ *Curvature* perception precision and the *Curvature* measurement of our *Curvature* changing prototype in the same plot. Points in this figure present the *Curvature* measurement of our two prototypes, i.e., R10 and R20, with inner air pressures changing in steps of 0.2 Psi¹. Bars with colors in this figure present users’ perception precision range in different softness conditions and *Curvature* conditions with their center located at the height of the respective reference *Curvature* value, i.e., 10 mm, 20 mm and 40 mm and with their tops and bottoms present respectively the value of $Curvature_{Reference} + Curvature_{JND}$ and $Curvature_{Reference} - Curvature_{JND}$ respectively. From this figure, we can see that our prototypes can well satisfy users’ *Curvature* perception precision when UIs are nearly flat (Radius \approx 40 mm) with a few points located at bars presenting users’ perception precision range, i.e., we can control our prototypes’ *Curvature* more precisely than users’ *Curvature* perception precision (JND). When UIs are medium-curved (Radius \approx 20 mm), bars barely touch two points, i.e., our prototypes’ *Curvature* controlling precision merely satisfy users’ *Curvature* perception precision (JND). This indicates that we should further improve the *Curvature* controlling precision of our

1. The system that we developed for controlling the pressure currently has a controlling precision of approximately 0.1 Psi. We control thus our prototypes in steps of 0.2 Psi to ensure the measurement accuracy.

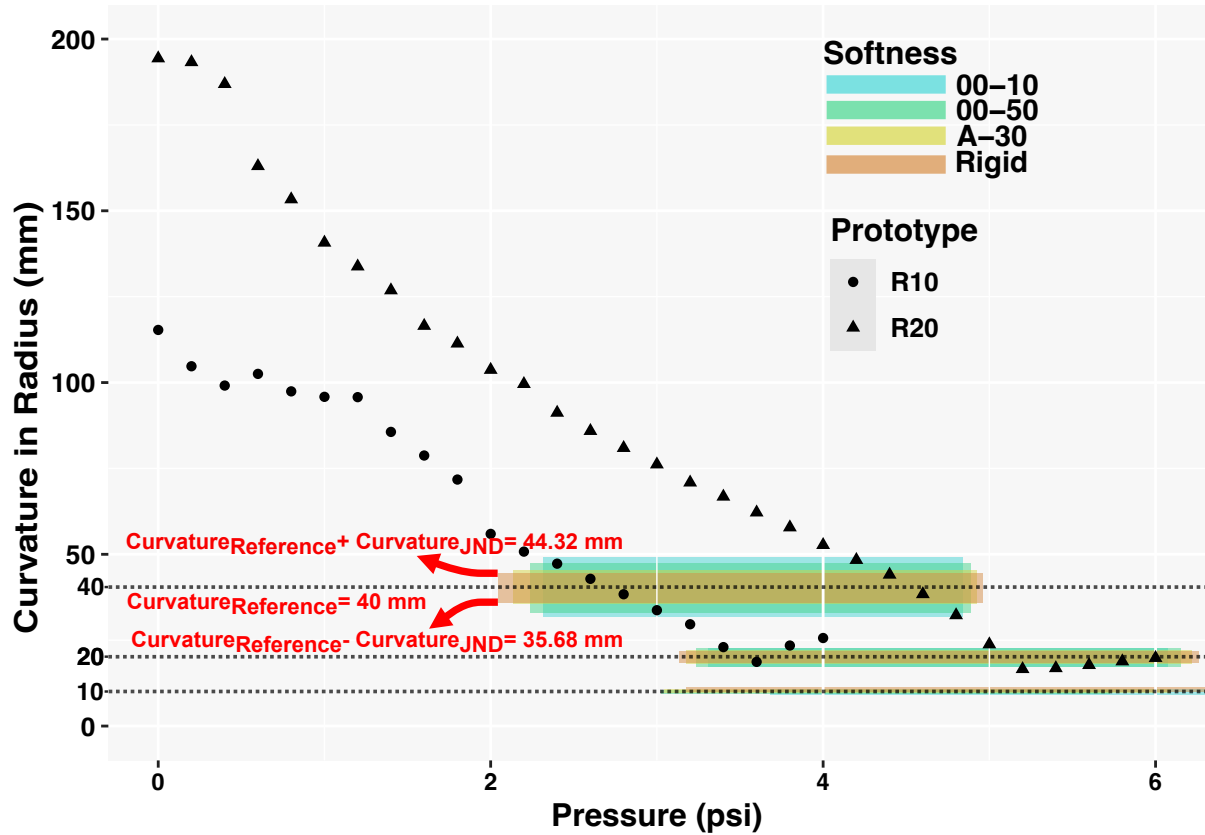


Figure 4.13 – *Curvature* measurements of our *Curvature* changing prototypes (Figure 4.4) and users’ *Curvature* perception precision measured in Chapter 3. Data points present the *Curvature* of our prototypes; we present them using their radius ($1/\text{Curvature}$) to keep consistent with Chapter 3 and improve the legibility. Bars in different colors present users’ perception precision range in different softness conditions. Bars’ center locates at the height of the respective reference *Curvature* value, i.e., 10 mm, 20 mm and 40 mm with their tops at the respective value of $\text{Curvature}_{\text{Reference}} + \text{Curvature}_{\text{JND}}$ and bottoms at $\text{Curvature}_{\text{Reference}} - \text{Curvature}_{\text{JND}}$. One example is indicated with text and arrows in red colors with users’ *Curvature* JND in rigid and 40 mm reference condition measured as 4.32 mm (Chapter 3). The widths of the bars are chosen to cover points in their ranges (if any) and to avoid complete overlaps among bars for better legibility.

prototypes. In contrast, as for UIs very curved (Radius ≈ 10 mm), our UIs can not currently create *Curvature* values located in users’ perception range. Thus, we should further work on creating more curved prototypes.

In fact, our *Curvature* changing prototypes are not exactly the same as stimuli in Chapter 3, e.g., our prototypes are not solid as stimuli in Chapter 3, and the air pressure

inside our prototypes might also impact the softness that users' perceived [430]. For this reason, Figure 4.13 roughly indicates how we should improve our prototype design; further psychophysical experiments should be conducted to measure users' *Curvature* perception precision using our prototypes directly. Similarly, psychophysical experiments should be conducted on users' perception precision of other shape-changing features on UIs in soft materials, e.g., with our other prototypes. With these measurements, future-designed SCIs' shape-controlling precision of these features should be fine enough to satisfy users' perception precision on them respectively.

Besides satisfying users' perception precision, another phenomenon we observed with our prototypes also suggests the importance of further improving shape-controlling precision: the sudden shape change. For instance, our *Closure* changing prototype's *Closure* increases suddenly from 32% to 100% when pressure increases from 4.4 Psi to 4.6 Psi, while its *Closure* increasing slowly before (Figure 4.10). With similar technology, we built a *Closure* changing flower (Figure 4.11). When pressure increases from 2.6 Psi to 2.8 Psi, the flower suddenly almost completely closes its petals. This suggests that we should control the inflation pressure more precisely to improve some of our prototype's shape-changing precision, e.g., with the pressure more precise than 0.2 Psi to get more precise control of the *Closure*.

4.4.3 Rigid materials involved in connecting pneumatically actuated soft shape-changing modules

In Section 2.1.10, the interconnection of various SCIs modules actuated by dielectric elastomers or SMA wires can be achieved using conductive wires to share actuation sources and control signals. In MorpheesPlug [227], authors proposed changing *Modularity* through attaching *Length*-changing modules to other modules in a slot, and then extend the *Length* to lock them through the slot. However, they just connect together but do not address the problem of sharing actuation sources. For sharing actuation sources in pneumatically actuated SCIs modules—utilizing pumps for air intake or evacuation—serial connectivity via air-proof tubes, as demonstrated [243], is feasible. To achieve independent control of each pneumatic module or to actuate specific modules within a connected series, such as under particular air pressure conditions (as illustrated in [301]), the incorporation of solenoid valves [401] or intricately designed and fabricated electronic-free valves [257] is necessary. Notably, solenoid valves typically require rigid

components, including springs, solenoids, and other electronic elements [212]. Similarly, current electronic-free valve systems often necessitate rigid materials, such as plastic tubing surrounding spring-ball systems (as depicted in Figure 2.17(a) of [59]), acrylic orifice plates (Figure 2.17(b) in [301]), and top and bottom acrylic components (Figure 2.17(c) in [257]). These rigid structures are essential to prevent deformation under pressurization and avoid unintended air passage; for instance, the inflation of the tube around the spring-ball system (Figure 2.17(a) in [59]) may lead to air leakage around the ball designed to block airflow. While specific microfluidic systems have successfully employed purely soft materials, predominantly PDMS elastomers [485], the high fabrication complexity associated with microfluidic systems [305] and the technologies specific to micron-scale applications pose challenges when applied directly to macroscopic systems (e.g., milli-scale or larger, typical in most pneumatic SCIs). Notably, laminar flow², a crucial criterion for microfluidic systems [204], is absent in macroscopic systems. Consequently, the development of valves using purely soft materials in macroscopic systems remains a challenging endeavor.

4.4.4 Strength/Stretchability changing technologies involving rigid materials

Two widely employed technologies for altering the *Strength/Stretchability* of user interfaces (UIs) are phase/glass transition materials (e.g., [385, 276, 217, 64, 520]) and jamming transition (e.g., [8, 107, 269, 406, 405, 319, 277]). Adjusting the temperature of phase/glass transition materials can transform their state from solid to liquid/glassy, making them soft with decreased *Strength* and increased *Stretchability*, respectively. However, using phase/glass transition materials for modifying *Strength/Stretchability* presents four evident disadvantages: (1) dichotomous *Strength* control, either soft when melted or rigid when not melted (e.g., [461]), leading to low *Strength* controlling precision (e.g., [7]); (2) necessitating additional heat insulation for wearable applications (e.g., [153]); (3) experiencing slow *Strength* increase due to the prolonged cooling time of melting materials (e.g., 7 min needed for cooling down melted LMM \approx 6 min at room temperature [184]); and (4) requiring continuous heating of materials to maintain a soft state³, resulting in

2. Laminar flow is the opposite of turbulent flow. Air or a liquid flows parallelly in different layers without mixing between layers in laminar flow. In contrast, it flows chaotically with convection between different layers in a turbulent flow.

3. For thermoresponsive hydrogel, it requires continuous heating to maintain a rigid state and needs to wait a long time for cooling down to get back to soft

low energy efficiency.

Compared with phase/glass transition materials, jamming transition actuated by vacuum offers a quicker, continuously tunable solution for *Strength/Stretchability* without heating. Various jamming media with different structures, such as granular (e.g., ground coffee used in [8]), fibrous (e.g., nylon fibers used in [44]), or laminar (e.g., sketch papers used in [319]), can be employed in jamming transitions. Aktaş et al. [7] analyzed the *Strength* of jamming systems using different jamming media under diverse load conditions, such as stretching, compressing, and bending. They observed that the *Strength* of systems after jamming transition is proportional to the rigidity of jamming materials (either Young's modulus or shear modulus⁴), especially when using laminar or fibrous jamming media. In contrast, the rigidity of granular jamming media has little impact on the *Strength* of systems. Soft materials, like foam beads, are also utilized in some granular jamming systems [277]. However, granular jamming systems still require rigid materials in the encasing membrane, such as thin plastic, to envelop them and provide sufficient *Strength* when used as haptic devices [8]. Rigid materials remain indispensable in jamming systems, whether as jamming media in laminar or fibrous jamming systems or as envelop in granular jamming systems, for efficiently tuning the *Strength* and *Stretchability* of the systems. The involvement of rigid materials might harm systems' stretchability as they are non-stretchable.

4.4.5 Limitations of building Size-changing UIs using solely soft materials

Soft materials, such as elastomers, exhibit significant stretchability compared to their original *Size*, with some instances of *Length* stretching exceeding 1000% [56]. However, when subjected to specific stimuli (e.g., increasing air pressure for air-proof elastomer bladders [509]), they typically undergo homogeneous changes in shape in all directions, posing challenges for achieving inhomogeneous shape changes, such as linearly increasing *Length* in one dimension. As detailed in Section 2.1.1, our technology for creating user interfaces (UIs) that change both *Length* and *Area* relies exclusively on soft materials, specifically silicone elastomers, utilizing in-plane expansion of embedded air channels un-

4. The Young's modulus and shear modulus are both measures of the rigidity of materials. Young's modulus is defined by the ratio between the lengthwise tension or compression on a material and its change of length [438]. The shear modulus is defined by the ratio between the force applied parallel or tangential to the face of a material and its deformation in the force direction [437]. Rigid materials usually have larger Young's modulus and shear modulus.

der pressurization. It is essential to ensure that the top and bottom membranes of the UIs have a uniform thickness to prevent curvature toward the thicker membrane side in a bi-layer structure. When fabricating the membrane to be glued with the molded part of our prototypes, we tried to spread the non-cured silicone with a high precision film casting knife [106] in different thicknesses and measured their thickness when dried. We found that non-cured silicone with a thickness of 1.7 mm will form a membrane of 1.2 mm, equal to the membrane thickness of the part molded for *Size* changing prototypes. 1.4 mm non-cured silicone will form a membrane of 1 mm and we use them in *Closure* and *Zero-crossing* prototypes which have one side of membrane thinner than another side for facilitating the bending toward the thinner side. Additionally, the external wall of the flat silicone plate must be thin enough to facilitate in-plane expansion, deviating from the original concept of Baromorph [402]. Although we fabricate *Size* changing prototypes with membrane thickness and external wall width carefully controlled, our prototypes still tend to curve when inflated to relatively high pressure, i.e., when *Length* increases approximately 24% under air pressure of 5 Psi (Figure 4.2(c)) and when *Area* increases approximately 46% under air pressure of 3 Psi (Figure 4.2(c)). This phenomenon may be attributed to the lower energy required for curving compared to stretching [337] when the plates are under tension. Another limitation of creating *Size*-changing interfaces using only soft materials is that *Volume* increase is confined to balloon-like inflated bladders (e.g., [284, 282, 157, 132, 114, 423, 81, 67, 160, 230]), where the membranes uniformly stretch to form a spherical shape, as depicted in Figure 2.2(a). To achieve inhomogeneous *Volume* changes in UIs, such as rectangular cuboid-like shape changes illustrated in Figure 2.2(c), rigid/non-stretchable materials like papers become indispensable to restrict their stretching in certain directions [509]. However, using non-stretchable materials will thus reversely limit the whole structure's stretchability.

4.5 Conclusion

In this chapter, we successfully created a series of shape-changing modules using exclusively soft materials, specifically silicone elastomers, to implement six distinct shape-change features in Morphees+: *Size*, *Curvature*, *Amplitude*, *Porosity*, *Closure* and *Zero-crossing*. However, challenges persist in developing UIs with changing *Volume*, *Modularity*, *Strength* and *Stretchability* features using only soft materials and current technologies. While soft materials offer great potential for constructing UIs with diverse shape-changing

abilities due to their high *Stretchability*, their elevated *Stretchability* often comes at the expense of reduced *Strength*. One key question that needs to be addressed is how we can integrate *Strength*-changing technologies with those affecting other shape-changing features such as *Curvature*. This question is pivotal in the development of UIs with significant shape-change capabilities while still maintaining high *Strength*—a crucial consideration for addressing the trade-off between *Strength* and *Stretchability* when employing programmable soft materials for building SCIs [358]. The next chapter will explore this research question (Chapter 5).

JAMMING ORIGAMI ENDOSKELETON: SHAPE-STRENGTH CONTROLLING TECHNOLOGY

5.1 Introduction

As we have seen in Chapter 2, recent advances in material science [358] make soft materials, such as elastomers [509] a promising choice for constructing shape-changing interfaces (SCIs). This provides a vital technology basis for developing SCIs with high shape-changing abilities. These materials possess high stretchability, allowing for easy deformation, with some examples being stretched over 1000% [56]. Deformability allows to change the geometric shapes of UIs—through some primary geometric shape-changes (Figure 2.20 such as size [119], curvature [509], amplitude [132], porosity [475], closure [510] and zero-crossing (e.g., [157]). The remarkable deformability of elastomers also holds the potential for achieving high-resolution SCIs [358, 376], for instance, overcoming the resolution constraints imposed by the size of actuators used in actuated pin-based 2.5D shape displays [349].

Because of their high deformability, soft materials present a trade-off between stretchability and strength [358]. Highly deformable materials typically exhibit low strength, while UI strength [376] also play a crucial role in providing users with essential haptic feedback, such as simulating the stiffness of different materials [107]. Meanwhile, our psychophysical experiment in Chapter 3 revealed that UIs with higher strength (lower softness) could give users more precise feedback on their geometric shapes, such as curvature. Addressing the trade-off between high deformability and strength is vital when utilizing soft materials to construct SCIs. Addressing this trade-off requires the development of novel technologies that leverage the stretchability of these materials while enhancing their range of strength. Such new technologies would enable richer haptic feedback.

By combining elastomers with jamming technologies [107], designers can control the strength of elastomer-based interfaces. For instance, using an air-proof bladder (e.g., silicone bladder [107]) filled with jamming media (e.g., glass beads [107]) allows for transforming the bladder from a soft state to a rigid state through vacuuming out air, effectively enhancing its strength. However, current research progress in this domain has mainly focused on separate aspects, with some studies concentrating on interfaces capable of geometrically changing their shapes and others on interfaces capable of controlling their strength. One notable challenge in developing such interfaces is that multiple independent actuating systems are required to control geometric shapes and strength. For example, a system [419] overlays an extra layer of jamming for strength control on an air chamber for geometric shape control, necessitating several pumps and resulting in bulky actuation systems and significantly increasing the thickness (e.g., 8 mm extra thickness because of the jamming layer [419]). Interfaces capable of controlling their geometric shapes and strength without importing extra actuators and significant thickness have yet to be developed, which is crucial to addressing the trade-off between high deformability and strength. In particular, for developing wearable applications where UIs' low bulkiness is critical [112, 288].

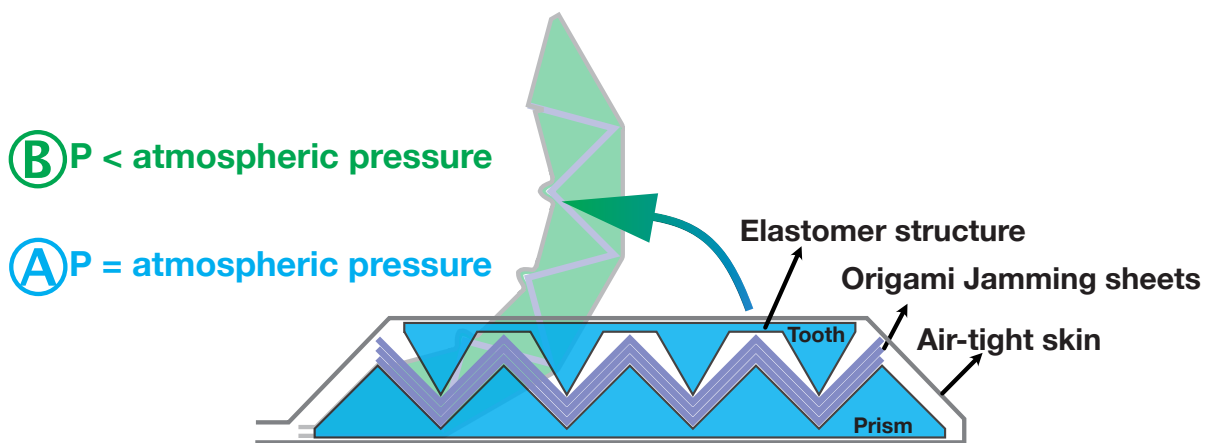


Figure 5.1 – Our curvature+stiffness actuation mechanism: (A) origami jamming sheets sandwiched between elastomer structures. (B) When air is vacuumed out of the airtight skin, the structure deforms to reach its maximum curvature and stiffness progressively.

This chapter presents a novel technology for SCIs capable of controlling their geometric shapes and strength using a single actuating system: a pump. As illustrated in

Figure 5.1, our system consists of a stretchable air-proof bladder (TPU membrane of 0.1 mm thickness) containing two layers of elastomer gears –whose shapes are designed for a specific final curvature–and several layers of plastic origami jamming sheets sandwiched between the elastomer gear layers. The two layers of gears are designed to have different shapes, which leaves spaces between them. When the air inside the bladder is vacuumed out, the pressure gradient inside and outside our prototype drives our elastomer structures to bend to squeeze out the air in the space between gears, causing the whole structure to change shape. Plastic origami jamming sheets are pre-cut to be able to fold with the elastomer structures (see details of our Fabrication process in section 5.5 and Figure 5.15) and change their shapes together with elastomer structures. To differentiate the two layers of gears, we call the thicker one “Prisms” and the thinner one “Teeth”, as in Figure 5.1. At the same time the vacuum driving the “Prisms” and “Teeth” close to each other and changes the prototype’s shape; the origami jamming sheets are more and more strongly pressed by ‘Prisms” and “Teeth” which can lead them to jam together and increasing the structure strength [107, 319, 7]. The shape-change and strength-change are driven by the pressure gradient inside and outside our prototype when air is vacuumed; thus, we can control geometric shapes and strength using a single actuating system: a pump. We currently focus on curvature control for geometric shape controlling in this chapter –as curvature-changing interfaces are prevalent in HCI research [509, 300, 236, 462, 157, 132, 114, 419, 423] . At the same time, it is a fundamental feature for realizing many other shape-changing features (Figure 2.20). In section 5.7.5, we will discuss the possibility of using our technology to create shape-change UIs other than curvature-changing ones.

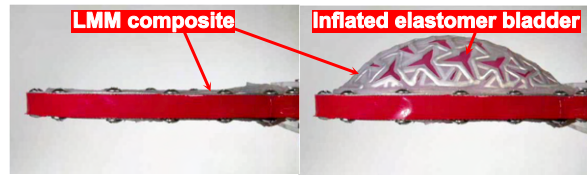
In this chapter, we first review existing related work controlling both geometric shape and strength control of UIs. Then, we describe our novel shape-changing technology and discuss the design space of our technology, exploring various design parameters and assessing their impact on the shape and strength of our structures. Finally, we envision applications based on this novel technology to enrich users’ interaction and discuss future work to improve our technology for creating UIs with richer shape-change ability.

5.2 Related work

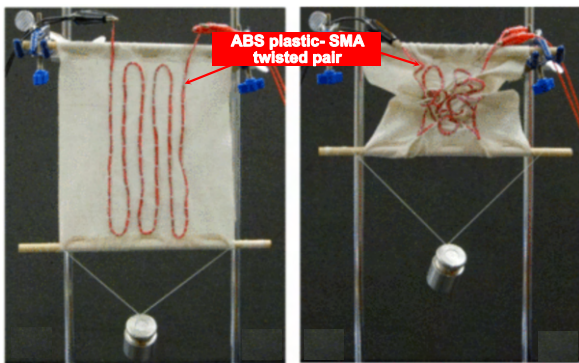
In Chapter 2, we have presented previous research addressing UIs’ geometric shape and strength control separately. Complementarily, this section summarizes prior work on UIs capable of controlling both geometric shapes and strength.



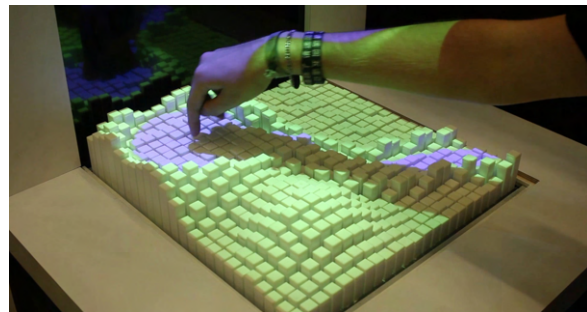
(a) **Pneumatically inflating + Jamming:** A matrix of jamming cells was added on the top of a pressure-controllable chamber. Before jamming, the matrix of cells can be bent with increasing pressure in the chamber, and each cell can be jammed to become rigid [418]



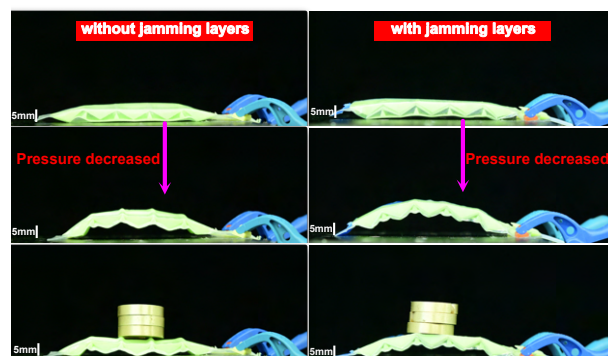
(b) **Pneumatically inflating + Phase-changing materials:** A layer of LMM composite was added to an elastomer bladder. When the composite is heated to soft, the composite layer can be pushed to change shape by the elastomer bladder inflated. The composite can return rigid when cooled down [184].



(c) **Shape-memory alloys + Phase-changing materials:** An ABS plastic-SMA twisted pair cabling is sewn into the fabric. The ABS plastic fiber can be heated to become soft; the SMA wire can be heated to change shape (curling up). When cooling down, the rigid ABS plastic fiber can help keep the shape [520].



(d) **Motorized 2.5D shape-display:** Each motorized bar in the matrix can change height when pressed by users according to respectively stimulated surface feature. [298]



(e) **Our technology:** two of our prototypes (left without origami jamming sheets and right with origami jamming sheets) change-shape with decreasing pressure and support load (a single wight is 20 g). Our technology with embedded origami jamming sheets (7 layers of 0.1 mm mylar film) slightly deformed under the weight of 60 g, while the prototype without origami jamming sheets collapses under the same wight.

Figure 5.2 – Different technologies for creating geometric shape and strength changing UIs.

Pneumatically inflating + Jamming Wall, Deimel, and Brock proposed to add an additional jamming system [471] on top of a pneumatically inflating SCI. This system can be inflated to bend (similar to [393]) and also for strength control. When the jamming system is not vacuumed, inflating the shape-changing system will bend it as the jamming media (e.g., ground coffee) is not pressed together and can slide freely. After vacuuming the jamming system, the jamming media is pressed together, increasing the system's strength to resist shape changes caused by external forces. Stanley and Okamura also proposed Haptic jamming [419, 416, 418] to achieve strength control and richer geometric shapes control, such as creating the shape of a Stanford bunny [495] from a planar surface. Haptic jamming consists of a 2D matrix of jamming cells (bladders of coffee) bonded over a pressure-controllable air chamber. Each jamming cell can be individually vacuumed by controlling its connection to the vacuum via valves. Increasing the pressure inside the air chamber, non-vacuumed cells are pushed up, while vacuumed cells remain locked in their original position, resulting in a 2.5D shape [246]. However, adding an extra jamming system to pneumatically inflating SCIs increases the thickness of the UI (e.g., extra thickness ≈ 8 mm in [419, 416, 418]). In contrast, our prototype does not add any extra thickness as the origami jamming sheets are placed directly in the gap between two elastomer structures. We have successfully fabricated thin prototypes with total thickness ≈ 4 mm (Figure 5.3). Furthermore, the whole system becomes less portable as needing at least two pumps as actuators, i.e., one for inflating shape-changing system and one for vacuuming jamming system, and more pumps or valves are needed to control each jamming cell in systems like [419, 416, 418].

Pneumatically inflating + Phase-changing materials Phase-changing materials like low melting point metals (LMM) can become soft when heated beyond their phase transition point (e.g., 62°C in [461]). Van Meerbeek et al. heated LMM until it became liquid and then filled it into porous silicone, creating a silicone/low melting point metals composite [461]. This composite softens when the LMM is heated to a liquid state and becomes rigid again when the LMM cools down. It can be bonded to a pneumatic SCI (e.g., PneuUI [509]) as an extra layer for controlling surface stiffness. A similar composite was fabricated in [48]. Hwang et al. [184] improved the technology by cutting the composite into kirigami shapes [65], enhancing its stretchability when the LMM melts, allowing it to stretch up to 100%. However, these systems using phase-changing materials for strength control inherit the same disadvantages as earlier discussed in section 4.4.4:

(1) dichotomous strength control of either soft when melted or rigid when not melted (e.g., [461]), thus lacking continuous stiffness feedback (e.g., [7]); (2) requiring additional heat insulation for wearable applications (e.g., [153]); (3) slow strength increase due to the long cooling time of melting materials (e.g., 7 min needed for cooling down melted LMM \approx 6 mm at room temperature [184]); and (4) continuous heating to maintain a soft state, resulting in low energy efficiency.

Shape-memory alloys + Phase-changing materials Shape-memory alloys [73] can be heated to change shape and phase-changing materials like thermoplastics (e.g., PLA and ABS used in [64, 520]) can be heated to become softer. This thus allows constructing UIs sharing one actuation system, i.e., heating system, for both shape and strength control. Yuen, Bilodeau, and Kramer [520] twisted together two wires: a shape-memory alloy (SMA) and a thermoplastics fiber containing a metal wire. The rigid thermoplastics fiber becomes soft by heating the metal wire above its glass transition point. Upon cooling, the thermoplastics fiber becomes rigid again. Leveraging the shape-memory effect of the SMA [73], the SMA wire can change shape to return to its programmed shape (e.g., from a straight wire to a helical coil in [520]) when heated above its activation temperature (e.g., 70 °C in [520]). When the thermoplastic fiber is heated to soften, the twisted SMA wire can actuate the thermoplastic fiber to change its shape. When the thermoplastics fiber cools and becomes rigid, it retains the shape of the SMA wire despite external forces. The advantage of [520] is that it only requires a single actuation, as geometric shape and strength control share the same heating source. However, similar to the technology mentioned above, *Pneumatically inflating + Phase-changing materials*, using phase-changing materials for strength control inherits all disadvantages as discussed in section 4.4.4 such as slow strength increase speed after heated.

Motorized 2.5D shape-display Emerging 2.5D shape displays (e.g., [246, 297, 244, 108]) were recently developed using a 2D matrix of height-changing bars, which can create various geometric shapes by controlling the height of each bar. It is like a relief sculpture: Carving a flat surface into different depths in different positions can form a richer shape globally. Materiable [298] expands on 2.5D shape display technologies by incorporating surface material properties rendering. When users touch or press on Materiable, the system can actively adapt the height of each bar to render the surface deformation according to its surface properties. For instance, when the user applies the same force on Materiable

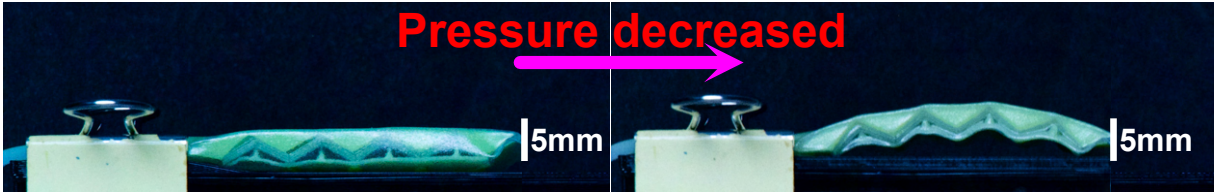


Figure 5.3 – A thin prototype made using our technology

with fingers, it can keep the height of each bar to render the effect of pressing on a rigid surface and can also vastly decrease the height of bars around fingers to render the effect of pressing on a soft surface. Thus, this technology can create UIs, i.e., surfaces on which users interact with controlled shape and strength. However, Materiable requires several actuation motors beneath, which makes it unsuitable for portable or wearable devices.

Our technology, the *Jamming Origami Endoskeleton* (Figure 5.1), achieves geometric shape control and strength control through pneumatically deflating. Compared with the work above, our technology can provide designers of SCIs with the following advantages: Geometric shape and strength control share (1) a single vacuum pump for actuation, making the device more portable. In our system, the jamming layer is inserted into the gap between the two layers of elastomer gears, thus (2) limiting extra thickness. We have currently successfully created thin prototypes with total thickness around 4 mm (Figure 5.3). The jamming-based strength controlling does not need continuous energy input to maintain strength, unlike heating LLM [461], resulting in (3) high energy efficiency. It also allows (4) fine-tunes stiffness, providing users with continuous haptic feedback, and (5) quick strength adjustment (less than 1 s to reach maximum vacuum with our current prototypes). Furthermore, as our system does not require heating for either shape control or strength control and has no rigid materials on both sides where it might come into contact with users, it is (6) better suited for wearable applications.

5.3 Design Space and technical evaluation

As our control of the geometric shapes controlling is based on the imperfectly compatible elastomer gears shapes, i.e., the shape of “*Prism*” and “*Tooth*” respectively in Figure 5.4 is different, we considered both the thickness difference $\Delta_{\text{Thickness}}$ and angle difference Δ_{Angle} (Figure 5.4) between two elastomer gears layers as design parameters.

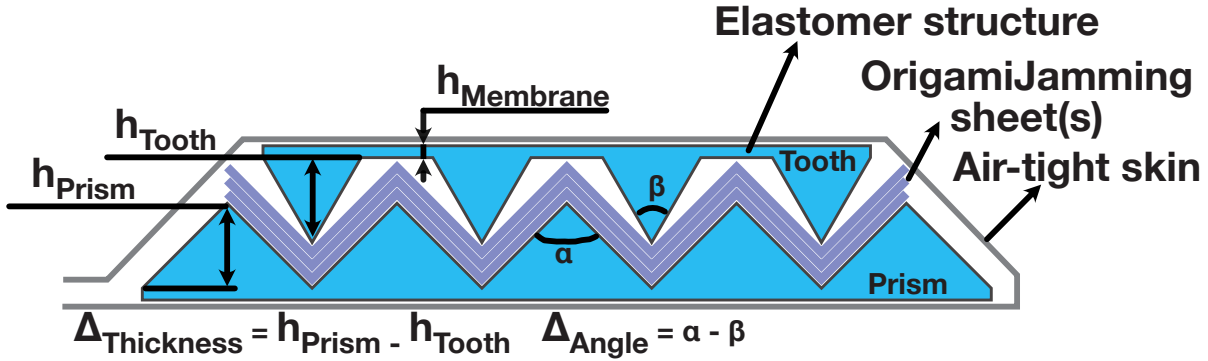
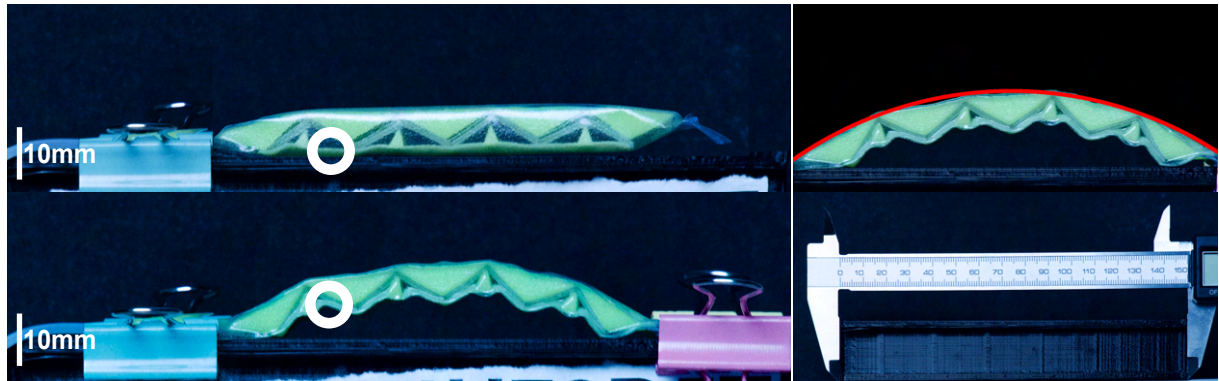


Figure 5.4 – Design parameters of our prototypes. To differentiate the two layers of gears, we call the thicker one “*Prism*” and the thinner one “*Tooth*”. Our current design parameters include the thickness and angle difference between “*Prism*” and “*Tooth*” ($\Delta_{\text{Thickness}}$ and Δ_{Angle}), thickness of “*Prism*” (h_{Prism}) and thickness of membrane (h_{Membrane}). We also study the impact of vacuum level P_{Vacuum} on our prototypes’ curvature and strength.

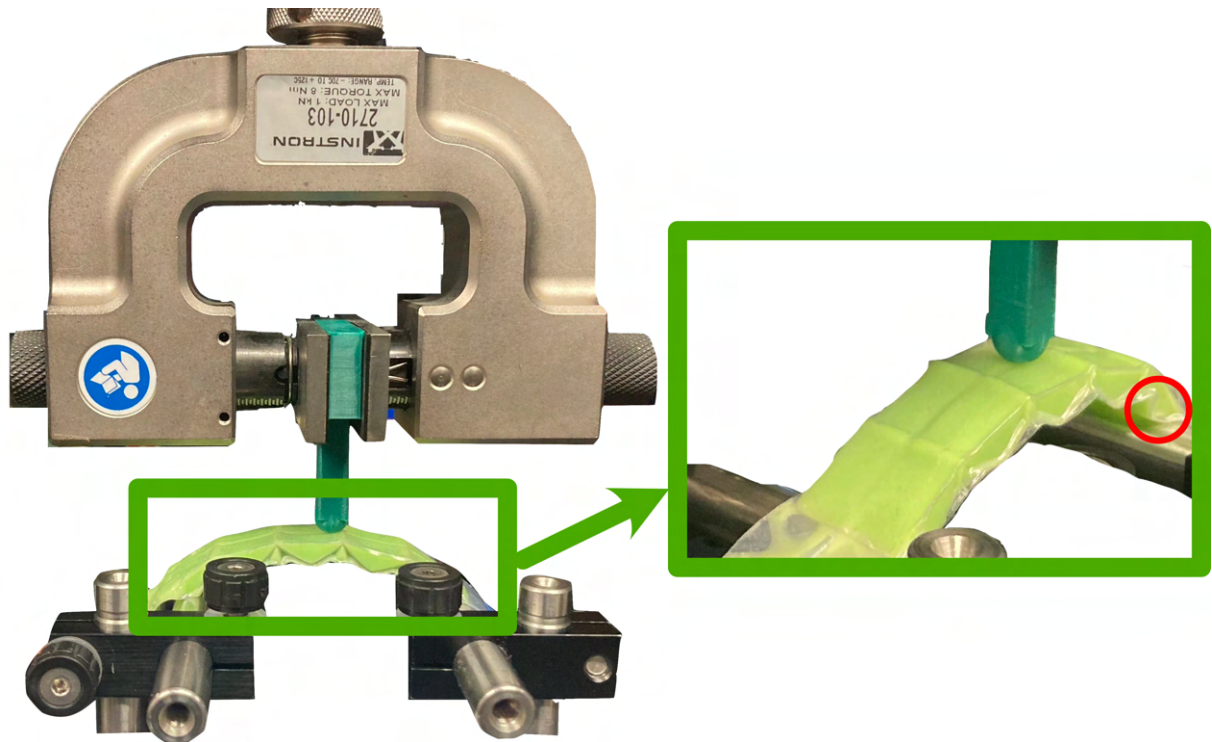
As the thickness is also an essential factor, in particular for wearable UIs [399], we also consider the thickness¹ as a design parameter. Besides, we also evaluate the impact on both geometric shapes (i.e., curvature) and strength of vacuum level P_{Vacuum} and whether having origami jamming sheets sandwiched. As presented in the white circles in Figure 5.5(a), we can see that the buckling [336] of membrane connecting each layer of elastomer gears hinders the full contact between elastomer gears, which might impact the geometric shapes of our prototypes. For this reason, we also evaluate the impact of the thickness of the membrane h_{Membrane} (Figure 5.4) connecting elastomer gears. In this section, we present how we measure the different curvature and strength of our prototypes with different design parameters (i.e., $\Delta_{\text{Thickness}}$, Δ_{Angle} , h_{Prism} , h_{Membrane} and P_{Vacuum}) and our measurement results.

Curvature measurement To measure the curvature of our prototypes, we took pictures of our stimuli after vacuuming out air (Figure 5.5(a) bottom left) with a Panasonic Lumix G Hybrides camera with a LUMIX G VARIO 14-140 lens (Focal length $f=135$ mm, resolution 1096×2160). As shown in Figure 5.5(a) (top left), the left side of one

1. We also consider the thickness difference between “*Prism*” and “*Tooth*” as a design parameter. In contrast, the thickness of each gear layer is coupled with the parameter of $\Delta_{\text{Thickness}}$. To simplify the analysis of the design parameter of thickness, we fix $\Delta_{\text{Thickness}}$ as 1mm and considering the thickness of the “*Prism*” (h_{Prism} in Figure 5.4) as the design parameter for thickness. The total thickness of a prototype equals the thickness of “*Prisms*” plus the thickness of membranes connecting gears and the thickness of membranes enveloping the prototype.



(a) Curvature measurement setup



(b) Strength measurement setup

Figure 5.5 – Curvature and strength measurement setup. (a) Curvature measurement. Top left: a prototype before vacuuming our air; Bottom left: a prototype with air vacuuming out; Top right: A prototype with edge detected, bolded and highlighted in red color for visualization; Bottom right: a vernier scale fixed on the support facilitating the conversion of pixels to millimeters. White circles in the left two figures show the buckling [336] of the elastomer membrane connecting elastomer structures and the TPU enveloping membrane. (b) Strength measurement setup. The measurement is done by the compression test with a 3D printed spherical indenter as in [418] and in Chapter 3. The red circle shows the form of "gear", which takes shape when vacuuming prototypes.

prototype was fixed on a 3D-printed support before vacuuming. After vacuuming air and the prototype curved (Figure 5.5(a) bottom left), we fixed the prototype's right side and took a photo. We then release the right side and the vacuum, and the prototype returns to flat (Figure 5.5(a) top left). To ensure measurement accuracy, we repeat the process of "Vacuuming-Releasing-Taking Pictures" of each prototype 10 times. We then detected the contour of the curved surface of each prototype with OpenCV 4.6.0 [315]. Before the contour detection, pictures were calibrated to remove the distortion of the camera lens with OpenCV 4.6.0 [315]. We fitted points to this contour (Figure 5.5(a) top right) using the circle-fit 0.1.3 [214] python package, to finally find its curvature. To convert curvature from pixels (px) to mm, we fixed a vernier scale on the support to ensure the precision of the conversion as in Figure 5.5(a) (bottom right). We found that 150.05 mm on the scale equals 3248 px in the pictures. Therefore, we convert our curvature measurements with 0.046 mm/px. In Figures 5.6(a), 5.7(a), 5.8(a), 5.9(a), 5.10(a), 5.11(a), we also present the 95% bootstrapping confidence interval through error bar based on the 10 repetitions of curvature measurement. All error bars in these figures are very small (smaller than data points, thus hidden in the points), suggesting that our prototypes' shape change during repetitive measurements is very stable, and the measured curvature is nearly the same among every 10 repetitions. In Figures 5.6(a), 5.7(a), 5.8(a), 5.9(a), 5.10(a), 5.11(a), we also present the linear regression with our curvature measurement result for different design parameters.

Strength measurement We conducted compression tests with a 3D printed spherical indenter to measure the prototypes' strength as in [418] using an INSTRON Universal Testing System [194]. The loading speed is 0.2 mm/s as in Chapter 3. As shown in Figure 5.12, referring to the standard flexural test methods [21], our prototypes were supported by two fixed metal cylinders, which allows the two extremities of each prototype to slide during the measurement freely. To calculate the strength of our prototypes (abbreviated as **S**) with each design parameter, we calculate the slope of force-displacement curves, by fitting data point between 0 and 4 mm (Figures 5.6(b), 5.7(b), 5.8(b), 5.9(b), 5.10(b), 5.11(b)), where the curves are all nearly linear [21]. In Figures 5.6(b), 5.7(b), 5.8(b), 5.9(b), 5.10(b), 5.11(b), we also present the linear regression of our strength measurement result of different design parameters. We also present all force-displacement curves in Annex A.5 with Figures A.10, A.11, A.12, A.13, A.14, A.15.

We provide detailed parameters of prototypes tested during our measurements with

Table A.1 in appendix A.4.

5.3.1 Thickness difference ($\Delta_{\text{Thickness}}$)

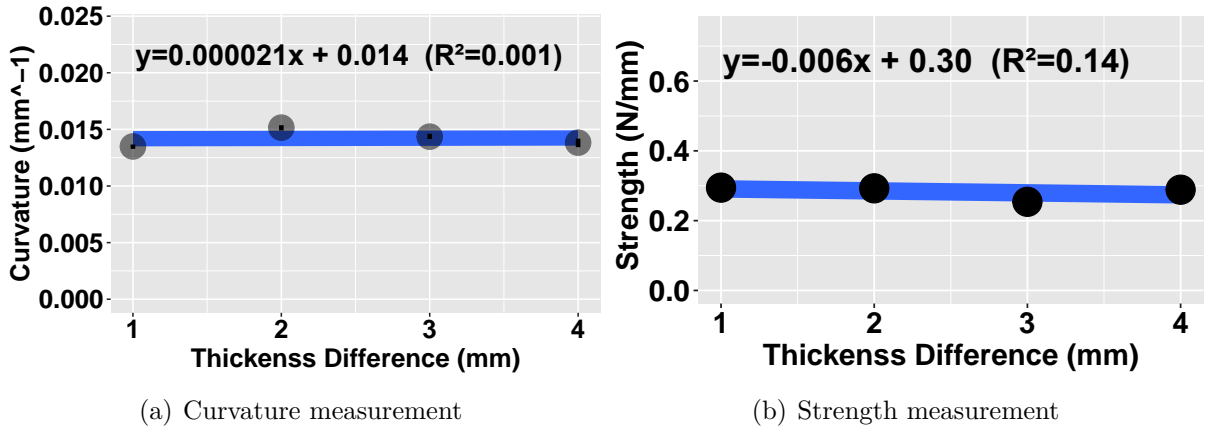


Figure 5.6 – Curvature (left) and strength (right) measurement under different thickness differences between “Prism” and “Tooth”.

As shown in Figure 5.6, both the curvature (Figure 5.6(a)) and strength (Figure 5.6(b)) show weak linear relationship with the thickness difference between “Prism” and “Tooth”, i.e., $\Delta_{\text{Thickness}}$. We can also see that both the curvature (Figure 5.6(a)) and strength (Figure 5.6(b)) nearly keep constant in our measurement range of $\Delta_{\text{Thickness}}$, which suggests that the thickness difference have little impact on our prototypes’ curvature and strength.

5.3.2 Angle difference (Δ_{Angle})

As shown in Figure 5.7, both the curvature (Figure 5.7(a)) and strength (Figure A.11) show a linear relationship with the angle difference between “Prism” and “Tooth”, i.e., Δ_{Angle} . We can see that both the curvature (Figure 5.7(a)) and strength (Figure 5.7(b)) show the tendency of decreasing when Δ_{Angle} increases, which suggests that larger Δ_{Angle} will lead to prototypes’ smaller shape-change and weaker strength.

5.3.3 Thickness (h_{Prism})

From Figure 5.8, we can see that our prototypes’ curvature (Figure 5.8(a)) shows linear relationship with the thickness of “Prism” h_{Prism} ¹, while the strength (Figure 5.8(b)) also

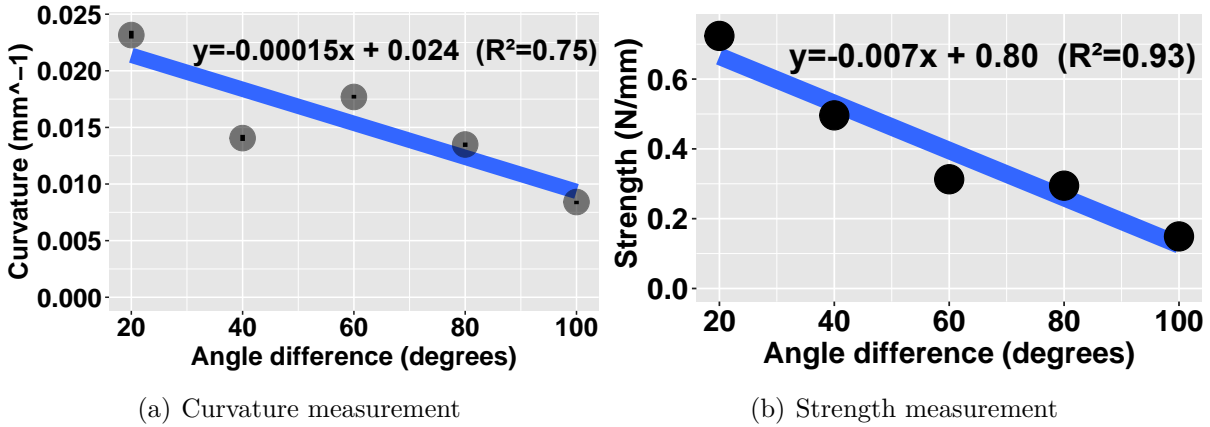


Figure 5.7 – Curvature (left) and strength (right) measurement under different angle differences between “Prism” and “Tooth”.

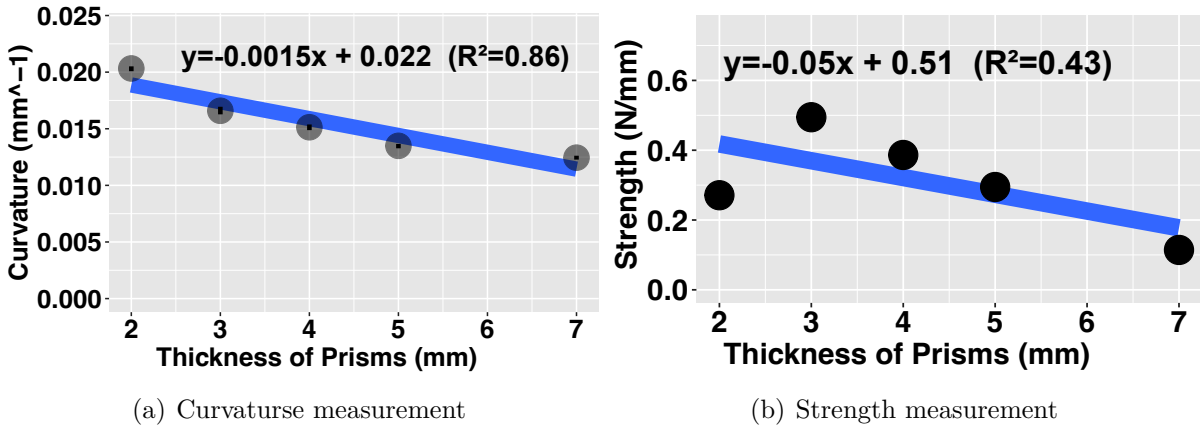


Figure 5.8 – Curvature (left) and strength (right) measurement under different thicknesses of “Prism”.

shows medium linear relationship with h_{Prism} . Figure 5.8(a) shows that with increasing h_{Prism} , the curvature of our prototypes decreases. The strength (Figure 5.8(b)) of our prototypes also decreases with larger h_{Prism} except when h_{Prism} is very small, i.e., 2 mm. The exception of small strength when h_{Prism} is as small as 2 mm might come from our measurement errors. In the condition of h_{Prism} being 2 mm, the length of the prototype is very short (≈ 35 mm), which is too short² to be stably placed on the

2. All our prototypes had the same numbers of “Prism” and “Tooth”, i.e., 5 “Prism” and 4 “Tooth” as in Figure 5.5(a). The whole length of a prototype equals to $5 \times$ the base length of a prism, thus equal to $5 \times \frac{2h_{\text{Prism}}}{\tan((180-\alpha)/2)}$. All prototypes tested for measuring the impact of h_{Prism} have the same angle values, i.e., $\alpha = 120^\circ$. The whole length of a prototype is thus linearly correlated with h_{Prism} , and smaller h_{Prism} corresponds to shorter prototypes.

two fixed metal cylinders supports (Figure 5.5(b)) during the compression test and thus impact the measurement accuracy. In our future work, we will verify this by redoing the measurement with an improved setup to avoid this error.

5.3.4 Thickness of membrane (h_{Membrane})

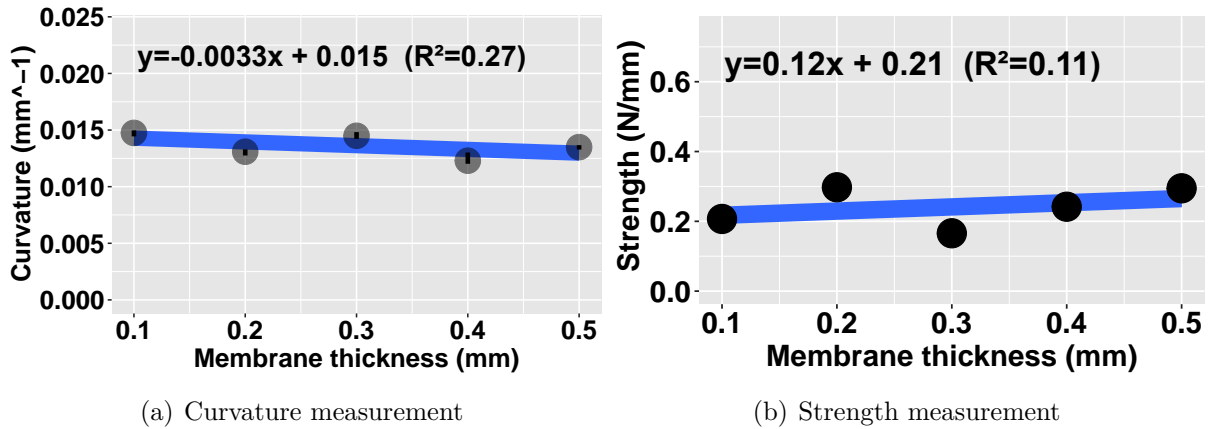


Figure 5.9 – Curvature (left) and strength (right) measurement under different thicknesses of membranes.

Figure 5.9 shows that both our prototypes' curvature (Figure 5.9(a)) and strength (Figure 5.9(b)) show a weak linear relationship with the thickness of membrane h_{Membrane} . These two figures also show that our prototypes' curvature (Figure 5.9(a)) tends to decrease slightly with a thicker membrane, and the strength tends to increase with a thicker membrane slightly.

5.3.5 Vacuum level (P_{Vacuum})

Figure 5.10 shows that, both our prototypes' curvature (Figure 5.10(a)) and strength (Figure 5.10(b)) show a linear relationship with the level of vacuum P_{Vacuum} . With Figure 5.10, we can also see that, with higher P_{Vacuum} , our prototypes tend towards being more curved (Figure 5.10(a)) and also exhibit larger strength (Figure 5.10(b)).

5.3.6 Whether having origami jamming sheets

Having origami jamming sheets sandwiched in elastomer structures is the principle of our technology. To know whether the impact of origami jamming sheets on our prototypes'

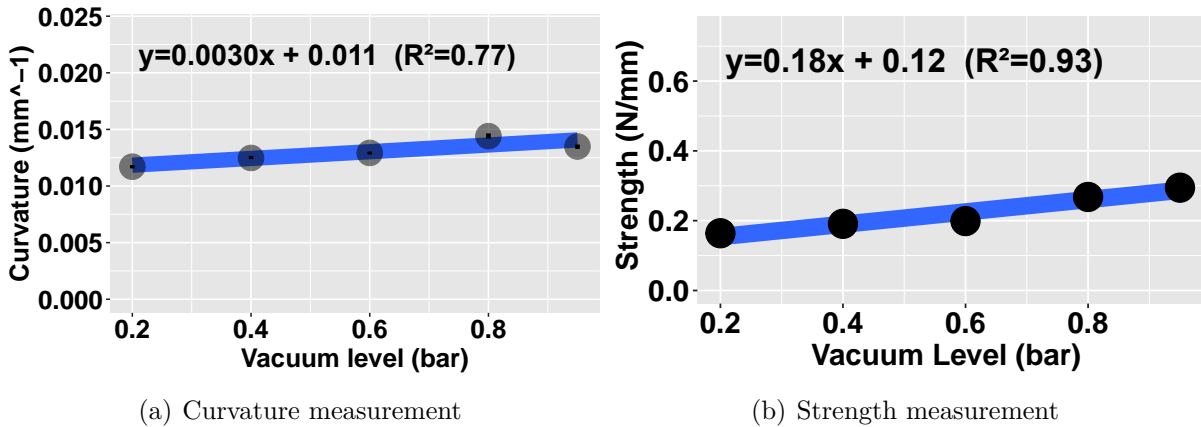


Figure 5.10 – Curvature (left) and strength (right) measurement under different vacuum levels.

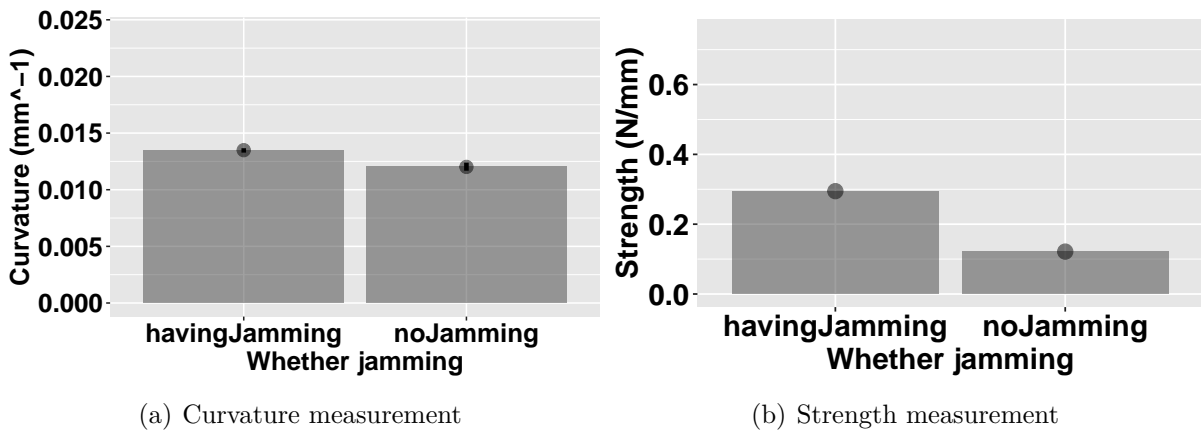


Figure 5.11 – Curvature (left) and strength (right) measurement under conditions of whether having origami jamming sheets between two layers of gears.

curvature and strength exists, we measured two prototypes: one without origami jamming sheets and one with 7 origami jamming sheets³. From Figure 5.11, we can see that adding origami jamming sheets between elastomer structures can help to slightly increase prototypes' curvature (Figure 5.11(a)) and increase nearly twice the strength with 0.29 N/mm vs. 0.12 N/mm (Figure 5.11(b)).

3. We decide the number of 7 layers from our first successfully fabricated and controlled prototype: Most thickness difference $\Delta_{\text{Thickness}}$ of our prototypes is 1 mm, which thus leaves 1 mm of gap between the apex of “Prism” and “Tooth” during our prototype assemblage. We used laser-cut Mylar film 0.1 mm thick as jamming media for prototypes. The 1 mm gap allows us to put up to 7 layers of such films inside without much effort.

5.3.7 Multiple linear regression on different design parameters

To further compare the impact of different design parameters on curvature and strength of our prototypes, we do the multiple linear regression of *Curvature* (**C**) and *Strength* (**S**) on different design parameters (i.e., the thickness difference between “Prism” and “Tooth” $\Delta_{\text{Thickness}}$, the angle difference Δ_{Angle} , the thickness of “Prism” h_{Prism} , the thickness of membrane h_{Membrane} and the level of vacuum P_{Vacuum}). Before the regression, we normalize all data, which allows us to compare different parameters on a common scale. Then, we can get the regression result:

$$C = 1.15 - 0.70\Delta_{\text{Angle}} - 0.57h_{\text{Prism}} + 0.10P_{\text{Vacuum}} + 0.056\Delta_{\text{Thickness}} + 0.033h_{\text{Membrane}} \quad (R^2 = 0.74) \quad (5.1)$$

$$S = 0.86 - 0.86\Delta_{\text{Angle}} - 0.39h_{\text{Prism}} + 0.18P_{\text{Vacuum}} + 0.097h_{\text{Membrane}} + 0.0088\Delta_{\text{Thickness}} \quad (R^2 = 0.81) \quad (5.2)$$

As shown in Equations 5.1 and 5.2, the Δ_{Angle} , h_{Prism} and P_{Vacuum} are the three first design parameters which impact both the curvature and strength. In contrast, the impact of other parameters is comparatively small. This is coherent with previously presented linearly fitting result on each design parameter (Figure 5.6, 5.7, 5.8, 5.9 and 5.10). The regression result indicates that decreasing the angle difference Δ_{Angle} , decreasing the thickness of “Prism” h_{Prism} or increasing the level of vacuum P_{Vacuum} can lead to increasing curvature of our prototypes and the increasing strength. Meanwhile, the P_{Vacuum} impacts more the *Strength* than the *Curvature*, with coefficient 0.18 vs. 0.10, which suggests that although the *Strength* and *Curvature* of our prototypes are coupled with the increasing P_{Vacuum} , the increasing of vacuum level lead to more important change on *Strength* than *Curvature*.

5.4 Supplementary strength measurement

With force-displacement curves (Figure A.10, A.11, A.12, A.13, A.14, A.15) that we obtained with measurements conducted in section 5.3, we can see clear “*fluctuation*” on the curves. During the compressing tests, we observed that the “*fluctuation*” comes from

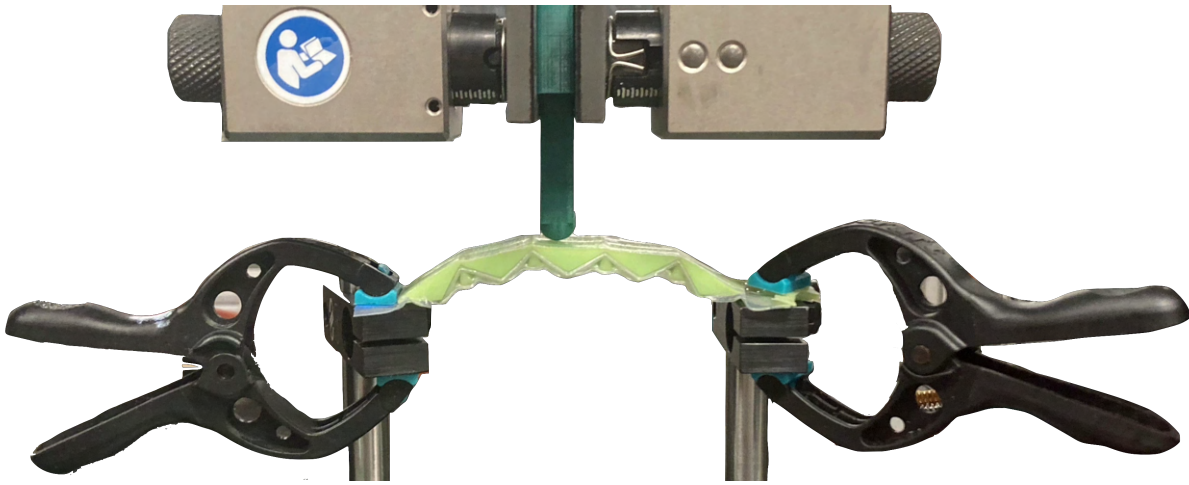


Figure 5.12 – Supplementary strength measurement with two extremities fixed.

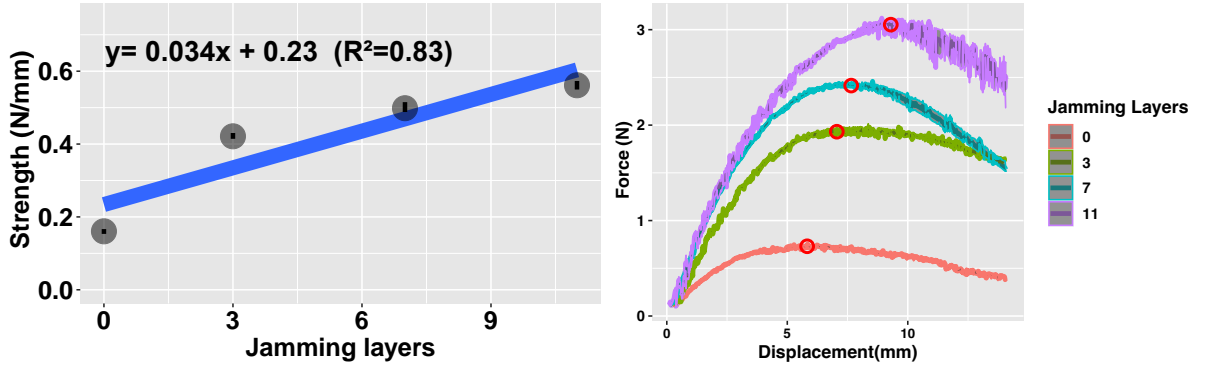
the sliding of “gears” (Figure 5.5(b)), which takes shape when prototypes are vacuumed on the surface of two metal cylinders. The sliding of "gears" might lead to switching gears that contact the metal cylinders, thus suddenly changing the contact force with the indenter. This might decrease the precision of the measurement. To improve our measurement precision, we did some supplementary measurements for the strength by fixing the two extremities of tested prototypes to avoid the sliding of “gears”. We did 7 repetitive measurements for each parameter. To calculate the strength of our prototypes with each design parameter, we calculate the average slope of the 7 force-displacement curves by fitting data points between 0 and 4 mm, where the curves are all nearly linear [21]. The measured strength results are presented as data points in Figures 5.13(a) and 5.14(a), with the error bar presenting the 95% bootstrapping confidence interval based on the 7 repetitions of measurements. The blue lines in Figures 5.13(a) and 5.14(a) present linear regression curves. We report here also the detailed force-displacement curves in Figures 5.13(b) and 5.14(b) where the shadow under curves also presents the 95% confidence interval estimated through the 7 repetitive measurements.

From section 5.3, we can see that having 7 origami jamming sheets leads to the strength increasing nearly twice compared with a prototype without origami jamming sheets (Figure 5.11(b)). To further confirm the key benefit of our new technology for strength enhancing and controlling, we conducted supplementary measurements to study further the impact of the numbers of layers of origami jamming sheets $N_{\text{JammingLayers}}$ on the strength of our prototypes. We also conducted supplementary measurements to study further the impact of vacuum levels P_{Vacuum} , as the P_{Vacuum} is the only parameter that

we can manipulate once the prototype is fabricated, i.e., can be manipulated during use.

Further measurements for the impact of other parameters will be conducted in future work. We provide detailed parameters of these prototypes with Table A.2 in appendix A.4.

5.4.1 Origami jamming sheets layers ($N_{\text{JammingLayers}}$)



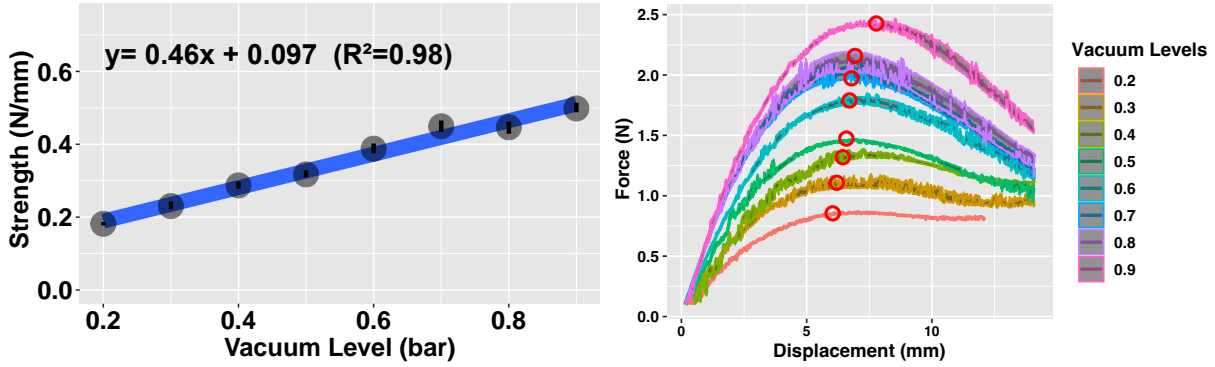
(a) Strength measurements and linear regression result. (b) Force-displacement curves. Red circles show where the force reaches its maximum values and decreases when the indenter compresses more deeply.

Figure 5.13 – Strength measurement in conditions of different layers of origami jamming sheets. (a) Strength (b) Force-displacement curves

With Figure 5.13(a), we can see that our prototypes' strength shows an apparent linear relationship with the number of layers of origami jamming sheets $N_{\text{JammingLayers}}$. We can clearly see that the strength increases with larger $N_{\text{JammingLayers}}$. Figure 5.13(b) presents the force-displacement curves under different $N_{\text{JammingLayers}}$ conditions. With Figure 5.13(b), we observed that the force increases when the indenter starts compressing the prototype, while the force reversely decreases when the indenter descends more deeply. Red circles in this Figure marked the position where the force arrives at the maximum value. Figure 5.13(b) shows the tendency of these points shifting to the upper right with larger $N_{\text{JammingLayers}}$ conditions, i.e., with larger $N_{\text{JammingLayers}}$, the maximum force is larger and needs to compress more deeply to arrive at the maximum force.

5.4.2 Vacuum level (P_{Vacuum})

On Figure 5.14(a), we can see that our prototypes' strength shows a strong linear relationship with vacuum levels P_{Vacuum} and higher P_{Vacuum} can lead to larger strength.



(a) Strength measurements and linear regression result. (b) Force-displacement curves. Red circles show where the force reaches its maximum values and decreases when the indenter compresses more deeply.

Figure 5.14 – Strength measurement under different vacuum levels.

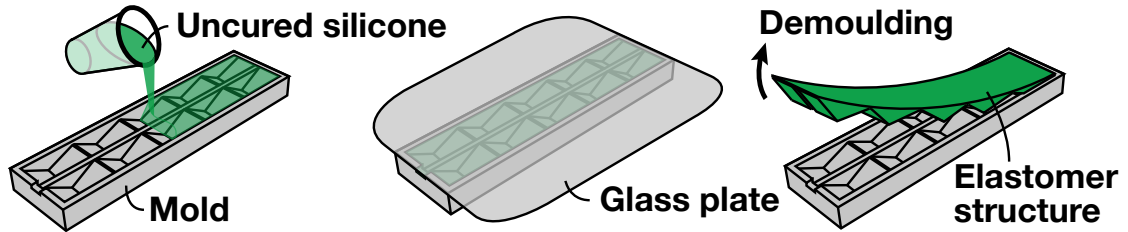
Figure 5.14(b) presents the force-displacement curves with different P_{vacuum} . Similarly to Figure 5.13(b), we also observed that the force will arrive at the maximum value when the indenter descends to a certain depth where marked by red circles in Figure 5.14(b). With Figure 5.14(b), we can see that the tendency of these points shifting to the upper right with higher P_{vacuum} conditions, i.e., with higher P_{vacuum} conditions the maximum force is larger and need to compress more deeply to arrive at the maximum force.

5.5 Fabrication

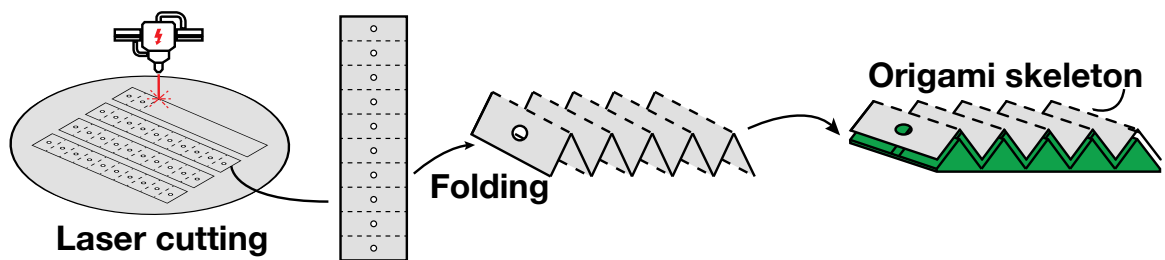
In this section, we present the fabrication process of our prototypes. Figure 5.15 illustrates the process as three major steps:

1. **Elastomer structures molding:** We firstly mold the elastomer structures with the silicone of Elite Double 32 [528], as its short cure time (≈ 20 minutes) allows fast prototype iteration. To fabricate the mold with high precision, we print them with photo-polymer resin (Formlabs standard clear resin [368]) using a stereolithography 3d printer (Formlabs Form3 [109]).
2. **Origami jamming sheets fabricating:** We then fabricate the origami jamming sheets by laser cutting Mylar film of 0.1 mm thickness as it provides a trade-off between thinness to be easily embedded between elastomer structures and rigidity for structure strength. The shape of each origami sheet is the same as the top surface of the elastomer structures (side Prism) when folded by their origami seams,

a Elastomer structure molding



b Origami jamming sheets fabricating



c Prototype enveloping

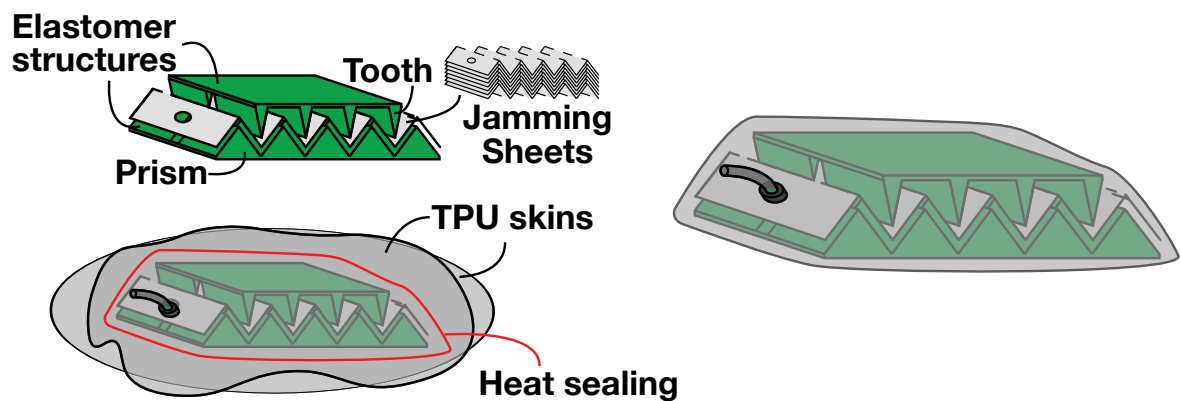


Figure 5.15 – Fabrication process. (a) Molding Elastomer structures. (b) Laser cutting origami jamming sheets. (c) Enveloping elastomer structures and origami jamming sheets together.

which can ensure the origami jamming sheets well fit our elastomer structures. We also cut a few holes on each origami sheet to ensure air circulation when vacuuming out air for actuation.

3. **Prototype enveloping:** We embed a few origami jamming sheets between our elastomer structures and then envelope them into a 0.1 mm thick TPU film by

heat sealing. Before the heat sealing, we insert a short air-tight tube between elastomer structures as the outlet for vacuuming. We chose the 0.1 mm thick TPU film because of its advantages of heat sealing compatibility and high stretchability.

5.6 Examples applications

This section presents some examples of applications of our novel technology for building shape- and strength-changing UIs.

5.6.1 Tuning the range of shape and stiffness of shape-changing physical buttons at the design stage

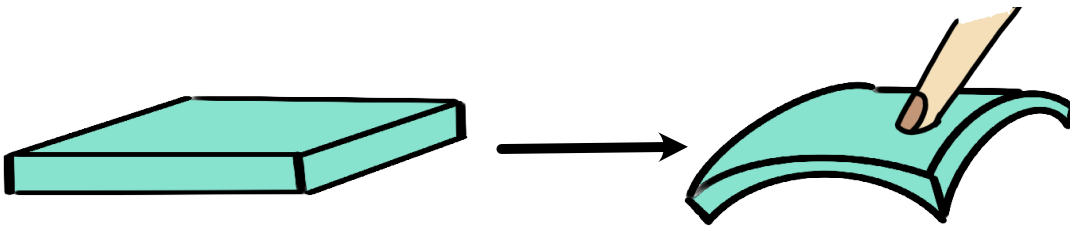


Figure 5.16 – A flat button can change shape into a curved button with higher strength.

Physical buttons represent a ubiquitous interface in our daily lives [9]. They play a crucial role in enhancing users' interaction experiences, such as improving input speed [482] and enabling eye-free interactions [261, 71]. Buttons that possess reconfigurable attributes in terms of shape and strength have the potential to enrich users' interaction experience further. For instance, the creation of a physical control panel with buttons that can be pneumatically inflated or deflated to modify their shape [157], buttons with adjustable actuation force levels [462] (e.g., requiring increased pressure for actuation when pneumatically inflated), and buttons capable of providing haptic feedback through the inflation and deflation of their top surface [132].

In addition to experimental prototypes (e.g., [157, 462, 132]), Alexander, Hardy, and Wattam [9] conducted a survey of 1515 physical buttons in household environments, characterizing them based on various properties, including the input force required to activate the button and the seating depth, defined as the height difference between the button's top surface and the surrounding plane. Their findings indicated that the average

input force for these buttons was 3.2 N ($\sigma = 4.4N$), with convex buttons having an average seating depth of 1.65 mm ($\sigma = 1.13mm$) and concave buttons measuring 0.89 mm ($\sigma = 0.85mm$).

Our technology can be employed during the design phase to assist designers in creating and fine-tuning their buttons' shape and stiffness characteristics. For example, we can generate buttons with varying strength levels by adjusting the vacuum levels (as depicted in Figure 5.14(b), where the maximum force our prototype can support ranges from ≈ 0.8 N to ≈ 2.5 N under different vacuum levels). Furthermore, it is feasible to create buttons with different seating depths, with our prototypes' protrusion height from the plane surface varying from 1.89 mm to 14.44 mm as the design parameter ((h_{Prism})) increases from 2 mm to 7 mm)⁴.

5.6.2 Tunable strength of wearable haptic device for notifications

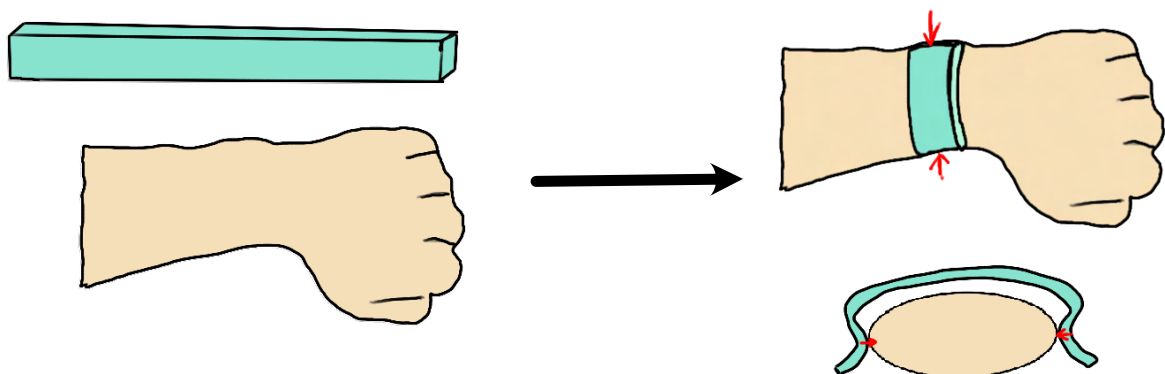


Figure 5.17 – A bracelet can change its shape to give wearer haptic feedback by contacting with wearers. With our technology's capability of strength controllability, we can tune the strength of the UI according to the wearing site, i.e., UI tuned to have higher strength for the body site where sensitivity is poorer.

In recent years, wearable haptic devices have emerged as a significant technological advancement [323, 4, 472, 380]. One common application of these devices is to provide wearers with notifications. Wearers can perceive various sensory inputs such as shape

4. Values corresponds to measurement result presented in section 5.3.3

changes (e.g., [67]), vibrations (e.g., [500]), air jets (e.g., [35]), motion (e.g., [152]), and temperature fluctuations (e.g., [151]) to receive notifications. Many of these applications have been designed with specific technologies tailored for predefined wearables, including finger pads (e.g., [151]), hands (e.g., [27]), forearms (e.g., [87]), wrists (e.g., [135]), and the head (e.g., [32]).

Through Lederman’s two-point touch and point localization thresholds test, we can discern variations in haptic sensitivity across different body sites in individuals [238, 240]. Consequently, a wearable haptic device designed for one specific body site may not be suitable for use on another. As demonstrated in our psychophysical experiment in Chapter 3, our research has revealed that users’ sensitivity can be enhanced, characterized by lower sensation thresholds when employing a more rigid UI for specific interaction positions, such as finger pads. Leveraging our technology, we can develop more versatile wearable haptic devices by precisely adjusting the UI strength based on the wearing position. For instance, higher UI strength may be applied to positions where sensitivity is lower. Furthermore, in conjunction with technologies like [59] of serially connecting different pneumatic shape-changing modules sharing pumps, it becomes feasible to interconnect multiple UIs developed using our approach to create scalable UI systems that accommodate various sizes and wearing positions.

5.6.3 Wearable sitting posture guidance

Numerous studies have indicated that prolonged sitting in office chairs with poor posture can lead to a growing number of health issues [477, 454], including neck pain [251], back pain [444], musculoskeletal discomfort [468], fatigue [162], reduced productivity, and diminished mood [321]. Therefore, it is imperative to develop user interfaces (UIs) that can guide individuals in correcting their posture when it becomes suboptimal.

Various technologies have been developed for detecting users’ sitting posture [477, 454]. When it comes to addressing posture guidance, current technologies primarily employ three approaches:

1. Alerting users when poor posture is detected [392, 218, 22], often through mechanisms like vibration [527]
2. Correcting users’ posture when they adopt poor postures [464, 463, 66], for example, by increasing the resistance of garments worn on the back to discourage further bending [464].

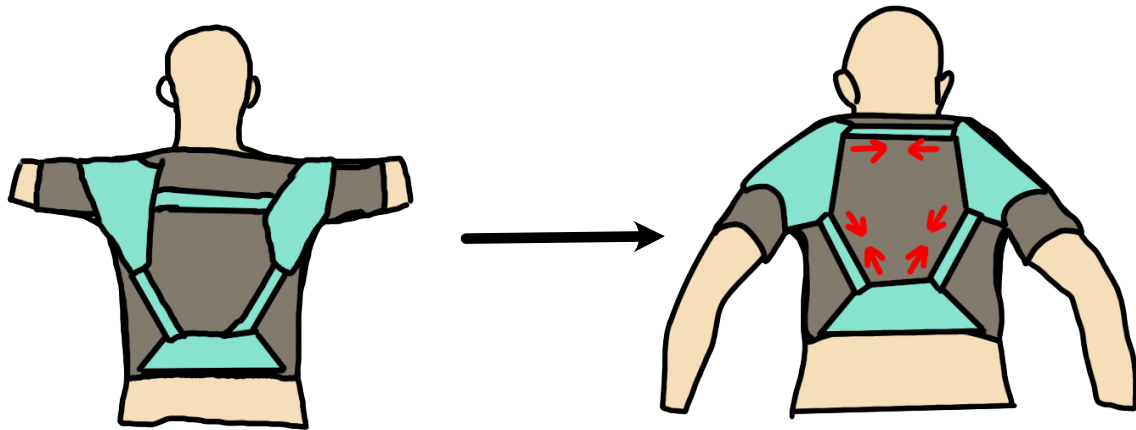


Figure 5.18 – A wearable posture guidance can change shape to alert users of their poor postures and increase movement resistance to correct them.

3. Adjusting the inclination of the chair (e.g., [122]) or the screen in front of users (e.g., [400]) to compel users to correct their posture, which typically necessitates bulky actuation systems, such as industrial robotic arms as seen in [400].

Our technology offers a wearable solution to create UIs capable of controlling posture and strength. This enables the development of wearable garments (see Figure 5.18) with dual functionalities: alerting users when having poor posture through shape changes and correcting their poor posture by enhancing strength, making it more difficult to maintain poor posture. Furthermore, our technology can be extended beyond posture guidance by incorporating haptic feedback and motion limitations based on the wearer’s posture-sensing capabilities. This can be achieved using conductive elastomers, as opposed to non-conductive ones like ours, to detect stretching, i.e., changes in the wearer’s posture, as demonstrated in previous works (e.g., [517, 480, 516]).

5.7 Discussion and future work

5.7.1 Setup for strength measurement

In previous sections 5.3 and 5.4, we introduced two distinct setups for strength measurement. In Section 5.4, we enhanced the setup presented in Section 5.3 by fixing both extremities of the prototypes to the testing support using clips. This modification ef-

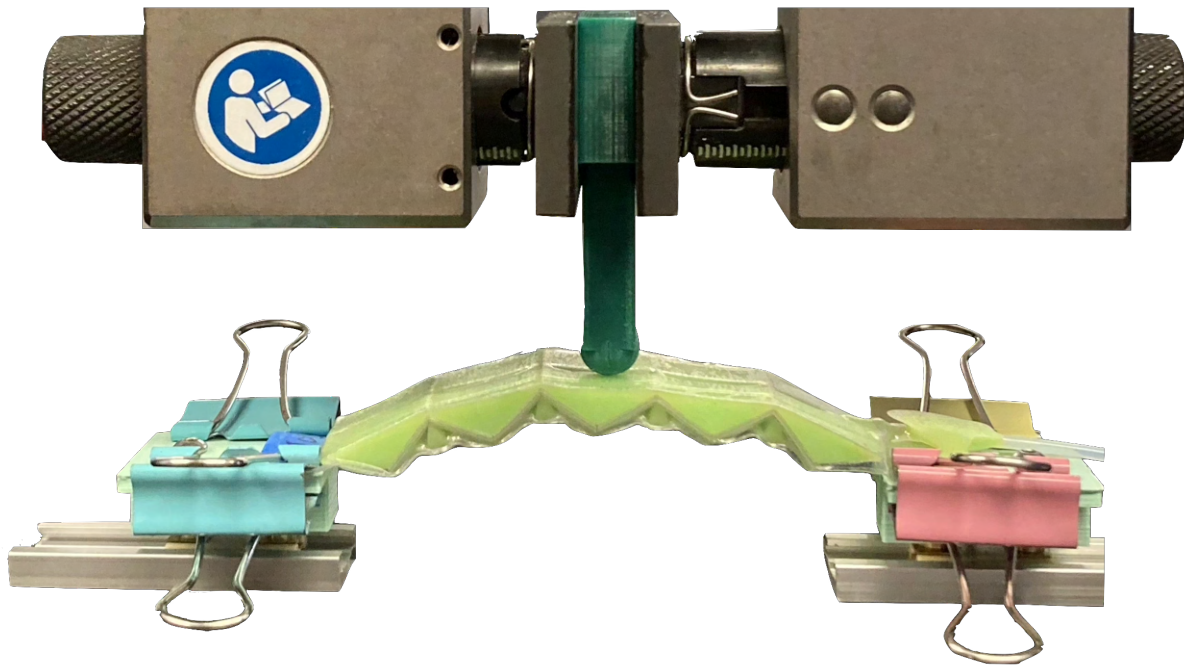


Figure 5.19 – Setup for strength measurement with two extremities fixed on the slider. With this setup, the two extremities of the prototype are fixed on the slider before the measurement. It can freely change its shape when vacuuming, releasing the vacuum, and compressing during the strength measurement.

fectively prevents the unintended sliding of the "gears" along the metal cylinders, which can introduce "fluctuations" in the force-displacement curves, potentially affecting measurement precision. However, this improved setup necessitates manually removing one or both clips before vacuuming to allow the prototype to change shape. Subsequently, the clips must be reattached for each strength measurement. This manual manipulation introduces the potential for measurement errors due to the release-fixing process.

Furthermore, the results obtained with the setup involving the fixation of both extremities may not directly apply to UI design scenarios in which at least one side of the UI should remain free to accommodate shape changes and enable users to interact with the UI's shape and strength without prior fixation. To address this limitation, we intend to conduct further strength measurements utilizing a setup that fixes both extremities of the prototypes on sliders, as depicted in Figure 5.19. In this setup, the prototype can undergo shape changes during vacuuming, release, and compression without requiring manual release-fixing steps, as seen in Figure 5.12.

In comparison to the configuration in Figure 5.5(b), where both extremities are placed on metal cylinders, the setup with both extremities fixed on sliders ensures smoother movement of the prototype’s extremities along the sliders, thus minimizing “fluctuations” in the force-displacement curves. The adoption of this slider-based setup (Figure 5.19) brings the measurement results closer to real-world application scenarios in which users can interact with UIs placed on a flat surface, such as a desktop, without the need for additional extremity fixation.

5.7.2 Shape and strength controlling mechanism

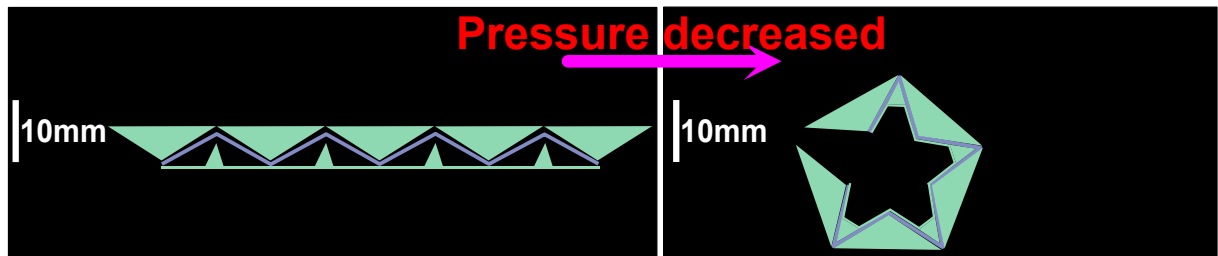


Figure 5.20 – Theoretical shape-change of the prototype presented in Figure 5.5(a). After the air has been vacuumed out, the neighbor inclined surfaces of the “Prisms” and “Teeth” should come into parallel and perfect contact with the jamming sheets (line in purple colors) between them.

Shape-controlling mechanism Our technology’s primary mechanism governing shape control is the pressure gradient inside and outside our prototype. This gradient, generated by the vacuum, compels our elastomer structures to bend, thereby expelling air between the “Prisms” and “Teeth”. This occurs because the shapes of " prisms " and " teeth " are inherently incompatible, leaving gaps between them. Ideally, once all the air inside our prototypes is completely vacuumed, the neighbor inclined surfaces of the “Prisms” and “Teeth” should come into parallel, resulting in the maximum achievable shape change for the entire prototype (Figure 5.20).

The prototype presented in Figure 5.5(a) theoretically has the potential to bend approximately 320° (Figure 5.20) when all the air is vacuumed out⁵, the neighbor inclined

5. In Figure 5.5(a), the vertex angle of “Tooth” is 40° (β) in Figure 5.4, and the vertex angle of “Prism” is 120° (β) in Figure 5.4. The respective base angle of “Prism” is 30° . There thus exists around a space of 80° that each “Prism” can turn around the apex of respective “Tooth” till their neighbor inclined surfaces parallel to each other. Considering that we have 4 “Teeth” in each prototype, the prototype can

surfaces of the “Prisms” and “Teeth” come into parallel and perfect contact with the jamming sheets between them. However, during our measurements, we observed that the prototype only bent to around 68° (as indicated by the central angle of the highlighted arc in Figure 5.5(a) top right) when the vacuum level reached 0.95 bar, representing the maximum vacuum level attainable in our experiments. We hypothesize that the measured shape change is significantly lower than the ideal one due to the buckling phenomenon of the membrane connecting each “tooth” and the TPU enveloping membrane. These factors prevent our structure from achieving further shape change, resulting in non-squeezed spaces between “Prisms” and “Teeth” (as shown in Figure 5.5(a)). This observation is consistent with the curvature measurements presented in Figure 5.9(a), where thicker membrane thickness h_{Membrane} leads to slightly smaller curvature. Thicker membranes introduce stronger resistance when undergoing bulk deformation during shape change.

Similar to the membranes of our elastomer structures, the enveloping TPU membrane may also introduce resistance during bulk deformation during shape change. Thus, future research should explore the enveloping membrane’s impact on our prototypes’ shape change, considering factors such as membrane thickness and materials. Future work should also address the design of these membranes to mitigate or reduce buckling.

Strength-controlling mechanism The fundamental mechanism governing strength control relies on jamming principles, as described in previous works [107, 319]. When we evacuate the air from the interior of our prototypes, a pressure gradient is established between the inside and outside, inducing bending in our elastomer structures. Simultaneously, the pre-cut origami jamming sheets adapt their shapes to coincide with these elastomer structures. When the origami jamming sheets come into contact with the elastomer structures on both sides, further air removal compresses these sheets, increasing inter-sheet friction. This, in turn, impedes the deformation of the prototype, resulting in enhanced strength [7]. This observation aligns with our experimental data, as illustrated in Figures 5.14(a) and 5.10(b).

Furthermore, as depicted in Figure 5.5(a), we observed that the buckling of the membranes creates gaps between the elastomer structures and origami jamming sheets. Addressing this issue by optimizing the design of the elastomer structure’s membranes to minimize or eliminate buckling could reduce the gaps between the elastomer structures and origami jamming sheets. This optimization may further augment the strength of our

ideally bend $80^\circ \times 4 = 320^\circ$.

prototypes. Future research should focus on addressing this challenge.

5.7.3 Design parameters and design tools

With our measurements of *Curvature* and *Strength* in section 5.3, we observed that the three main design parameters that impact both our prototypes' *Curvature* and *Strength* are Δ_{Angle} , h_{Prism} and P_{Vacuum} . With supplementary strength measurements in section 5.4, we further confirmed that increasing P_{Vacuum} can lead to larger *Strength*. Besides, we also found increasing layers of origami jamming sheets $N_{\text{JammingLayers}}$ can lead to increased *Strength*. These measurements suggest that further prototype improvements can focus on the aforementioned design parameters. To facilitate other researchers' research based on our technologies, we are developing a design tool that allows designers to tune different design parameters and simulate the *Curvature* and *Strength* change based on our measurements in section 5.3 and 5.4. Once we finish designing our UI with this design tool, it should also provide users with STL files for 3D printing the mold of elastomer structures and SVG files that can later be imported to a laser cutting machine for fabricating the origami jamming sheets. Providing such a design tool should significantly lower the barrier of constricting SCIs from technological aspects [10].

5.7.4 Force reverse during compression test



Figure 5.21 – Two shape status of a popper toy: convex (Left) and concave (Right). It can suddenly turn from a convex to a concave shape and vice versa when a user continuously pushes on it [427].

In Figures 5.13(b) and 5.14(b), we present force-displacement curves, revealing an intriguing observation during the compression test. These curves indicate that, while undergoing compression, the force reaches its maximum value at a certain depth and decreases with further compression. This phenomenon can be elucidated through the Snap-through effect, which has been extensively studied in the field of material science [29,

325, 174]. The Snap-through effect refers to the abrupt change in shape observed in curved surfaces when subjected to pressure. For instance, if you continuously push the center of a popper’s toy (as shown in Figure 5.21), it can suddenly transition from a convex to a concave shape and vice versa. During this sudden shape change, you can perceive a decrease in the force applied to the toy.

Leveraging the Snap-through effect, we can enhance haptic feedback when interacting with user interfaces developed using our technology. As demonstrated in Figures 5.13(b) and 5.14(b), a prototype equipped with additional origami jamming sheets or subjected to a higher vacuum level can result in an increased maximum force that users must apply and a deeper compression required to reach this maximum force.

Current theories [29, 325, 174] for analyzing and modeling the Snap-through point, i.e., determining the maximum force value and the depth at which it occurs, are primarily designed for homogeneous materials, such as the Silicon (Si) beam studied in [174]. Our prototypes, however, consist of multiple layers of different materials, including TPU membrane, elastomer structures, Mylar sheets, and air gaps between them. Consequently, applying these current theories to analyze and model the Snap-through point in our prototypes becomes challenging.

Future research will involve finite-element simulations (e.g., [58]) and synchronized video recordings capturing the deformation of our prototypes during the compression test and real-time force-displacement curves. This comprehensive approach aims to provide a deeper understanding of the behavior of our prototypes at various positions along the force-displacement curves, particularly concerning the Snap-through point. A more nuanced comprehension of the Snap-through point will enable us to design user interfaces using our technology with enhanced haptic feedback by predefining both the maximum input force and the depth of force reversal indentation.

5.7.5 Shape-changing capability

In our current study, each “Prism” and “Tooth” within a single prototype share an identical shape and are evenly distributed in parallel across the elastomer membrane, resulting in consistent shape changes for every pair of “Prism” and “Tooth”, i.e., uniform local shape changes. Simultaneously, we focused solely on analyzing the curvature change of the entire prototype and did not investigate further to examine local shape changes, i.e., the between each pair of “Prism” and “Tooth”. We drew inspiration from previous research, specifically CurveUps [147] (Figure 5.22). CurveUps [147] presents a technology

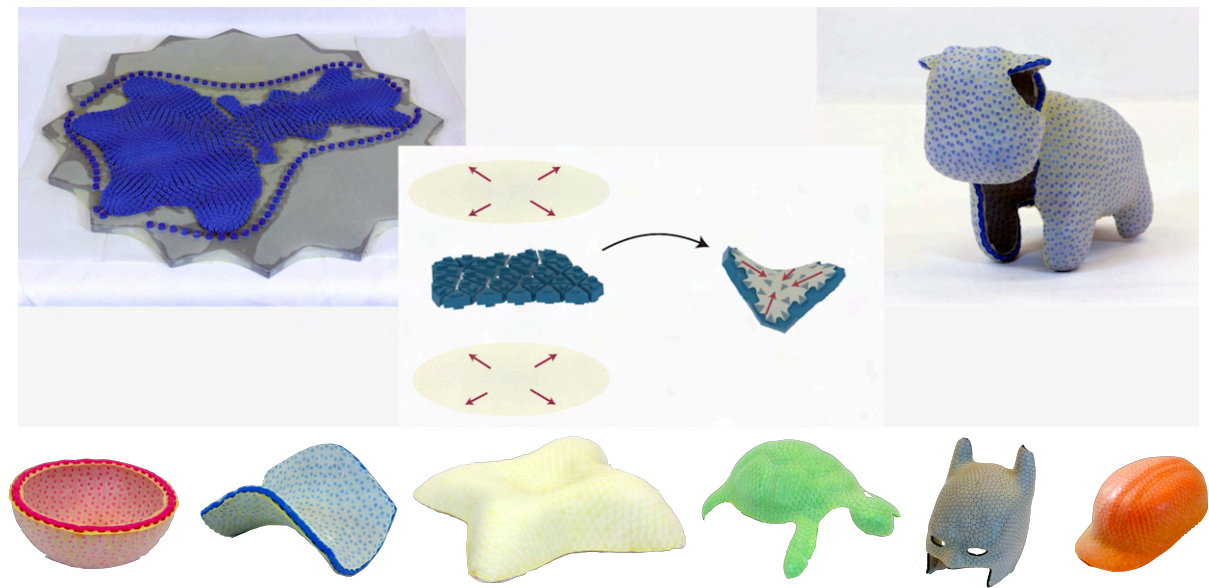


Figure 5.22 – This Figure [147] presents CurveUps, the technology of 3D printing spaced prisms on pre-stretched latex membrane to create 3D shapes when releasing the fixation around the membrane and some examples of 3D objects created with this technology. Top left: a flat latex membrane with 3D-printed spaced prisms on it, with the membrane’s boundary fixed on the support plate. Top center: This demonstrates what happens as a local shape changes when the membrane’s fixation is released. Top right: the flat surface turns into the shape of a cow when the fixation is released. Bottom: Some other exemplary 3D objects were created with CurveUps technology. From left to right: Half-Sphere, Hyperboloid, Lilium, Turtle, Bump Cap and Mask.

that employs 3D printing of sparse prisms on a pre-stretched latex membrane to generate 3D shapes upon releasing the membrane’s tension. The release of tension in the pre-stretched latex membrane causes it to contract, bringing the 3D-printed prisms closer together and reducing their spacing. When adjacent prisms come into contact due to this reduction in distance, they rotate around the point of contact, resulting in localized deformation. CurveUps [147] also provides an algorithm for determining the shape and distribution of each prism to achieve a specific 3D shape. Our JOE technology shares a similar mechanism of shape change with the rotation of each pair of “Prism” and “Tooth” when subjected to a vacuum, causing them to decrease the space between them. In our future work, we can draw upon the insights from CurveUps [147] to create other shape changes by meticulously designing the size and orientation of each “Prism” and “Tooth” as well as the distances between them by our desired 3D shape.

5.8 Conclusion

In this chapter, we present an innovative technology termed “Jamming Origami Endoskeleton (JOE)”. This technology facilitates concurrent control over both the strength and geometric shape, specifically the curvature of UIs. This technological advancement can help to address soft programmable materials’ stretchability-strength trade-off [10] and offer a new opportunity for an immersive haptic feedback experience. Through comprehensive measurements of curvature and strength in our prototypes, we have identified three key design factors influencing the strength and curvature of UIs utilizing our technology. These factors encompass the angle differences between "Prism" and "Tooth" Δ_{Angle} , the height of "Prism" $\mathbf{h}_{\text{Prism}}$, and the vacuum level $\mathbf{P}_{\text{vacuum}}$. Moreover, our research demonstrates that an increased number of origami jamming layers $\mathbf{N}_{\text{JammingLayers}}$ can augment the strength of UIs. Future research endeavors to enhance our technology should prioritize the optimization of these design parameters.

In conjunction with the preceding chapter, we emphasize the potential of utilizing soft materials for the development of SCIs with high shape-changing abilities. The subsequent chapter will address the design challenges of SCIs research by delving into specific HCI application development with SCIs in programmable soft materials.

PART III

SCIs design

SHAPE MORPHING WATCH

6.1 Introduction

One design challenge of shape-changing interfaces (SCIs) research is to develop HCI applications for users. In this chapter, we will address this challenge by developing an HCI application with SCIs in programmable soft materials and evaluating users' interaction experience with them. We will focus on wearable SCIs since the high stretchability of soft materials like elastomers [509] makes them stand out for wearable applications [480]. Wearable UIs endowed with shape-changing capabilities have emerged to deliver haptic and visual experiences on the human body [220]. Notably, notifications conveyed through shape changes have been overlooked less frequently than vibrations [85]. As the exploration of soft and shape-changing technologies for wearable UIs gains momentum (e.g., [146, 160, 391, 135, 181]), there is a timely need to empirically investigate their potential applications on one of the most probable body locations—the wrist [522]—and for one of the most crucial functions of smartwatches, i.e., notifications [6]. Additionally, users tend to associate highly noticeable modalities with important notifications [267], underscoring the significance of understanding the perceptibility of these novel modalities.

Among various forms of shape changes [226], curvature change stands out as one of the most prevalent [226]. Our earlier study in Chapter 3 has already affirmed users' ability to precisely perceive the curvature of soft UIs, especially when they exhibit pronounced curvature. The central question addressed in this chapter pertains to **determining the optimal maximum curvature at which users are most likely to notice soft shape changes on their wrist**. While prior work studied (1) noticeability on the wrist of many modalities, (2) shape-change on the wrist, (3) noticeability of shape-change, and (4) tactile perception of soft and curved surfaces, none of these prior work has studied

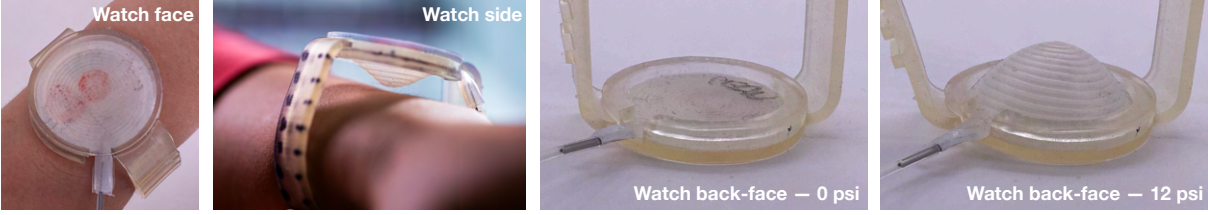
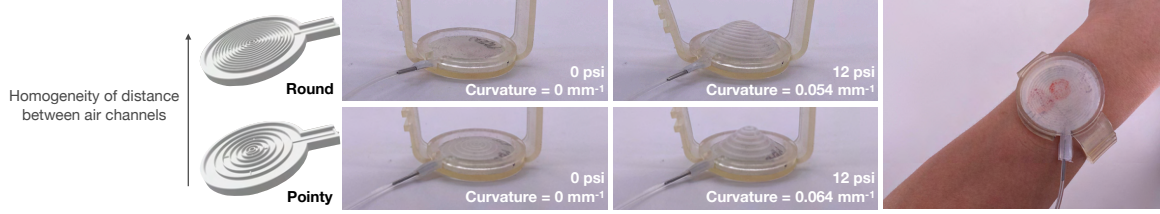


Figure 6.1 – We present a novel haptic notification mechanism for soft watches, through the change of curvature and contact area of its back surface. The second picture (watch side) shows a loosely tied bracelet for illustration purpose, unlike our experiment.

the impact of the curvature for users to notice soft shape-change on their wrist.

Addressing this research question poses a significant challenge, primarily involving the isolation of parameters [10]. Specifically, it necessitates controlling the maximum curvature while maintaining a constant watch size. Prior pneumatically-actuated prototypes –based on simple air chambers–cannot keep the watch size constant to vary the maximum curvature. With technologies we have explored in Chapter 4 on constructing SCIs with soft materials primarily based on recent advances from material sciences: Baromorph [402] materials, we introduce our original (1) **fabrication of a wrist-worn Baromorph surface measuring $\varnothing 42$ mm in and 3 mm-thin**. Furthermore, we (2) **conduct a psychophysical experiment to measure the absolute detection threshold (ADT) on the posterior side of the wrist at 3.86 psi**—prior to the surface starting curving. Through participant interviews, we demonstrate that (3) **participants found this novel feedback enjoyable**, and (4) **participants felt different sensations for each maximum curvature**.

6.2 Related work

We position our work (Figure 6.2) to the following research areas: (1) noticeability studies on the wrist, (2) shape-change on the wrist, (3) perception of shape change, and more particularly of curvature change, and (4) impact of curvature and softness on the tactile experience.

6.2.1 Noticeability on the wrist

Notifications on the wrist are already common on smartwatches. Most research and industrial wrist-worn systems deliver vibrotactile feedback, e.g., [329, 17]. As an example, Graham-Knight et al. studied the use of vibrations on a smartwatch for non-visual communication for intimate people [141]. Vibrotactile feedback on the wrist was shown to increase speakers' awareness of time, help the coordination between a speaker and her session chair, and reduced distraction [431].

Visual notifications were also studied. E.g., Kao et al. studied the perception of on-skin visual notifications in social contexts [216]. Pohl, Medrek, and Rohs explored indirect illumination on the wrist as a way to provide notifications to users [343]. Vibrotactile and visual feedback have also been combined. E.g., Schäfer et al. studied visual (light), audio, and haptic (vibration) notifications on the wrist to monitor questions and feedback during online presentations [384]. Further modalities have been studied to provide notifications to users on their wrists. E.g., Lee and Lee studied the absolute detection threshold of airflow on the wrist [241].

Stronger push on users' skin has been studied for notification. E.g., HapticClench [146] uses shape-memory alloys to provide a squeezing sensation around the arm, and InContact [407] compares pinch, squeeze, and twist sensations to vibrotactile feedback for mediated social touch. However, both provide shear force feedback on the skin, in addition to feedback perpendicular to the skin that we study here. In addition, these devices do not use curvature for haptic feedback as we do.

PneuHaptic [160] pneumatically & independently actuates five silicone chambers worn around the arm. In an informal evaluation, the authors show the effectiveness of PneuHaptic. However, the curvature of the inflated silicone chambers is fixed by their size (isotropic deformation, Figure 6.3). In addition, chambers are always in contact with the users' skin. On the contrary, we propose to explore the impact of *two different curvatures* temporarily touching the skin on the absolute detection threshold, for the *same watch size*.

6.2.2 Shape-change on the wrist

Shape change on the wrist has been studied. E.g., Doppio [391] explores the design space of a modular screen for smartwatches. WristOrigami explores the design space for foldable multi-display smartwatches [529]. On the contrary, we explore a more organic and soft design providing surface continuity and study the noticeability of its curvature

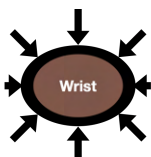
						
OUR WORK and [160, 181, 329]	Compression [146, 160, 342]	Shear [146, 407]	Vibrotactile [17, 141, 329, 384, 431]	Airflow [241]	Light [216, 343, 384]	Audio [384]

Figure 6.2 – Positioning to prior wrist-worn feedback: we explore curvature change, while prior work explored different types of feedback.

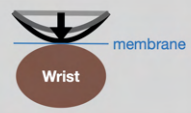
			
OUR WORK	PneuHaptic [160]	RetroShape [181]	Haptic wristwatch [329]
Anisotropic deformation		X	X
Continuous surface	X		X
Soft surface	X		X
Low voltage	X	X	
High amplitude	X	X	
Temporary contact		X	

Figure 6.3 – Positioning to prior curvature-changing wrist-worn devices: PneuHaptic’s airbag deforms in the same way in all directions (isotropic deformation), making the curvature linked to the diameter of the airbag. In addition, it is always in contact with the users’ wrist [160]. RetroShape provides low curvature resolution through its discrete 4 × 4 surface and its surface is made of hard material [181]. The eyes-free haptic wristwatch relies on a membrane that is always in contact with the user’s wrist, requires high voltage (up to 160V compared to our 12V) and provides limited maximum amplitude (a few mm compared to our >15mm) [329].

change.

Cito [135] explores movements of the watch face, namely orbiting the face around the wrist, translating it out of the sleeve, rotating it around its orthogonal axis, tilting it, and raising it. While rising, it provides the same kind of haptic feedback that we study here, but it does not allow to vary the curvature of the watch face.

AmbienBeat [68] sticks electromagnets on silicone membranes to provide users with haptic feedback with the repulsion and attraction force of electromagnets. The authors find that haptic feedback from ambienBeat can better guide users' heart rate regulation comparing with auditory and visual guidance. However, they do not explore the feedback from surfaces with different curvatures.

RetroShape [181] provides a 2.5D shape-display on the back side of a smartwatch. The authors study the impact of the resolution of the 2.5D display on the illusion of the presence of virtual objects. The shape display that we provide is different as it is soft and continuous (Figure 6.3).

A haptic wristwatch [329] was proposed, where a piezoelectric disc on the back side of a watch changes curvature to hit a membrane in contact with the users' skin. However, Pasquero, Stobbe, and Stonehouse's change of curvature does not change the contact area on the users' skin as we do and requires higher voltage while providing lower amplitude of shape-change (Figure 6.3).

6.2.3 Perception of shape-change

Prior work studied the noticeability of shape change. E.g., Lee, Lee, and Choe studied visual notifications provided through a shape-changing plant [242]. Among other kinds of shape change, the authors study the change in the plant's curvature. However, its absolute visual detection threshold has not been studied. Bending a flat panel has also been studied as a way to provide visual notifications from the users' environment [211]. Authors found that such feedback in the users' near periphery was efficient and not distracting. However, these prior works study ambient notifications.

Closer to the users' bodies, different types of shape-changing notifications were studied in a video-based study [333]. In particular, around 82% of their participants said they would attend to curvature-based notifications. MorePhone [134] provides notifications by bending the whole mobile phone or its corners independently. Authors found that bending the whole phone was rather matched to urgent notifications. Leveraging the haptic information provided by the change of shape, Hoggan et al. studied if users can

distinguish mobile shape-changing textures [167] at the surface of a mobile phone. On the contrary, we investigate the noticeability of curvature change on the wrist. Dimitriadis and Alexander studied if different types of shape-changing mobile phones were noticeable in the front pocket of trousers [85]. However, it is hard to generalize these results to another body part (wrist vs. thigh) and to different types of shape-change.

Prior work studied more particularly curvature-changing interfaces (e.g., [63, 361, 157, 132]). E.g., HapTag [63] provides haptic feedback through the deformation of a thin surface located on users' skin. However, this prior work did not study the impact of the curvature of the surface on noticeability. Pneumatibles [132] decrease the air pressure step-by-step in a "detents" pattern. The authors studied users' recognition precision with different combinations of the number of detents and the initial maximum pressure in the button. However, they did not study the combination of participants' absolute detection threshold and curvature of a wrist-worn device.

6.2.4 Touch, curvature, and softness

Touch between a system and users can happen actively or passively. Active touch happens when users initiate the touch, e.g., when users voluntarily touch their capacitive screen. Passive touch happens when users are touched without controlling the movement, e.g., for haptic notifications.

When actively touching, humans can distinguish with their index finger a curved surface—with a base-to-peak height of 0.09 mm—from a flat surface [139]. We have studied in Chapter 3 the just-noticeable difference in curvature in different softness conditions. However, we haven't studied the absolute detection threshold on the wrist for passive touch. Hu and Hoffman explored round and spiky bumps on a robot skin for emotional expression [176, 177, 178]. However, they do not explore if these shapes can be used as any other type of feedback.

Other work on active touch studied perception when users slide their finger over the surface to explore the curvature [347]. However, active touch perception does not involve the same perception mechanisms as passive touch, i.e. when receiving a notification. Users only use cutaneous cues¹ when passively touched. On the contrary, active touch

1. Kinesthetic cues refer to the sense of position and motion of limbs, along with associated forces, conveyed by the sensory receptors in the skin around the joints, joint capsules, tendons and muscles [240, 415]. The cutaneous cues refer to the responses of mechanoreceptors [209] innervating the finger pad skin within and in the neighborhood of the contact area [240, 415].

[129] involves kinesthetic cues¹ [240].

When being passively touched on their index finger, humans judge stimuli slightly less curved than they actually are when the contact force increases (e.g., from 0.196 N to 0.588 N) [136]. In addition, humans' discrimination threshold slightly decreases when the contact area increases [137]. While contact force and area play a role when being notified through curvature change, both the effect of contact force [136] and contact area [137] are much smaller than the effect of the surface curvature itself. For this reason and for the sake of simplicity, we present our exploration around the exploration of the surface curvature to provide notification feedback, although we are aware that the resulting contact area and force play a role.

Actively touching *soft* objects, like passive touch, involves cutaneous cues. The contact area of a finger with another soft surface increases as the finger presses deeper into the surface [207]. The softer the surface, the more rapidly this contact area increases. Leveraging this phenomenon, Bicchi, Scilingo, and De Rossi proposed the Contact Area Spread Rate (CASR) device [36, 386]. Through the contact area between the finger and the device, this device provides users with cutaneous information. The hard device can vary its contact area with the user's finger pad through telescopic concentric cylinders. The finger presses at the top of the device and indents the cylinders more deeply. When the finger comes in contact with larger cylinders, the contact area increases. Bicchi, Scilingo, and De Rossi adapt the speed of the enlargement of the contact area according to the softness of the simulated surface: the softer the simulated surface, the more rapidly the contact area increases. The authors found that with this simulation, users recognize the softness almost as well as with real objects: 75% with CASR vs. 87% with real objects. This shows the important role of cutaneous cues, in particular the contact area, in softness perception. In our study, users are *passively* touched by a soft surface. Depending on its curvature, we expect the contact area to vary. Therefore, we expect cutaneous cues to play a major role in the detection of the notification.

While prior work explored areas close to the problem addressed in this chapter, this section shows that no prior work studied the absolute detection threshold of the soft curvature-changing back-face of a watch. In addition, the work closest to ours use different technologies, e.g., either confounding maximum curvature and size [160], with low curvature resolution [181], or with limited maximum curvature [329].

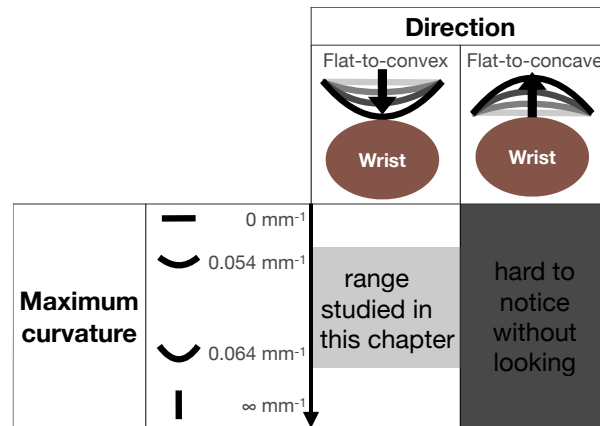


Figure 6.4 – Design space of the maximum curvature.

6.3 Watch design

To design our watch, we considered the following parameters: shape change, temporal pattern, and location.

Shape-change Among the many possible features for shape change, such as porosity, modularity, or size [226, 363], we choose to first focus on curvature (Figure 6.4), as this is one of the most common changes of shape studied in the literature. We leave for future work the full exploration of the space for alternative shape change, and particularly focus on the range of curvature that a surface can offer. In order to limit the number of experimental variables for this first experiment, we chose the same curvature all around the surface (rotational symmetry).

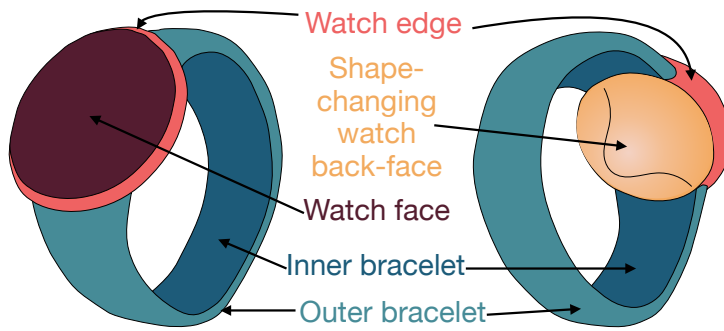
We considered concave and convex curvatures (Figure 6.4). We explored in a pilot study flat-to-concave curvatures –away from the wrist as shown in Figure 6.4. It was hardly noticeable without looking at the wrist. For this reason, we only consider flat-to-convex deformation –towards the wrist. We then considered a range of maximum curvatures from round to spiky. We discarded extremely spiky curvatures for user safety, as even a low pressure on the skin can hurt if the contact area is extremely small [201]. As shown in Figure 6.4, the spikiest prototype we could fabricate offers a maximum curvature of 0.064 mm⁻¹. We then fabricated an intermediate prototype, less spiky but able to touch the skin when inflated, with a maximum curvature from 0.054 mm⁻¹.

Temporal pattern Kinetic parameters of the change of shape, such as speed, path and direction [363], open a large design space for notifications through shape-change. Such patterns are often studied for other notification mechanisms such as vibration, e.g., [141]. In this chapter, we study a simple ramp pattern: the surface linearly goes from flat to curvy, stays constantly curvy for a certain amount of time, and then linearly goes back to flat at the same speed as before.

Location We considered alternative locations for the curvature-changing surfaces, all around the watch (Figure 6.5). The outside of the watch –watch face and outer bracelet in Figure 6.5(a), left– allows for visual feedback, while the inside of the watch –watch back-face and inner bracelet in Figure 6.5(a), right– allows for haptic feedback as it contacts with the skin. We also considered the different sides of the wrist (Figure 6.5(b)): posterior, medial, anterior, and lateral sides of the wrist. We only explore the watch back-face for the study presented in this chapter (Figure 6.1) based on the following rationale: As prior work already studied the visual feedback provided by the change of curvature very close to the users’ wrist [211], we choose in this chapter to focus on the haptic feedback provided by the change of curvature, i.e. the inner side of the watch. As the posterior side of the forearm is the most sensitive side of the forearm [95], we choose to start with the back-face of the watch (yellow in Figure 6.5(a)), rather than the other sides of the wrist.

To fabricate a soft, round surface that changes curvature on the back face of a watch, we leverage previous work in material sciences on soft shape-changing materials [402], namely silicone surfaces with embedded air channels called baromorphs (Figure 6.1). The arrangement of air channels defines the surface deformation when inflated. The distinguishing characteristic of different designs is the local curvature of the resulting inflated material: varying arrangements of air channels show different local curvatures under the same inner pressure. We focus in this chapter on rotation-invariant arrangements of air channels (Figure 6.6) which allows us to explore the different maximum curvature (and resulting contact areas and pressure) when inflated. This material is the single one we found that allows the deformation of a continuous, soft surface in a single direction, with low voltage (12V) and >1cm amplitude of shape-change (Figure 6.2).

outside	edge	inside

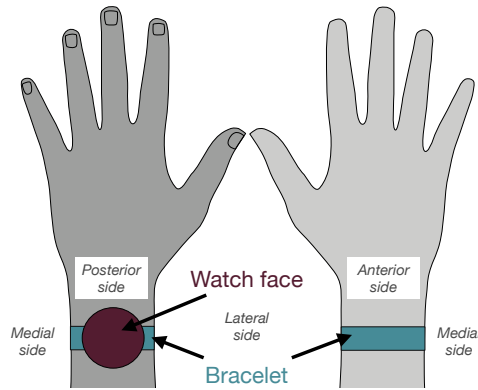


(a) Alternative shape-changing areas.

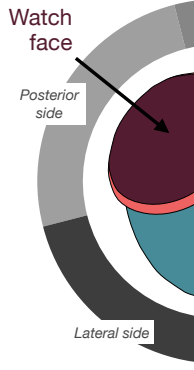
width=368px

width=1902px

lateral side anterior side



	outside	edge	inside
posterior side			
lateral side			
anterior side			
medial side			



width=567px

width=368px

width=1902px

Figure 6.5 – Location of shape-changing areas

6.4 Watch fabrication

We are the first to fabricate such small baromorph surfaces. Making small prototypes is a grand challenge in shape-changing research and an essential step to leverage results from material science for wearable interaction [10]. We faced the three following challenges when fabricating our $\varnothing 42$ mm and 3 mm-thick baromorph surface following Siéfert et al.’s instructions –made for larger surfaces [173].

3D printing a small and high-resolution mold To precisely control the shape of a $\varnothing 42$ mm and 3 mm-thick baromorph, the challenge lies in achieving a high density of air channels in such a limited volume. We used a Form3 high precision Stereolithography (SLA) 3D printer [109] and faced a printing precision challenge and a cleaning challenge. The printer precision and the resin we used were bottlenecks to achieve thin air channels. When cleaning with isopropyl alcohol [197] in FormWash [110] after printing, the mold slightly deforms. At this scale, such fabrication defects lead to relatively large unwanted deformation of the inflated surface. To solve these problems, we systematically tried to print the molds for 0.1 mm- to 1 mm-wide air channels with the 3D printer. We tried to print with Formlabs General Purpose black, white, and clear resins [368] and noticed that the clear resin worked best. We also noticed that changing the isopropyl alcohol [197] in the FormWash [110] more often than required by the manufacturer, prevented any residue at the surface of the mold. The smallest air channels whose mold was of sufficient quality to achieve the designed deformation were 0.4 mm wide.

Removing air bubbles trapped in the uncured silicone As the inner structure of our baromorph is very thin, even one small air bubble inside the baromorph will lead to strong local deformation around the bubble and thus lead to an unpredicted shape when inflating the baromorph. To solve this problem when molding the silicone, we carefully remove all entrapped air inside the mixture of silicone after pouring the silicone into the mold. To do this, we vacuum degas the mixture for 3 minutes and use a needle to bring bubbles entrapped in the mold to the surface.

Gluing the cover to the channels To complete the baromorph fabrication, we unmold the baromorph, and we spread and cure a 0.4 mm-thin silicone membrane for the cover. When gluing such a thin membrane on top of such thin and low channels, the risk lies in obstructing the 0.6mm-high channels. Air channels that are obstructed by the glue or not

perfectly glued to the cover lead to relatively large unwanted deformation of the inflated surface. To solve this problem, we use the Sil-Poxy glue [403] instead of silicone [402]. The higher viscosity of the glue enables a more precise control of the thickness. We use a high precision film casting knife [106] to precisely control the thickness of the glue [403] to 0.3 mm, which is thick enough to strongly glue all inner structures but thin enough to avoid the obstruction of channels.

We tested different silicone (Smooth On Ecoflex and Dragon Skin silicone series [191]) in a pilot: Shore 00-10, Shore 00-50, Shore A-10, Shore A-20, and Shore A-30. We selected the Shore A-10 silicone, as it provided a trade-off between large shape-changing ability, and fast curing and fabrication.

We 3D print the watch case and bracelet with Formlabs Flexible 50A Resin [368] with the same printer [109].

To actuate the change of shape at the back of the watch, we developed a Python script that controls three 12 V two-way peristaltic air pumps [140] connected in parallel to inflate and deflate the shape-changing surface. The pumps are connected directly to the shape-changing surface with a long and thin Flexible PVC Tube [**PVCtube**]: 1.5 m long, 0.8 mm inner diameter and 2.4 mm outer diameter. Through this technical design, the shape-changing surface can rapidly increase its inner pressure from 0 psi to 12 psi within 1 second. We paid particular attention to the parameters of the proportional–integral–derivative (PID) controller in the software, to avoid the tingling sensation that we noticed during early testing. We share all the necessary materials to fabricate our prototype, including 3D models and Python scripts with the parameters of the PID controller.

6.5 Absolute detection threshold

The absolute detection threshold is an important and fundamental initial psychophysical measurement [127] that defines the threshold at which users can notice the feedback from the backside of the watch. Rather than measuring human sensitivity, the aim of our experiment is to determine a baseline when triggering the notification. This measure is necessary to design future interfaces and applications with the soft curvature-changing back face. We conducted this study in the lab with no distractions, to identify the baseline notification. First, determining the ADT with no distraction is a standard procedure in prior work, e.g., [146, 342, 28]. To reduce unintentional false positive inflation of

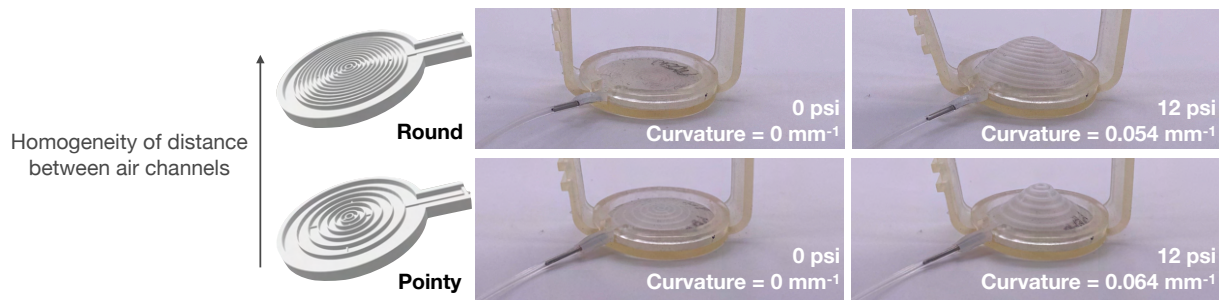
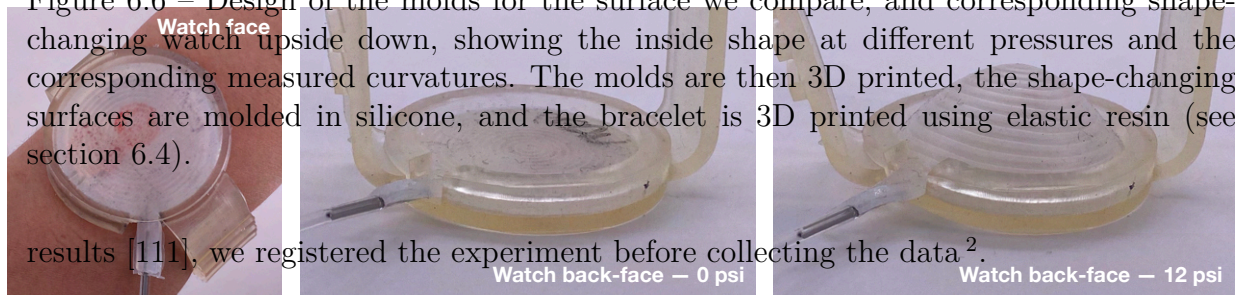


Figure 6.6 – Design of the molds for the surface we compare, and corresponding shape-changing watch upside down, showing the inside shape at different pressures and the corresponding measured curvatures. The molds are then 3D printed, the shape-changing surfaces are molded in silicone, and the bracelet is 3D printed using elastic resin (see section 6.4).



results [111], we registered the experiment before collecting the data².

6.5.1 Experimental design

We conduct a within-subject experiment to find the absolute threshold at which users notice the haptic feedback provided by the watch. Participants experience two different designs of shape-change (Figure 6.6).

Independent variable We vary the *homogeneity of the distance* between air channels as shown in Figure 6.6 in order to compare the two following MAXIMUM CURVATURES:

- R:** The flat-to-round surface has dense and regularly spaced air channels (Figure 6.6, top). With baromorphs of $\varnothing 42$ mm, we find that this design results at 12 psi in the curvature of 0.054 mm^{-1} , i.e. a curvature radius of 18.52 mm (Annex A.6).
- P:** The flat-to-pointy surface has air channels far from each other at the periphery and air channels close to each other at the center (Figure 6.6, bottom). With baromorphs of $\varnothing 42$ mm, we find that this design results at 12 psi in the curvature at the top of 0.064 mm^{-1} , i.e. a curvature radius of 15.53 mm (Annex A.6).

We measured experimentally the curvature of our prototypes in the range of 1-13 psi. We explain our procedure in detail in Annex A.6. In the range of 1-10 psi, curvatures are

2. https://osf.io/cqv7f/?view_only=3f9b0f47a67b40268e7204286bd9a458

very similar as shown in Figures A.16(b) and A.16(c) in Annex A.6. In the range of 10-13 psi, the center of the P surface is curvier than the center of the R surface.

Half of the participants start the experiment with R and the other half starts with P.

Dependent variables We collect participants' answers –whether they notice a stimulus– at each trial. We also collect their answers to an AttrakDiff questionnaire [158] for each MAXIMUM CURVATURE, their ranking of MAXIMUM CURVATURES in terms of preference and subjective detectability, and their qualitative feedback through semi-structured interviews. We chose not to collect physical data, like the pressure on the skin or the resulting indentation of the skin, because we aim to design a usable device (HCI) rather than understanding biological mechanisms (psychophysics).

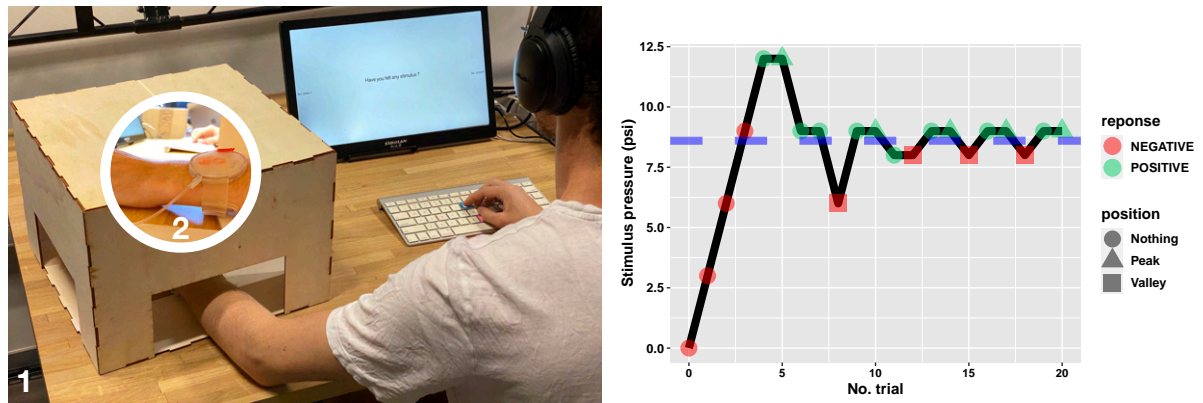
6.5.2 Apparatus

Participants wear the bracelet shown in Figure 6.1, 6.6, and 6.7(a). We fabricate the prototype as explained in section 6.4. The watch face is a closed surface to ensure the baromorph deforms towards the participants' wrists. The experimenter kept the bracelet securely closed with tape during the experiment. We control the fit of the bracelet by measuring participants' wrist circumference (C in cm) and adjusting the bracelet length (L in cm) to this circumference following $L = 0.8 \times C + 5.8$. To find this model, we performed a fitting pilot with 5 participants (adjusted $R^2 = 0.93$), where we made sure that the bracelet was as tight as possible while comfortable to wear.

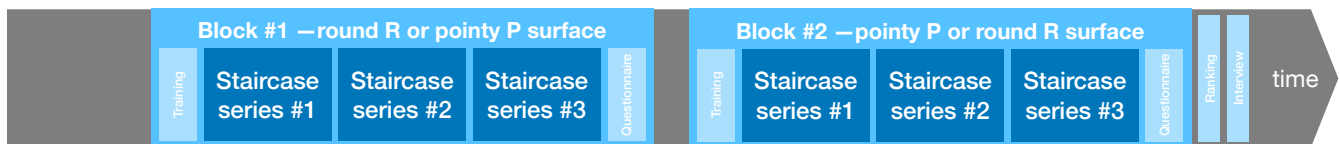
We developed Python software to run the experiment. We provide all the necessary files to reproduce our hardware and software experimental apparatus in the supplementary material.

6.5.3 Participants

We recruited 12 participants from our university campus. Twelve participants allow us to test both orders of presentation of the two MAXIMUM CURVATURES. In addition, 12 participants are the most common sample size [52]. Participants were 21 to 40 years old (median = 27). Six self-reported as women and six as men. Four of them own a smartwatch providing vibrotactile feedback that they wear regularly or every day. All participants have normal sensitivity on all sides of the wrist, except P7's sensitivity on the anterior side of the wrist (Figure 6.5(b)) which is slightly impaired.



(a) (1) Overview of the experimental setup and (b) Third staircase series for P9 with the flat-to- (2) close-up of the non-dominant hand wearing the pointy surface (P). The blue dashed line shows the watch inside the box. The pumps and Arduino are absolute detection threshold computed for this placed in a box on a separate table on the right (card-ries. board box in the background in (2)).



(c) Experimental timeline.

Figure 6.7 – Experimental setup.

6.5.4 Procedure

Participants sit and rest their forearm at a table (Figure 6.7(a)). We first measure participants' wrist circumference, and sensitivity using a Semmes-Weinstein monofilament test [388] on the posterior, anterior, lateral and medial sides of the wrist (Figure 6.5(b)).

The experimenter installs the shape-changing watch back-face with the first MAXIMUM CURVATURE. To control a tight while comfortable fitting of the bracelet, homogeneous among participants according to the model presented in section 6.5.2, the experimenter closes the bracelet at the position line corresponding to participants' measured wrist circumference –black lines labeled with wrist circumferences as shown in Figure 6.1. We asked participants to confirm if the fitting was tight while comfortable. To isolate the haptic sensation and avoid visual feedback, participants hide their forearm in a box as in [146, 531]. The experimenter installs the prototype inside the box around the participants' non-dominant wrist as in [146, 342, 531] (Figure 6.7(a)). While the dominant side is more sensitive than the non-dominant side at the mid-posterior forearm [95], testing the

feedback on the non-dominant side is more ecological: most users wear their watch on the non-dominant arm [512]. In addition, to avoid any impact of the noise of the pumps, participants wear headphones playing Brownian noise.

At the beginning of each block (one for each MAXIMUM CURVATURE, Figure 6.7(c)), the experimenter asks participants to test the prototype, as this type of feedback is novel. To do so, the experimenter presents in a pseudo-random order either no stimulus (0 psi) or a strong stimulus (10 psi). The training stops after participants correctly judged both two zero stimuli and two strong stimuli successively³.

We then follow a standard two-down, one-up staircase procedure [247]. In each staircase series, the first trial starts with the baromorph at 0 psi (Figure 6.7(b)). We maintain the desired pressure for 1s as in [241, 531]. We do not consider longer times such as 2s [146] or 5s [342] as our pilot study showed that users rather notice changes in curvature and get used to a stable curvature. We then decrease the pressure to 0 psi before participants report whether they felt any stimulus by pressing the corresponding key on a keyboard (Figure 6.7(a)). This is the standard procedure for non-distracted absolute detection threshold experiments [146, 342, 531, 241].

As shown in Figure 6.7(b), if participants do not feel any stimulus, we increase the target pressure of the next trial by a constant step of 3 psi. If participants feel the stimulus, we keep the same target pressure for the next trial. If participants feel a stimulus twice in a row, the target pressure of the next trial is reduced by the same constant step.

The increase/decrease steps are equal and constant before each reversal⁴ [247]. Between the third and the fourth reversals, we decrease the step value to 1 psi to improve threshold accuracy [146, 531]. The staircase series ends after nine reversals [146]. We later compute the threshold as the mean of the last five reversals [146].

Participants take a break after each staircase series (Figure 6.7(c)). We repeat each staircase series three times for each MAXIMUM CURVATURE to further improve the accuracy. Thus, we collect $2 \text{ MAXIMUM CURVATURE} \times 3 \text{ repetitions} \times 12 \text{ participants} = 72$ measurements of the threshold.

At the end of each block, participants fill an AttrakDiff questionnaire [158]. At the end of the experiment, they rank the prototypes in terms of preference and subjective

3. Most participants succeeded in training in the first 4 trials with both 2 zero stimuli and 2 strong stimuli. Only 3 participants needed slightly more trials for training with the pointy surface, i.e., 5 trials for P5 and P11 and 7 trials for P10.

4. A reversal is a change in direction, i.e. a local extremum shown as a triangle (peak) or a square (valley) in Figure 6.7(a).

detectability. We then conduct a semi-structured interview to collect participants' qualitative feedback. The topics planned in our interview guide were the location and descriptions of the sensations, if users felt any difference between experimental conditions, and if they had any strategy to answer the perception question. The experiment lasts around 60 min for each participant.

6.5.5 Data analysis

From participants' answers, we compute the absolute detection threshold as the mean of the last five reversals –as in, e.g., [531, 342, 146]. We report to computed thresholds in psi –that can be converted to bar or kPa as in [531] and to mm^{-1} (Annex A.6). We use estimation techniques based on geometric means. Figures between brackets show 95% bootstrapped confidence intervals (CI) as recommended [90]. We use pairwise differences to show effect sizes. These methods are recommended by the APA [20] and largely adopted (e.g., [83, 221, 80, 206, 237, 293]). Rather than the dichotomous inference supported by p-values, we opted for this more nuanced analysis of the direction and magnitude of the effect. A p-value-approach reading of the results presented in this chapter can be done by comparing the CIs spacing with common p-value spacing, as shown in Figure 3 in [235]. A pairwise difference is an intra-subject measurement that expresses the effect size and is computed between each of the geometric means.

We analyzed the interviews' transcripts using thematic analysis [379]. We chose thematic analysis to find out participants' experiences from our interview transcripts. Our research question was *What are users' experience with the wristwatch?* We combined inductive and deductive approaches to analyse the transcripts: While, e.g., location and sensation were topics that we questioned explicitly during interviews (deductive approach), we analyse their subthemes through an inductive approach (bottom-up from participants own words). In addition, we adopted a semantic approach, i.e. we analyzed the explicit content of the transcripts, and did not rely on assumptions underlying the data. We followed the six steps of thematic analysis:

1. **Familiarization:** we first transcribed the audio and read thoroughly the resulting transcripts.
2. **Coding:** we thoroughly coded all the data using the taguette software. We highlighted and labeled/coded everything we found potentially interesting regarding participants' experience with the watch.

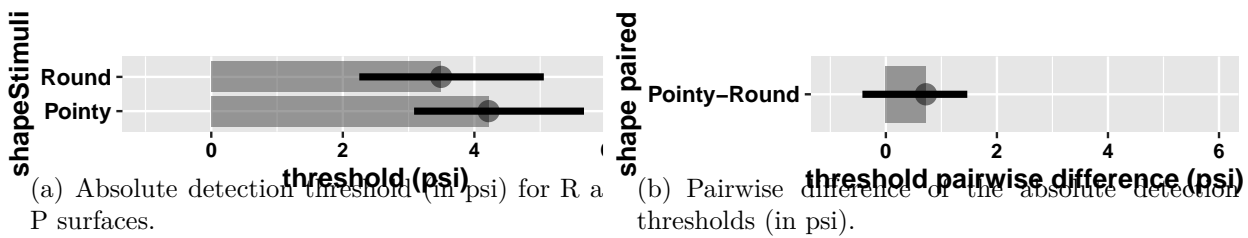


Figure 6.8 – Analysis of the absolute detection thresholds. Error bars indicate bootstrapped 95% confidence intervals.

3. **Generating themes:** we then looked over all the codes previously defined, and grouped them into themes
4. **Reviewing themes:** we then read the transcripts again and analyzed if the generated themes were accurately and relevant representing the data. This lead us to readjust some of our coding.
5. **Naming themes:** we finally reviewed the naming of each theme to make sure each precisely pictures the data.

6.5.6 Results

Absolute detection threshold

Figure 6.8 presents the absolute detection threshold. Figure 6.8(a) shows that the flat-to-round (R) surface has an average absolute detection threshold of 3.49 psi ([2.25, 5.07]), and that the flat-to-pointy (P) surface has an average absolute detection threshold of 4.22 psi ([3.11, 5.65]). Although the P surface has a slightly higher absolute detection threshold ($M = +0.72$ [-0.44, 1.46]) than the R surface (Figure 6.8(b)), the difference is very small, and the 95% confidence interval crosses 0, meaning that the actual difference might even be a little reverse. When looking at each surface at such low pressures (< 10 psi, Figure A.16(b) in Annex A.6), we find no curvature difference between the top center of R and P surfaces.

To conclude, the MAXIMUM CURVATURE of the surface has very little to no impact *on the absolute detection threshold*. Overall, this notification modality has a low absolute detection threshold ($M = 3.86$ psi [2.96, 4.91]).

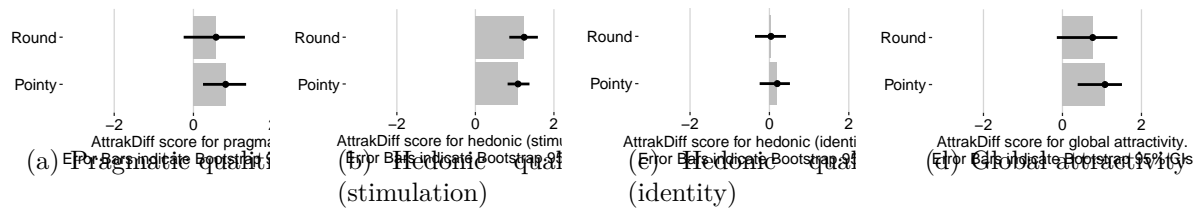


Figure 6.9 – AttrakDiff scores. Error bars indicate bootstrapped 95% confidence intervals.

Pragmatic and Hedonic Qualities

Figure 6.9 presents the AttrakDiff questionnaire results [158]. An interface rated as neutral lies in the range $[-1, 1]$, while $[-3, 1]$ or $[1, 3]$ denotes respectively rather negative or positive ratings. Figure 6.9(a) shows that participants found both watches rather neutral in terms of usability and perceived ease of use (Pointy $M=0.81$ $[0.24, 1.33]$, Round $M=0.57$ $[-0.25, 1.30]$). This can be explained by the fact that the stimulus levels were very low to measure the absolute detection threshold. Figure 6.9(b) shows that participants found that both watches have rather positive stimulation qualities (Pointy $M=1.09$ $[0.82, 1.38]$, Round $M=1.24$ $[0.86, 1.59]$). Figure 6.9(c) shows that participants rated as neutral the ability of both watches to support a social function and to communicate users' identity (Pointy $M=0.20$ $[-0.25, 0.52]$, Round $M=0.1$ $[-0.36, 0.42]$). Figure 6.9(d) shows that participants found the P surface slightly attractive ($M=1.08$ $[0.38, 1.51]$), while they found the R surface slightly more neutral ($M=0.77$ $[-0.14, 1.39]$).

Ranking

At the very low levels of stimuli that participants experienced in this experiment, we found no difference in the ranking of both R and P surfaces. Among 12 participants, half of the participants preferred the R surface, while the other half preferred the P surface. Seven participants think the deformation of the R surface was easier to perceive, while the other 5 participants found the contrary. As P10 mentioned that he preferred P because it was the first time he experienced this novel and pleasant stimulus, we explored if the order of presentation of each surface had an impact on the ranking and found no impact.

Qualitative feedback

We identified the four following main themes in the final interviews. While location, sensation and differences were themes that we asked explicitly during the interviews (top-

down) while their subthemes were bottom-up (participants own words), enjoyment was a theme that emerged during our bottom-up thematic analysis.

Enjoyment Five participants explicitly mentioned that the sensation was pleasant. For instance, P9 said that it was “very smooth, delicate”, P10 said it was “soothing” and “nice”, and P12 said it was “attractive”. P10 said that “there’s also a great deal of emotion involved”. Prior work studied the relationship between shape-change and emotions [333, 424, 432]. However, these works are based on visual stimuli and not haptic ones, as in this chapter. Although further work is needed to quantitatively measure how this prototype positively affects users, this positive qualitative feedback from our participants shows that this novel notification modality can be complementary to existing ones. Indeed, when comparing to their smartphones –they did not own a smartwatch– P2 and P8 mentioned that this novel type of feedback was more pleasant than vibrotactile (P2) and sound (P8) feedback.

Location of the sensations As expected, all participants –except P9– mentioned feelings on the posterior wrist side. P1 explicitly mentioned that she felt “at the top, for the big pressures”. I.e., the main sensation was at the posterior side of the wrist when the stimulus was higher than the threshold. The second most mentioned locations were the wrist lateral and medial sides. Participants could feel the very low stimuli strength that we tested during this experiment already on the sides of the wrist. As P4 said, “On the sides, I felt less, well, I had the feeling that I could feel less on the sides”. Participants mentioned less the anterior side of the wrist and for the same feeling as the lateral and medial sides. As our experiment studied very subtle stimuli, P12 even mentioned that he could feel these stimuli at the location of the cable connection. This shows that users are very sensitive to this novel type of notification modality. This is promising for future experiments exploring distracted detection threshold when users experience additional haptic sensations, like when driving a bicycle.

Description of the sensations We found 21 subthemes describing participants’ sensations from their own words: inflation (24 occurrences), deflation (15 occurrences), pressing and vibrating (14 occurrences each), touching (10 occurrences), hairs (9 occurrences), breathing (8 occurrences), squeezing (5 occurrences), spreading (3 occurrences), pricking, curvature, release, waves, moving and air blowing (2 occurrences each), massaging, sucking, tingling, pulse, skin (1 occurrence each).

The most discussed theme during interviews was inflation (9 participants). Five participants said they could feel the inflation more clearly (P4-8) than the deflation, while only one found the deflation easier to detect (P2).

The second most discussed themes were touching (P2-5, P9-11), pressing (P4, P6-7, P9, P11-12), and vibrating (P3, P4, P8, P10, P12). Participants described a local pressing sensation: “It was pressing at a point” (P7). Participants also felt the spreading of the pressure: “It really felt like it was crushing and spreading on my skin” (P11) and “it touches a corner and then spreads out” (P2).

P3-4-8 mentioned that the vibration was very subtle. P3 said “I’m in a controlled environment here, but I think that if I make everyday gestures, I might not notice the vibration”. As said above, as we tested very low stimuli levels, participants could already feel the vibration before the actual change of shape.

Subjective differences between R and P surfaces As our quantitative measurement of the ADT predicts, P1-2, P4-6, P8, and P12 mentioned that both R and P surfaces were similar during this absolute detection threshold experiment, e.g., “I had the feeling that they were the same” (P1).

However, P2-5, P7 and P11-12 were able to discuss their different sensations: “it was not the same sensation” (P11). P2 said, for instance, that “[R] must be more flat”, and “with [P] you have the feeling that it touches”. P4 said that “[R] had a larger surface. [P] was smaller, I think”. P1 and P5 also discussed a difference in the location of their sensation: Both felt R stimulated them rather on the sides, while P stimulated them rather at the center of the posterior wrist side.

Consistently with the results of the pragmatic qualities (Figure 6.9(a)) and the global attractivity (Figure 6.9(d)), P1-4 and P10 explained during the interviews why they preferred P: “It was easier to know if I felt it” (P1), “[I found R] less detectable, and since it’s less detectable, it’s my least favorite.” (P2), “I had more sensations with P” (P3), and “when [the stimuli] were clear, I think it was a bit clearer in P” (P4).

6.6 Discussion

Variance inter-participants We found that there are differences between our participants. We made sure that all participants had normal sensitivity on the posterior side of their wrist, but we did not test their actual sensitivity threshold with a more precise

Semmes-Weinstein monofilament test [388]. We hypothesize that variations in users' sensory threshold might have an impact on the ADT of this prototype. During interviews, two men (P2&11) mentioned their sensation came from hairs on the skin of the wrist: both could feel the movement before any contact with the skin because the device attracted their hair or made their hair move. Previous work [123] found that people can perceive tactile sensation with hair on their skin, e.g., perceiving the vibration of an object contacting with the hair on the dorsal part of the middle finger. Besides, in Pohl et al.'s experiment [342] measuring users' detection threshold of compression from a blood pressure cuff on the forearm, they observed that participants with larger diameter arms have a higher detection threshold. They supposed participants' arms shape might influence the cuff's inflation characteristics. Further studies can investigate whether participants' anthropometric measurements, such as arm shape and hair on the skin, can impact users' threshold with our watch. Ecological testing of this novel notification modality should include an initial calibration in order to adapt the threshold to individual sensitivity.

Fitting of the bracelet We paid great care to control the fitting of the bracelet (see section 6.5.2) so that we could reliably compare the results between participants and between blocks. However, in more ecological situations, users may fit the bracelet of their watch differently: some like to have it tightly adjusted to their wrist, while others prefer to wear it more loosely. Future work could explore the impact of the fitting of the bracelet on the detectability. As above, ecological testing of this novel notification modality should include an initial calibration in order to adapt to individual preferences, as this is already the case with vibrotactile feedback on smartwatches.

Memory effect During interviews, three participants mentioned a possible memory effect. P1&11 mentioned that they were not sure if the sensation they had was from before or from the current stimulus. On the contrary, P4 mentioned that it was hard to remember the sensation. The impact of memory on users' haptic perception was observed in previous research [459, 456, 469]. For example, Vogels, Kappers, and Koenderink found that after touching a convex (resp. concave) surface, their participants perceived a flat surface as concave (resp. convex) [469]. They also found that the memory effect can last more than 40 seconds. In another study, Gilson and Baddeley found that their participants can recall the position of a pen touching their forearm, while their remembered position precision decreases over time [130]: E.g., three seconds after been touched, the average

remembered position error was measured as 15 cm. Furthermore, our experiment studied users' haptic perception on the forearm which involves hairy skin [3]. In addition to the mechanoreceptive afferents with high conduction speed (20-80 m/s) [272] that exist both in glabrous and hairy skin⁵, one unique characteristic of hairy skin is the presence of C-tactile (CT) fibres, another kind of mechanoreceptive afferents with low conduction speed (0.5-2 m/s) [272], which might introduce latency in neural signal processing [479]. We could not explore the existence of a memory effect with our experimental setting. Future work should measure if there is any memory effect in order to compensate in future design, and measure the minimum interval needed between two successive stimuli to eliminate any confusion between stimuli like P1&11 mentioned.

ADT and vibrations Our initial registered hypothesis was that participants would have a lower absolute detection threshold when wearing a watch with higher curvature. We therefore designed our experiment to compare curvatures. We eventually found little difference between curvatures. During the experiment, the cable coming out of the watch connects it to three pumps and does not touch the participants' skin (Figure 6.7(a)-2). The absolute detection threshold without distraction is so low that it might not imply shape change as shown in Figure A.16(c) at 3 psi. However, we noted that the difference between curvatures is greater when the deformable surface is enclosed inside the watch (Figure 6.6 at 12 psi) compared to outside any enclosure (Figure A.16(b) at 12 psi). Nevertheless, we believe the experimental procedure does not question the ADT we measured because we eliminated any contact with the cable and pumps (placed on another table). In fact, our prototypes feature long and thin air channels (e.g., for the rounded prototype, 664 mm long and 0.4 mm wide). Radial inflation of the channels can induce vibrations in the channels themselves due to the turbulence of the airflow [42, 302]. Therefore, these vibrations are an integral part of the haptic modality presented. These vibrations are perceptible to our participants and come from beneath our prototype, unlike those coming from a pipe or a motor. Ultimately, we think that we cannot untie the impact of vibrations caused by the inflation, barely perceptible, and the impact of the curvature, at such a low level of stimulus needed for absolute detection.

Besides quantitative results, seven out of twelve participants explained during interviews (section 6.5.6) that they actually felt differences between round and pointy curva-

5. In contrast to hairy skin, glabrous skin is devoid of hairs. Glabrous skin mainly covers the palmar region of the hand and and plantar region of the feet [3].

tures. Ultimately, our results actually tell the scientific community that this novel feedback is easily detectable, and that curvature plays little role in the *undistracted* absolute detection threshold. This does not mean that curvature will not play a role in other levels of detection, like *distracted* absolute detection threshold or just noticeable difference, as qualitative feedback showed that participants might be able to tell the difference.

Comparison To better understand this new modality, in this study we chose to compare two alternative curvatures for the same modality. However, we have not compared this new modality to existing ones, such as those presented in figures 6.2 and 6.3. Positioning this new modality in relation to the state of the art will be necessary in future work. In comparison, PneuHaptic [160] offers a different feedback through a series of inflatable air chambers around the arm. Their authors did not measure users' absolute detection threshold with the device. SqueezeBack [342] offers a different feedback –compression– through a blood pressure cuff applying pressure around users' forearm. Their authors measured an average detection threshold of 0.1 psi. This threshold is lower than the one we found (3.49 or 4.22 psi depending on the curvature). Designers can balance this difference with other requirements, such as multimodality, as the feedback we propose in this chapter is different and relies on surface curvature change rather than compression. To further enable designers to make a decision, future work should compare users' subjective evaluation of these different haptic modalities.

Mobility Although we have studied this new modality in the case of a connected watch, the current prototype is not mobile yet. Although the technology is not yet ready to enable this type of feedback on current watches, it is important to study the opportunities for interaction with users today [156], in parallel with technological advances such as the miniaturization of pumps.

6.7 Conclusion

In Chapter 4, we established that soft materials possess significant potential for constructing SCIs with versatile shape-changing capabilities. Building upon insights from our psychophysical experiment in Chapter 3, we found that users can accurately and precisely perceive the shape of highly curved UIs (Radius ≈ 10 mm) even when constructed on very soft materials (Shore 00-10). To address the SCIs design challenges, this chapter

introduces a novel soft material-based watch designed to notify users through dynamic changes in curvature on the back face of their smartwatch. To control the maximum curvature, we utilize Baromorph surfaces [402], maintaining constant parameters such as watch size. The adaptation of soft materials and our effort of making a Baromorph surface as small as $\varnothing 42$ mm and 3 mm-thin to well ensure its wearability on the wrist. Through a standard two-down, one-up adaptive staircase procedure, we determined the absolute detection threshold (ADT) to be 3.86 psi—the minimum pressure required for users to detect the inflation of the watch. Impressively, users exhibited a remarkably low threshold for detecting notifications in a controlled laboratory environment with no distractions. Under such low pressure, the shape changes in our prototypes are barely discernible in photos taken by a camera (Figure A.16(c)). Qualitative findings reveal that participants not only enjoyed this innovative feedback mechanism but also experienced distinct sensations with each watch. While these results highlight the promising potential of our approach, further user studies are warranted. Future investigations should explore users' ADT measurements during primary tasks like walking or cycling.

CONCLUSION

7.1 Thesis Contributions

Soft materials like elastomers [509] are attracting more and more HCI researchers' interest. Their high stretchability and deformability make them instantly soft and safe [377], which is particularly important when UIs are worn on the body [480]. With the advancement of sensing technologies [40, 57], UIs made of soft materials are already capable of sending users' various inputs interaction with them, such as touch [484, 480], press [517, 441], bend [366] and stretch [225]. At the same time, the advancement of programmable soft materials makes UIs in soft materials capable of changing their shapes for different purposes (Figures 1.1 and 1.2). Considering the high potential of integrating programmable soft materials into SCIs and the growing synergies between material science and HCI [358], it is opportune to investigate how to incorporate programmable soft materials more effectively into SCIs design. In this thesis, we focus on investing in using programmable soft materials to construct SCIs, which sets them apart from traditional rigid planar UIs like LCD screens. In Chapter 2, we first review different HCI research using programmable soft materials used to construct SCIs as the background of our research. This chapter also serves as a takeaway for HCI researchers, giving them an overview of new materials adopted in SCIs creation. We then investigate three major HCI research questions with respective challenges coming from user behavior, technological, and design aspects [10]: (1) Understanding the user experience of SCIs, (2) Technological barriers to SCIs development using programable soft materials, and Design and implementation of SCIs application using programable soft materials. In this section, we summarize our contributions in these three dimensions.

User behavior. Users' experiences with SCIs are multifaceted, including both the perception of UIs' physical properties like curvature [435] and association with multiple affective sensations like emotion [271]. When UIs change shape, they can also bring multiple

effects, such as visual effects [333] and haptic effects [107]. One key difficulty in understanding the user experience of SCIs is the factors isolating [10]. For this purpose, this thesis starts from the fundamental point of how effectively (precisely and accurately) users can perceive the SCIs' shapes under different softness conditions through touch. Our study starts from this point as one critical distinction between SCIs and GUIs behind rigid planar LCD screens is that users can physically touch SCIs, perceive their physical shapes, and interact with them directly using their body, such as their fingers and hands [169]. Despite the increasing use of soft materials for constructing SCIs, the study of users' shape perception performance with UIs on soft materials still needs to be explored. To better understand how soft UIs' shape can convey tactile information to users, we conducted psychophysical experiments to determine the just-noticeable-difference (JND) of UIs' shape under different softness. Our current focus is on a fundamental shape feature in our thesis, curvature, which is critical for developing UIs capable of changing many other shape features (Section 2.2). We employed static stimuli instead of dynamic curvature-changing UIs (e.g., PneuUI [509]) to eliminate additional parameters, such as air pressure, which can impact both curvature [509] and softness [39, 262]. We kept other parameters, such as UIs' size (i.e., height and diameter), constant to isolate the impact of softness. We have made our experiment protocol, materials for fabricating experiment stimuli, experimental data collecting software, empirical data, and the respective script for data analysis publicly accessible¹. This transparency facilitates the reproducibility of our experiment and encourages similar experiments on various shape features. For example, with our public materials, Ghosh [128] recently extended our experiment from convex to concave surfaces. Our experiment revealed that users can precisely and accurately perceive UIs' shape even when made of very soft materials, particularly when the UIs are highly curved. This establishes the groundwork for using soft materials to create other UIs, providing users with precise and accurate shape information through tactile feedback.

Technological. The technological barriers to SCIs development using programable soft materials come from two aspects: (1) the lack of toolkits [10, 358] for HCI researchers developing UIs with various shape-changing abilities using programmable soft materials and (2) the stretchability-strength trade-off [358] of programmable soft materials limit their applications. Initially, we comprehensively reviewed various programmable soft materials to realize the common shape-changing features studied in HCI [226]. Additionally, we

1. <https://osf.io/r5w7x/>

introduced *SoftMorphees*, a series of shape-changing modules primarily utilizing a novel programmable soft material, Baromorph [402], to achieve diverse shape-changing features exclusively through soft materials. We also provide their feature measurements when actuated, i.e., under different air pressures, with respective regression equations to facilitate other researchers' designs. The insights from our review and *SoftMorphees* prototypes will help other HCI researchers efficiently realize their desired shape-changing features using programmable soft materials. Our work paves the way for technological aspects to further develop SCI toolkits in programmable soft materials. Then, we addressed a significant limitation of soft materials, such as elastomers, characterized by a trade-off between stretchability and strength [358]. While high stretchability [56] offers increased deformability and potential for shape change, it compromises strength due to easy deformation. To overcome this challenge, we introduced the "Jamming Origami Endoskeleton (JOE)" technology, enabling simultaneous control of UIs' shape (currently focused on curvature) and strength. This innovation is expected to broaden the applications of UIs by incorporating geometric shape and strength changes.

Design. Finally, leveraging our understanding of users' shape perception with UIs made of soft materials and technologies for building SCIs with various shape-changing abilities in soft materials, we designed new HCI applications with SCIs with different shapes in programmable soft materials. We also conducted respective user studies to evaluate users' interaction experience with them to answer SCI design questions such as what shape changes we should apply and what applications we should build. More specifically, we developed SCIs installed at the BoD of a smartwatch with different shape changes for delivering notifications to users. We meticulously designed thin SCIs with a total thickness of 3 mm and developed two variations (pointy vs. round) to measure users' absolute detection threshold (ADT). The low ADT value of approximately 3.86 psi for both two watches, obtained under laboratory conditions, indicates the effectiveness of this innovative feedback mechanism. Qualitative findings also reveal that participants enjoyed this innovative feedback mechanism. This paved the way for developing such SCIs to provide users with notifications effectively and addressed design challenges in SCIs research by providing insights into how programmable soft materials can be integrated into SCIs design.

7.2 Short-term Future Work

Limitations exist in our current studies, raising questions for future studies. Here, we discuss the short-term future work of this thesis.

7.2.1 Users' shape perception ability for UIs dynamically changing shapes

Soft materials with emerging properties have been employed to develop SCIs for various applications. Focusing on the curvature of UIs, our psychophysical experiment in Chapter 3 demonstrates that soft materials can offer users highly precise and accurate feedback on the shape of UIs. To isolate different experimental parameters [10] and emphasize the influence of UIs' softness on users' shape-perception performance, our experiment maintains other parameters, such as UIs' sizes (all stimuli with a base-to-peak height and diameter of 16 mm, as illustrated in Figure 3.2(b)), at a constant level. However, applications of SCIs typically involve multiple changes in shape features. For instance, pneumatic actuation [509] is one of the most commonly used technologies for realizing shape changes. Concurrent with the curvature change, when an airtight bladder is inflated with inner air pressure, its diameter [119], height [132], and strength [39, 262] also increase. Our empirical results indicate the high potential of using soft materials to convey shape information to users through psychophysics experiments with static curved UIs. Further experiments should be conducted with UIs dynamically changing their shapes, possibly involving haptic cues [116] (e.g., height and size changes) in addition to surface curvature. Moreover, with UIs dynamically changing their shape, such as curvature, an exciting avenue for future work is the absolute estimation of curvature (magnitude estimation) and the perception of continuous change in curvature, such as when users keep their finger on top of the UI and experience a transition between two curvatures.

Furthermore, both in HCI research [376, 363] and everyday life [226], we encounter UIs with shape-changing abilities beyond curvature change. In this thesis, we specifically focused on studying UIs' curvature for three main reasons: (1) Curved objects surround our world, and we are familiar with them [169, 362]. (2) Curvature-changing UIs are prevalent in current HCI research (e.g., [509, 300, 236, 462, 157, 132, 114, 419, 423]). (3) Curvature-changing technologies play a crucial role in constructing other shape-changing UIs (Figure 2.20), and curvature is a critical feature for encoding any 3D shapes [378].

However, as discussed in Chapter 3, current studies on users’ shape perception are primarily conducted with rigid UIs, either focusing on curvature [139, 347, 255, 137, 136] or other shape features [219]. With advances in new materials and the synergies between material science and HCI research [358], we can anticipate the proliferation of SCIs constructed with soft materials featuring various shape-changing abilities in the coming years. Therefore, the impact of softness on users’ shape perception abilities for features other than curvature should capture researchers’ interest.

7.2.2 Design tools for SCIs

In Chapter 4, we developed a series of soft material-based shape-changing modules, termed *SoftMorphees*, showcasing various shape-changing features such as size, curvature, amplitude, porosity, zero-crossing, closure, and speed. These modules underscore the potential of utilizing programmable soft materials to create diverse SCIs. The foundation of these technologies lies in the novel material called Baromorph [402]. Siéfert et al. outlined their approach to designing Baromorph, which involves projecting a 3D objective shape onto a plane to determine the configuration of air channels embedded in a silicone plate, akin to outlining contour lines on a map to represent a mountain. This methodology results in increased channel density corresponding to greater stretch strain (steeper surface) on the 3D shape after pressurizing these channels. However, this remains an idealized design approach based on Baromorph’s theoretical shape-changing principle without considering measurements on actual prototypes. For instance, based on Baromorph, as detailed in Chapter 6, the shape change observed in our prototypes deviates from our predictions. Notably, pointy prototypes exhibit lower channel density and steeper surfaces (Figure A.16(c)) when strongly inflated, and the prototype with isometry air channels was inflated into a demi-sphere-like shape instead of a cone shape predicted in [402]. This discrepancy may be attributed to the inflation pressure applied to Baromorph (≈ 13 psi), surpassing its previous actuating pressure (≈ 5 psi) [402]. This underscores the significance of combining theoretical calculations of Baromorph’s channel shape for objective 3D shapes with verification through measurements on actual prototypes. Our work in Chapter 4 extends the capabilities of Baromorph and connects it with HCI research by employing Baromorphs to realize specific shape-changing features commonly encountered in HCI [376, 226]. We provide detailed shape measurements to assist other HCI researchers in utilizing Baromorph to develop their desired SCIs. However, a notable gap remains in the absence of a design tool, similar to software tools developed in previous

work [409, 318, 225, 256, 476, 510, 474] that aids designers in directly creating modules to fabricate prototypes (i.e., STL files for 3D printing) from desired 3D shapes. This tool should accommodate not only primitive shapes, as explored in Chapter 4, but also more complex shapes that may involve a combination of various shape-changing features.

In Chapter 5, we introduce a novel technology called *Jamming Origami Endoskeleton (JOE)*, designed to control the shapes and strength of UIs concurrently. This innovation addresses the inherent trade-off between soft materials’ high stretchability and low strength [358]. JOE achieves shape-change through two imperfectly compatible layers of elastomer gears, namely “Prism” and “Tooth”, creating gaps between them. Evacuating air from the prototype induces gear rotation and expelling air, resulting in a global shape change. Simultaneously, origami sheets jam between the layers, enhancing strength. The development of SCIs using JOE involves consideration of multiple design parameters. We provide measurements for curvature and strength, identifying three key design parameters affecting UIs: the angle differences between “Prism” and “Tooth” Δ_{Angle} , the height of “Prism” h_{Prism} and the vacuum level P_{vacuum} . The number of origami jamming layers $N_{\text{JammingLayers}}$ also significantly impacts UIs’ strength. Our current study isolates each factor’s impact on UIs’ curvature and strength, maintaining other parameters constant without exploring their interactions. A comprehensive analysis, considering interactions between different design parameters, is essential to guide designers in selecting parameters for desired UI shapes and strengths.

Like *SoftMorphees*, we lack a dedicated design tool software for directly generating modules (STL files for 3D printing) for elastomer gears and form patterns (SVG files for laser cutting) for origami jamming layers based on designers’ specifications. Such a design tool should be developed, leveraging our prototype measurements under various design parameters (including interactions), to aid designers in adopting our technology for SCIs development. As discussed in Chapter 5, *CurveUps* [147], a non-reversible shape-change technology, inspires us to expand our technology from curvature-changing UIs to those with more intricate shape changes. The design tool can also integrate features from *CurveUps* to refine our “Prisms” and “Teeth” shapes to assist designers in creating SCIs with both strength and shape changes, surpassing mere curvature alterations.

7.2.3 Extending User study with our novel SCIs

In Chapter 6, we measured users’ Absolute Detection Threshold (ADT) using our watches, novel SCIs changing curvature to convey notifications. In a controlled laboratory

environment without distractions, users demonstrated a remarkably low threshold (3.86 psi) for detecting notifications. The subtle shape changes in our prototypes at such low-pressure levels were scarcely discernible in photographs taken by a camera. This outcome underscores the potential of employing our shape-changing watch for notification functions. Qualitative insights also indicate that participants appreciated this innovative feedback mechanism, opening avenues for further studies to deepen our understanding of this novel feedback type.

On the perception side, having established the minimal detectable feedback, future investigations could measure users' ADT when engaged in primary tasks such as walking or cycling and during cognitively demanding activities [146]. Additionally, future research could explore users' JND between two curvatures. Considering prior findings that users desire persistent modalities for notifications [267], shape-change presents an opportunity for such continuity, necessitating the exploration of users' long-term perceptions.

On the design side, future work could integrate the system into bracelets or even the entire body, recognizing variations in human sensitivity [397, 95] and exploring alternative forms of shape change [226]. We plan a design workshop to investigate soft shape-changing on-skin notifications systematically.

On the usage side, smartwatches serve as both personal devices and public displays [332], and the unique feature of shape-changing UIs lies in the combination of haptic and visual feedback. Consequently, we aim to evaluate the visual and haptic feedback provided by such surfaces on other parts of the watch, gauging responses from both wearers and those in their vicinity. *On the technical side*, future efforts could explore mechanisms to accelerate shape changes, utilizing more potent pumps or compressed air for actuation. Additionally, we plan to extend the use of an air pressure sensor, previously applied to a simple air balloon [342], to Baromorph surfaces, leveraging users' actions to interact with the system. In line with prior research [160, 181, 329], a critical aspect for future adoption is the miniaturization of the hardware controlling the prototype.

7.3 Perspectives for Future SCIs

In this section, we discuss future research questions for SCIs developments and applications and envision SCIs' future evolution based on current society and technology trends.

7.3.1 Lower technical barriers for customized SCIs

Navigating beyond the industrial age marked by the mass production of standardized commodities in pipelines, we presently inhabit a post-industrial society characterized by a growing demand for personalized everyday objects [164, 362]. This surge is driven by diverse motivations, including the pursuit of individual identities [263], the democratization of technologies [26, 273], advancements in technical and cultural innovations [49, 118], and the creation of more sustainable objects [50, 310]. The advent of electronic platforms, such as Arduino [18], portable computing platforms like Raspberry Pi [338], hardware design accessibility facilitated by entities like Adafruit [193], open-source development platforms exemplified by GitHub [131], and technical-oriented Q&A websites like Stack Overflow [320], has significantly lowered the barriers for electronic prototyping and software programming. This barrier reduction is attributed to their ease of learning, utilization, and the continuous support and inspiration from the burgeoning communities associated with these platforms. The widespread adoption of technologies like 3D Printing [289, 183, 60] and open-source 3D modeling software such as OpenSCAD [316] has further empowered individuals to fabricate personal artifacts and prototype tests efficiently across various forms and materials. Beyond electronic prototyping, software programming, and 3D model printing, the development of SCIs involves the intricate control of programmable materials like shape-memory alloys [274], pneumatically inflatable elastomers [509], dielectric elastomers [113] and hydrogels [203]. In contrast to the accessible landscape of electronic prototyping, software programming, and 3D printing, new materials for SCIs still present significant entry barriers and require specialized training for designers. Nevertheless, many researchers, particularly in HCI [357, 358], are working to lower these barriers. They contribute by creating design toolkits and tutorials [401, 113, 428, 292, 227, 202, 266, 282] to facilitate the learning path for other designers.

Our thesis work aims to help designers and researchers integrate soft programmable materials into their projects. This facilitation spans understanding user interactions with SCIs made from soft programmable materials and delving into the technologies necessary for their development. Further studies on user perception and toolkit development, as discussed in section 7.2, will extend this assistance beyond designers and researchers to end-users, progressively making it easier for them to develop their SCIs. As material science becomes more deeply integrated into HCI and researchers continue democratizing associated technologies, we envision a future where users can effortlessly conceive, prototype, and utilize their SCIs as easily as they currently do with 3D printing.

7.3.2 SCIs as standalone everyday objects

In Chapter 6, we introduced SCIs installed on the BoD of smartwatches. These SCIs currently serve as accessories for standard electronic devices, i.e., shape-changing haptic surfaces at the BoD of a smartwatch providing notifications. This aligns seamlessly with the overarching SCIs research focus [10]-exploring SCIs' shape-changing capabilities and diverse applications. Meanwhile, *Output* capabilities through shape-changing abilities [363, 376] and *Input* through sensing capabilities [40] are important when developing HCI applications. Regarding *Output*, we have systematically presented different programmable soft materials in Chapter 2 for UIs' shape control. Regarding *Input*, emerging sensing technologies based on soft materials [40, 414] were developed and can enhance UIs' sensing capabilities. Some recent advance in materials science [452] allows 3D printing direct structures using multiple materials, which integrates both *Output* (i.e., capable of being inflated to bend) and *Input* (i.e., capable of changing materials' resistance when bent). Beyond materials themselves sensing users' input and changing shape, current SCIs usually need extra actuators like pumps [509] for actuating their shape-change and extra controlling modules like Arduino [326] and smartphone [440] for processing sensing data or sending commands to control actuators. For this reason, current SCIs prototypes usually include tethered actuators and/or wired controlling boards and batteries. Soft programmable materials like shape-memory alloys [295] and dielectric elastomers [113] can be actuated by applying current or voltage to them; thus no need for tethered actuators. However, they may still need connections to batteries and controlling modules for power supply and control.

To move from vision to successfully embedding SCIs in everyday life [363], two technological trends are emerging. One is the miniaturization of batteries, actuators, and controllers [163, 124, 41], making these conspicuous electronic components easier to embed. Another is the development of electronic-free components to replace existing ones. As for electronic-free components, Lu et al. recently introduced the Fluidic Computation Kit [257], capable of realizing control logics activated under specific pressure conditions, thereby replacing some electronic controlling modules for pneumatically actuated SCIs. Sustainflatable [257], another development by Lu et al., utilizes pressure changes within an airtight box during physical transformations like evaporation/liquefaction to inflate/deflate pneumatically SCIs, replacing traditional pumps. Other works like [59, 383, 301, 375] also provide insights into constructing electronic-free control components, especially for pneumatically actuated UIs. Some other studies leverage pressure changes

during chemical reactions [478] and explosions [394] to replace pumps in pneumatically actuated SCIs. Additionally, emerging new technologies in material science, such as displays made of soft materials like textile [396], various energy harvesting technologies [268], and soft circuitry [322], could help eliminate current rigid and conspicuous electronic components, such as LED screens, batteries, PCB boards, and controllers, making UIs better integrated into our everyday environments. With advancements in these technologies, coupled with the ability of UIs to sense user interactions and changing shapes, we anticipate a future where everyday objects respond to our interactions by altering their shapes and/or colors. These standalone SCIs will operate without needing external batteries, actuators, and controllers, representing a significant step forward in the evolution of user interfaces. One approach to achieve this goal is to develop synergies between material science and HCI to develop toolkits for facilitating HCI researchers to develop SCIs using new materials [358].

7.3.3 Wearable SCIs

Wearable devices represent a captivating trend in the mobile device market, with the global wearables market projected to grow at a compound annual growth rate (CAGR) of 11.3% from 2019, reaching \$62.82 billion by 2025 [367]. Among the diverse range of wearable devices, smartwatches (e.g., Apple Watch [489]), earwear devices (e.g., AirPods [487]), and smart wristbands (e.g., Xiaomi Mi Band [496]) stand out as the three most popular types [367]. Primarily utilized for functions such as navigation [13], notifications [504], financial payments [15], and basic health data monitoring (e.g., blood oxygen [16]) and sports data tracking (e.g., active calories [14]), these devices currently lack shape-changing capabilities.

Recent research in HCI has seen a growing interest in wearable devices with shape-changing abilities. For example, the surface shape of a watch [329, 181] or a wristband [160] in contact with the wearer's skin can change its curvature to deliver notifications, replacing the traditional vibration used in commercial smartwatches or smart wristbands [504]. Innovations also extend to shoes with internally adaptable shapes conforming to the wearer's foot morphology [25]. Some applications involve inflatable bladders worn on the user's body, controlling bladders' inflation pressure, frequency, and positions to change the pressure applied to the wearers' body to offer different tactile sensations such as simulating being hugged or hit by a snowball [81]. This technology has also been used to guide wearers' breathing rates [69]. Additionally, length change UIs attached to the

user's body [531, 150] can generate shearing forces on the skin, providing notifications through skin stretching rather than vibration [531]. Another noteworthy category of shape-changing UIs is wearable exoskeletons [323], typically composed of bendable structures worn on joints like the phalangeal joints of hands, offering external force to aid physical movements [523].

Beyond HCI research, designers and artists, particularly in the fashion industry, have explored more dramatic changes with shape-changing garments, enabling wearers to express their identity and personal values and build social connections [77, 324, 390]. For instance, transforming a day dress into a ball gown involves several motors pushing outwards to alter its silhouette and hemline [304] to adapt to a person's multitasking lifestyle. A spider-like structure [499] worn on the shoulder extends its legs, actuated by motors, to protect the wearer and signal others to maintain a distance when a proximity sensor detects intrusion into personal space. Similar work also designed shape-changing garments to protect wearers' personal space [498, 515]. Further explorations in fashion design include garments made of silicone [514], actuated by actuators to continuously ripple, expand, and contract, presenting the philosophical concept of the complexity of individuals' alternating identities. Another example involves a cloth with spikes actuated by shape-memory alloy [104], responding to onlookers' gaze to increase wearers' awareness of their social context. Such avant-garde designs showcased during fashion shows [390, 447] indicate the immense potential of interactive garments and wearable UIs, transcending conventional boundaries.

When designing wearables for a broader population, subtlety becomes crucial [526, 112, 288], ensuring users can interact with UIs to achieve their objectives without compromising privacy or social interaction (i.e., being observed) [344, 11]. Traditional garment materials like fabric offer comfort due to their excellent air permeability and flexibility [399]. Technologies such as embedding shape-memory alloys [229, 34], coating with hydration-swelling materials [475], sewing conductive fibers [313], and incorporating luminescent fibers [313, 396] enable fabrics to change shape [229, 34, 475], sense user input gestures [313], and display colorful images [396]. Consequently, fabric, a conventional garment-making material [490], becomes easily adaptable for developing subtle wearable SCIs. Soft programmable materials like elastomers [402] further enhance wearable UIs' shape-changing [303] and sensing abilities [513], expanding their application context. Their high stretchability makes them inherently body-compliant, ensuring comfort for wearers [399]. Future studies should explore integrating emerging soft programmable

materials seamlessly into wearable applications, taking subtlety, low bulkiness, and comfortability into consideration [112, 288, 526].

7.3.4 SCIs in Metaverse

With recent news in high-tech, such as Facebook renaming itself to Meta and introducing the concept of the Metaverse to outline its future plans [493], and Apple commercially releasing its mixed reality (MR) headset, the Apple Vision Pro [488], the concept of the Metaverse [294] is gaining increasing attention beyond the research realm. Metaverse researchers are actively working towards enhancing crucial features, such as the sense of presence and user immersion in a synthetic world amalgamated with digital information, including visual effects, sound, and the physical surroundings that users can perceive with their physical bodies [294]. In addition to highly advanced visual [410] and audio [453] display technologies, as well as emerging smell rendering [47] and taste rendering [46] technologies, the incorporation of physical objects into the Metaverse, allowing users to experience haptic sensations as they interact with virtual elements, can significantly amplify the sense of immersion and presence [166, 369, 172].

However, when compared to the visually rendered complex environments filled with objects of various shapes [404], creating physical UIs to simulate diverse shapes of objects in a virtual environment remains challenging. Current technologies like TilePoP [436] enable the construction of objects in a Minecraft style with a limited set of shapes using inflatable cube airbags of varying sizes. Nevertheless, the resolution is constrained, with a minimum edge size of 10 cm for their constructed objects. Addressing this limitation, our research focuses on continuously enhancing the shape-changing capabilities of UIs. Unlike TilePoP [436] or other technologies such as 2.5D displays [108] composed of matrices of actuated pins to provide numbers of different shapes (discrete) using one UI in limited resolution, SCIs in programmable soft materials typically have limited numbers of (continuous) shapes specialized for specific contexts [168]. Despite these limitations, users can integrate information from different senses, such as haptic and visual, to form a robust perception of an object's features [97, 98] even when they are not perfectly matched. Previous work has validated and measured users' tolerance of the incoherence of softness [43], curvature [443] and size [435] between physical objects and their visually rendered counterparts in Metaverse. Considering this, we anticipate that SCIs will not only become pervasive in our physical world, as previously discussed but their integration into the Metaverse is poised to significantly enhance user interaction experiences with

haptic feedback, even within the constraints of their shape-changing abilities. Moreover, recent research has demonstrated that users can relate their haptic experiences of touching physical objects with different shapes to other senses, such as smells [275], colors [250], softness [420] and emotions [105, 175]. Consequently, envisioning SCIs with dynamic shapes provides users tactile sensations in the Metaverse, coupled with other technologies rendering visual [410], auditory [453], olfactory [47], and gustatory [46] senses, promises to elevate the immersive experience within the Metaverse substantially.

BIBLIOGRAPHY

- [1] A. W. 10.1007/BF02259120, V. G. Macefield, and J. W. Bisley, « Encoding of Object Curvature by Tactile Afferents From Human Fingers », *in: Journal of Neurophysiology* 78.6 (1997), PMID: 9405508, pp. 2881–2888, DOI: 10.1152/jn.1997.78.6.2881, eprint: <https://doi.org/10.1152/jn.1997.78.6.2881>, URL: <https://doi.org/10.1152/jn.1997.78.6.2881>.
- [2] Moaed A Abd, Joseph Ingicco, Douglas T Hutchinson, Emmanuelle Tognoli, and Erik D Engeberg, « Multichannel haptic feedback unlocks prosthetic hand dexterity », *in: Scientific Reports* 12.1 (2022), p. 2323, DOI: 10.1038/s41598-022-04953-1.
- [3] Rochelle Ackerley, Karin Saar, Francis McGlone, and Helena Backlund Wasling, « Quantifying the sensory and emotional perception of touch: differences between glabrous and hairy skin », *in: Frontiers in behavioral neuroscience* 8 (2014), p. 34, DOI: 10.3389/fnbeh.2014.00034.
- [4] Adilzhan Adilkhanov, Matteo Rubagotti, and Zhanat Kappassov, « Haptic Devices: Wearability-Based Taxonomy and Literature Review », *in: IEEE Access* 10 (2022), pp. 91923–91947, DOI: 10.1109/ACCESS.2022.3202986.
- [5] Sung Hee Ahn, Sanghyun Kwon, Sangwoo Bahn, Myung Hwan Yun, and Wooyeon Yu, « Effects of Grip Curvature and Hand Anthropometry for the Unimanual Operation of Touchscreen Handheld Devices », *in: Human Factors and Ergonomics in Manufacturing & Service Industries* 26.3 (2016), pp. 367–380, DOI: <https://doi.org/10.1002/hfm.20662>, eprint: <https://onlinelibrary.wiley.com/doi/pdf/10.1002/hfm.20662>, URL: <https://onlinelibrary.wiley.com/doi/abs/10.1002/hfm.20662>.
- [6] Neil Aitken, *Most Used Features of Smartwatches*, Last retrieved: 2023-06-15, 2023, URL: <https://whatphone.com.au/guide/most-used-features-of-smartwatches/>.

- [7] Buse Aktaş, Yashraj S. Narang, Nikolaos Vasios, Katia Bertoldi, and Robert D. Howe, « A Modeling Framework for Jamming Structures », *in: Advanced Functional Materials* 31.16 (2021), p. 2007554, DOI: <https://doi.org/10.1002/adfm.202007554>, eprint: <https://onlinelibrary.wiley.com/doi/pdf/10.1002/adfm.202007554>, URL: <https://onlinelibrary.wiley.com/doi/abs/10.1002/adfm.202007554>.
- [8] Ahmed Al Maimani and Anne Roudaut, « Frozen Suit: Designing a Changeable Stiffness Suit and Its Application to Haptic Games », *in: Proceedings of the 2017 CHI Conference on Human Factors in Computing Systems*, CHI '17, Denver, Colorado, USA: Association for Computing Machinery, 2017, pp. 2440–2448, ISBN: 9781450346559, DOI: 10.1145/3025453.3025655, URL: <https://doi.org/10.1145/3025453.3025655>.
- [9] Jason Alexander, John Hardy, and Stephen Wattam, « Characterising the Physicality of Everyday Buttons », *in: Proceedings of the Ninth ACM International Conference on Interactive Tabletops and Surfaces*, ITS '14, Dresden, Germany: Association for Computing Machinery, 2014, pp. 205–208, ISBN: 9781450325875, DOI: 10.1145/2669485.2669519.
- [10] Jason Alexander, Anne Roudaut, Jürgen Steimle, Kasper Hornbæk, Miguel Bruns Alonso, Sean Follmer, and Timothy Merritt, « Grand Challenges in Shape-Changing Interface Research », *in: Proceedings of the 2018 CHI Conference on Human Factors in Computing Systems*, CHI '18, Montreal QC, Canada: Association for Computing Machinery, 2018, pp. 1–14, ISBN: 9781450356206, DOI: 10.1145/3173574.3173873, URL: <https://doi.org/10.1145/3173574.3173873>.
- [11] Fraser Anderson, Tovi Grossman, Daniel Wigdor, and George Fitzmaurice, « Supporting Subtlety with Deceptive Devices and Illusory Interactions », *in: Proceedings of the 33rd Annual ACM Conference on Human Factors in Computing Systems*, CHI '15, Seoul, Republic of Korea: Association for Computing Machinery, 2015, pp. 1489–1498, ISBN: 9781450331456, DOI: 10.1145/2702123.2702336.
- [12] Santosh V. Angadi and Robert L. Jackson, « A critical review on the solenoid valve reliability, performance and remaining useful life including its industrial applications », *in: Engineering Failure Analysis* 136 (2022), p. 106231, ISSN: 1350-6307, DOI: <https://doi.org/10.1016/j.engfailanal.2022.106231>, URL: <https://www.sciencedirect.com/science/article/pii/S1350630722002059>.

-
- [13] Apple, *Get directions on Apple Watch*, Last retrieved January 25, 2024, URL: <https://support.apple.com/en-eg/guide/watch/apdea7480950/watchos>.
- [14] Apple, *Get started with the Workout app on Apple Watch*, Last retrieved January 25, 2024, URL: <https://support.apple.com/en-gu/guide/watch/apd4edc9bc20/watchos>.
- [15] Apple, *Make purchases using Apple Pay*, Last retrieved January 25, 2024, URL: <https://support.apple.com/en-us/102626>.
- [16] Apple, *Track important health information with Apple Watch*, Last retrieved January 25, 2024, URL: <https://support.apple.com/guide/watch/track-important-health-information-apple-apdc2bf82d90/watchos>.
- [17] Taylor Dixon, *Good Vibrations: How Apple Dominates the Touch Feedback Game*, Last retrieved July 13, 2023, 2019, URL: <https://www.ifixit.com/News/16768/apple-taptic-engine-haptic-feedback>.
- [18] Arduino, *Arduino*, Last retrieved January 22, 2024, URL: <https://www.arduino.cc/>.
- [19] M. Ashtiani, S.H. Hashemabadi, and A. Ghaffari, « A review on the magnetorheological fluid preparation and stabilization », *in: Journal of Magnetism and Magnetic Materials* 374 (2015), pp. 716–730, ISSN: 0304-8853, DOI: <https://doi.org/10.1016/j.jmmm.2014.09.020>, URL: <https://www.sciencedirect.com/science/article/pii/S0304885314008403>.
- [20] American Psychological Association, *Publication Manual of the American Psychological Association*, (2020), Washington, D.C., United States: American Psychological Association, 2019.
- [21] International ASTM, « Standard test methods for flexural properties of unreinforced and reinforced plastics and electrical insulating materials », *in: ASTM D790-15* (2015), DOI: 10.1520/D0790-15.
- [22] Jacob Astocondor-Villar, Juan Grados, Fernando Mendoza-Apaza, Wilmer Chavez-Sanchez, Kennedy Narciso-Gomez, Anna Grados-Espinoza, and Paolo Pascual-Panduro, « Low-Cost Biomechanical System for Posture Rectification Using IoT Technology », *in: Proceedings of the 2023 6th International Conference on Electronics, Communications and Control Engineering*, ICECC '23, Fukuoka, Japan: Association for Computing Machinery, 2023, pp. 271–277, ISBN: 9798400700002,

- DOI: 10.1145/3592307.3592350, URL: <https://doi.org/10.1145/3592307.3592350>.
- [23] S. Sandra Bae, Clement Zheng, Mary Etta West, Ellen Yi-Luen Do, Samuel Huron, and Danielle Albers Szafer, « Making Data Tangible: A Cross-Disciplinary Design Space for Data Physicalization », *in: Proceedings of the 2022 CHI Conference on Human Factors in Computing Systems*, CHI '22, New Orleans, LA, USA: Association for Computing Machinery, 2022, ISBN: 9781450391573, DOI: 10.1145/3491102.3501939, URL: <https://doi.org/10.1145/3491102.3501939>.
- [24] Fariborz Baghaei Naeni, Aamna M. AlAli, Raghad Al-Husari, Amin Rigi, Mohammad K. Al-Sharman, Dimitrios Makris, and Yahya Zweiri, « A Novel Dynamic-Vision-Based Approach for Tactile Sensing Applications », *in: IEEE Transactions on Instrumentation and Measurement* 69.5 (2020), pp. 1881–1893, DOI: 10.1109/TIM.2019.2919354.
- [25] Katerina Baousi, Nate Fear, Christos Mourouzis, Ben Stokes, Henry Wood, Paul Worgan, and Anne Roudaut, « Inflashoe: A Shape Changing Shoe to Control Underfoot Pressure », *in: Proceedings of the 2017 CHI Conference Extended Abstracts on Human Factors in Computing Systems*, CHI EA '17, <conf-loc>, <city>Denver</city>, <state>Colorado</state>, <country>USA</country>, </conf-loc>: Association for Computing Machinery, 2017, pp. 2381–2387, ISBN: 9781450346566, DOI: 10.1145/3027063.3053190, URL: <https://doi.org/10.1145/3027063.3053190>.
- [26] Jeffrey Bardzell, Shaowen Bardzell, and Austin Toombs, « "now that's definitely a proper hack": self-made tools in hackerspaces », *in: Proceedings of the SIGCHI Conference on Human Factors in Computing Systems*, CHI '14, Toronto, Ontario, Canada: Association for Computing Machinery, 2014, pp. 473–476, ISBN: 9781450324731, DOI: 10.1145/2556288.2557221, URL: <https://doi.org/10.1145/2556288.2557221>.
- [27] Jose Barreiros, Houston Claire, Bryan Peele, Omer Shapira, Josef Spjut, David Luebke, Malte Jung, and Robert Shepherd, « Fluidic Elastomer Actuators for Haptic Interactions in Virtual Reality », *in: IEEE Robotics and Automation Letters* 4.2 (2019), pp. 277–284, DOI: 10.1109/LRA.2018.2888628.
- [28] Olivier Bau, Ivan Poupyrev, Ali Israr, and Chris Harrison, « TeslaTouch: Electrovi-
bration for Touch Surfaces », *in: Proceedings of the 23rd Annual ACM Symposium on User Interface Software and Technology*, UIST '10, New York, New York, USA:

- Association for Computing Machinery, 2010, pp. 283–292, ISBN: 9781450302715, DOI: 10.1145/1866029.1866074.
- [29] Zdeněk P. Bažant, L. Cedolin, and Zdeněk P. Bažant, *Stability of Structures: Elastic, Inelastic, Fracture and Damage Theories*, English, Oxford University Press, 1991, pp. 231–236, URL: <https://www.scholars.northwestern.edu/en/publications/stability-of-structures-elastic-inelastic-fracture-and-damage-the>.
- [30] Stephan Bergbauer and David D. Pollard, « How to calculate normal curvatures of sampled geological surfaces », *in: Journal of Structural Geology* 25.2 (2003), pp. 277–289, ISSN: 0191-8141, DOI: [https://doi.org/10.1016/S0191-8141\(02\)00019-6](https://doi.org/10.1016/S0191-8141(02)00019-6), URL: <https://www.sciencedirect.com/science/article/pii/S0191814102000196>.
- [31] Wouter M. Bergmann Tiest and Astrid M. L. Kappers, « Cues for Haptic Perception of Compliance », *in: IEEE Transactions on Haptics* 2.4 (2009), pp. 189–199, DOI: 10.1109/TOH.2009.16.
- [32] Matthias Berning, Florian Braun, Till Riedel, and Michael Beigl, « ProximityHat: A Head-Worn System for Subtle Sensory Augmentation with Tactile Stimulation », *in: Proceedings of the 2015 ACM International Symposium on Wearable Computers, ISWC '15, Osaka, Japan: Association for Computing Machinery, 2015*, pp. 31–38, ISBN: 9781450335782, DOI: 10.1145/2802083.2802088.
- [33] N.A. Bernstein, *Dexterity and Its Development*, ed. by M.L. Latash M.L. Latash and M.T. Turvey, Psychology Press, 1996, DOI: 10.4324/9781410603357, URL: <https://doi.org/10.4324/9781410603357>.
- [34] J. Berzowska and M. Coelho, « Kukkia and Vilkas: kinetic electronic garments », *in: Ninth IEEE International Symposium on Wearable Computers (ISWC'05)*, 2005, pp. 82–85, DOI: 10.1109/ISWC.2005.29.
- [35] Arpit Bhatia, Dhruv Kundu, Suyash Agarwal, Varnika Kairon, and Aman Par-nami, « Soma-Noti: Delivering Notifications Through Under-Clothing Wearables », *in: Proceedings of the 2021 CHI Conference on Human Factors in Computing Systems, CHI '21, Yokohama, Japan: Association for Computing Machinery, 2021*, ISBN: 9781450380966, DOI: 10.1145/3411764.3445123, URL: <https://doi.org/10.1145/3411764.3445123>.

- [36] A. Bicchi, E.P. Scilingo, and D. De Rossi, « Haptic discrimination of softness in teleoperation: the role of the contact area spread rate », *in: IEEE Transactions on Robotics and Automation* 16.5 (2000), pp. 496–504, DOI: 10.1109/70.880800.
- [37] A. Bicchi, E.P. Scilingo, and D. De Rossi, « Haptic discrimination of softness in teleoperation: the role of the contact area spread rate », *in: IEEE Transactions on Robotics and Automation* 16.5 (2000), pp. 496–504, DOI: 10.1109/70.880800.
- [38] Loïc Blanc, Alain Delchambre, and Pierre Lambert, « Flexible Medical Devices: Review of Controllable Stiffness Solutions », *in: Actuators* 6.3 (2017), ISSN: 2076-0825, DOI: 10.3390/act6030023, URL: <https://www.mdpi.com/2076-0825/6/3/23>.
- [39] Alberto Boem, Yuuki Enzaki, Hiroaki Yano, and Hiroo Iwata, « Human Perception of a Haptic Shape-changing Interface with Variable Rigidity and Size », *in: 2019 IEEE Conference on Virtual Reality and 3D User Interfaces (VR)*, 2019, pp. 858–859, DOI: 10.1109/VR.2019.8798214.
- [40] Alberto Boem and Giovanni Maria Troiano, « Non-Rigid HCI: A Review of Deformable Interfaces and Input », *in: Proceedings of the 2019 on Designing Interactive Systems Conference*, DIS '19, San Diego, CA, USA: Association for Computing Machinery, 2019, pp. 885–906, ISBN: 9781450358507, DOI: 10.1145/3322276.3322347, URL: <https://doi.org/10.1145/3322276.3322347>.
- [41] Jessica Danielle Boles, « Power Electronics Meet Piezoelectrics: Converters, Components, and Miniaturization », PhD thesis, Massachusetts Institute of Technology, 2022, URL: <https://hdl.handle.net/1721.1/147383>.
- [42] W N Bond, « Turbulent flow through tubes », *in: Proceedings of the Physical Society* 43.1 (Jan. 1931), p. 46, DOI: 10.1088/0959-5309/43/1/306, URL: <https://dx.doi.org/10.1088/0959-5309/43/1/306>.
- [43] Elodie Bouzbib, Claudio Pacchierotti, and Anatole Lécuyer, « When Tangibles Become Deformable: Studying Pseudo-Stiffness Perceptual Thresholds in a VR Grasping Task », *in: IEEE Transactions on Visualization and Computer Graphics* 29.5 (2023), pp. 2743–2752, DOI: 10.1109/TVCG.2023.3247083.
- [44] Margherita Brancadoro, Mariangela Manti, Selene Tognarelli, and Matteo Cianchetti, « Preliminary experimental study on variable stiffness structures based on fiber

- jamming for soft robots », *in: 2018 IEEE International Conference on Soft Robotics (RoboSoft)*, 2018, pp. 258–263, DOI: 10.1109/ROBOSOFT.2018.8404929.
- [45] Victor Bret, « A Brief Rant On The Future Of Interaction Design. », *in: Worry Dream.com* (2011), URL: <http://worrydream.com/ABriefRantOnTheFutureOfInteractionD>
- [46] Jas Brooks, Noor Amin, and Pedro Lopes, « Taste Retargeting via Chemical Taste Modulators », *in: Proceedings of the 36th Annual ACM Symposium on User Interface Software and Technology, UIST '23*, <conf-loc>, <city>San Francisco</city>, <state>CA</state>, <country>USA</country>, </conf-loc>: Association for Computing Machinery, 2023, ISBN: 9798400701320, DOI: 10.1145/3586183.3606818.
- [47] Jas Brooks and Pedro Lopes, « Smell & Paste: Low-Fidelity Prototyping for Olfactory Experiences », *in: Proceedings of the 2023 CHI Conference on Human Factors in Computing Systems, CHI '23*, <conf-loc>, <city>Hamburg</city>, <country>Germany</country>, </conf-loc>: Association for Computing Machinery, 2023, ISBN: 9781450394215, DOI: 10.1145/3544548.3580680.
- [48] Trevor L. Buckner, Michelle C. Yuen, Sang Yup Kim, and Rebecca Kramer-Bottiglio, « Enhanced Variable Stiffness and Variable Stretchability Enabled by Phase-Changing Particulate Additives », *in: Advanced Functional Materials* 29.50 (2019), p. 1903368, DOI: <https://doi.org/10.1002/adfm.201903368>, eprint: <https://onlinelibrary.wiley.com/doi/pdf/10.1002/adfm.201903368>, URL: <https://onlinelibrary.wiley.com/doi/abs/10.1002/adfm.201903368>.
- [49] Leah Buechley and Hannah Perner-Wilson, « Crafting technology: Reimagining the processes, materials, and cultures of electronics », *in: ACM Trans. Comput.-Hum. Interact.* 19.3 (Oct. 2012), ISSN: 1073-0516, DOI: 10.1145/2362364.2362369, URL: <https://doi.org/10.1145/2362364.2362369>.
- [50] Leah Buechley, Daniela K. Rosner, Eric Paulos, and Amanda Williams, « DIY for CHI: methods, communities, and values of reuse and customization », *in: CHI '09 Extended Abstracts on Human Factors in Computing Systems, CHI EA '09*, <conf-loc>, <city>Boston</city>, <state>MA</state>, <country>USA</country>, </conf-loc>: Association for Computing Machinery, 2009, pp. 4823–4826, ISBN: 9781605582474, DOI: 10.1145/1520340.1520750.

- [51] Mohamad Adam Bujang, Nadiah Sa'at, and Tg Mohd Ikhwan Tg Abu Bakar, « Determination of minimum sample size requirement for multiple linear regression and analysis of covariance based on experimental and non-experimental studies », *in: Epidemiology, Biostatistics, and Public Health* 14.3 (2017), DOI: <https://doi.org/10.2427/12117>.
- [52] Kelly Caine, « Local Standards for Sample Size at CHI », *in: Proceedings of the 2016 CHI Conference on Human Factors in Computing Systems*, CHI '16, San Jose, California, USA: Association for Computing Machinery, 2016, pp. 981–992, ISBN: 9781450333627, DOI: 10.1145/2858036.2858498.
- [53] M. E. Cates, J. P. Wittmer, J.-P. Bouchaud, and P. Claudin, « Jamming, Force Chains, and Fragile Matter », *in: Phys. Rev. Lett.* 81 (9 Aug. 1998), pp. 1841–1844, DOI: 10.1103/PhysRevLett.81.1841, URL: <https://link.aps.org/doi/10.1103/PhysRevLett.81.1841>.
- [54] Ahmed Amine Chafik, Jaafar Gaber, Souad Tayane, and Mohamed Ennaji, « Behavioral modeling of knitted shape memory membrane », *in: 2022 XXVIII International Conference on Information, Communication and Automation Technologies (ICAT)*, 2022, pp. 1–6, DOI: 10.1109/ICAT54566.2022.9811236.
- [55] Dow Chemical, *SYLGAR 184*, Last retrieved January 4, 2024, URL: <https://www.dow.com/en-us/pdp/sylgard-184-silicone-elastomer-kit.01064291z.html#overview>.
- [56] Chao Chen, Zhengjin Wang, and Zhigang Suo, « Flaw sensitivity of highly stretchable materials », *in: Extreme Mechanics Letters* 10 (2017), Filling Gaps in Material Property Space: IUTAM Symposium, pp. 50–57, ISSN: 2352-4316, DOI: <https://doi.org/10.1016/j.eml.2016.10.002>, URL: <https://www.sciencedirect.com/science/article/pii/S2352431616301523>.
- [57] Dustin Chen and Qibing Pei, « Electronic Muscles and Skins: A Review of Soft Sensors and Actuators », *in: Chemical Reviews* 117.17 (2017), PMID: 28816043, pp. 11239–11268, DOI: 10.1021/acs.chemrev.7b00019, eprint: <https://doi.org/10.1021/acs.chemrev.7b00019>, URL: <https://doi.org/10.1021/acs.chemrev.7b00019>.

- [58] Tian Chen, Mark Pauly, and Pedro M Reis, « A reprogrammable mechanical metamaterial with stable memory », *in: Nature* 589.7842 (2021), pp. 386–390, DOI: 10.1038/s41586-020-03123-5, URL: <https://doi.org/10.1038/s41586-020-03123-5>.
- [59] Yu-Wen Chen, Wei-Ju Lin, Yi Chen, and Lung-Pan Cheng, « PneuSeries: 3D Shape Forming with Modularized Serial-Connected Inflatables », *in: The 34th Annual ACM Symposium on User Interface Software and Technology, UIST '21, Virtual Event, USA: Association for Computing Machinery, 2021*, pp. 431–440, ISBN: 9781450386357, DOI: 10.1145/3472749.3474760, URL: <https://doi.org/10.1145/3472749.3474760>.
- [60] Xiang 'Anthony' Chen, Jeeun Kim, Jennifer Mankoff, Tovi Grossman, Stelian Coros, and Scott E. Hudson, « Reprise: A Design Tool for Specifying, Generating, and Customizing 3D Printable Adaptations on Everyday Objects », *in: Proceedings of the 29th Annual Symposium on User Interface Software and Technology, UIST '16, Tokyo, Japan: Association for Computing Machinery, 2016*, pp. 29–39, ISBN: 9781450341899, DOI: 10.1145/2984511.2984512, URL: <https://doi.org/10.1145/2984511.2984512>.
- [61] Xiaojuan Chen, Fei Shao, CJ Barnes, Tom Childs, and Brian Henson, « Exploring relationships between touch perception and surface physical properties », *in: International Journal of Design* 3.2 (2009), pp. 67–76, URL: <https://www.ijdesign.org/index.php/IJDesign/article/view/596/261>.
- [62] Yang Chen, Katherine Fennedy, Anna Fogel, Shengdong Zhao, Chao Zhang, Lijuan Liu, and Chingchiuan Yen, « SSpoon: A Shape-Changing Spoon That Optimizes Bite Size for Eating Rate Regulation », *in: Proc. ACM Interact. Mob. Wearable Ubiquitous Technol.* 6.3 (Sept. 2022), DOI: 10.1145/3550312, URL: <https://doi.org/10.1145/3550312>.
- [63] Yanjun Chen, Xuewei Liang, Si Chen, Yuwen Chen, Hongnan Lin, Hechuan Zhang, Chutian Jiang, Feng Tian, Yu Zhang, Shanshan Yao, and Teng Han, « HapTag: A Compact Actuator for Rendering Push-Button Tactility on Soft Surfaces », *in: Proceedings of the 35th Annual ACM Symposium on User Interface Software and Technology, UIST '22, Bend, OR, USA: Association for Computing Machinery, 2022*, ISBN: 9781450393201, DOI: 10.1145/3526113.3545644.

- [64] Thomas P. Chenal, Jennifer C. Case, Jamie Paik, and Rebecca K. Kramer, « Variable stiffness fabrics with embedded shape memory materials for wearable applications », *in: 2014 IEEE/RSJ International Conference on Intelligent Robots and Systems*, 2014, pp. 2827–2831, DOI: 10.1109/IRoS.2014.6942950.
- [65] Gary PT Choi, Levi H Dudte, and L Mahadevan, « Programming shape using kirigami tessellations », *in: Nature materials* 18.9 (2019), pp. 999–1004, DOI: <https://doi.org/10.1038/s41563-019-0452-y>.
- [66] Inrak Choi, Nick Corson, Lizzie Peiros, Elliot W. Hawkes, Sean Keller, and Sean Follmer, « A Soft, Controllable, High Force Density Linear Brake Utilizing Layer Jamming », *in: IEEE Robotics and Automation Letters* 3.1 (2018), pp. 450–457, DOI: 10.1109/LRA.2017.2761938.
- [67] Kyung Yun Choi, Neska ElHaouij, Jinmo Lee, Rosalind W. Picard, and Hiroshi Ishii, « Design and Evaluation of a Clippable and Personalizable Pneumatic-Haptic Feedback Device for Breathing Guidance », *in: Proc. ACM Interact. Mob. Wearable Ubiquitous Technol.* 6.1 (Mar. 2022), DOI: 10.1145/3517234, URL: <https://doi.org/10.1145/3517234>.
- [68] Kyung Yun Choi and Hiroshi Ishii, « AmbienBeat: Wrist-Worn Mobile Tactile Biofeedback for Heart Rate Rhythmic Regulation », *in: Proceedings of the Fourteenth International Conference on Tangible, Embedded, and Embodied Interaction*, TEI '20, Sydney NSW, Australia: Association for Computing Machinery, 2020, pp. 17–30, ISBN: 9781450361071, DOI: 10.1145/3374920.3374938, URL: <https://doi.org/10.1145/3374920.3374938>.
- [69] Kyung Yun Choi, Jinmo Lee, Neska ElHaouij, Rosalind Picard, and Hiroshi Ishii, « ASpire: Clippable, Mobile Pneumatic-Haptic Device for Breathing Rate Regulation via Personalizable Tactile Feedback », *in: Extended Abstracts of the 2021 CHI Conference on Human Factors in Computing Systems*, CHI EA '21, Yokohama, Japan: Association for Computing Machinery, 2021, ISBN: 9781450380959, DOI: 10.1145/3411763.3451602, URL: <https://doi.org/10.1145/3411763.3451602>.
- [70] G. Cini, A. Frisoli, S. Marcheschi, F. Salsedo, and M. Bergamasco, « A novel fingertip haptic device for display of local contact geometry », *in: First Joint Eurohaptics Conference and Symposium on Haptic Interfaces for Virtual Environment and Teleoperator Systems. World Haptics Conference*, Pisa, Italy: Institute of Electrical and Electronics Engineers, 2005, pp. 602–605, DOI: 10.1109/WHC.2005.16.

- [71] J. Clawson, K. Lyons, T. Starner, and E. Clarkson, « The impacts of limited visual feedback on mobile text entry for the Twiddler and mini-QWERTY keyboards », *in: Ninth IEEE International Symposium on Wearable Computers (ISWC'05)*, 2005, pp. 170–177, DOI: 10.1109/ISWC.2005.49.
- [72] Marcelo Coelho and Pattie Maes, « Shutters: A Permeable Surface for Environmental Control and Communication », *in: Proceedings of the 3rd International Conference on Tangible and Embedded Interaction*, TEI '09, Cambridge, United Kingdom: Association for Computing Machinery, 2009, pp. 13–18, ISBN: 9781605584935, DOI: 10.1145/1517664.1517671, URL: <https://doi.org/10.1145/1517664.1517671>.
- [73] Marcelo Coelho and Jamie Zigelbaum, « Shape-changing interfaces », *in: Personal and Ubiquitous Computing* 15 (2011), pp. 161–173, DOI: 10.1007/s00779-010-0311-y.
- [74] Kerstyn Comley and Norman A. Fleck, « A micromechanical model for the Young's modulus of adipose tissue », *in: International Journal of Solids and Structures* 47.21 (2010), pp. 2982–2990, ISSN: 0020-7683, DOI: <https://doi.org/10.1016/j.ijsolstr.2010.07.001>, URL: <https://www.sciencedirect.com/science/article/pii/S0020768310002465>.
- [75] Melia Condon, Ingvars Birznieks, Kathryn Hudson, David K. Chelvanayagam, David Mahns, Håkan Olausson, and Vaughan G. Macefield, « Differential sensitivity to surface compliance by tactile afferents in the human finger pad », *in: Journal of Neurophysiology* 111.6 (2014), PMID: 24371291, pp. 1308–1317, DOI: 10.1152/jn.00589.2013, eprint: <https://doi.org/10.1152/jn.00589.2013>, URL: <https://doi.org/10.1152/jn.00589.2013>.
- [76] Matt Craddock and Rebecca Lawson, « The effects of size changes on haptic object recognition », *in: Attention, Perception, & Psychophysics* 71.4 (2009), pp. 910–923, DOI: 10.3758/APP.71.4.910.
- [77] Diana Crane, *Fashion and its social agendas: Class, gender, and identity in clothing*, University of Chicago Press, 2012, URL: <https://press.uchicago.edu/ucp/books/book/chicago/F/bo3777018.html>.
- [78] Zhitong Cui, Shuhong Wang, Junxian Li, Shijian Luo, and Alexandra Ion, « MiuraKit: A Modular Hands-On Construction Kit For Pneumatic Shape-Changing And Robotic Interfaces », *in: Proceedings of the 2023 ACM Designing Interactive*

- Systems Conference*, DIS '23, Pittsburgh, PA, USA: Association for Computing Machinery, 2023, pp. 2066–2078, ISBN: 9781450398930, DOI: 10.1145/3563657.3596108.
- [79] Kiran Dandekar, Balasundar I. Raju, and Mandayam A. Srinivasan, « 3-D Finite-Element Models of Human and Monkey Fingertips to Investigate the Mechanics of Tactile Sense », *in: Journal of Biomechanical Engineering* 125.5 (Oct. 2003), pp. 682–691, ISSN: 0148-0731, DOI: 10.1115/1.1613673, eprint: <https://asmedigitalcollection.asme.org/biomechanical/article-pdf/125/5/682/5767639/682\1.pdf>, URL: <https://doi.org/10.1115/1.1613673>.
- [80] Kurtis Danyluk, Bernhard Jenny, and Wesley Willett, « Look-From Camera Control for 3D Terrain Maps », *in: Proceedings of the 2019 CHI Conference on Human Factors in Computing Systems*, CHI '19, Glasgow, Scotland Uk: Association for Computing Machinery, 2019, pp. 1–12, ISBN: 9781450359702, DOI: 10.1145/3290605.3300594, URL: <https://doi.org/10.1145/3290605.3300594>.
- [81] Alexandra Delazio, Ken Nakagaki, Roberta L. Klatzky, Scott E. Hudson, Jill Fain Lehman, and Alanson P. Sample, « Force Jacket: Pneumatically-Actuated Jacket for Embodied Haptic Experiences », *in: Proceedings of the 2018 CHI Conference on Human Factors in Computing Systems*, CHI '18, Montreal QC, Canada: Association for Computing Machinery, 2018, pp. 1–12, ISBN: 9781450356206, DOI: 10.1145/3173574.3173894, URL: <https://doi.org/10.1145/3173574.3173894>.
- [82] Harvard Natural Sciences Lecture Demonstrations, *Egg Shell Strength*, (last retrieved January 3, 2024), URL: <https://sciencedemonstrations.fas.harvard.edu/presentations/egg-shell-strength>.
- [83] Ruta Desai, Fraser Anderson, Justin Matejka, Stelian Coros, James McCann, George Fitzmaurice, and Tovi Grossman, « Geppetto: Enabling Semantic Design of Expressive Robot Behaviors », *in: Proceedings of the 2019 CHI Conference on Human Factors in Computing Systems*, CHI '19, Glasgow, Scotland Uk: Association for Computing Machinery, 2019, pp. 1–14, ISBN: 9781450359702, DOI: 10.1145/3290605.3300599, URL: <https://doi.org/10.1145/3290605.3300599>.
- [84] Naga Sai Gopi K. Devaraju and Marc A. Unger, « Pressure driven digital logic in PDMS based microfluidic devices fabricated by multilayer soft lithography », *in: Lab Chip* 12 (22 2012), pp. 4809–4815, DOI: 10.1039/C2LC21155F, URL: <http://dx.doi.org/10.1039/C2LC21155F>.

-
- [85] Panteleimon Dimitriadis and Jason Alexander, « Evaluating the Effectiveness of Physical Shape-Change for in-Pocket Mobile Device Notifications », *in: Proceedings of the SIGCHI Conference on Human Factors in Computing Systems*, CHI '14, Toronto, Ontario, Canada: Association for Computing Machinery, 2014, pp. 2589–2592, ISBN: 9781450324731, DOI: 10.1145/2556288.2557164.
- [86] Yuran Ding, Craig Shultz, and Chris Harrison, « Surface I/O: Creating Devices with Functional Surface Geometry for Haptics and User Input », *in: Proceedings of the 2023 CHI Conference on Human Factors in Computing Systems*, CHI '23, Hamburg, Germany: Association for Computing Machinery, 2023, ISBN: 9781450394215, DOI: 10.1145/3544548.3581037, URL: <https://doi.org/10.1145/3544548.3581037>.
- [87] David Dobbstein, Evgeny Stemasov, Daniel Besserer, Irina Stenske, and Enrico Rukzio, « Movelet: A Self-Actuated Movable Bracelet for Positional Haptic Feedback on the User's Forearm », *in: Proceedings of the 2018 ACM International Symposium on Wearable Computers*, ISWC '18, Singapore, Singapore: Association for Computing Machinery, 2018, pp. 33–39, ISBN: 9781450359672, DOI: 10.1145/3267242.3267249, URL: <https://doi.org/10.1145/3267242.3267249>.
- [88] Ioannis Douros, *Calculating the curvature shape characteristics of the human body from 3D scanner data*, University of London, University College London (United Kingdom), 2004.
- [89] Catherine J Dowell, J Farley Norman, Jackie R Moment, Lindsey M Shain, Hideko F Norman, Flip Phillips, and Astrid ML Kappers, « Haptic shape discrimination and interhemispheric communication », *in: Scientific Reports* 8.1 (2018), p. 377, DOI: 10.1038/s41598-017-18691-2.
- [90] Pierre Dragicevic, « Fair Statistical Communication in HCI », *in: Modern Statistical Methods for HCI*, Springer, 2016, pp. 291–330, DOI: 10.1007/978-3-319-26633-6_13, URL: <https://hal.inria.fr/hal-01377894>.
- [91] Pierre Dragicevic, « Fair statistical communication in HCI », *in: Modern statistical methods for HCI*, Berlin, Germany: Springer, 2016, pp. 291–330, DOI: https://doi.org/10.1007/978-3-319-26633-6_13.
- [92] Philip N. Duncan, Siavash Ahrar, and Elliot E. Hui, « Scaling of pneumatic digital logic circuits », *in: Lab Chip* 15 (5 2015), pp. 1360–1365, DOI: 10.1039/C4LC01048E, URL: <http://dx.doi.org/10.1039/C4LC01048E>.

- [93] Soya Eguchi, Claire Okabe, Mai Ohira, and Hiroya Tanaka, « Pneumatic Auxetics: Inverse Design and 3D Printing of Auxetic Pattern for Pneumatic Morphing », *in: Extended Abstracts of the 2022 CHI Conference on Human Factors in Computing Systems*, CHI EA '22, New Orleans, LA, USA: Association for Computing Machinery, 2022, ISBN: 9781450391566, DOI: 10.1145/3491101.3519801.
- [94] Andrew Engel, « Validation and Modeling of a Subject-Driven Device for In Vivo Finger Indentation Using a Finger Mimic », PhD thesis, University of Cincinnati, 2017, URL: https://etd.ohiolink.edu/apexprod/rws_etd/send_file/send?accession=ucin1491557931643749&disposition=inline.
- [95] Cem Erçalık and Seçil Özkurt, « Two-point discrimination assessment of the upper extremities of healthy young Turkish individuals », *in: Turkish journal of physical medicine and rehabilitation* 68 (1 Mar. 2022), pp. 136–141, DOI: 10.5606/tftrd.2022.6263.
- [96] Zackory Erickson, Eliot Xing, Bharat Srirangam, Sonia Chernova, and Charles C. Kemp, « Multimodal Material Classification for Robots using Spectroscopy and High Resolution Texture Imaging », *in: 2020 IEEE/RSJ International Conference on Intelligent Robots and Systems (IROS)*, Las Vegas, NV, USA: Institute of Electrical and Electronics Engineers, 2020, pp. 10452–10459, DOI: 10.1109/IROS45743.2020.9341165.
- [97] Marc O Ernst and Martin S Banks, « Humans integrate visual and haptic information in a statistically optimal fashion », *in: Nature* 415.6870 (2002), pp. 429–433, DOI: 10.1038/415429a.
- [98] Marc O Ernst and Heinrich H Bülthoff, « Merging the senses into a robust percept », *in: Trends in cognitive sciences* 8.4 (2004), pp. 162–169, DOI: 10.1016/j.tics.2004.02.002.
- [99] Vincent Falanga and Brian Bucalo, « Use of a durometer to assess skin hardness », *in: Journal of the American Academy of Dermatology* 29.1 (1993), pp. 47–51, ISSN: 0190-9622, DOI: [https://doi.org/10.1016/0190-9622\(93\)70150-R](https://doi.org/10.1016/0190-9622(93)70150-R), URL: <https://www.sciencedirect.com/science/article/pii/019096229370150R>.
- [100] Zhuzhi Fan and Céline Coutrix, « Impact of Softness on Users' Perception of Curvature for Future Soft Curvature-Changing UIs », *in: Proceedings of the 2023 CHI Conference on Human Factors in Computing Systems*, CHI '23, Hamburg, Ger-

- many: Association for Computing Machinery, 2023, ISBN: 9781450394215, DOI: 10.1145/3544548.3581179.
- [101] Zhuzhi Fan, Alexis Sanson, Thomas Rames, and Céline Coutrix, « Conception et perception d'un changement de forme molle au dos d'une montre connectée », *in: Actes de La 35ième Conference Francophone Sur l'Interaction Homme-Machine, IHM '24*, Paris, France: Association for Computing Machinery, 2024, DOI: 10.1145/3649792.3649800, URL: <https://doi.org/10.1145/3649792.3649800>.
- [102] Zhuzhi Fan, Alexis Sanson, Thomas Rames, and Céline Coutrix, « Design and Perception of a Soft Shape Change Beneath a Smart watch », *in: Proceedings of The ACM International Conference on Mobile Human-Computer Interaction, MobileHCI '24*, Melbourne, Australia: Association for Computing Machinery, 2024, DOI: 10.1145/3676495.
- [103] Cathy Mengying Fang and Chris Harrison, « Retargeted Self-Haptics for Increased Immersion in VR without Instrumentation », *in: The 34th Annual ACM Symposium on User Interface Software and Technology, UIST '21*, Virtual Event, USA: Association for Computing Machinery, 2021, pp. 1109–1121, ISBN: 9781450386357, DOI: 10.1145/3472749.3474810, URL: <https://doi.org/10.1145/3472749.3474810>.
- [104] Behnaz Farahi, « D Caress of the Gaze », *in: Behnaz Farahi, Neil Leach (eds.) (2015)*, p. 176, URL: <https://behnazfarahi.com/publications/>.
- [105] Feng Feng, Dan Bennett, Zhi-jun Fan, and Oussama Metatla, « It's Touching: Understanding Touch-Affect Association in Shape-Change with Kinematic Features », *in: Proceedings of the 2022 CHI Conference on Human Factors in Computing Systems, CHI '22*, <conf-loc>, <city>New Orleans</city>, <state>LA</state>, <country>USA</country>, </conf-loc>: Association for Computing Machinery, 2022, ISBN: 9781450391573, DOI: 10.1145/3491102.3502003, URL: <https://doi.org/10.1145/3491102.3502003>.
- [106] BYK, *Film Casting Knife*, Last retrieved July 26, 2023, 2023, URL: <https://www.byk-instruments.com/en/Physical-Properties/Paint-Application/Manual-Film-Applicators/Film-Casting-Knife/c/p-5974?variant=2328>.

- [107] Sean Follmer, Daniel Leithinger, Alex Olwal, Nadia Cheng, and Hiroshi Ishii, « Jamming User Interfaces: Programmable Particle Stiffness and Sensing for Malleable and Shape-Changing Devices », *in: Proceedings of the 25th Annual ACM Symposium on User Interface Software and Technology*, UIST '12, Cambridge, Massachusetts, USA: Association for Computing Machinery, 2012, pp. 519–528, ISBN: 9781450315807, DOI: 10.1145/2380116.2380181.
- [108] Sean Follmer, Daniel Leithinger, Alex Olwal, Akimitsu Hogge, and Hiroshi Ishii, « InFORM: Dynamic Physical Affordances and Constraints through Shape and Object Actuation », *in: Proceedings of the 26th Annual ACM Symposium on User Interface Software and Technology*, UIST '13, St. Andrews, Scotland, United Kingdom: Association for Computing Machinery, 2013, pp. 417–426, ISBN: 9781450322683, DOI: 10.1145/2501988.2502032, URL: <https://doi.org/10.1145/2501988.2502032>.
- [109] FormLabs, *Form3 high precision Stereolithography (SLA) 3D printer*, Last retrieved July 25, 2023, 2023, URL: <https://formlabs.com/3d-printers/form-3/>.
- [110] FormLabs, *Form Wash*, Last retrieved July 25, 2023, 2023, URL: <https://formlabs.com/post-processing/wash-cure/>.
- [111] Wolfgang Forstmeier, Eric-Jan Wagenmakers, and Timothy H. Parker, « Detecting and avoiding likely false-positive findings – a practical guide », *in: Biological Reviews* 92 (4 Nov. 2017), pp. 1941–1968, DOI: 10.1111/brv.12315, URL: <https://doi.org/10.1111/brv.12315>.
- [112] Leire Francés-Morcillo, Paz Morer-Camo, María Isabel Rodríguez-Ferradas, and Aitor Cazón-Martín, « Wearable Design Requirements Identification and Evaluation », *in: Sensors* 20.9 (2020), ISSN: 1424-8220, DOI: 10.3390/s20092599, URL: <https://www.mdpi.com/1424-8220/20/9/2599>.
- [113] Karmen Franinović and Luke Franzke, « Shape Changing Surfaces and Structures: Design Tools and Methods for Electroactive Polymers », *in: Proceedings of the 2019 CHI Conference on Human Factors in Computing Systems*, CHI '19, Glasgow, Scotland Uk: Association for Computing Machinery, 2019, pp. 1–12, ISBN: 9781450359702, DOI: 10.1145/3290605.3300355, URL: <https://doi.org/10.1145/3290605.3300355>.

-
- [114] Gabriele Frediani and Federico Carpi, « Tactile display of softness on fingertip », *in: Scientific reports* 10.1 (2020), pp. 1–10, DOI: <https://doi.org/10.1038/s41598-020-77591-0>.
- [115] Robert M Friedman, Kim D Hester, Barry G Green, and Robert H LaMotte, « Magnitude estimation of softness », *in: Experimental brain research* 191.2 (2008), pp. 133–142, DOI: <https://doi.org/10.1007/s00221-008-1507-5>.
- [116] A. Frisoli, M. Solazzi, F. Salsedo, and M. Bergamasco, « A Fingertip Haptic Display for Improving Curvature Discrimination », *in: Presence: Teleoperators and Virtual Environments* 17.6 (Dec. 2008), pp. 550–561, DOI: 10.1162/pres.17.6.550, eprint: <https://direct.mit.edu/pvar/article-pdf/17/6/550/1624873/pres.17.6.550.pdf>, URL: <https://doi.org/10.1162/pres.17.6.550>.
- [117] Bruno Fruchard, Paul Strohmeier, Roland Bennewitz, and Jürgen Steimle, « Squish This: Force Input on Soft Surfaces for Visual Targeting Tasks », *in: Proceedings of the 2021 CHI Conference on Human Factors in Computing Systems*, CHI '21, Yokohama, Japan: Association for Computing Machinery, 2021, ISBN: 9781450380966, DOI: 10.1145/3411764.3445623, URL: <https://doi.org/10.1145/3411764.3445623>.
- [118] Verena Fuchsberger, Martin Murer, Manfred Tscheligi, Silvia Lindtner, Shaowen Bardzell, Jeffrey Bardzell, Andreas Reiter, and Pernille Bjorn, « Fabrication & HCI: Hobbyist Making, Industrial Production, and Beyond », *in: Proceedings of the 2016 CHI Conference Extended Abstracts on Human Factors in Computing Systems*, CHI EA '16, San Jose, California, USA: Association for Computing Machinery, 2016, pp. 3550–3557, ISBN: 9781450340823, DOI: 10.1145/2851581.2856491, URL: <https://doi.org/10.1145/2851581.2856491>.
- [119] Juri Fujii, Takuya Matsunobu, and Yasuaki Kakehi, « COLORISE: Shape- and Color-Changing Pixels with Inflatable Elastomers and Interactions », *in: Proceedings of the Twelfth International Conference on Tangible, Embedded, and Embodied Interaction*, TEI '18, Stockholm, Sweden: Association for Computing Machinery, 2018, pp. 199–204, ISBN: 9781450355681, DOI: 10.1145/3173225.3173228, URL: <https://doi.org/10.1145/3173225.3173228>.
- [120] Juri Fujii, Satoshi Nakamaru, and Yasuaki Kakehi, « LayerPump: Rapid Prototyping of Functional 3D Objects with Built-in Electrohydrodynamics Pumps Based on Layered Plates », *in: Proceedings of the Fifteenth International Conference on*

- Tangible, Embedded, and Embodied Interaction*, TEI '21, Salzburg, Austria: Association for Computing Machinery, 2021, ISBN: 9781450382137, DOI: 10.1145/3430524.3442453, URL: <https://doi.org/10.1145/3430524.3442453>.
- [121] Kaori Fujinami, « Implicit Interaction with Daily Objects: Applications and Issues », in: *Proceedings of the 3rd International Universal Communication Symposium*, IUCS '09, Tokyo, Japan: Association for Computing Machinery, 2009, pp. 163–168, ISBN: 9781605586410, DOI: 10.1145/1667780.1667813, URL: <https://doi.org/10.1145/1667780.1667813>.
- [122] Kazuyuki Fujita, Aoi Suzuki, Kazuki Takashima, Kaori Ikematsu, and Yoshifumi Kitamura, « TiltChair: Manipulative Posture Guidance by Actively Inclining the Seat of an Office Chair », in: *Proceedings of the 2021 CHI Conference on Human Factors in Computing Systems*, CHI '21, Yokohama, Japan: Association for Computing Machinery, 2021, ISBN: 9781450380966, DOI: 10.1145/3411764.3445151, URL: <https://doi.org/10.1145/3411764.3445151>.
- [123] Masahiro Furukawa, Naohisa Nagaya, Yuki Hashimoto, Hiroyuki Kajimoto, and Masahiko Inami, « Measurement of the detection thresholds of hair on human hairy skin using direct vibrotactile stimulation », in: *World Haptics 2009 - Third Joint EuroHaptics conference and Symposium on Haptic Interfaces for Virtual Environment and Teleoperator Systems*, 2009, pp. 127–132, DOI: 10.1109/WHC.2009.4810819.
- [124] Run Ze Gao and Carolyn L. Ren, « Synergizing microfluidics with soft robotics: A perspective on miniaturization and future directions », in: *Biomicrofluidics* 15.1 (Feb. 2021), p. 011302, ISSN: 1932-1058, DOI: 10.1063/5.0036991, eprint: https://pubs.aip.org/aip/bmf/article-pdf/doi/10.1063/5.0036991/13639721/011302\1_online.pdf, URL: <https://doi.org/10.1063/5.0036991>.
- [125] Tian Gao, Emmanuel Siéfert, Antonio DeSimone, and Benoît Roman, « Shape Programming by Modulating Actuation over Hierarchical Length Scales », in: *Advanced Materials* 32.47 (2020), p. 2004515, DOI: <https://doi.org/10.1002/adma.202004515>, eprint: <https://onlinelibrary.wiley.com/doi/pdf/10.1002/adma.202004515>, URL: <https://onlinelibrary.wiley.com/doi/abs/10.1002/adma.202004515>.

-
- [126] Seval Genc and Bora Derin, « Field Responsive Fluids - A Review », in: *Key Engineering Materials* 521 (Sept. 2012), pp. 87–99, DOI: 10.4028/www.scientific.net/KEM.521.87.
- [127] George A Gescheider, *Psychophysics: the fundamentals*, Third, Milton Park, Abingdon-on-Thames, Oxfordshire, England, UK: Routledge, 2016, pp. 46–54, 183–186, URL: <https://www.routledge.com/Psychophysics-The-Fundamentals/Gescheider/p/book/9781138984158>.
- [128] Shinjini Ghosh, « Investigating the influence of curvature on User Experience in TUIs- A Comparative Study of Concave and Convex Buttons », MA thesis, University of Birmingham, 2024, URL: <https://www.scribd.com/document/696708932/Investigating-the-influence-of-curvature-on-User-Experience-in-TUIs-A-Comparative-Study-of-Concave-and-Convex-Buttons>.
- [129] James J Gibson, « Observations on active touch. », in: *Psychological review* 69.6 (1962), p. 477.
- [130] Elizabeth Q. Gilson and A. D. Baddeley, « Tactile Short-Term Memory », in: *Quarterly Journal of Experimental Psychology* 21.2 (1969), pp. 180–184, DOI: 10.1080/14640746908400211, eprint: <https://doi.org/10.1080/14640746908400211>, URL: <https://doi.org/10.1080/14640746908400211>.
- [131] GitHub, *GitHub*, Last retrieved January 22, 2024, URL: <https://github.com/>.
- [132] Kristian Gohlke, Eva Hornecker, and Wolfgang Sattler, « Pneumatibles: Exploring Soft Robotic Actuators for the Design of User Interfaces with Pneumotactile Feedback », in: *Proceedings of the TEI '16: Tenth International Conference on Tangible, Embedded, and Embodied Interaction*, TEI '16, Eindhoven, Netherlands: Association for Computing Machinery, 2016, pp. 308–315, ISBN: 9781450335829, DOI: 10.1145/2839462.2839489.
- [133] Kristian Gohlke, Wolfgang Sattler, and Eva Hornecker, « AirPinch – An Inflatable Touch Fader with Pneumatic Tactile Feedback », in: *Sixteenth International Conference on Tangible, Embedded, and Embodied Interaction*, TEI '22, Daejeon, Republic of Korea: Association for Computing Machinery, 2022, ISBN: 9781450391474, DOI: 10.1145/3490149.3505568.

- [134] Antonio Gomes, Andrea Nesbitt, and Roel Vertegaal, « MorePhone: A Study of Actuated Shape Deformations for Flexible Thin-Film Smartphone Notifications », *in: Proceedings of the SIGCHI Conference on Human Factors in Computing Systems*, CHI '13, Paris, France: Association for Computing Machinery, 2013, pp. 583–592, ISBN: 9781450318990, DOI: 10.1145/2470654.2470737.
- [135] Jun Gong, Lan Li, Daniel Vogel, and Xing-Dong Yang, « Cito: An Actuated Smartwatch for Extended Interactions », *in: Proceedings of the 2017 CHI Conference on Human Factors in Computing Systems*, CHI '17, Denver, Colorado, USA: Association for Computing Machinery, 2017, pp. 5331–5345, ISBN: 9781450346559, DOI: 10.1145/3025453.3025568, URL: <https://doi.org/10.1145/3025453.3025568>.
- [136] AW Goodwin, KT John, and AH Marceglia, « Tactile discrimination of curvature by humans using only cutaneous information from the fingerpads », *in: Experimental brain research* 86.3 (1991), pp. 663–672, DOI: <https://doi.org/10.1007/BF00230540>.
- [137] AW Goodwin and HE Wheat, « Human tactile discrimination of curvature when contact area with the skin remains constant », *in: Experimental brain research* 88.2 (1992), pp. 447–450, DOI: <https://doi.org/10.1007/BF02259120>.
- [138] Ian E Gordon and Victoria Morison, « The haptic perception of curvature », *in: Perception and psychophysics* 31.5 (1982), pp. 446–450, DOI: 10.3758/BF03204854.
- [139] Ian E Gordon and Victoria Morison, « The haptic perception of curvature », *in: Perception & psychophysics* 31.5 (1982), pp. 446–450, DOI: <https://doi.org/10.3758/BF03204854>.
- [140] Goso, *Peristaltic Pump*, Last retrieved July 29, 2023, 2023, URL: https://www.amazon.fr/dp/B079GRP174/ref=pe_3044141_189395771_TE_3p_dp_1.
- [141] John Brandon Graham-Knight, Jon Michael Robert Corbett, Patricia Lasserre, Hai-Ning Liang, and Khalad Hasan, « Exploring Haptic Feedback for Common Message Notification Between Intimate Couples with Smartwatches », *in: Proceedings of the 32nd Australian Conference on Human-Computer Interaction*, OzCHI '20, Sydney, NSW, Australia: Association for Computing Machinery, 2021, pp. 245–252, ISBN: 9781450389754, DOI: 10.1145/3441000.3441012.

-
- [142] Joseph N Grima and Kenneth E Evans, « Auxetic behavior from rotating triangles », *in: Journal of materials science* 41.10 (2006), pp. 3193–3196, DOI: 10.1007/s10853-006-6339-8.
- [143] Daniel Groeger and Jürgen Steimle, « LASEC: Instant Fabrication of Stretchable Circuits Using a Laser Cutter », *in: Proceedings of the 2019 CHI Conference on Human Factors in Computing Systems*, CHI '19, Glasgow, Scotland Uk: Association for Computing Machinery, 2019, pp. 1–14, ISBN: 9781450359702, DOI: 10.1145/3290605.3300929, URL: <https://doi.org/10.1145/3290605.3300929>.
- [144] Daniel Groeger and Jürgen Steimle, « ObjectSkin: Augmenting Everyday Objects with Hydroprinted Touch Sensors and Displays », *in: Proc. ACM Interact. Mob. Wearable Ubiquitous Technol.* 1.4 (Jan. 2018), DOI: 10.1145/3161165, URL: <https://doi.org/10.1145/3161165>.
- [145] David Gueorguiev, Dimitrios Tzionas, Claudio Pacchierotti, Michael J. Black, and Katherine J. Kuchenbecker, *Statistical Modelling of Fingertip Deformations and Contact Forces during Tactile Interaction*, Extended abstract presented at the Hand, Brain and Technology conference (HBT), Ascona, Switzerland, Aug. 2018.
- [146] Aakar Gupta, Antony Albert Raj Irudayaraj, and Ravin Balakrishnan, « Haptic-Clench: Investigating Squeeze Sensations Using Memory Alloys », *in: Proceedings of the 30th Annual ACM Symposium on User Interface Software and Technology*, UIST '17, Québec City, QC, Canada: Association for Computing Machinery, 2017, pp. 109–117, ISBN: 9781450349819, DOI: 10.1145/3126594.3126598.
- [147] Ruslan Guseinov, Eder Miguel, and Bernd Bickel, « CurveUps: Shaping Objects from Flat Plates with Tension-Actuated Curvature », *in: ACM Trans. Graph.* 36.4 (July 2017), ISSN: 0730-0301, DOI: 10.1145/3072959.3073709.
- [148] Ehsan Hajiesmaili, Natalie M. Larson, Jennifer A. Lewis, and David R. Clarke, « Programmed shape-morphing into complex target shapes using architected dielectric elastomer actuators », *in: Science Advances* 8.28 (2022), eabn9198, DOI: 10.1126/sciadv.abn9198, eprint: <https://www.science.org/doi/pdf/10.1126/sciadv.abn9198>, URL: <https://www.science.org/doi/abs/10.1126/sciadv.abn9198>.
- [149] Lars Hallnäs and Johan Redström, « Slow Technology – Designing for Reflection », *in: Personal Ubiquitous Comput.* 5.3 (Jan. 2001), pp. 201–212, ISSN: 1617-4909, DOI: 10.1007/PL00000019, URL: <https://doi.org/10.1007/PL00000019>.

- [150] Nur Al-huda Hamdan, Adrian Wagner, Simon Voelker, Jürgen Steimle, and Jan Borchers, « Springlets: Expressive, Flexible and Silent On-Skin Tactile Interfaces », *in: Proceedings of the 2019 CHI Conference on Human Factors in Computing Systems*, CHI '19, Glasgow, Scotland Uk: Association for Computing Machinery, 2019, pp. 1–14, ISBN: 9781450359702, DOI: 10.1145/3290605.3300718.
- [151] Teng Han, Fraser Anderson, Pourang Irani, and Tovi Grossman, « HydroRing: Supporting Mixed Reality Haptics Using Liquid Flow », *in: Proceedings of the 31st Annual ACM Symposium on User Interface Software and Technology*, UIST '18, Berlin, Germany: Association for Computing Machinery, 2018, pp. 913–925, ISBN: 9781450359481, DOI: 10.1145/3242587.3242667, URL: <https://doi.org/10.1145/3242587.3242667>.
- [152] Teng Han, Shubhi Bansal, Xiaochen Shi, Yanjun Chen, Baogang Quan, Feng Tian, Hongan Wang, and Sriram Subramanian, « HapBead: On-Skin Microfluidic Haptic Interface Using Tunable Bead », *in: Proceedings of the 2020 CHI Conference on Human Factors in Computing Systems*, CHI '20, Honolulu, HI, USA: Association for Computing Machinery, 2020, pp. 1–10, ISBN: 9781450367080, DOI: 10.1145/3313831.3376190.
- [153] Youngshang Han, Leif-Erik Simonsen, and Mohammad H. Malakooti, « Printing Liquid Metal Elastomer Composites for High-Performance Stretchable Thermo-electric Generators », *in: Advanced Energy Materials* 12.34 (2022), p. 2201413, DOI: <https://doi.org/10.1002/aenm.202201413>, eprint: <https://onlinelibrary.wiley.com/doi/pdf/10.1002/aenm.202201413>, URL: <https://onlinelibrary.wiley.com/doi/abs/10.1002/aenm.202201413>.
- [154] Laura E Hanzly, Kristofer A Kristofferson, Natasha Chauhan, and Justin R Barone, « Biologically controlled gelatin actuators », *in: Green Materials* 9.4 (2021), pp. 157–166, DOI: 10.1680/jgrma.20.00069, eprint: <https://doi.org/10.1680/jgrma.20.00069>, URL: <https://doi.org/10.1680/jgrma.20.00069>.
- [155] John Hardy, Christian Weichel, Faisal Taher, John Vidler, and Jason Alexander, « ShapeClip: Towards Rapid Prototyping with Shape-Changing Displays for Designers », *in: Proceedings of the 33rd Annual ACM Conference on Human Factors in Computing Systems*, CHI '15, Seoul, Republic of Korea: Association for Computing Machinery, 2015, pp. 19–28, ISBN: 9781450331456, DOI: 10.1145/2702123.2702599, URL: <https://doi.org/10.1145/2702123.2702599>.

-
- [156] Chris Harrison, « The HCI Innovator's Dilemma », *in: Interactions* 25.6 (Oct. 2018), pp. 26–33, ISSN: 1072-5520, DOI: 10.1145/3274564, URL: <https://doi-org.ins2i.bib.cnrs.fr/10.1145/3274564>.
- [157] Chris Harrison and Scott E. Hudson, « Providing Dynamically Changeable Physical Buttons on a Visual Display », *in: Proceedings of the SIGCHI Conference on Human Factors in Computing Systems*, CHI '09, Boston, MA, USA: Association for Computing Machinery, 2009, pp. 299–308, ISBN: 9781605582467, DOI: 10.1145/1518701.1518749, URL: <https://doi.org/10.1145/1518701.1518749>.
- [158] Marc Hassenzahl, « The Thing and I: Understanding the Relationship between User and Product », *in: Funology: From Usability to Enjoyment*, USA: Kluwer Academic Publishers, 2005, pp. 31–42, ISBN: 1402029667.
- [159] Simon Hauser, Matthew Robertson, Auke Ijspeert, and Jamie Paik, « JammJoint: A Variable Stiffness Device Based on Granular Jamming for Wearable Joint Support », *in: IEEE Robotics and Automation Letters* 2.2 (2017), pp. 849–855, DOI: 10.1109/LRA.2017.2655109.
- [160] Liang He, Cheng Xu, Ding Xu, and Ryan Brill, « PneuHaptic: Delivering Haptic Cues with a Pneumatic Armband », *in: Proceedings of the 2015 ACM International Symposium on Wearable Computers*, ISWC '15, Osaka, Japan: Association for Computing Machinery, 2015, pp. 47–48, ISBN: 9781450335782, DOI: 10.1145/2802083.2802091, URL: <https://doi.org/10.1145/2802083.2802091>.
- [161] Felix Heibeck, Basheer Tome, Clark Della Silva, and Hiroshi Ishii, « UniMorph: Fabricating Thin Film Composites for Shape-Changing Interfaces », *in: Proceedings of the 28th Annual ACM Symposium on User Interface Software and Technology*, UIST '15, Charlotte, NC, USA: Association for Computing Machinery, 2015, pp. 233–242, ISBN: 9781450337793, DOI: 10.1145/2807442.2807472, URL: <https://doi.org/10.1145/2807442.2807472>.
- [162] Martin G Helander and Lijian Zhang, « Field studies of comfort and discomfort in sitting », *in: Ergonomics* 40.9 (1997), PMID: 9306741, pp. 895–915, DOI: 10.1080/001401397187739, eprint: <https://doi.org/10.1080/001401397187739>, URL: <https://doi.org/10.1080/001401397187739>.
- [163] Adam Heller, « Potentially implantable miniature batteries », *in: Analytical and bioanalytical chemistry* 385 (2006), pp. 469–473, DOI: 10.1007/s00216-006-0326-4.

- [164] Guido Hermans and Erik Stolterman, « Exploring parametric design: Consumer customization of an everyday object », *in*: (2012), URL: <https://dl.designresearchsociety.org/drs-conference-papers/drs2012/researchpapers/51/>.
- [165] Anuruddha Hettiarachchi and Daniel Wigdor, « Annexing Reality: Enabling Opportunistic Use of Everyday Objects as Tangible Proxies in Augmented Reality », *in*: *Proceedings of the 2016 CHI Conference on Human Factors in Computing Systems*, CHI '16, San Jose, California, USA: Association for Computing Machinery, 2016, pp. 1957–1967, ISBN: 9781450333627, DOI: 10.1145/2858036.2858134, URL: <https://doi.org/10.1145/2858036.2858134>.
- [166] H.G. Hoffman, « Physically touching virtual objects using tactile augmentation enhances the realism of virtual environments », *in*: *Proceedings. IEEE 1998 Virtual Reality Annual International Symposium (Cat. No.98CB36180)*, 1998, pp. 59–63, DOI: 10.1109/VRAIS.1998.658423.
- [167] Eve Hoggan, Yi-Ta Hsieh, Kalle Myllymaa, Vuokko Lantz, Johan Kildal, Julian Eiler, and Giulio Jacucci, « An Exploration of Mobile Shape-Changing Textures », *in*: *Proceedings of the Eleventh International Conference on Tangible, Embedded, and Embodied Interaction*, TEI '17, Yokohama, Japan: Association for Computing Machinery, 2017, pp. 275–282, ISBN: 9781450346764, DOI: 10.1145/3024969.3024983.
- [168] David Holman, Audrey Girouard, Hrvoje Benko, and Roel Vertegaal, « The Design of Organic User Interfaces: Shape, Sketching and Hypercontext », *in*: *Interacting with Computers* 25.2 (Mar. 2013), pp. 133–142, ISSN: 0953-5438, DOI: 10.1093/iwc/iws018, eprint: <https://academic.oup.com/iwc/article-pdf/25/2/133/2300729/iws018.pdf>, URL: <https://doi.org/10.1093/iwc/iws018>.
- [169] David Holman and Roel Vertegaal, « Organic User Interfaces: Designing Computers in Any Way, Shape, or Form », *in*: *Commun. ACM* 51.6 (June 2008), pp. 48–55, ISSN: 0001-0782, DOI: 10.1145/1349026.1349037, URL: <https://doi.org/10.1145/1349026.1349037>.
- [170] David Holman, Roel Vertegaal, Mark Altosaar, Nikolaus Troje, and Derek Johns, « Paper Windows: Interaction Techniques for Digital Paper », *in*: *Proceedings of the SIGCHI Conference on Human Factors in Computing Systems*, CHI '05, Portland, Oregon, USA: Association for Computing Machinery, 2005, pp. 591–599, ISBN:

- 1581139985, DOI: 10.1145/1054972.1055054, URL: <https://doi.org/10.1145/1054972.1055054>.
- [171] Bernard J van der Horst and Astrid M L Kappers, « Haptic Curvature Comparison of Convex and Concave Shapes », *in: Perception* 37.8 (2008), PMID: 18853551, pp. 1137–1151, DOI: 10.1068/p5780, eprint: <https://doi.org/10.1068/p5780>, URL: <https://doi.org/10.1068/p5780>.
- [172] Kei Hoshi and John Waterworth, « Tangible presence in blended reality space », *in: PRESENCE 2009*, 2009, pp. 1–10, URL: <https://www.diva-portal.org/smash/get/diva2:311021/FULLTEXT01.pdf>.
- [173] Emmanuel Siefert and Benoit Roman, Last retrieved July 13, 2023, 2019, URL: <https://vimeo.com/420256797>.
- [174] Glenn Hrinda, « Snap-Through Instability Patterns in Truss Structures », *in: 51st AIAA/ASME/ASCE/AHS/ASC Structures, Structural Dynamics, and Materials Conference*, DOI: 10.2514/6.2010-2611, eprint: <https://arc.aiaa.org/doi/pdf/10.2514/6.2010-2611>, URL: <https://arc.aiaa.org/doi/abs/10.2514/6.2010-2611>.
- [175] Yuhan Hu and Guy Hoffman, « Using Skin Texture Change to Design Emotion Expression in Social Robots », *in: 2019 14th ACM/IEEE International Conference on Human-Robot Interaction (HRI)*, 2019, pp. 2–10, DOI: 10.1109/HRI.2019.8673012.
- [176] Yuhan Hu and Guy Hoffman, « Using Skin Texture Change to Design Emotion Expression in Social Robots », *in: Proceedings of the 14th ACM/IEEE International Conference on Human-Robot Interaction*, HRI '19, Daegu, Republic of Korea: IEEE Press, 2020, pp. 2–10, ISBN: 9781538685556.
- [177] Yuhan Hu and Guy Hoffman, « What Can a Robot’s Skin Be? Designing Texture-Changing Skin for Human–Robot Social Interaction », *in: J. Hum.-Robot Interact.* 12.2 (Apr. 2023), DOI: 10.1145/3532772, URL: <https://doi.org/10.1145/3532772>.
- [178] Yuhan Hu, Isabel Neto, Jin Ryu, Ali Shtarbanov, Hugo Nicolau, Ana Paiva, and Guy Hoffman, « Touchibo: Multimodal Texture-Changing Robotic Platform for Shared Human Experiences », *in: Adjunct Proceedings of the 35th Annual ACM Symposium on User Interface Software and Technology*, UIST '22 Adjunct, Bend,

- OR, USA: Association for Computing Machinery, 2022, ISBN: 9781450393218, DOI: 10.1145/3526114.3558643.
- [179] Mutian Hua, Dong Wu, Shuwang Wu, Yanfei Ma, Yousif Alsaïd, and Ximin He, « 4D printable tough and thermoresponsive hydrogels », *in: ACS applied materials & interfaces* 13.11 (2020), pp. 12689–12697, DOI: 10.1021/acsami.0c17532.
- [180] Xiaonan Huang, Kitty Kumar, Mohammad K. Jawed, Amir Mohammadi Nasab, Zisheng Ye, Wanliang Shan, and Carmel Majidi, « Highly Dynamic Shape Memory Alloy Actuator for Fast Moving Soft Robots », *in: Advanced Materials Technologies* 4.4 (2019), p. 1800540, DOI: <https://doi.org/10.1002/admt.201800540>, eprint: <https://onlinelibrary.wiley.com/doi/pdf/10.1002/admt.201800540>, URL: <https://onlinelibrary.wiley.com/doi/abs/10.1002/admt.201800540>.
- [181] Da-Yuan Huang, Ruizhen Guo, Jun Gong, Jingxian Wang, John Graham, De-Nian Yang, and Xing-Dong Yang, « RetroShape: Leveraging Rear-Surface Shape Displays for 2.5D Interaction on Smartwatches », *in: Proceedings of the 30th Annual ACM Symposium on User Interface Software and Technology*, UIST '17, Québec City, QC, Canada: Association for Computing Machinery, 2017, pp. 539–551, ISBN: 9781450349819, DOI: 10.1145/3126594.3126610, URL: <https://doi.org/10.1145/3126594.3126610>.
- [182] John H. Hubbard and Beverly H. West, « Structural Stability », *in: Differential Equations: A Dynamical Systems Approach: Higher-Dimensional Systems*, New York, NY: Springer New York, 1995, pp. 203–264, ISBN: 978-1-4612-4192-8, DOI: 10.1007/978-1-4612-4192-8_4, URL: https://doi.org/10.1007/978-1-4612-4192-8_4.
- [183] Nathaniel Hudson, Celena Alcock, and Parmit K. Chilana, « Understanding New-comers to 3D Printing: Motivations, Workflows, and Barriers of Casual Makers », *in: Proceedings of the 2016 CHI Conference on Human Factors in Computing Systems*, CHI '16, San Jose, California, USA: Association for Computing Machinery, 2016, pp. 384–396, ISBN: 9781450333627, DOI: 10.1145/2858036.2858266, URL: <https://doi.org/10.1145/2858036.2858266>.
- [184] Dohgyu Hwang, Edward J. Barron, A. B. M. Tahidul Haque, and Michael D. Bartlett, « Shape morphing mechanical metamaterials through reversible plasticity », *in: Science Robotics* 7.63 (2022), eabg2171, DOI: 10.1126/scirobotics.abg2171, eprint: <https://www.science.org/doi/pdf/10.1126/scirobotics.abg2171>.

- abg2171, URL: <https://www.science.org/doi/abs/10.1126/scirobotics.abg2171>.
- [185] Celine Coutrix Hyunyoung Kim and Anne Roudaut, « Collection of everyday reconfigurable objects. », *in: phyflex.imag.fr* (2018), URL: <http://phyflex.imag.fr/EverydayObjects.html>.
- [186] Celine Coutrix Hyunyoung Kim and Anne Roudaut., *Collection of everyday reconfigurable objects*. siteweb, 2018, URL: <http://phyflex.imag.fr/EverydayObjects.html>.
- [187] T. Iberall, J. Jackson, L. Labbe, and R. Zampano, « Knowledge-based prehension: capturing human dexterity », *in: Proceedings. 1988 IEEE International Conference on Robotics and Automation*, 1988, 82–87 vol.1, DOI: 10.1109/ROBOT.1988.12027.
- [188] Filip Ilievski, Aaron D Mazzeo, Robert F Shepherd, Xin Chen, and George M Whitesides, « Soft robotics for chemists », *in: Angewandte Chemie* 123.8 (2011), pp. 1930–1935, DOI: 10.1002/ange.201006464.
- [189] Seiji Inaba, Shigeru Fujino, and Kenji Morinaga, « Young’s Modulus and Compositional Parameters of Oxide Glasses », *in: Journal of the American Ceramic Society* 82.12 (1999), pp. 3501–3507, DOI: <https://doi.org/10.1111/j.1151-2916.1999.tb02272.x>, eprint: <https://ceramics.onlinelibrary.wiley.com/doi/pdf/10.1111/j.1151-2916.1999.tb02272.x>, URL: <https://ceramics.onlinelibrary.wiley.com/doi/abs/10.1111/j.1151-2916.1999.tb02272.x>.
- [190] Dynalloy Inc, *Technical Characteristics of Flexinol Actuator Wires*, (last retrieved November 14, 2023), 2007, URL: <https://www.dynalloy.com/pdfs/TCF1140.pdf>.
- [191] Smooth On Inc., *Dragon Skin 10 NV*, Last retrieved July 24, 2023, URL: <https://www.smooth-on.com/products/dragon-skin-10-nv/>.
- [192] Smooth On Inc., *Ecoflex 00-30*, Last retrieved January 4, 2024, URL: <https://www.smooth-on.com/products/ecoflex-00-30/>.
- [193] Adafruit Industries, *Adafruit*, Last retrieved January 22, 2024, URL: <https://www.adafruit.com/>.
- [194] Instron, *INSTRON Universal Testing System*, Last retrieved January 4, 2024, URL: <https://www.instron.com/en/products/testing-systems/universal-testing-systems/3400-and-6800-series-system-retrofits>.

- [195] Inc. Interlink Electronics, *Interlink FSR 406*, Last retrieved January 4, 2024, URL: <https://www.interlinkelectronics.com/fsr-406>.
- [196] Alexandra Ion, Johannes Frohnhofen, Ludwig Wall, Robert Kovacs, Mirela Alistar, Jack Lindsay, Pedro Lopes, Hsiang-Ting Chen, and Patrick Baudisch, « Metamaterial Mechanisms », *in: Proceedings of the 29th Annual Symposium on User Interface Software and Technology, UIST '16*, Tokyo, Japan: Association for Computing Machinery, 2016, pp. 529–539, ISBN: 9781450341899, DOI: 10.1145/2984511.2984540, URL: <https://doi.org/10.1145/2984511.2984540>.
- [197] FormLabs, *Isopropyl Alcohol*, Last retrieved July 25, 2023, 2023, URL: https://support.formlabs.com/s/article/Isopropyl-Alcohol-IPA?language=en_US.
- [198] Yoshio Ishiguro and Ivan Poupyrev, « 3D Printed Interactive Speakers », *in: Proceedings of the SIGCHI Conference on Human Factors in Computing Systems, CHI '14*, Toronto, Ontario, Canada: Association for Computing Machinery, 2014, pp. 1733–1742, ISBN: 9781450324731, DOI: 10.1145/2556288.2557046, URL: <https://doi.org/10.1145/2556288.2557046>.
- [199] Hiroshi Ishii, « Tangible Bits: Beyond Pixels », *in: Proceedings of the 2nd International Conference on Tangible and Embedded Interaction, TEI '08*, Bonn, Germany: Association for Computing Machinery, 2008, pp. xv–xxv, ISBN: 9781605580043, DOI: 10.1145/1347390.1347392, URL: <https://doi.org/10.1145/1347390.1347392>.
- [200] Hiroki Ishizuka, Nicolo Lorenzoni, and Norihisa Miki, « Characterization of tactile display for stiffness distribution using Magneto-rheological fluid », *in: 2014 International Conference on Electronics Packaging (ICEP)*, 2014, pp. 400–404, DOI: 10.1109/ICEP.2014.6826717.
- [201] *Robotics — Safety requirements for robot systems in an industrial environment — Part 1: Robots*, Standard, Geneva, CH: International Organization for Standardization, 2018.
- [202] Harshika Jain, Melinda Chen, Alisha Collins, Lining Yao, Sunniva Liu, Riya Bobde, and Cindy Liu, « Demonstrating DIY Methods for Actuating Morphing Matter: Hands-on methods with off-the-shelf materials to actuate flexible substrates. », *in: Proceedings of the 14th Conference on Creativity and Cognition, C&C '22*, Venice, Italy: Association for Computing Machinery, 2022, pp. 593–596, ISBN: 9781450393270, DOI: 10.1145/3527927.3535196.

-
- [203] Harshika Jain, Kexin Lu, and Lining Yao, « Hydrogel-Based DIY Underwater Morphing Artifacts: A Morphing and Fabrication Technique to Democratize the Creation of Controllable Morphing 3D Underwater Structures with Low-Cost, Easily Available Hydrogel Beads Adhered to a Substrate. », *in: Designing Interactive Systems Conference 2021*, DIS '21, Virtual Event, USA: Association for Computing Machinery, 2021, pp. 1242–1252, ISBN: 9781450384766, DOI: 10.1145/3461778.3462136, URL: <https://doi.org/10.1145/3461778.3462136>.
- [204] Dirk Janasek, Joachim Franzke, and Andreas Manz, « Scaling and the design of miniaturized chemical-analysis systems », *in: Nature* 442.7101 (2006), pp. 374–380, DOI: 10.1038/nature05059.
- [205] Yvonne Jansen, Thorsten Karrer, and Jan Borchers, « MudPad: Tactile Feedback and Haptic Texture Overlay for Touch Surfaces », *in: ACM International Conference on Interactive Tabletops and Surfaces*, ITS '10, Saarbrücken, Germany: Association for Computing Machinery, 2010, pp. 11–14, ISBN: 9781450303996, DOI: 10.1145/1936652.1936655.
- [206] Yvonne Jansen, Jonas Schjerlund, and Kasper Hornbæk, « Effects of Locomotion and Visual Overview on Spatial Memory When Interacting with Wall Displays », *in: Proceedings of the 2019 CHI Conference on Human Factors in Computing Systems*, CHI '19, Glasgow, Scotland Uk: Association for Computing Machinery, 2019, pp. 1–12, ISBN: 9781450359702, DOI: 10.1145/3290605.3300521, URL: <https://doi.org/10.1145/3290605.3300521>.
- [207] K. L. Johnson, « Normal contact of elastic solids – Hertz theory », *in: Contact Mechanics*, Cambridge, United Kingdom: Cambridge University Press, 1985, pp. 84–106, DOI: 10.1017/CB09781139171731.005.
- [208] K. L. Johnson, « Normal contact of elastic solids – Hertz theory », *in: Contact Mechanics*, Cambridge, United Kingdom: Cambridge University Press, 1985, pp. 84–106, DOI: 10.1017/CB09781139171731.005.
- [209] Kenneth O Johnson, « The roles and functions of cutaneous mechanoreceptors », *in: Current Opinion in Neurobiology* 11.4 (2001), pp. 455–461, ISSN: 0959-4388, DOI: [https://doi.org/10.1016/S0959-4388\(00\)00234-8](https://doi.org/10.1016/S0959-4388(00)00234-8), URL: <https://www.sciencedirect.com/science/article/pii/S0959438800002348>.

- [210] L.A. Jones and M. Berris, « The psychophysics of temperature perception and thermal-interface design », *in: Proceedings 10th Symposium on Haptic Interfaces for Virtual Environment and Teleoperator Systems. HAPTICS 2002*, 2002, pp. 137–142, DOI: 10.1109/HAPTIC.2002.998951.
- [211] Lee Jones, John McClelland, Phonesavanh Thongsouksanoumane, and Audrey Girouard, « Ambient Notifications with Shape Changing Circuits in Peripheral Locations », *in: Proceedings of the 2017 ACM International Conference on Interactive Surfaces and Spaces, ISS '17*, Brighton, United Kingdom: Association for Computing Machinery, 2017, pp. 405–408, ISBN: 9781450346917, DOI: 10.1145/3132272.3132291.
- [212] T. Kajima and Y. Kawamura, « Development of a high-speed solenoid valve: investigation of solenoids », *in: IEEE Transactions on Industrial Electronics* 42.1 (1995), pp. 1–8, DOI: 10.1109/41.345838.
- [213] Alexander Kalus, Martin Kocur, Johannes Klein, Manuel Mayer, and Niels Henze, « PumpVR: Rendering the Weight of Objects and Avatars through Liquid Mass Transfer in Virtual Reality », *in: Proceedings of the 2023 CHI Conference on Human Factors in Computing Systems, CHI '23*, Hamburg, Germany: Association for Computing Machinery, 2023, ISBN: 9781450394215, DOI: 10.1145/3544548.3581172, URL: <https://doi.org/10.1145/3544548.3581172>.
- [214] Kenichi Kanatani and Prasanna Rangarajan, « Hyper least squares fitting of circles and ellipses », *in: Computational Statistics and Data Analysis* 55.6 (2011), pp. 2197–2208, DOI: <https://doi.org/10.1016/j.csda.2010.12.012>.
- [215] Kenichi Kanatani and Prasanna Rangarajan, « Hyper least squares fitting of circles and ellipses », *in: Computational Statistics & Data Analysis* 55.6 (2011), pp. 2197–2208, DOI: <https://doi.org/10.1016/j.csda.2010.12.012>.
- [216] Cindy Hsin-Liu (Cindy) Kao, Min-Wei Hung, Ximeng Zhang, Po-Chun Huang, and Chuang-Wen You, « Probing User Perceptions of On-Skin Notification Displays », *in: Proc. ACM Hum.-Comput. Interact.* 4.CSCW3 (Jan. 2021), DOI: 10.1145/3432943.
- [217] Hsin-Liu (Cindy) Kao, Miren Bamforth, David Kim, and Chris Schmandt, « Skinmorph: Texture-Tunable on-Skin Interface through Thin, Programmable Gel », *in: ISWC '18*, Singapore, Singapore: Association for Computing Machinery, 2018,

- pp. 196–203, ISBN: 9781450359672, DOI: 10.1145/3267242.3267262, URL: <https://doi.org/10.1145/3267242.3267262>.
- [218] Rithik Kapoor, Ashish Jaiswal, and Fillia Makedon, « Light-Weight Seated Posture Guidance System with Machine Learning and Computer Vision », *in: Proceedings of the 15th International Conference on PErvasive Technologies Related to Assis-tive Environments*, PETRA '22, Corfu, Greece: Association for Computing Machin-ery, 2022, pp. 595–600, ISBN: 9781450396318, DOI: 10.1145/3529190.3535341, URL: <https://doi.org/10.1145/3529190.3535341>.
- [219] Astrid M.L. Kappers and Wouter M. Bergmann Tiest, « Haptic perception », *in: WIREs Cognitive Science* 4.4 (2013), pp. 357–374, DOI: <https://doi.org/10.1002/wcs.1238>, eprint: <https://wires.onlinelibrary.wiley.com/doi/pdf/10.1002/wcs.1238>, URL: <https://wires.onlinelibrary.wiley.com/doi/abs/10.1002/wcs.1238>.
- [220] Pavel Karpashevich, Pedro Sanches, Rachael Garrett, Yoav Luft, Kelsey Cotton, Vasiliki Tsaknaki, and Kristina Höök, « Touching Our Breathing through Shape-Change: Monster, Organic Other, or Twisted Mirror », *in: ACM Trans. Comput.-Hum. Interact.* 29.3 (Feb. 2022), ISSN: 1073-0516, DOI: 10.1145/3490498.
- [221] Elio Keddisseh, Marcos Serrano, and Emmanuel Dubois, « KeyTch: Combining the Keyboard with a Touchscreen for Rapid Command Selection on Toolbars », *in: Proceedings of the 2021 CHI Conference on Human Factors in Computing Systems*, CHI '21, Yokohama, Japan: Association for Computing Machinery, 2021, ISBN: 9781450380966, DOI: 10.1145/3411764.3445288, URL: <https://doi.org/10.1145/3411764.3445288>.
- [222] Crane Keenan, *A Quick and Dirty Introduction to the Curvature of Surfaces*, (last retrieved December 05, 2023), 2007, URL: <http://wordpress.discretization.de/geometryprocessingandapplicationsws19/a-quick-and-dirty-introduction-to-the-curvature-of-surfaces/>.
- [223] Jonas Kellermeyer, Jan Torpus, Toni Kovacevic, Sophie Stephanie Kellner, and Cedric Julian Spindler, « To Touch or not to Touch? Differences in Affordance Resonating with Materialities. Hard and Soft Sensors embedded in an Artistic Research Setting », *in: Proceedings of the Seventeenth International Conference on Tangible, Embedded, and Embodied Interaction*, TEI '23, Warsaw, Poland: As-

- sociation for Computing Machinery, 2023, ISBN: 9781450399777, DOI: 10.1145/3569009.3572749, URL: <https://doi.org/10.1145/3569009.3572749>.
- [224] William M Kier, « The musculature of coleoid cephalopod arms and tentacles », *in: Frontiers in cell and developmental biology* 4 (2016), p. 10, DOI: 10.3389/fcell.2016.00010.
- [225] Ozgun Kilic Afsar, Ali Shtarbanov, Hila Mor, Ken Nakagaki, Jack Forman, Karen Modrei, Seung Hee Jeong, Klas Hjort, Kristina Höök, and Hiroshi Ishii, « OmniFiber: Integrated Fluidic Fiber Actuators for Weaving Movement Based Interactions into the ‘Fabric of Everyday Life’ », *in: The 34th Annual ACM Symposium on User Interface Software and Technology*, UIST ’21, Virtual Event, USA: Association for Computing Machinery, 2021, pp. 1010–1026, ISBN: 9781450386357, DOI: 10.1145/3472749.3474802, URL: <https://doi.org/10.1145/3472749.3474802>.
- [226] Hyunyoung Kim, Celine Coutrix, and Anne Roudaut, « Morphees+: Studying Everyday Reconfigurable Objects for the Design and Taxonomy of Reconfigurable UIs », *in: Proceedings of the 2018 CHI Conference on Human Factors in Computing Systems*, CHI ’18, Montreal QC, Canada: Association for Computing Machinery, 2018, pp. 1–14, ISBN: 9781450356206, DOI: 10.1145/3173574.3174193, URL: <https://doi.org/10.1145/3173574.3174193>.
- [227] Hyunyoung Kim, Aluna Everitt, Carlos Tejada, Mengyu Zhong, and Daniel Ashbrook, « MorpheesPlug: A Toolkit for Prototyping Shape-Changing Interfaces », *in: Proceedings of the 2021 CHI Conference on Human Factors in Computing Systems*, CHI ’21, Yokohama, Japan: Association for Computing Machinery, 2021, ISBN: 9781450380966, DOI: 10.1145/3411764.3445786, URL: <https://doi.org/10.1145/3411764.3445786>.
- [228] Jeeun Kim, Qingnan Zhou, Amanda Ghassaei, and Xiang ‘Anthony’ Chen, « OmniSoft: A Design Tool for Soft Objects by Example », *in: Proceedings of the Fifteenth International Conference on Tangible, Embedded, and Embodied Interaction*, TEI ’21, Salzburg, Austria: Association for Computing Machinery, 2021, ISBN: 9781450382137, DOI: 10.1145/3430524.3440634.
- [229] Jin Hee (Heather) Kim, Kunpeng Huang, Simone White, Melissa Conroy, and Cindy Hsin-Liu Kao, « KnitDermis: Fabricating Tactile On-Body Interfaces Through Machine Knitting », *in: Proceedings of the 2021 ACM Designing Interactive Systems Conference*, DIS ’21, Virtual Event, USA: Association for Computing Machin-

- ery, 2021, pp. 1183–1200, ISBN: 9781450384766, DOI: 10.1145/3461778.3462007, URL: <https://doi.org/10.1145/3461778.3462007>.
- [230] Seoktae Kim, Hyunjung Kim, Boram Lee, Tek-Jin Nam, and Woohun Lee, « Inflatable Mouse: Volume-Adjustable Mouse with Air-Pressure-Sensitive Input and Haptic Feedback », *in: Proceedings of the SIGCHI Conference on Human Factors in Computing Systems*, CHI '08, Florence, Italy: Association for Computing Machinery, 2008, pp. 211–224, ISBN: 9781605580111, DOI: 10.1145/1357054.1357090.
- [231] Roberta L Klatzky, Susan J Lederman, and Catherine Reed, « Haptic integration of object properties: texture, hardness, and planar contour. », *in: Journal of Experimental Psychology: Human Perception and Performance* 15.1 (1989), p. 45, DOI: 10.1037/0096-1523.15.1.45.
- [232] Umut Koçak, Karljohan Palmerius, Camilla Forsell, Anders Ynnerman, and Matthew Cooper, « Analysis of the JND of Stiffness in Three Modes of Comparison », *in: Proceedings of Haptic and Audio Interaction Design - 6th International Workshop, HAID 2011, Kusatsu, Japan, August 25-26*, vol. 6851, Berlin, Germany: Springer, Aug. 2011, pp. 22–31, ISBN: 978-3-642-22949-7, DOI: 10.1007/978-3-642-22950-3_3.
- [233] Sushil Koirala, Sangeeta Prakash, Azharul Karim, and Bhesh Bhandari, « Shape morphing of foods: Mechanism, strategies, and applications », *in: Trends in Food Science & Technology* 139 (2023), p. 104135, ISSN: 0924-2244, DOI: <https://doi.org/10.1016/j.tifs.2023.104135>, URL: <https://www.sciencedirect.com/science/article/pii/S0924224423002509>.
- [234] Ig Mo Koo, Kwangmok Jung, Ja Choon Koo, Jae-Do Nam, Young Kwan Lee, and Hyouk Ryeol Choi, « Development of Soft-Actuator-Based Wearable Tactile Display », *in: IEEE Transactions on Robotics* 24.3 (2008), pp. 549–558, DOI: 10.1109/TR0.2008.921561.
- [235] Martin Krzywinski and Naomi Altman, « Error bars: The meaning of error bars is often misinterpreted, as is the statistical significance of their overlap. », *in: Nature Methods* 10 (10 2013), pp. 921–922, ISSN: ISSN 1548-7105, DOI: 10.1038/nmeth.2659, URL: <https://doi.org/10.1038/nmeth.2659>.

- [236] Pin-Sung Ku, Kungpeng Huang, and Cindy Hsin-Liu Kao, « Patch-O: Deformable Woven Patches for On-Body Actuation », *in: Proceedings of the 2022 CHI Conference on Human Factors in Computing Systems*, CHI '22, New Orleans, LA, USA: Association for Computing Machinery, 2022, ISBN: 9781450391573, DOI: 10.1145/3491102.3517633, URL: <https://doi.org/10.1145/3491102.3517633>.
- [237] Caitlin Kuhlman, Diana Doherty, Malika Nurbekova, Goutham Deva, Zarni Phyo, Paul-Henry Schoenhagen, MaryAnn VanValkenburg, Elke Rundensteiner, and Lane Harrison, « Evaluating Preference Collection Methods for Interactive Ranking Analytics », *in: Proceedings of the 2019 CHI Conference on Human Factors in Computing Systems*, CHI '19, Glasgow, Scotland Uk: Association for Computing Machinery, 2019, pp. 1–11, ISBN: 9781450359702, DOI: 10.1145/3290605.3300742, URL: <https://doi.org/10.1145/3290605.3300742>.
- [238] Susan J Lederman, « Skin and touch », *in: Encyclopedia of human biology* 7 (1991), pp. 51–63.
- [239] Susan J Lederman and Roberta L Klatzky, « Hand movements: A window into haptic object recognition », *in: Cognitive psychology* 19.3 (1987), pp. 342–368, DOI: 10.1016/0010-0285(87)90008-9.
- [240] Susan J Lederman and Roberta L Klatzky, « Haptic perception: A tutorial », *in: Attention, Perception and Psychophysics* 71.7 (2009), pp. 1439–1459, DOI: 10.3758/APP.71.7.1439.
- [241] Jaeyeon Lee and Geehyuk Lee, « Designing a Non-Contact Wearable Tactile Display Using Airflows », *in: Proceedings of the 29th Annual Symposium on User Interface Software and Technology*, UIST '16, Tokyo, Japan: Association for Computing Machinery, 2016, pp. 183–194, ISBN: 9781450341899, DOI: 10.1145/2984511.2984583.
- [242] Jarrett G.W. Lee, Bongshin Lee, and Eun Kyoung Choe, « Decorative, Evocative, and Uncanny: Reactions on Ambient-to-Disruptive Health Notifications via Plant-Mimicking Shape-Changing Interfaces », *in: Proceedings of the 2023 CHI Conference on Human Factors in Computing Systems*, CHI '23, Hamburg, Germany: Association for Computing Machinery, 2023, ISBN: 9781450394215, DOI: 10.1145/3544548.3581486.

-
- [243] Jun-Young Lee, Jaemin Eom, Woo-Young Choi, and Kyu-Jin Cho, « Soft LEGO: Bottom-Up Design Platform for Soft Robotics », *in: 2018 IEEE/RSJ International Conference on Intelligent Robots and Systems (IROS)*, 2018, pp. 7513–7520, DOI: 10.1109/IROS.2018.8593546.
- [244] Daniel Leithinger, Sean Follmer, Alex Olwal, and Hiroshi Ishii, « Physical Telepresence: Shape Capture and Display for Embodied, Computer-Mediated Remote Collaboration », *in: Proceedings of the 27th Annual ACM Symposium on User Interface Software and Technology*, UIST '14, Honolulu, Hawaii, USA: Association for Computing Machinery, 2014, pp. 461–470, ISBN: 9781450330695, DOI: 10.1145/2642918.2647377, URL: <https://doi.org/10.1145/2642918.2647377>.
- [245] Daniel Leithinger and Hiroshi Ishii, « Relief: A Scalable Actuated Shape Display », *in: Proceedings of the Fourth International Conference on Tangible, Embedded, and Embodied Interaction*, TEI '10, Cambridge, Massachusetts, USA: Association for Computing Machinery, 2010, pp. 221–222, ISBN: 9781605588414, DOI: 10.1145/1709886.1709928, URL: <https://doi.org/10.1145/1709886.1709928>.
- [246] Daniel Leithinger, David Lakatos, Anthony DeVincenzi, Matthew Blackshaw, and Hiroshi Ishii, « Direct and Gestural Interaction with Relief: A 2.5D Shape Display », *in: Proceedings of the 24th Annual ACM Symposium on User Interface Software and Technology*, UIST '11, Santa Barbara, California, USA: Association for Computing Machinery, 2011, pp. 541–548, ISBN: 9781450307161, DOI: 10.1145/2047196.2047268.
- [247] H. Levitt, « Transformed Up-Down Methods in Psychoacoustics », *in: The Journal of the Acoustical Society of America* 49.2B (Aug. 2005), pp. 467–477, ISSN: 0001-4966, DOI: 10.1121/1.1912375, eprint: https://pubs.aip.org/asa/jasa/article-pdf/49/2B/467/12184369/467\1_online.pdf, URL: <https://doi.org/10.1121/1.1912375>.
- [248] Meng Li, Aniket Pal, Amirreza Aghakhani, Abdon Pena-Francesch, and Metin Sitti, « Soft actuators for real-world applications », *in: Nature Reviews Materials* 7.3 (2022), pp. 235–249, DOI: 10.1038/s41578-021-00389-7.
- [249] Riverbank Computing Limited, *PyQt5*, (last retrieved January 18, 2024), 2023, URL: <https://pypi.org/project/PyQt5/>.

- [250] Anan Lin, Meike Scheller, Feng Feng, Michael J Proulx, and Oussama Metatla, « Feeling Colours: Crossmodal Correspondences Between Tangible 3D Objects, Colours and Emotions », *in: Proceedings of the 2021 CHI Conference on Human Factors in Computing Systems*, CHI '21, <conf-loc>, <city>Yokohama</city>, <country>Japan</country>, </conf-loc>: Association for Computing Machinery, 2021, ISBN: 9781450380966, DOI: 10.1145/3411764.3445373, URL: <https://doi.org/10.1145/3411764.3445373>.
- [251] Angela Maria Lis, Katia M Black, Hayley Korn, and Margareta Nordin, « Association between sitting and occupational LBP », *in: European spine journal* 16.2 (2007), pp. 283–298, DOI: 10.1007/s00586-006-0143-7.
- [252] Andrea J Liu and Sidney R Nagel, « Jamming is not just cool any more », *in: Nature* 396.6706 (1998), pp. 21–22, DOI: 10.1038/23819.
- [253] W. Liu and C. R. Rahn, « Fiber-Reinforced Membrane Models of McKibben Actuators », *in: Journal of Applied Mechanics* 70.6 (Jan. 2004), pp. 853–859, ISSN: 0021-8936, DOI: 10.1115/1.1630812, eprint: https://asmedigitalcollection.asme.org/appliedmechanics/article-pdf/70/6/853/5470497/853_1.pdf, URL: <https://doi.org/10.1115/1.1630812>.
- [254] Yuhu Liu, Satoshi Nishikawa, Young ah Seong, Ryuma Niiyama, and Yasuo Kuniyoshi, « ThermoCaress: A Wearable Haptic Device with Illusory Moving Thermal Stimulation », *in: Proceedings of the 2021 CHI Conference on Human Factors in Computing Systems*, CHI '21, Yokohama, Japan: Association for Computing Machinery, 2021, ISBN: 9781450380966, DOI: 10.1145/3411764.3445777, URL: <https://doi.org/10.1145/3411764.3445777>.
- [255] Stefan Louw, Astrid ML Kappers, and Jan J Koenderink, « Haptic detection thresholds of Gaussian profiles over the whole range of spatial scales », *in: Experimental brain research* 132.3 (2000), pp. 369–374, DOI: 10.1007/s002210000350.
- [256] Qiuyu Lu, Jifei Ou, João Wilbert, André Haben, Haipeng Mi, and Hiroshi Ishii, « MilliMorph – Fluid-Driven Thin Film Shape-Change Materials for Interaction Design », *in: Proceedings of the 32nd Annual ACM Symposium on User Interface Software and Technology*, UIST '19, New Orleans, LA, USA: Association for Computing Machinery, 2019, pp. 663–672, ISBN: 9781450368162, DOI: 10.1145/3332165.3347956, URL: <https://doi.org/10.1145/3332165.3347956>.

- [257] Qiuyu Lu, Haiqing Xu, Yijie Guo, Joey Yu Wang, and Lining Yao, « Fluidic Computation Kit: Towards Electronic-Free Shape-Changing Interfaces », *in: Proceedings of the 2023 CHI Conference on Human Factors in Computing Systems*, CHI '23, Hamburg, Germany: Association for Computing Machinery, 2023, ISBN: 9781450394215, DOI: 10.1145/3544548.3580783, URL: <https://doi.org/10.1145/3544548.3580783>.
- [258] Tongqing Lu, Cheng Ma, and Tiejun Wang, « Mechanics of dielectric elastomer structures: A review », *in: Extreme Mechanics Letters* 38 (2020), p. 100752, ISSN: 2352-4316, DOI: <https://doi.org/10.1016/j.eml.2020.100752>, URL: <https://www.sciencedirect.com/science/article/pii/S2352431620300912>.
- [259] Danli Luo, Aditi Maheshwari, Andreea Danielescu, Jiaji Li, Yue Yang, Ye Tao, Lingyun Sun, Dinesh K Patel, Guanyun Wang, Shu Yang, Teng Zhang, and Lining Yao, « Autonomous self-burying seed carriers for aerial seeding », *in: Nature* 614.7948 (2023), pp. 463–470, DOI: 10.1038/s41586-022-05656-3.
- [260] Qingyun Lv, Min Wu, and Yong Shen, « Enhanced swelling ratio and water retention capacity for novel super-absorbent hydrogel », *in: Colloids and Surfaces A: Physicochemical and Engineering Aspects* 583 (2019), p. 123972, ISSN: 0927-7757, DOI: <https://doi.org/10.1016/j.colsurfa.2019.123972>, URL: <https://www.sciencedirect.com/science/article/pii/S0927775719309628>.
- [261] Kent Lyons, Thad Starner, Daniel Plaisted, James Fusia, Amanda Lyons, Aaron Drew, and E. W. Looney, « Twiddler Typing: One-Handed Chording Text Entry for Mobile Phones », *in: Proceedings of the SIGCHI Conference on Human Factors in Computing Systems*, CHI '04, Vienna, Austria: Association for Computing Machinery, 2004, pp. 671–678, ISBN: 1581137028, DOI: 10.1145/985692.985777, URL: <https://doi.org/10.1145/985692.985777>.
- [262] Robert Mangan and Michel Destrade, « Gent models for the inflation of spherical balloons », *in: International Journal of Non-Linear Mechanics* 68 (2015), Mechanics of Rubber - in Memory of Alan Gent, pp. 52–58, ISSN: 0020-7462, DOI: <https://doi.org/10.1016/j.ijnonlinmec.2014.05.016>, URL: <https://www.sciencedirect.com/science/article/pii/S0020746214001292>.
- [263] Sampada Marathe and S. Shyam Sundar, « What drives customization? control or identity? », *in: Proceedings of the SIGCHI Conference on Human Factors in Computing Systems*, CHI '11, <conf-loc>, <city>Vancouver</city>, <state>BC</state>,</p></div>
<div data-bbox="865 967 907 984" data-label="Page-Footer">263</div>

- <country>Canada</country>, </conf-loc>: Association for Computing Machinery, 2011, pp. 781–790, ISBN: 9781450302289, DOI: 10.1145/1978942.1979056.
- [264] Ramses V. Martinez, Carina R. Fish, Xin Chen, and George M. Whitesides, « Elastomeric Origami: Programmable Paper-Elastomer Composites as Pneumatic Actuators », *in: Advanced Functional Materials* 22.7 (2012), pp. 1376–1384, DOI: <https://doi.org/10.1002/adfm.201102978>, eprint: <https://onlinelibrary.wiley.com/doi/pdf/10.1002/adfm.201102978>, URL: <https://onlinelibrary.wiley.com/doi/abs/10.1002/adfm.201102978>.
- [265] Jonàs Martínez, Jérémie Dumas, and Sylvain Lefebvre, « Procedural Voronoi Foams for Additive Manufacturing », *in: ACM Trans. Graph.* 35.4 (July 2016), ISSN: 0730-0301, DOI: 10.1145/2897824.2925922.
- [266] Jose Francisco Martinez Castro, Alice Buso, Jun Wu, and Elvin Karana, « TEX(alive): A TOOLKIT TO EXPLORE TEMPORAL EXPRESSIONS IN SHAPE-CHANGING TEXTILE INTERFACES », *in: Proceedings of the 2022 ACM Designing Interactive Systems Conference, DIS '22*, <conf-loc>, <city>Virtual Event</city>, <country>Australia</country>, </conf-loc>: Association for Computing Machinery, 2022, pp. 1162–1176, ISBN: 9781450393584, DOI: 10.1145/3532106.3533515, URL: <https://doi.org/10.1145/3532106.3533515>.
- [267] Afra Mashhadi, Akhil Mathur, and Fahim Kawsar, « The Myth of Subtle Notifications », *in: Proceedings of the 2014 ACM International Joint Conference on Pervasive and Ubiquitous Computing: Adjunct Publication, UbiComp '14 Adjunct*, Seattle, Washington: Association for Computing Machinery, 2014, pp. 111–114, ISBN: 9781450330473, DOI: 10.1145/2638728.2638759.
- [268] Loreto Mateu and Francesc Moll, « Review of energy harvesting techniques and applications for microelectronics », *in: VLSI Circuits and Systems II*, ed. by Jose Fco. Lopez, Francisco V. Fernandez, Jose Maria Lopez-Villegas, and Jose M. de la Rosa, vol. 5837, International Society for Optics and Photonics, SPIE, 2005, pp. 359–373, DOI: 10.1117/12.613046, URL: <https://doi.org/10.1117/12.613046>.
- [269] Yasushi Matoba, Toshiki Sato, Nobuhiro Takahashi, and Hideki Koike, « Claytric-Surface: An Interactive Surface with Dynamic Softness Control Capability », *in: ACM SIGGRAPH 2012 Emerging Technologies, SIGGRAPH '12*, Los Angeles,

- California: Association for Computing Machinery, 2012, ISBN: 9781450316804, DOI: 10.1145/2343456.2343462, URL: <https://doi.org/10.1145/2343456.2343462>.
- [270] Joselle M. McCracken, Brian R. Donovan, and Timothy J. White, « Materials as Machines », *in: Advanced Materials* 32.20 (2020), p. 1906564, DOI: <https://doi.org/10.1002/adma.201906564>, eprint: <https://onlinelibrary.wiley.com/doi/pdf/10.1002/adma.201906564>, URL: <https://onlinelibrary.wiley.com/doi/abs/10.1002/adma.201906564>.
- [271] Francis McGlone, Ake B Vallbo, Hakan Olausson, Line Loken, and Johan Wessberg, « Discriminative touch and emotional touch. », *in: Canadian Journal of Experimental Psychology/Revue canadienne de psychologie expérimentale* 61.3 (2007), p. 173, DOI: 10.1037/cjep2007019.
- [272] Francis McGlone, Johan Wessberg, and Håkan Olausson, « Discriminative and Affective Touch: Sensing and Feeling », *in: Neuron* 82.4 (2014), pp. 737–755, ISSN: 0896-6273, DOI: <https://doi.org/10.1016/j.neuron.2014.05.001>, URL: <https://www.sciencedirect.com/science/article/pii/S0896627314003870>.
- [273] David Mellis, Sean Follmer, Björn Hartmann, Leah Buechley, and Mark D. Gross, « FAB at CHI: digital fabrication tools, design, and community », *in: CHI '13 Extended Abstracts on Human Factors in Computing Systems*, CHI EA '13, Paris, France: Association for Computing Machinery, 2013, pp. 3307–3310, ISBN: 9781450319522, DOI: 10.1145/2468356.2479673, URL: <https://doi.org/10.1145/2468356.2479673>.
- [274] Moritz Alexander Messerschmidt, Sachith Muthukumarana, Nur Al-Huda Hamdan, Adrian Wagner, Haimo Zhang, Jan Borchers, and Suranga Chandima Nanayakkara, « ANISMA: A Prototyping Toolkit to Explore Haptic Skin Deformation Applications Using Shape-Memory Alloys », *in: ACM Trans. Comput.-Hum. Interact.* 29.3 (Jan. 2022), ISSN: 1073-0516, DOI: 10.1145/3490497.
- [275] Oussama Metatla, Emanuela Maggioni, Clare Cullen, and Marianna Obrist, « "Like Popcorn": Crossmodal Correspondences Between Scents, 3D Shapes and Emotions in Children », *in: Proceedings of the 2019 CHI Conference on Human Factors in Computing Systems*, CHI '19, Glasgow, Scotland Uk: Association for Computing Machinery, 2019, pp. 1–13, ISBN: 9781450359702, DOI: 10.1145/3290605.3300689, URL: <https://doi.org/10.1145/3290605.3300689>.

- [276] Viktor Miruchna, Robert Walter, David Lindlbauer, Maren Lehmann, Regine von Klitzing, and Jörg Müller, « GelTouch: Localized Tactile Feedback Through Thin, Programmable Gel », in: *Proceedings of the 28th Annual ACM Symposium on User Interface Software and Technology*, UIST '15, Charlotte, NC, USA: Association for Computing Machinery, 2015, pp. 3–10, ISBN: 9781450337793, DOI: 10.1145/2807442.2807487, URL: <https://doi.org/10.1145/2807442.2807487>.
- [277] T. Mitsuda, S. Kuge, M. Wakabayashi, and S. Kawamura, « Wearable haptic display by the use of a Particle Mechanical Constraint », in: *Proceedings 10th Symposium on Haptic Interfaces for Virtual Environment and Teleoperator Systems. HAPTICS 2002*, 2002, pp. 153–158, DOI: 10.1109/HAPTIC.2002.998953.
- [278] AW Mix and AJ Giacomini, « Dimensionless Durometry », in: *Polymer-Plastics Technology and Engineering* 50.3 (2011), pp. 288–296, DOI: 10.1080/03602559.2010.531867, eprint: <https://doi.org/10.1080/03602559.2010.531867>, URL: <https://doi.org/10.1080/03602559.2010.531867>.
- [279] Motoki Miyoshi, Parinya Punpongsanon, Daisuke Iwai, and Kosuke Sato, « Soft-Print: Investigating Haptic Softness Perception of 3D Printed Soft Object in FDM 3D Printers », in: *NIP and Digital Fabrication Conference*, 1, Society for Imaging Science and Technology, Springfield, Virginia: Society for Imaging Science and Technology, 2021, pp. 78–85, DOI: <https://doi.org/10.2352/J.ImagingSci.Technol.2021.65.4.040406>.
- [280] Jaronie Mohd Jani, Martin Leary, Aleksandar Subic, and Mark A. Gibson, « A review of shape memory alloy research, applications and opportunities », in: *Materials and Design (1980-2015)* 56 (2014), pp. 1078–1113, ISSN: 0261-3069, DOI: <https://doi.org/10.1016/j.matdes.2013.11.084>, URL: <https://www.sciencedirect.com/science/article/pii/S0261306913011345>.
- [281] Gregory Mone, « The Future is Flexible Displays », in: *Commun. ACM* 56.6 (June 2013), pp. 16–17, ISSN: 0001-0782, DOI: 10.1145/2461256.2461263, URL: <https://doi.org/10.1145/2461256.2461263>.
- [282] Hedieh Moradi and César Torres, « Siloseam: A Morphogenetic Workflow for the Design and Fabrication of Inflatable Silicone Bladders », in: *Proceedings of the 2020 ACM Designing Interactive Systems Conference*, DIS '20, Eindhoven, Netherlands: Association for Computing Machinery, 2020, pp. 1995–2006, ISBN: 9781450369749,

- DOI: 10.1145/3357236.3395473, URL: <https://doi.org/10.1145/3357236.3395473>.
- [283] Christopher Moraes, Yu Sun, and Craig A Simmons, « Solving the shrinkage-induced PDMS alignment registration issue in multilayer soft lithography », *in: Journal of Micromechanics and Microengineering* 19.6 (May 2009), p. 065015, DOI: 10.1088/0960-1317/19/6/065015, URL: <https://dx.doi.org/10.1088/0960-1317/19/6/065015>.
- [284] Stephen A. Morin, Sen Wai Kwok, Joshua Lessing, Jason Ting, Robert F. Shepherd, Adam A. Stokes, and George M. Whitesides, « Elastomeric Tiles for the Fabrication of Inflatable Structures », *in: Advanced Functional Materials* 24.35 (2014), pp. 5541–5549, DOI: <https://doi.org/10.1002/adfm.201401339>, eprint: <https://onlinelibrary.wiley.com/doi/pdf/10.1002/adfm.201401339>, URL: <https://onlinelibrary.wiley.com/doi/abs/10.1002/adfm.201401339>.
- [285] Bobak Mosadegh, Chuan-Hsien Kuo, Yi-Chung Tung, Yu-suke Torisawa, Tommaso Bersano-Begey, Hossein Tavana, and Shuichi Takayama, « Integrated elastomeric components for autonomous regulation of sequential and oscillatory flow switching in microfluidic devices », *in: Nature physics* 6.6 (2010), pp. 433–437, DOI: 10.1038/nphys1637.
- [286] Bobak Mosadegh, Panagiotis Polygerinos, Christoph Keplinger, Sophia Wennstedt, Robert F. Shepherd, Unmukt Gupta, Jongmin Shim, Katia Bertoldi, Conor J. Walsh, and George M. Whitesides, « Pneumatic Networks for Soft Robotics that Actuate Rapidly », *in: Advanced Functional Materials* 24.15 (2014), pp. 2163–2170, DOI: <https://doi.org/10.1002/adfm.201303288>, eprint: <https://onlinelibrary.wiley.com/doi/pdf/10.1002/adfm.201303288>, URL: <https://onlinelibrary.wiley.com/doi/abs/10.1002/adfm.201303288>.
- [287] Alessandro Moscatelli, Maura Mezzetti, and Francesco Lacquaniti, « Modeling psychophysical data at the population-level: The generalized linear mixed model », *in: Journal of Vision* 12.11 (Oct. 2012), pp. 26–26, ISSN: 1534-7362, DOI: 10.1167/12.11.26, eprint: https://arvojournals.org/arvo/content/_public/journal/jov/933489/i1534-7362-12-11-26.pdf, URL: <https://doi.org/10.1167/12.11.26>.

- [288] Vivian Genaro Motti and Kelly Caine, « Human Factors Considerations in the Design of Wearable Devices », *in: Proceedings of the Human Factors and Ergonomics Society Annual Meeting 58.1* (2014), pp. 1820–1824, DOI: 10.1177/1541931214581381, eprint: <https://doi.org/10.1177/1541931214581381>, URL: <https://doi.org/10.1177/1541931214581381>.
- [289] Stefanie Mueller, « 3D Printing for Human-Computer Interaction », *in: Interactions 24.5* (Aug. 2017), pp. 76–79, ISSN: 1072-5520, DOI: 10.1145/3125399, URL: <https://doi.org/10.1145/3125399>.
- [290] Thomas Muender, Anke Verena Reinschluessel, Daniela Salzmann, Thomas Lück, Andrea Schenk, Dirk Weyhe, Tanja Döring, and Rainer Malaka, « Evaluating Soft Organ-Shaped Tangibles for Medical Virtual Reality », *in: Extended Abstracts of the 2022 CHI Conference on Human Factors in Computing Systems, CHI EA '22*, New Orleans, LA, USA: Association for Computing Machinery, 2022, ISBN: 9781450391566, DOI: 10.1145/3491101.3519715.
- [291] Sachith Muthukumarana, Don Samitha Elvitigala, Juan Pablo Forero Cortes, Denys J.C. Matthies, and Suranga Nanayakkara, « Touch Me Gently: Recreating the Perception of Touch Using a Shape-Memory Alloy Matrix », *in: Proceedings of the 2020 CHI Conference on Human Factors in Computing Systems, CHI '20*, Honolulu, HI, USA: Association for Computing Machinery, 2020, pp. 1–12, ISBN: 9781450367080, DOI: 10.1145/3313831.3376491, URL: <https://doi.org/10.1145/3313831.3376491>.
- [292] Sachith Muthukumarana, Moritz Alexander Messerschmidt, Denys J.C. Matthies, Jürgen Steimle, Philipp M. Scholl, and Suranga Nanayakkara, « ClothTiles: A Prototyping Platform to Fabricate Customized Actuators on Clothing Using 3D Printing and Shape-Memory Alloys », *in: Proceedings of the 2021 CHI Conference on Human Factors in Computing Systems, CHI '21*, Yokohama, Japan: Association for Computing Machinery, 2021, ISBN: 9781450380966, DOI: 10.1145/3411764.3445613.
- [293] Pranathi Mylavarapu, Adil Yalcin, Xan Gregg, and Niklas Elmqvist, « Ranked-List Visualization: A Graphical Perception Study », *in: Proceedings of the 2019 CHI Conference on Human Factors in Computing Systems, CHI '19*, Glasgow, Scotland Uk: Association for Computing Machinery, 2019, pp. 1–12, ISBN: 9781450359702,

- DOI: 10.1145/3290605.3300422, URL: <https://doi.org/10.1145/3290605.3300422>.
- [294] Stylianos Mystakidis, « Metaverse », in: *Encyclopedia 2.1* (2022), pp. 486–497, ISSN: 2673-8392, DOI: 10.3390/encyclopedia2010031, URL: <https://www.mdpi.com/2673-8392/2/1/31>.
- [295] Sara Nabil, Jan Kučera, Nikoletta Karastathi, David S. Kirk, and Peter Wright, « Seamless Seams: Crafting Techniques for Embedding Fabrics with Interactive Actuation », in: *Proceedings of the 2019 on Designing Interactive Systems Conference, DIS '19*, San Diego, CA, USA: Association for Computing Machinery, 2019, pp. 987–999, ISBN: 9781450358507, DOI: 10.1145/3322276.3322369, URL: <https://doi.org/10.1145/3322276.3322369>.
- [296] Sara Nabil, Thomas Plötz, and David S. Kirk, « Interactive Architecture: Exploring and Unwrapping the Potentials of Organic User Interfaces », in: *Proceedings of the Eleventh International Conference on Tangible, Embedded, and Embodied Interaction, TEI '17*, Yokohama, Japan: Association for Computing Machinery, 2017, pp. 89–100, ISBN: 9781450346764, DOI: 10.1145/3024969.3024981, URL: <https://doi.org/10.1145/3024969.3024981>.
- [297] Ken Nakagaki, Daniel Fitzgerald, Zhiyao (John) Ma, Luke Vink, Daniel Levine, and Hiroshi Ishii, « InFORCE: Bi-Directional ‘Force’ Shape Display for Haptic Interaction », in: *Proceedings of the Thirteenth International Conference on Tangible, Embedded, and Embodied Interaction, TEI '19*, Tempe, Arizona, USA: Association for Computing Machinery, 2019, pp. 615–623, ISBN: 9781450361965, DOI: 10.1145/3294109.3295621, URL: <https://doi.org/10.1145/3294109.3295621>.
- [298] Ken Nakagaki, Luke Vink, Jared Counts, Daniel Windham, Daniel Leithinger, Sean Follmer, and Hiroshi Ishii, « Materiable: Rendering Dynamic Material Properties in Response to Direct Physical Touch with Shape Changing Interfaces », in: *Proceedings of the 2016 CHI Conference on Human Factors in Computing Systems*, New York, NY, USA: Association for Computing Machinery, 2016, pp. 2764–2772, ISBN: 9781450333627, DOI: 10.1145/2858036.2858104.
- [299] Satoshi Nakamaru, Ryosuke Nakayama, Ryuma Niiyama, and Yasuaki Kakehi, « FoamSense: Design of Three Dimensional Soft Sensors with Porous Materials », in: *Proceedings of the 30th Annual ACM Symposium on User Interface Software and Technology, UIST '17*, Québec City, QC, Canada: Association for Computing

- Machinery, 2017, pp. 437–447, ISBN: 9781450349819, DOI: 10.1145/3126594.3126666, URL: <https://doi.org/10.1145/3126594.3126666>.
- [300] Ryosuke Nakayama, Ryo Suzuki, Satoshi Nakamaru, Ryuma Niiyama, Yoshihiro Kawahara, and Yasuaki Kakehi, « MorphIO: Entirely Soft Sensing and Actuation Modules for Programming Shape Changes through Tangible Interaction », *in: Proceedings of the 2019 on Designing Interactive Systems Conference, DIS '19*, San Diego, CA, USA: Association for Computing Machinery, 2019, pp. 975–986, ISBN: 9781450358507, DOI: 10.1145/3322276.3322337, URL: <https://doi.org/10.1145/3322276.3322337>.
- [301] Nils Napp, Brandon Araki, Michael T. Tolley, Radhika Nagpal, and Robert J. Wood, « Simple passive valves for addressable pneumatic actuation », *in: 2014 IEEE International Conference on Robotics and Automation (ICRA)*, 2014, pp. 1440–1445, DOI: 10.1109/ICRA.2014.6907041.
- [302] R. Neelamegam and V. Shankar, « Experimental study of the instability of laminar flow in a tube with deformable walls », *in: Physics of Fluids 27.2* (Feb. 2015), p. 024102, ISSN: 1070-6631, DOI: 10.1063/1.4907246, eprint: https://pubs.aip.org/aip/pof/article-pdf/doi/10.1063/1.4907246/14843752/024102_1_online.pdf, URL: <https://doi.org/10.1063/1.4907246>.
- [303] Kristin Neidlinger, Khiet P. Truong, Caty Telfair, Loe Feijs, Edwin Dertien, and Vanessa Evers, « AWElectric: That Gave Me Goosebumps, Did You Feel It Too? », *in: Proceedings of the Eleventh International Conference on Tangible, Embedded, and Embodied Interaction, TEI '17*, Yokohama, Japan: Association for Computing Machinery, 2017, pp. 315–324, ISBN: 9781450346764, DOI: 10.1145/3024969.3025004, URL: <https://doi.org/10.1145/3024969.3025004>.
- [304] Anina Net, Bruce Bateman, and StMichal Starosta, *Robotic Dress*, Last retrieved January 24, 2024, URL: <https://wardrobetrendsfashion.com/robotic-dress-powered-360fash-tech-kits/>.
- [305] Adelina-Gabriela Niculescu, Cristina Chircov, Alexandra Cătălina Bîrcă, and Alexandru Mihai Grumezescu, « Fabrication and Applications of Microfluidic Devices: A Review », *in: International Journal of Molecular Sciences 22.4* (2021), ISSN: 1422-0067, DOI: 10.3390/ijms22042011, URL: <https://www.mdpi.com/1422-0067/22/4/2011>.

-
- [306] Ryuma Niiyama, Xu Sun, Cynthia Sung, Byoungkwon An, Daniela Rus, and Sangbae Kim, « Pouch motors: Printable soft actuators integrated with computational design », *in: Soft Robotics 2.2* (2015), pp. 59–70, DOI: 10.1089/soro.2014.0023.
- [307] Ryuma Niiyama, Lining Yao, and Hiroshi Ishii, « Weight and Volume Changing Device with Liquid Metal Transfer », *in: Proceedings of the 8th International Conference on Tangible, Embedded and Embodied Interaction, TEI '14*, Munich, Germany: Association for Computing Machinery, 2014, pp. 49–52, ISBN: 9781450326353, DOI: 10.1145/2540930.2540953, URL: <https://doi.org/10.1145/2540930.2540953>.
- [308] Ailish O'Halloran, Fergal O'Malley, and Peter McHugh, « A review on dielectric elastomer actuators, technology, applications, and challenges », *in: Journal of Applied Physics* 104.7 (2008), p. 071101, DOI: 10.1063/1.2981642, eprint: <https://aip.scitation.org/doi/pdf/10.1063/1.2981642>, URL: <https://aip.scitation.org/doi/abs/10.1063/1.2981642>.
- [309] Dan Odell and Peter Johnson, « Evaluation of flat, angled, and vertical computer mice and their effects on wrist posture, pointing performance, and preference », *in: Work* 52.2 (2015), pp. 245–253, DOI: 10.3233/WOR-152167.
- [310] William Odom, James Pierce, Erik Stolterman, and Eli Blevis, « Understanding why we preserve some things and discard others in the context of interaction design », *in: Proceedings of the SIGCHI Conference on Human Factors in Computing Systems, CHI '09*, Boston, MA, USA: Association for Computing Machinery, 2009, pp. 1053–1062, ISBN: 9781605582467, DOI: 10.1145/1518701.1518862, URL: <https://doi.org/10.1145/1518701.1518862>.
- [311] Shogo Okamoto, Hikaru Nagano, and Yoji Yamada, « Psychophysical Dimensions of Tactile Perception of Textures », *in: IEEE Transactions on Haptics* 6.1 (2013), pp. 81–93, DOI: 10.1109/TOH.2012.32.
- [312] A.G. Olabi and A. Grunwald, « Design and application of magneto-rheological fluid », *in: Materials & Design* 28.10 (2007), pp. 2658–2664, ISSN: 0261-3069, DOI: <https://doi.org/10.1016/j.matdes.2006.10.009>, URL: <https://www.sciencedirect.com/science/article/pii/S0261306906002962>.
- [313] Alex Olwal, Jon Moeller, Greg Priest-Dorman, Thad Starner, and Ben Carroll, « I/O Braid: Scalable Touch-Sensitive Lighted Cords Using Spiraling, Repeating Sensing Textiles and Fiber Optics », *in: Proceedings of the 31st Annual ACM Sym-*

- posium on User Interface Software and Technology*, UIST '18, Berlin, Germany: Association for Computing Machinery, 2018, pp. 485–497, ISBN: 9781450359481, DOI: 10.1145/3242587.3242638, URL: <https://doi.org/10.1145/3242587.3242638>.
- [314] Kas Oosterhuis and Nimish Bioria, « Interactions with Proactive Architectural Spaces: The Muscle Projects », *in: Commun. ACM* 51.6 (June 2008), pp. 70–78, ISSN: 0001-0782, DOI: 10.1145/1349026.1349041, URL: <https://doi.org/10.1145/1349026.1349041>.
- [315] OpenCV, *OpenCV*, Last retrieved January 4, 2024, URL: <https://docs.opencv.org/4.x/>.
- [316] OpenSCAD, *OpenSCAD*, (last retrieved January 22, 2024), URL: <https://openscad.org/>.
- [317] C Opreșan, V Cârlescu, A Barnea, Gh Prisacaru, D N Olaru, and Gh Plesu, « Experimental determination of the Young's modulus for the fingers with application in prehension systems for small cylindrical objects », *in: IOP Conference Series: Materials Science and Engineering* 147 (Aug. 2016), p. 012058, DOI: 10.1088/1757-899x/147/1/012058, URL: <https://doi.org/10.1088/1757-899x/147/1/012058>.
- [318] Jifei Ou, Mélina Skouras, Nikolaos Vlavianos, Felix Heibeck, Chin-Yi Cheng, Jan-nik Peters, and Hiroshi Ishii, « AeroMorph - Heat-Sealing Inflatable Shape-Change Materials for Interaction Design », *in: Proceedings of the 29th Annual Symposium on User Interface Software and Technology*, UIST '16, Tokyo, Japan: Association for Computing Machinery, 2016, pp. 121–132, ISBN: 9781450341899, DOI: 10.1145/2984511.2984520, URL: <https://doi.org/10.1145/2984511.2984520>.
- [319] Jifei Ou, Lining Yao, Daniel Tauber, Jürgen Steimle, Ryuma Niiyama, and Hiroshi Ishii, « JamSheets: Thin Interfaces with Tunable Stiffness Enabled by Layer Jamming », *in: Proceedings of the 8th International Conference on Tangible, Embedded and Embodied Interaction*, TEI '14, Munich, Germany: Association for Computing Machinery, 2014, pp. 65–72, ISBN: 9781450326353, DOI: 10.1145/2540930.2540971, URL: <https://doi.org/10.1145/2540930.2540971>.
- [320] Stack Overflow, *Stack Overflow*, Last retrieved January 22, 2024, URL: <https://stackoverflow.com/>.

-
- [321] Neville Owen, Geneviève N Healy, Charles E Matthews, and David W Dunstan, « Too much sitting: the population-health science of sedentary behavior », *in: Exercise and sport sciences reviews* 38.3 (2010), p. 105, DOI: 10.1097/JES.0b013e3181e373a2.
- [322] Kadri Bugra Ozutemiz, James Wissman, Osman Burak Ozdoganlar, and Carmel Majidi, « EGaIn–Metal Interfacing for Liquid Metal Circuitry and Microelectronics Integration », *in: Advanced Materials Interfaces* 5.10 (2018), p. 1701596, DOI: 10.1002/admi.201701596.
- [323] Claudio Pacchierotti, Stephen Sinclair, Massimiliano Solazzi, Antonio Frisoli, Vincent Hayward, and Domenico Prattichizzo, « Wearable Haptic Systems for the Fingertip and the Hand: Taxonomy, Review, and Perspectives », *in: IEEE Transactions on Haptics* 10.4 (2017), pp. 580–600, DOI: 10.1109/TOH.2017.2689006.
- [324] Yue Pan and Erik Stolterman, « What if HCI Becomes a Fashion Driven Discipline? », *in: Proceedings of the 33rd Annual ACM Conference on Human Factors in Computing Systems, CHI '15*, Seoul, Republic of Korea: Association for Computing Machinery, 2015, pp. 2565–2568, ISBN: 9781450331456, DOI: 10.1145/2702123.2702544, URL: <https://doi.org/10.1145/2702123.2702544>.
- [325] A. Pandey, D. E. Moulton, D. Vella, and D. P. Holmes, « Dynamics of snapping beams and jumping poppers », *in: Europhysics Letters* 105.2 (Feb. 2014), p. 24001, DOI: 10.1209/0295-5075/105/24001, URL: <https://dx.doi.org/10.1209/0295-5075/105/24001>.
- [326] Joohee Park, Young-Woo Park, and Tek-Jin Nam, « Wrigglo: Shape-Changing Peripheral for Interpersonal Mobile Communication », *in: Proceedings of the SIGCHI Conference on Human Factors in Computing Systems, CHI '14*, Toronto, Ontario, Canada: Association for Computing Machinery, 2014, pp. 3973–3976, ISBN: 9781450324731, DOI: 10.1145/2556288.2557166, URL: <https://doi.org/10.1145/2556288.2557166>.
- [327] Amanda Parkes and Hiroshi Ishii, « Bosu: A Physical Programmable Design Tool for Transformability with Soft Mechanics », *in: Proceedings of the 8th ACM Conference on Designing Interactive Systems, DIS '10*, Aarhus, Denmark: Association for Computing Machinery, 2010, pp. 189–198, ISBN: 9781450301039, DOI: 10.1145/1858171.1858205.

- [328] Achille Pasqualotto, Megan Ng, Zheng Yee Tan, and Ryo Kitada, « Tactile perception of pleasantness in relation to perceived softness », *in: Scientific reports* 10.1 (2020), p. 11189, DOI: 10.1038/s41598-020-68034-x.
- [329] Jerome Pasquero, Scott J. Stobbe, and Noel Stonehouse, « A Haptic Wristwatch for Eyes-Free Interactions », *in: Proceedings of the SIGCHI Conference on Human Factors in Computing Systems*, CHI '11, Vancouver, BC, Canada: Association for Computing Machinery, 2011, pp. 3257–3266, ISBN: 9781450302289, DOI: 10.1145/1978942.1979425.
- [330] Anupam Pathak, Diann Brei, and Jonathan Luntz, « Experimental characterization of the convective heat transfer from shape memory alloy SMA wire to various ambient environments », *in: International Conference on Adaptive Structures and Technologies (ICAST 2008)*, 2008, pp. 6–9, URL: https://library.eawag-empa.ch/icast_proceedings_2008_open_access/ICAST2008039.pdf.
- [331] Mariola Pawlaczyk, Monika Lelonkiewicz, and Michał Wieczorowski, « Review papers Age-dependent biomechanical properties of the skin », *in: Advances in Dermatology and Allergology/Postępy Dermatologii i Alergologii* 30.5 (2013), pp. 302–306, ISSN: 1642-395X, DOI: 10.5114/pdia.2013.38359, URL: <http://dx.doi.org/10.5114/pdia.2013.38359>.
- [332] Jennifer Pearson, Simon Robinson, and Matt Jones, « It's About Time: Smartwatches as Public Displays », *in: Proceedings of the 33rd Annual ACM Conference on Human Factors in Computing Systems*, CHI '15, Seoul, Republic of Korea: Association for Computing Machinery, 2015, pp. 1257–1266, ISBN: 9781450331456, DOI: 10.1145/2702123.2702247.
- [333] Esben W. Pedersen, Sriram Subramanian, and Kasper Hornbæk, « Is My Phone Alive? A Large-Scale Study of Shape Change in Handheld Devices Using Videos », *in: Proceedings of the SIGCHI Conference on Human Factors in Computing Systems*, CHI '14, Toronto, Ontario, Canada: Association for Computing Machinery, 2014, pp. 2579–2588, ISBN: 9781450324731, DOI: 10.1145/2556288.2557018.
- [334] Qibing Pei, Marcus Rosenthal, Scott Stanford, Harsha Prahlad, and Ron Pelrine, « Multiple-degrees-of-freedom electroelastomer roll actuators », *in: Smart Materials and Structures* 13.5 (Sept. 2004), N86, DOI: 10.1088/0964-1726/13/5/N03, URL: <https://dx.doi.org/10.1088/0964-1726/13/5/N03>.

- [335] Marianne Graves Petersen, Majken Kirkegaard Rasmussen, and Johan Trettvik, « Affordances of Shape-Changing Interfaces: An Information Perspective on Transformability and Movement », *in: Proceedings of the 2020 ACM Designing Interactive Systems Conference*, DIS '20, Eindhoven, Netherlands: Association for Computing Machinery, 2020, pp. 1959–1971, ISBN: 9781450369749, DOI: 10.1145/3357236.3395521, URL: <https://doi.org/10.1145/3357236.3395521>.
- [336] P Peyla, « Buckling of a compressed elastic membrane: a simple model », *in: The European Physical Journal B-Condensed Matter and Complex Systems* 48 (2005), pp. 379–383, DOI: 10.1140/epjb/e2005-00415-9, URL: <https://doi.org/10.1140/epjb/e2005-00415-9>.
- [337] Matteo Pezulla, Gabriel P. Smith, Paola Nardinocchi, and Douglas P. Holmes, « Geometry and mechanics of thin growing bilayers », *in: Soft Matter* 12 (19 2016), pp. 4435–4442, DOI: 10.1039/C6SM00246C, URL: <http://dx.doi.org/10.1039/C6SM00246C>.
- [338] Raspberry Pi, *Raspberry Pi*, Last retrieved January 22, 2024, URL: <https://www.raspberrypi.org/>.
- [339] V.C. Pinto, Tiago Ramos, Sofia Alves, J. Xavier, Paulo Tavares, P.M.G.P. Moreira, and Rui Miranda Guedes, « Comparative Failure Analysis of PLA, PLA/GNP and PLA/CNT-COOH Biodegradable Nanocomposites thin Films », *in: Procedia Engineering* 114 (2015), ICSI 2015 The 1st International Conference on Structural Integrity Funchal, Madeira, Portugal 1st to 4th September, 2015, pp. 635–642, ISSN: 1877-7058, DOI: <https://doi.org/10.1016/j.proeng.2015.08.004>, URL: <https://www.sciencedirect.com/science/article/pii/S1877705815016434>.
- [340] Michal Piovarči, David I. W. Levin, Jason Rebello, Desai Chen, Roman Ďurikovič, Hanspeter Pfister, Wojciech Matusik, and Piotr Didyk, « An Interaction-Aware, Perceptual Model for Non-Linear Elastic Objects », *in: ACM Trans. Graph.* 35.4 (July 2016), ISSN: 0730-0301, DOI: 10.1145/2897824.2925885, URL: <https://doi.org/10.1145/2897824.2925885>.
- [341] Ben Piper, Carlo Ratti, and Hiroshi Ishii, « Illuminating Clay: A 3-D Tangible Interface for Landscape Analysis », *in: Proceedings of the SIGCHI Conference on Human Factors in Computing Systems*, CHI '02, Minneapolis, Minnesota, USA: Association for Computing Machinery, 2002, pp. 355–362, ISBN: 1581134533, DOI: 10.1145/503376.503439, URL: <https://doi.org/10.1145/503376.503439>.

- [342] Henning Pohl, Peter Brandes, Hung Ngo Quang, and Michael Rohs, « Squeeze-back: Pneumatic Compression for Notifications », *in: Proceedings of the 2017 CHI Conference on Human Factors in Computing Systems*, CHI '17, Denver, Colorado, USA: Association for Computing Machinery, 2017, pp. 5318–5330, ISBN: 9781450346559, DOI: 10.1145/3025453.3025526.
- [343] Henning Pohl, Justyna Medrek, and Michael Rohs, « ScatterWatch: Subtle Notifications via Indirect Illumination Scattered in the Skin », *in: Proceedings of the 18th International Conference on Human-Computer Interaction with Mobile Devices and Services*, MobileHCI '16, Florence, Italy: Association for Computing Machinery, 2016, pp. 7–16, ISBN: 9781450344081, DOI: 10.1145/2935334.2935351.
- [344] Henning Pohl, Andreea Muresan, and Kasper Hornbæk, « Charting Subtle Interaction in the HCI Literature », *in: Proceedings of the 2019 CHI Conference on Human Factors in Computing Systems*, CHI '19, Glasgow, Scotland Uk: Association for Computing Machinery, 2019, pp. 1–15, ISBN: 9781450359702, DOI: 10.1145/3290605.3300648.
- [345] Panagiotis Polygerinos, Zheng Wang, Kevin C. Galloway, Robert J. Wood, and Conor J. Walsh, « Soft robotic glove for combined assistance and at-home rehabilitation », *in: Robotics and Autonomous Systems* 73 (2015), Wearable Robotics, pp. 135–143, ISSN: 0921-8890, DOI: <https://doi.org/10.1016/j.robot.2014.08.014>, URL: <https://www.sciencedirect.com/science/article/pii/S0921889014001729>.
- [346] Sylvia C Pont, Astrid ML Kappers, and Jan J Koenderink, « Haptic curvature discrimination at several regions of the hand », *in: Perception and Psychophysics* 59.8 (1997), pp. 1225–1240, DOI: <https://doi.org/10.3758/BF03214210>.
- [347] Sylvia C Pont, Astrid ML Kappers, and Jan J Koenderink, « Similar mechanisms underlie curvature comparison by static and dynamic touch », *in: Perception & Psychophysics* 61.5 (1999), pp. 874–894, DOI: <https://doi.org/10.3758/BF03206903>.
- [348] Sylvia C Pont, Astrid ML Kappers, and Jan J Koenderink, « Similar mechanisms underlie curvature comparison by static and dynamic touch », *in: Perception and Psychophysics* 61.5 (1999), pp. 874–894, DOI: <https://doi.org/10.3758/BF03206903>.

-
- [349] Ivan Poupyrev, Tatsushi Nashida, Shigeaki Maruyama, Jun Rekimoto, and Yasufumi Yamaji, « Lumen: Interactive Visual and Shape Display for Calm Computing », *in: ACM SIGGRAPH 2004 Emerging Technologies*, SIGGRAPH '04, Los Angeles, California: Association for Computing Machinery, 2004, p. 17, ISBN: 1581138962, DOI: 10.1145/1186155.1186173, URL: <https://doi.org/10.1145/1186155.1186173>.
- [350] Andrew N Pressley, *Elementary differential geometry*, 2nd ed., Springer London, 2010, pp. 165–213, DOI: 10.1007/978-1-84882-891-9.
- [351] William R. Provancher, Katherine J. Kuchenbecker, Günter Niemeyer, and Mark R. Cutkosky, « Perception of Curvature and Object Motion via Contact Location Feedback », *in: Robotics Research. The Eleventh International Symposium*, ed. by Paolo Dario and Raja Chatila, Berlin, Heidelberg: Springer Berlin Heidelberg, 2005, pp. 456–465, ISBN: 978-3-540-31508-7, DOI: 10.1007/11008941_49, URL: https://doi.org/10.1007/11008941_49.
- [352] William Ronald Provancher, *On tactile sensing and display*, Stanford, California, USA: Stanford University, 2003, URL: http://www-cdr.stanford.edu/DML/publications/provancher_thesis.pdf.
- [353] Laura Pruszko, Céline Coutrix, Yann Laurillau, Benoît Piranda, and Julien Bourgeois, « Molecular HCI: Structuring the Cross-disciplinary Space of Modular Shape-changing User Interfaces », *in: Proc. ACM Hum.-Comput. Interact. 5.EICS* (May 2021), DOI: 10.1145/3461733, URL: <https://doi.org/10.1145/3461733>.
- [354] Junhong Pu, Yuan Meng, Zhixin Xie, Zihang Peng, Jianghan Wu, Ye Shi, Roshan Plamthottam, Wei Yang, and Qibing Pei, « A unimorph nanocomposite dielectric elastomer for large out-of-plane actuation », *in: Science Advances* 8.9 (2022), eabm6200, DOI: 10.1126/sciadv.abm6200, eprint: <https://www.science.org/doi/pdf/10.1126/sciadv.abm6200>, URL: <https://www.science.org/doi/abs/10.1126/sciadv.abm6200>.
- [355] Wei Pu, Fanan Wei, Ligang Yao, and Shuangxi Xie, « A review of humidity-driven actuator: toward high response speed and practical applications », *in: Journal of Materials Science* 57.26 (2022), pp. 12202–12235, DOI: <https://doi.org/10.1007/s10853-022-07344-z>.

- [356] Purnendu, Eric Acome, Christoph Keplinger, Mark D Gross, Carson Bruns, and Daniel Leithinger, « Soft Electrohydraulic Actuators for Origami Inspired Shape-Changing Interfaces », *in: Extended Abstracts of the 2021 CHI Conference on Human Factors in Computing Systems*, CHI EA '21, Yokohama, Japan: Association for Computing Machinery, 2021, ISBN: 9781450380959, DOI: 10.1145/3411763.3451590, URL: <https://doi.org/10.1145/3411763.3451590>.
- [357] Isabel Qamar, Rainer Groh, David Holman, and Anne Roudaut, « Bridging the gap between material science and human-computer interaction », *in: Interactions* 26.5 (Aug. 2019), pp. 64–69, ISSN: 1072-5520, DOI: 10.1145/3344943.
- [358] Isabel P. S. Qamar, Rainer Groh, David Holman, and Anne Roudaut, « HCI Meets Material Science: A Literature Review of Morphing Materials for the Design of Shape-Changing Interfaces », *in: Proceedings of the 2018 CHI Conference on Human Factors in Computing Systems*, CHI '18, Montreal QC, Canada: Association for Computing Machinery, 2018, pp. 1–23, ISBN: 9781450356206, DOI: 10.1145/3173574.3173948, URL: <https://doi.org/10.1145/3173574.3173948>.
- [359] Fang Qin, Huai-Yu Cheng, Rachel Sneeringer, Maria Vlachostergiou, Sampada Acharya, Haolin Liu, Carmel Majidi, Mohammad Islam, and Lining Yao, « Exo-Form: Shape Memory and Self-Fusing Semi-Rigid Wearables », *in: Extended Abstracts of the 2021 CHI Conference on Human Factors in Computing Systems*, CHI EA '21, Yokohama, Japan: Association for Computing Machinery, 2021, ISBN: 9781450380959, DOI: 10.1145/3411763.3451818, URL: <https://doi.org/10.1145/3411763.3451818>.
- [360] Hayes Solos Raffle, Amanda J. Parkes, and Hiroshi Ishii, « Topobo: A Constructive Assembly System with Kinetic Memory », *in: Proceedings of the SIGCHI Conference on Human Factors in Computing Systems*, CHI '04, Vienna, Austria: Association for Computing Machinery, 2004, pp. 647–654, ISBN: 1581137028, DOI: 10.1145/985692.985774, URL: <https://doi.org/10.1145/985692.985774>.
- [361] Michael Raitor, Julie M. Walker, Allison M. Okamura, and Heather Culbertson, « WRAP: Wearable, restricted-aperture pneumatics for haptic guidance », *in: 2017 IEEE International Conference on Robotics and Automation (ICRA)*, 2017, pp. 427–432, DOI: 10.1109/ICRA.2017.7989055.
- [362] Karim Rashid, *I want to change the world*, Thames & Hudson, 2001, ISBN: 0-500-28316-8.

-
- [363] Majken K. Rasmussen, Esben W. Pedersen, Marianne G. Petersen, and Kasper Hornbæk, « Shape-Changing Interfaces: A Review of the Design Space and Open Research Questions », *in: Proceedings of the SIGCHI Conference on Human Factors in Computing Systems*, CHI '12, Austin, Texas, USA: Association for Computing Machinery, 2012, pp. 735–744, ISBN: 9781450310154, DOI: 10.1145/2207676.2207781, URL: <https://doi.org/10.1145/2207676.2207781>.
- [364] Majken K. Rasmussen, Giovanni M. Troiano, Marianne G. Petersen, Jakob G. Simonsen, and Kasper Hornbæk, « Sketching Shape-Changing Interfaces: Exploring Vocabulary, Metaphors Use, and Affordances », *in: Proceedings of the 2016 CHI Conference on Human Factors in Computing Systems*, CHI '16, San Jose, California, USA: Association for Computing Machinery, 2016, pp. 2740–2751, ISBN: 9781450333627, DOI: 10.1145/2858036.2858183, URL: <https://doi.org/10.1145/2858036.2858183>.
- [365] Wim M. van Rees, Etienne Vouga, and L. Mahadevan, « Growth patterns for shape-shifting elastic bilayers », *in: Proceedings of the National Academy of Sciences* 114.44 (2017), pp. 11597–11602, DOI: 10.1073/pnas.1709025114, eprint: <https://www.pnas.org/doi/pdf/10.1073/pnas.1709025114>, URL: <https://www.pnas.org/doi/abs/10.1073/pnas.1709025114>.
- [366] Christian Rendl, David Kim, Sean Fanello, Patrick Parzer, Christoph Rhemann, Jonathan Taylor, Martin Zirkl, Gregor Scheipl, Thomas Rothländer, Michael Haller, and Shahram Izadi, « FlexSense: A Transparent Self-Sensing Deformable Surface », *in: Proceedings of the 27th Annual ACM Symposium on User Interface Software and Technology*, UIST '14, Honolulu, Hawaii, USA: Association for Computing Machinery, 2014, pp. 129–138, ISBN: 9781450330695, DOI: 10.1145/2642918.2647405, URL: <https://doi.org/10.1145/2642918.2647405>.
- [367] Meticulous Research, *Wearable Devices Market by Product Type (Smartwatch, Earwear, Eyewear, and others), End-Use Industry (Consumer Electronics, Healthcare, Enterprise and Industrial, Media and Entertainment), Connectivity Medium, and Region - Global Forecast to 2025*, [meticulousresearch.com/product/wearable-devices-market-5050](https://www.meticulousresearch.com/product/wearable-devices-market-5050), Last accessed Dec 2020, 2019.
- [368] FormLabs, *Formlabs materials*, Last retrieved July 25, 2023, 2023, URL: <https://formlabs.com/materials-hub/>.

- [369] Maximilian Rettinger and Gerhard Rigoll, « Touching the future of training: investigating tangible interaction in virtual reality », *in: Frontiers in Virtual Reality* 4 (2023), DOI: 10.3389/frvir.2023.1187883.
- [370] Helge Ritter and Robert Haschke, *Humanoid Robotics and Neuroscience: Science, Engineering and Society*, ed. by Cheng G PhD, Boca Raton (FL): CRC Press/Taylor and Francis, 2015, chap. Hands, Dexterity, and the Brain, URL: <https://www.ncbi.nlm.nih.gov/books/NBK299038/>.
- [371] Michael L. Rivera, Jack Forman, Scott E. Hudson, and Lining Yao, « Hydrogel-Textile Composites: Actuators for Shape-Changing Interfaces », *in: Extended Abstracts of the 2020 CHI Conference on Human Factors in Computing Systems*, CHI EA '20, Honolulu, HI, USA: Association for Computing Machinery, 2020, pp. 1–9, ISBN: 9781450368193, DOI: 10.1145/3334480.3382788, URL: <https://doi.org/10.1145/3334480.3382788>.
- [372] Matthew A. Robertson, Masato Murakami, Wyatt Felt, and Jamie Paik, « A Compact Modular Soft Surface With Reconfigurable Shape and Stiffness », *in: IEEE/ASME Transactions on Mechatronics* 24.1 (2019), pp. 16–24, DOI: 10.1109/TMECH.2018.2878621.
- [373] Benoît Roman, *How to make a baromorph*, Last retrieved February 29, 2024, URL: <https://vimeo.com/420256797>.
- [374] Beat Rossmly, Sonja Rümelin, and Alexander Wiethoff, « StringTouch - From String Instruments towards New Interface Morphologies », *in: Proceedings of the Fifteenth International Conference on Tangible, Embedded, and Embodied Interaction*, TEI '21, Salzburg, Austria: Association for Computing Machinery, 2021, ISBN: 9781450382137, DOI: 10.1145/3430524.3440628.
- [375] Philipp Rothemund, Alar Ainla, Lee Belding, Daniel J. Preston, Sarah Kurihara, Zhigang Suo, and George M. Whitesides, « A soft, bistable valve for autonomous control of soft actuators », *in: Science Robotics* 3.16 (2018), eaar7986, DOI: 10.1126/scirobotics.aar7986, eprint: <https://www.science.org/doi/pdf/10.1126/scirobotics.aar7986>, URL: <https://www.science.org/doi/abs/10.1126/scirobotics.aar7986>.

-
- [376] Anne Roudaut, Abhijit Karnik, Markus Löchtefeld, and Sriram Subramanian, « Morphees: Toward High "Shape Resolution" in Self-Actuated Flexible Mobile Devices », *in: Proceedings of the SIGCHI Conference on Human Factors in Computing Systems*, CHI '13, Paris, France: Association for Computing Machinery, 2013, pp. 593–602, ISBN: 9781450318990, DOI: 10.1145/2470654.2470738, URL: <https://doi.org/10.1145/2470654.2470738>.
- [377] Daniela Rus and Michael T Tolley, « Design, fabrication and control of soft robots », *in: Nature* 521.7553 (2015), pp. 467–475, DOI: <https://doi.org/10.1038/nature14543>.
- [378] S. Rusinkiewicz, « Estimating curvatures and their derivatives on triangle meshes », *in: Proceedings. 2nd International Symposium on 3D Data Processing, Visualization and Transmission, 2004. 3DPVT 2004*. 2004, pp. 486–493, DOI: 10.1109/TDPVT.2004.1335277.
- [379] Sage, ed., *Thematic analysis: A practical guide*, 2022.
- [380] Vanessa Sanchez, Conor J. Walsh, and Robert J. Wood, « Textile Technology for Soft Robotic and Autonomous Garments », *in: Advanced Functional Materials* 31.6 (2021), p. 2008278, DOI: <https://doi.org/10.1002/adfm.202008278>, eprint: <https://onlinelibrary.wiley.com/doi/pdf/10.1002/adfm.202008278>, URL: <https://onlinelibrary.wiley.com/doi/abs/10.1002/adfm.202008278>.
- [381] Harpreet Sareen, Udayan Umaphathi, Patrick Shin, Yasuaki Kakehi, Jifei Ou, Hiroshi Ishii, and Pattie Maes, « Printflatables: Printing Human-Scale, Functional and Dynamic Inflatable Objects », *in: Proceedings of the 2017 CHI Conference on Human Factors in Computing Systems*, CHI '17, Denver, Colorado, USA: Association for Computing Machinery, 2017, pp. 3669–3680, ISBN: 9781450346559, DOI: 10.1145/3025453.3025898, URL: <https://doi.org/10.1145/3025453.3025898>.
- [382] Munehiko Sato, Ivan Poupyrev, and Chris Harrison, « Touché: Enhancing Touch Interaction on Humans, Screens, Liquids, and Everyday Objects », *in: Proceedings of the SIGCHI Conference on Human Factors in Computing Systems*, CHI '12, Austin, Texas, USA: Association for Computing Machinery, 2012, pp. 483–492, ISBN: 9781450310154, DOI: 10.1145/2207676.2207743, URL: <https://doi.org/10.1145/2207676.2207743>.

- [383] Valkyrie Savage, Carlos Tejada, Mengyu Zhong, Raf Ramakers, Daniel Ashbrook, and Hyunyoung Kim, « AirLogic: Embedding Pneumatic Computation and I/O in 3D Models to Fabricate Electronics-Free Interactive Objects », *in: Proceedings of the 35th Annual ACM Symposium on User Interface Software and Technology*, UIST '22, Bend, OR, USA: Association for Computing Machinery, 2022, ISBN: 9781450393201, DOI: 10.1145/3526113.3545642, URL: <https://doi.org/10.1145/3526113.3545642>.
- [384] René Schäfer, Tobias Wagner, Ulyana Lavnikovich, and Jan Borchers, « Enhancing Notification Awareness for Online Presenters via a Wrist-Worn Device », *in: Extended Abstracts of the 2023 CHI Conference on Human Factors in Computing Systems*, CHI EA '23, Hamburg, Germany: Association for Computing Machinery, 2023, ISBN: 9781450394222, DOI: 10.1145/3544549.3585855.
- [385] Bryan E Schubert and Dario Floreano, « Variable stiffness material based on rigid low-melting-point-alloy microstructures embedded in soft poly (dimethylsiloxane)(PDMS) », *in: Rsc Advances* 3.46 (2013), pp. 24671–24679, DOI: <https://doi.org/10.1039/C3RA44412K>.
- [386] Enzo Pasquale Scilingo, Matteo Bianchi, Giorgio Grioli, and Antonio Bicchi, « Rendering Softness: Integration of Kinesthetic and Cutaneous Information in a Haptic Device », *in: IEEE Transactions on Haptics* 3.2 (2010), pp. 109–118, DOI: 10.1109/TOH.2010.2.
- [387] Enzo Pasquale Scilingo, Matteo Bianchi, Giorgio Grioli, and Antonio Bicchi, « Rendering Softness: Integration of Kinesthetic and Cutaneous Information in a Haptic Device », *in: IEEE Transactions on Haptics* 3.2 (2010), pp. 109–118, DOI: 10.1109/TOH.2010.2.
- [388] Jamar, *Semmes-Weinstein monofilament sensory tests*, Last retrieved July 29, 2023, 2023, URL: <https://www.performancehealth.com/jamar-monofilaments>.
- [389] Marcos Serrano, Jolee Finch, Pourang Irani, Andrés Lucero, and Anne Roudaut, « Mold-It: Understanding How Physical Shapes Affect Interaction with Handheld Freeform Devices », *in: Proceedings of the 2022 CHI Conference on Human Factors in Computing Systems*, CHI '22, New Orleans, LA, USA: Association for Computing Machinery, 2022, ISBN: 9781450391573, DOI: 10.1145/3491102.3502022.

- [390] Teddy Seyed, James Devine, Joe Finney, Michal Moskal, Peli de Halleux, Steve Hodges, Thomas Ball, and Asta Roseway, « Rethinking the Runway: Using Avant-Garde Fashion To Design a System for Wearables », *in: Proceedings of the 2021 CHI Conference on Human Factors in Computing Systems*, CHI '21, <conf-loc>, <city>Yokohama</city>, <country>Japan</country>, </conf-loc>: Association for Computing Machinery, 2021, ISBN: 9781450380966, DOI: 10.1145/3411764.3445643, URL: <https://doi.org/10.1145/3411764.3445643>.
- [391] Teddy Seyed, Xing-Dong Yang, and Daniel Vogel, « Doppio: A Reconfigurable Dual-Face Smartwatch for Tangible Interaction », *in: Proceedings of the 2016 CHI Conference on Human Factors in Computing Systems*, CHI '16, San Jose, California, USA: Association for Computing Machinery, 2016, pp. 4675–4686, ISBN: 9781450333627, DOI: 10.1145/2858036.2858256.
- [392] Zuyu Shen, Xi Wan, Yucheng Jin, Ge Gao, Qianying Wang, and Wei Liu, « Seat-Plus: A Smart Health Chair Supporting Active Sitting Posture Correction », *in: International Conference on Human-Computer Interaction*, Springer, 2021, pp. 531–547, DOI: 10.1007/978-3-030-78224-5_37.
- [393] Robert F. Shepherd, Filip Ilievski, Wonjae Choi, Stephen A. Morin, Adam A. Stokes, Aaron D. Mazzeo, Xin Chen, Michael Wang, and George M. Whitesides, « Multigait soft robot », *in: Proceedings of the National Academy of Sciences* 108.51 (2011), pp. 20400–20403, ISSN: 0027-8424, DOI: 10.1073/pnas.1116564108, eprint: <https://www.pnas.org/content/108/51/20400.full.pdf>, URL: <https://www.pnas.org/content/108/51/20400>.
- [394] Robert F. Shepherd, Adam A. Stokes, Jacob Freake, Jabulani Barber, Phillip W. Snyder, Aaron D. Mazzeo, Ludovico Cademartiri, Stephen A. Morin, and George M. Whitesides, « Using Explosions to Power a Soft Robot », *in: Angewandte Chemie International Edition* 52.10 (2013), pp. 2892–2896, DOI: <https://doi.org/10.1002/anie.201209540>, eprint: <https://onlinelibrary.wiley.com/doi/pdf/10.1002/anie.201209540>, URL: <https://onlinelibrary.wiley.com/doi/abs/10.1002/anie.201209540>.
- [395] Hu Shi, Kun Tan, Boyang Zhang, and Wenqiao Liu, « Review on Research Progress of Hydraulic Powered Soft Actuators », *in: Energies* 15.23 (2022), ISSN: 1996-1073, DOI: 10.3390/en15239048, URL: <https://www.mdpi.com/1996-1073/15/23/9048>.

- [396] Xiang Shi, Yong Zuo, Peng Zhai, Jiahao Shen, Yangyiwei Yang, Zhen Gao, Meng Liao, Jingxia Wu, Jiawei Wang, Xiaojie Xu, Qi Tong, Bo Zhang, Bingjie Wang, Xuemei Sun, Lihua Zhang, Qibing Pei, Dayong Jin, Peining Chen, and Huisheng Peng, « Large-area display textiles integrated with functional systems », *in: Nature* 591.7849 (2021), pp. 240–245, DOI: 10.1038/s41586-021-03295-8.
- [397] Kannathu Shibin and Asir Samuel, « The Discrimination of Two-point Touch Sense for the Upper Extremity in Indian Adults », *in: International Journal of Health and Rehabilitation Sciences* 2 (Jan. 2013), pp. 38–43.
- [398] SHIMADZU, *SHIMADZU Autograph AGS-X Precision Universal Tester*, (last retrieved February 3, 2023), 2022, URL: <https://www.shimadzu.eu/ags-x-series-0>.
- [399] Tokihiko Shimura, Shun Sato, Peter Zalar, and Naoji Matsuhisa, « Engineering the Comfort-of-Wear for Next Generation Wearables », *in: Advanced Electronic Materials* 9.9 (2023), p. 2200512, DOI: <https://doi.org/10.1002/aelm.202200512>, eprint: <https://onlinelibrary.wiley.com/doi/pdf/10.1002/aelm.202200512>, URL: <https://onlinelibrary.wiley.com/doi/abs/10.1002/aelm.202200512>.
- [400] Joon-Gi Shin, Eiji Onchi, Maria Jose Reyes, Junbong Song, Uichin Lee, Seung-Hee Lee, and Daniel Saakes, « Slow Robots for Unobtrusive Posture Correction », *in: Proceedings of the 2019 CHI Conference on Human Factors in Computing Systems*, CHI '19, Glasgow, Scotland Uk: Association for Computing Machinery, 2019, pp. 1–10, ISBN: 9781450359702, DOI: 10.1145/3290605.3300843, URL: <https://doi.org/10.1145/3290605.3300843>.
- [401] Ali Shtarbanov, « FlowIO Development Platform – the Pneumatic “Raspberry Pi” for Soft Robotics », *in: Extended Abstracts of the 2021 CHI Conference on Human Factors in Computing Systems*, CHI EA '21, Yokohama, Japan: Association for Computing Machinery, 2021, ISBN: 9781450380959, DOI: 10.1145/3411763.3451513, URL: <https://doi.org/10.1145/3411763.3451513>.
- [402] Emmanuel Siéfert, Etienne Reyssat, José Bico, and Benoît Roman, « Bio-inspired pneumatic shape-morphing elastomers », *in: Nature materials* 18.1 (2019), pp. 24–28, DOI: 10.1038/s41563-018-0219-x, URL: <https://blog.espci.fr/benoitroman/en/baromorph/>.

-
- [403] Smooth-on, *Sil Poxxy Glue*, Last retrieved July 25, 2023, 2023, URL: <https://www.smooth-on.com/products/sil-poxy/>.
- [404] Adalberto L. Simeone, Eduardo Velloso, and Hans Gellersen, « Substitutional Reality: Using the Physical Environment to Design Virtual Reality Experiences », in: *Proceedings of the 33rd Annual ACM Conference on Human Factors in Computing Systems*, CHI '15, Seoul, Republic of Korea: Association for Computing Machinery, 2015, pp. 3307–3316, ISBN: 9781450331456, DOI: 10.1145/2702123.2702389, URL: <https://doi.org/10.1145/2702123.2702389>.
- [405] Timothy M. Simon, Ross T. Smith, and Bruce H. Thomas, « Wearable Jamming Mitten for Virtual Environment Haptics », in: *Proceedings of the 2014 ACM International Symposium on Wearable Computers*, ISWC '14, Seattle, Washington: Association for Computing Machinery, 2014, pp. 67–70, ISBN: 9781450329699, DOI: 10.1145/2634317.2634342, URL: <https://doi.org/10.1145/2634317.2634342>.
- [406] Timothy M. Simon, Bruce H. Thomas, and Ross T. Smith, « Controlling Stiffness with Jamming for Wearable Haptics », in: *Proceedings of the 2015 ACM International Symposium on Wearable Computers*, ISWC '15, Osaka, Japan: Association for Computing Machinery, 2015, pp. 45–46, ISBN: 9781450335782, DOI: 10.1145/2802083.2808401, URL: <https://doi.org/10.1145/2802083.2808401>.
- [407] Melanie F. Simons, Alice C. Haynes, Yan Gao, Yihua Zhu, and Jonathan Rossiter, « In Contact: Pinching, Squeezing and Twisting for Mediated Social Touch », in: *Extended Abstracts of the 2020 CHI Conference on Human Factors in Computing Systems*, CHI EA '20, Honolulu, HI, USA: Association for Computing Machinery, 2020, pp. 1–9, ISBN: 9781450368193, DOI: 10.1145/3334480.3382798.
- [408] Gurpreet Singh and Arnab Chanda, « Mechanical properties of whole-body soft human tissues: a review », in: *Biomedical Materials* 16.6 (Oct. 2021), p. 062004, DOI: 10.1088/1748-605x/ac2b7a, URL: <https://doi.org/10.1088/1748-605x/ac2b7a>.
- [409] Mélina Skouras, Bernhard Thomaszewski, Bernd Bickel, and Markus Gross, « Computational Design of Rubber Balloons », in: *Computer Graphics Forum* 31.2pt4 (2012), pp. 835–844, DOI: <https://doi.org/10.1111/j.1467-8659.2012.03064.x>, eprint: <https://onlinelibrary.wiley.com/doi/pdf/10.1111/j.1467-8659.2012.03064.x>, URL: <https://onlinelibrary.wiley.com/doi/abs/10.1111/j.1467-8659.2012.03064.x>.

- [410] Mel Slater, Pankaj Khanna, Jesper Mortensen, and Insu Yu, « Visual Realism Enhances Realistic Response in an Immersive Virtual Environment », *in: IEEE Computer Graphics and Applications* 29.3 (2009), pp. 76–84, DOI: 10.1109/MCG.2009.55.
- [411] Harshal Arun Sonar, Jian-Lin Huang, and Jamie Paik, « Soft Touch using Soft Pneumatic Actuator–Skin as a Wearable Haptic Feedback Device », *in: Advanced Intelligent Systems* 3.3 (2021), p. 2000168, DOI: <https://doi.org/10.1002/aisy.202000168>, eprint: <https://onlinelibrary.wiley.com/doi/pdf/10.1002/aisy.202000168>, URL: <https://onlinelibrary.wiley.com/doi/abs/10.1002/aisy.202000168>.
- [412] Harshal Arun Sonar, Sagar Dattatray Joshi, Matthew Aaron Robertson, and Jamie Paik, « Interactive soft pneumatic actuator skin », *in: IEEE/RSJ International Conference on Intelligent Robots and Systems*, POST_TALK, 2017, URL: <https://infoscience.epfl.ch/record/231732>.
- [413] Harshal Arun Sonar, Matthew Aaron Robertson, Sagar Dattatray Joshi, Tigmanshu Bhatnagar, and Jamie Paik, *Soft portable wearable pneumatic interactive suit*, US Patent 11,458,067, Oct. 2022, URL: <https://patents.google.com/patent/US11458067B2/en>.
- [414] Hamid Souri, Hritwick Banerjee, Ardian Jusufi, Norbert Radacsi, Adam A. Stokes, Inkyu Park, Metin Sitti, and Morteza Amjadi, « Wearable and Stretchable Strain Sensors: Materials, Sensing Mechanisms, and Applications », *in: Advanced Intelligent Systems* 2.8 (2020), p. 2000039, DOI: <https://doi.org/10.1002/aisy.202000039>, eprint: <https://onlinelibrary.wiley.com/doi/pdf/10.1002/aisy.202000039>, URL: <https://onlinelibrary.wiley.com/doi/abs/10.1002/aisy.202000039>.
- [415] M. A. Srinivasan and R. H. LaMotte, « Tactual discrimination of softness », *in: Journal of Neurophysiology* 73.1 (1995), PMID: 7714593, pp. 88–101, DOI: 10.1152/jn.1995.73.1.88, eprint: <https://doi.org/10.1152/jn.1995.73.1.88>, URL: <https://doi.org/10.1152/jn.1995.73.1.88>.
- [416] Andrew A. Stanley, James C. Gwilliam, and Allison M. Okamura, « Haptic jamming: A deformable geometry, variable stiffness tactile display using pneumatics and particle jamming », *in: 2013 World Haptics Conference (WHC)*, Daejeon, Ko-

-
- rea (South): Institute of Electrical and Electronics Engineers, 2013, pp. 25–30, DOI: 10.1109/WHC.2013.6548379.
- [417] Andrew A. Stanley, James C. Gwilliam, and Allison M. Okamura, « Haptic jamming: A deformable geometry, variable stiffness tactile display using pneumatics and particle jamming », *in: 2013 World Haptics Conference (WHC)*, Daejeon, Korea (South): Institute of Electrical and Electronics Engineers, 2013, pp. 25–30, DOI: 10.1109/WHC.2013.6548379.
- [418] Andrew A. Stanley and Allison M. Okamura, « Controllable Surface Haptics via Particle Jamming and Pneumatics », *in: IEEE Transactions on Haptics* 8.1 (2015), pp. 20–30, DOI: 10.1109/TOH.2015.2391093.
- [419] Andrew A. Stanley and Allison M. Okamura, « Deformable Model-Based Methods for Shape Control of a Haptic Jamming Surface », *in: IEEE Transactions on Visualization and Computer Graphics* 23.2 (2017), pp. 1029–1041, DOI: 10.1109/TVCG.2016.2525788.
- [420] Cameron Steer, Teodora Dinca, Crescent Jicol, Michael J Proulx, and Jason Alexander, « Feel the Force, See the Force: Exploring Visual-tactile Associations of Deformable Surfaces with Colours and Shapes », *in: Proceedings of the 2023 CHI Conference on Human Factors in Computing Systems, CHI '23*, <conf-loc>, <city>Hamburg</city>, <country>Germany</country>, </conf-loc>: Association for Computing Machinery, 2023, ISBN: 9781450394215, DOI: 10.1145/3544548.3580830, URL: <https://doi.org/10.1145/3544548.3580830>.
- [421] Jürgen Steimle, Andreas Jordt, and Pattie Maes, « Flexpad: Highly Flexible Bending Interactions for Projected Handheld Displays », *in: Proceedings of the SIGCHI Conference on Human Factors in Computing Systems, CHI '13*, Paris, France: Association for Computing Machinery, 2013, pp. 237–246, ISBN: 9781450318990, DOI: 10.1145/2470654.2470688, URL: <https://doi.org/10.1145/2470654.2470688>.
- [422] Stanley Smith Stevens, « Matching functions between loudness and ten other continua1 », *in: Perception and Psychophysics* 1.1 (1966), pp. 5–8, DOI: <https://doi.org/10.3758/BF03207813>.
- [423] Andrew Stevenson, Christopher Perez, and Roel Vertegaal, « An Inflatable Hemispherical Multi-Touch Display », *in: Proceedings of the Fifth International Conference on Tangible, Embedded, and Embodied Interaction, TEI '11*, Funchal, Portugal: Association for Computing Machinery, 2010, pp. 289–292, ISBN: 9781450304788,

- DOI: 10.1145/1935701.1935766, URL: <https://doi.org/10.1145/1935701.1935766>.
- [424] Paul Strohmeier, Juan Pablo Carrascal, Bernard Cheng, Margaret Meban, and Roel Vertegaal, « An Evaluation of Shape Changes for Conveying Emotions », *in: Proceedings of the 2016 CHI Conference on Human Factors in Computing Systems*, CHI '16, San Jose, California, USA: Association for Computing Machinery, 2016, pp. 3781–3792, ISBN: 9781450333627, DOI: 10.1145/2858036.2858537.
- [425] Yuta Sugiura, Masahiko Inami, and Takeo Igarashi, « A Thin Stretchable Interface for Tangential Force Measurement », *in: Proceedings of the 25th Annual ACM Symposium on User Interface Software and Technology*, UIST '12, Cambridge, Massachusetts, USA: Association for Computing Machinery, 2012, pp. 529–536, ISBN: 9781450315807, DOI: 10.1145/2380116.2380182, URL: <https://doi.org/10.1145/2380116.2380182>.
- [426] Saiganesh Swaminathan, Michael Rivera, Runchang Kang, Zheng Luo, Kadri Bugra Ozutemiz, and Scott E. Hudson, « Input, Output and Construction Methods for Custom Fabrication of Room-Scale Deployable Pneumatic Structures », *in: Proc. ACM Interact. Mob. Wearable Ubiquitous Technol.* 3.2 (June 2019), DOI: 10.1145/3328933, URL: <https://doi.org/10.1145/3328933>.
- [427] Matteo Taffetani, Xin Jiang, Douglas P. Holmes, and Dominic Vella, « Static bistability of spherical caps », *in: Proceedings of the Royal Society A: Mathematical, Physical and Engineering Sciences* 474.2213 (2018), Figure from <https://www.youtube.com/watch?p.20170910>, DOI: 10.1098/rspa.2017.0910, eprint: <https://royalsocietypublishing.org/doi/pdf/10.1098/rspa.2017.0910>, URL: <https://royalsocietypublishing.org/doi/abs/10.1098/rspa.2017.0910>.
- [428] Yasaman Tahouni, Isabel P. S. Qamar, and Stefanie Mueller, « NURBSforms: A Modular Shape-Changing Interface for Prototyping Curved Surfaces », *in: Proceedings of the Fourteenth International Conference on Tangible, Embedded, and Embodied Interaction*, TEI '20, Sydney NSW, Australia: Association for Computing Machinery, 2020, pp. 403–409, ISBN: 9781450361071, DOI: 10.1145/3374920.3374927, URL: <https://doi.org/10.1145/3374920.3374927>.
- [429] Nobuhiro Takahashi, Shinichi Furuya, and Hideki Koike, « Soft Exoskeleton Glove with Human Anatomical Architecture: Production of Dexterous Finger Movements

- and Skillful Piano Performance », *in: IEEE Transactions on Haptics* 13.4 (2020), pp. 679–690, DOI: 10.1109/TOH.2020.2993445.
- [430] Naoki Takizawa, Hiroaki Yano, Hiroo Iwata, Yukio Oshiro, and Nobuhiro Ohkouchi, « Encountered-Type Haptic Interface for Representation of Shape and Rigidity of 3D Virtual Objects », *in: IEEE Transactions on Haptics* 10.4 (2017), pp. 500–510, DOI: 10.1109/TOH.2017.2740934.
- [431] Diane Tam, Karon E. MacLean, Joanna McGrenere, and Katherine J. Kuchenbecker, « The Design and Field Observation of a Haptic Notification System for Timing Awareness during Oral Presentations », *in: Proceedings of the SIGCHI Conference on Human Factors in Computing Systems*, CHI '13, Paris, France: Association for Computing Machinery, 2013, pp. 1689–1698, ISBN: 9781450318990, DOI: 10.1145/2470654.2466223.
- [432] Haodan Tan, John Tiab, Selma Šabanović, and Kasper Hornbæk, « Happy Moves, Sad Grooves: Using Theories of Biological Motion and Affect to Design Shape-Changing Interfaces », *in: Proceedings of the 2016 ACM Conference on Designing Interactive Systems*, DIS '16, Brisbane, QLD, Australia: Association for Computing Machinery, 2016, pp. 1282–1293, ISBN: 9781450340311, DOI: 10.1145/2901790.2901845, URL: <https://doi.org/10.1145/2901790.2901845>.
- [433] X. Tang, X. Zhang, R. Tao, and Yiming Rong, « Structure-enhanced yield stress of magnetorheological fluids », *in: Journal of Applied Physics* 87.5 (Mar. 2000), pp. 2634–2638, ISSN: 0021-8979, DOI: 10.1063/1.372229, eprint: https://pubs.aip.org/aip/jap/article-pdf/87/5/2634/10602386/2634\1_online.pdf, URL: <https://doi.org/10.1063/1.372229>.
- [434] Yujie Tao, Shan-Yuan Teng, and Pedro Lopes, « Altering Perceived Softness of Real Rigid Objects by Restricting Fingerpad Deformation », *in: The 34th Annual ACM Symposium on User Interface Software and Technology*, UIST '21, Virtual Event, USA: Association for Computing Machinery, 2021, pp. 985–996, ISBN: 9781450386357, DOI: 10.1145/3472749.3474800.
- [435] Shan-Yuan Teng, Tzu-Sheng Kuo, Chi Wang, Chi-huan Chiang, Da-Yuan Huang, Liwei Chan, and Bing-Yu Chen, « PuPoP: Pop-up Prop on Palm for Virtual Reality », *in: Proceedings of the 31st Annual ACM Symposium on User Interface Software and Technology*, UIST '18, Berlin, Germany: Association for Computing

- Machinery, 2018, pp. 5–17, ISBN: 9781450359481, DOI: 10.1145/3242587.3242628, URL: <https://doi.org/10.1145/3242587.3242628>.
- [436] Shan-Yuan Teng, Cheng-Lung Lin, Chi-huan Chiang, Tzu-Sheng Kuo, Liwei Chan, Da-Yuan Huang, and Bing-Yu Chen, « TilePoP: Tile-type Pop-up Prop for Virtual Reality », *in: Proceedings of the 32nd Annual ACM Symposium on User Interface Software and Technology*, UIST '19, New Orleans, LA, USA: Association for Computing Machinery, 2019, pp. 639–649, ISBN: 9781450368162, DOI: 10.1145/3332165.3347958, URL: <https://doi.org/10.1145/3332165.3347958>.
- [437] American Society for Testing and Materials, « ASTM D2240-15 standard test method for rubber property: durometer hardness », *in: ASTM Volume 03.01: Metals – Mechanical Testing; Elevated And Low-temperature Tests; Metallography*, ASTM West Conshohocken, West Conshohocken, Pennsylvania, United States: American Society for Testing and Materials, 2015, p. 13, DOI: 10.1520/D2240-15.
- [438] American Society for Testing and Materials, « Standard Test Method for Young's Modulus, Tangent Modulus, and Chord Modulus », *in: ASTM Volume 03.01: Metals – Mechanical Testing; Elevated And Low-temperature Tests; Metallography*, ASTM West Conshohocken, West Conshohocken, Pennsylvania, United States: American Society for Testing and Materials, 2010, p. 7, DOI: 10.1520/E0111-04R10.
- [439] American Society for Testing and Materials, « Standard Test Methods for Rubber Properties in Compression », *in: ASTM Volume 09.01: Rubber, Natural And Synthetic — General Test Methods; Carbon Black*, ASTM West Conshohocken, West Conshohocken, Pennsylvania, United States: American Society for Testing and Materials, 2018, p. 4, DOI: 10.1520/D0575-91R18.
- [440] Marc Teyssier, Gilles Bailly, Catherine Pelachaud, and Eric Lecolinet, « MobiLimb: Augmenting Mobile Devices with a Robotic Limb », *in: Proceedings of the 31st Annual ACM Symposium on User Interface Software and Technology*, UIST '18, Berlin, Germany: Association for Computing Machinery, 2018, pp. 53–63, ISBN: 9781450359481, DOI: 10.1145/3242587.3242626, URL: <https://doi.org/10.1145/3242587.3242626>.
- [441] Marc Teyssier, Gilles Bailly, Catherine Pelachaud, Eric Lecolinet, Andrew Conn, and Anne Roudaut, « Skin-On Interfaces: A Bio-Driven Approach for Artificial Skin Design to Cover Interactive Devices », *in: Proceedings of the 32nd Annual*

- ACM Symposium on User Interface Software and Technology*, UIST '19, New Orleans, LA, USA: Association for Computing Machinery, 2019, pp. 307–322, ISBN: 9781450368162, DOI: 10.1145/3332165.3347943, URL: <https://doi.org/10.1145/3332165.3347943>.
- [442] John Tiab and Kasper Hornbæk, « Understanding Affordance, System State, and Feedback in Shape-Changing Buttons », *in: Proceedings of the 2016 CHI Conference on Human Factors in Computing Systems*, CHI '16, San Jose, California, USA: Association for Computing Machinery, 2016, pp. 2752–2763, ISBN: 9781450333627, DOI: 10.1145/2858036.2858350, URL: <https://doi.org/10.1145/2858036.2858350>.
- [443] Xavier de Tinguay, Claudio Pacchierotti, Mathieu Emily, Mathilde Chevalier, Aurélie Guignardat, Morgan Guillaudeux, Chloé Six, Anatole Lécuyer, and Maud Marchal, « How Different Tangible and Virtual Objects Can Be While Still Feeling the Same? », *in: 2019 IEEE World Haptics Conference (WHC)*, 2019, pp. 580–585, DOI: 10.1109/WHC.2019.8816164.
- [444] Sarah Tinitali, Kelly-Ann Bowles, Jennifer L. Keating, and Terry Haines, « Sitting Posture During Occupational Driving Causes Low Back Pain; Evidence-Based Position or Dogma? A Systematic Review », *in: Human Factors* 63.1 (2021), PMID: 31513435, pp. 111–123, DOI: 10.1177/0018720819871730, eprint: <https://doi.org/10.1177/0018720819871730>, URL: <https://doi.org/10.1177/0018720819871730>.
- [445] B. Tondu and P. Lopez, « Modeling and control of McKibben artificial muscle robot actuators », *in: IEEE Control Systems Magazine* 20.2 (2000), pp. 15–38, DOI: 10.1109/37.833638.
- [446] Bertrand Tondu, « Modelling of the McKibben artificial muscle: A review », *in: Journal of Intelligent Material Systems and Structures* 23.3 (2012), pp. 225–253, DOI: 10.1177/1045389X11435435, eprint: <https://doi.org/10.1177/1045389X11435435>, URL: <https://doi.org/10.1177/1045389X11435435>.
- [447] Manuel Martínez Torán, Alicia Bonillo, Emilio Espí, and Manuel Martínez Torán, « Future Trends about Fashion and Technology: A Forward Planning », *in: Current Trends in Fashion Technology & Textile Engineering* 2.2 (2018), pp. 21–22, DOI: 10.19080/CTFTTE.2018.02.555582.

- [448] Cesar Torres, Tim Campbell, Neil Kumar, and Eric Paulos, « HapticPrint: Designing Feel Aesthetics for Digital Fabrication », *in: Proceedings of the 28th Annual ACM Symposium on User Interface Software and Technology*, UIST '15, Charlotte, NC, USA: Association for Computing Machinery, 2015, pp. 583–591, ISBN: 9781450337793, DOI: 10.1145/2807442.2807492, URL: <https://doi.org/10.1145/2807442.2807492>.
- [449] RN Traxler, « The effect of temperature on rate of osmosis », *in: The Journal of Physical Chemistry* 32.1 (2002), pp. 127–141, DOI: 10.1021/j150283a010.
- [450] Bernhard Treutwein, « Adaptive psychophysical procedures », *in: Vision Research* 35.17 (1995), pp. 2503–2522, ISSN: 0042-6989, DOI: [https://doi.org/10.1016/0042-6989\(95\)00016-X](https://doi.org/10.1016/0042-6989(95)00016-X), URL: <https://www.sciencedirect.com/science/article/pii/004269899500016X>.
- [451] Giovanni Maria Troiano, Esben Warming Pedersen, and Kasper Hornbæk, « User-Defined Gestures for Elastic, Deformable Displays », *in: Proceedings of the 2014 International Working Conference on Advanced Visual Interfaces*, AVI '14, Como, Italy: Association for Computing Machinery, 2014, pp. 1–8, ISBN: 9781450327756, DOI: 10.1145/2598153.2598184, URL: <https://doi.org/10.1145/2598153.2598184>.
- [452] Ryan L. Truby, Michael Wehner, Abigail K. Grosskopf, Daniel M. Vogt, Sebastien G. M. Uzel, Robert J. Wood, and Jennifer A. Lewis, « Soft Somatosensitive Actuators via Embedded 3D Printing », *in: Advanced Materials* 30.15 (2018), p. 1706383, DOI: <https://doi.org/10.1002/adma.201706383>, eprint: <https://onlinelibrary.wiley.com/doi/pdf/10.1002/adma.201706383>, URL: <https://onlinelibrary.wiley.com/doi/abs/10.1002/adma.201706383>.
- [453] Nicolas Tsingos, Emmanuel Gallo, and George Drettakis, « Perceptual audio rendering of complex virtual environments », *in: ACM Trans. Graph.* 23.3 (Aug. 2004), pp. 249–258, ISSN: 0730-0301, DOI: 10.1145/1015706.1015710, URL: <https://doi.org/10.1145/1015706.1015710>.
- [454] Catrine Tudor-Locke, John M Schuna, Lauren J Frensham, and Mahara Proenca, « Changing the way we work: elevating energy expenditure with workstation alternatives », *in: International journal of obesity* 38.6 (2014), pp. 755–765, DOI: 10.1038/ijo.2013.223.

-
- [455] André B Valdez and Eric L Amazeen, « Sensory and perceptual interactions in weight perception », *in: Perception and psychophysics* 70.4 (2008), pp. 647–657, DOI: <https://doi.org/10.3758/PP.70.4.647>.
- [456] Bernard J Van der Horst, Maarten JA Duijndam, Myrna FM Ketels, Martine TJM Wilbers, Sandra A Zwijsen, and Astrid ML Kappers, « Intramanual and intermanual transfer of the curvature aftereffect », *in: Experimental Brain Research* 187.3 (2008), pp. 491–496, DOI: <https://doi.org/10.1007/s00221-008-1390-0>.
- [457] Bernard J Van der Horst and Astrid ML Kappers, « Curvature discrimination in various finger conditions », *in: Experimental brain research* 177.3 (2007), pp. 304–311, DOI: <https://doi.org/10.1007/s00221-006-0670-9>.
- [458] Bernard J Van der Horst and Astrid ML Kappers, « Using curvature information in haptic shape perception of 3D objects », *in: Experimental brain research* 190 (2008), pp. 361–367, DOI: <https://doi.org/10.1007/s00221-008-1478-6>.
- [459] Bernard J. van der Horst, Wouter P. Willebrands, and Astrid M.L. Kappers, « Transfer of the curvature aftereffect in dynamic touch », *in: Neuropsychologia* 46.12 (2008), pp. 2966–2972, ISSN: 0028-3932, DOI: <https://doi.org/10.1016/j.neuropsychologia.2008.06.003>, URL: <https://www.sciencedirect.com/science/article/pii/S0028393208002674>.
- [460] Albert Van Eeckhout, Enrique Garcia-Caurel, Teresa Garnatje, Juan Carlos Escalera, Mercè Durfort, Josep Vidal, José J Gil, Juan Campos, and Angel Lizana, « Polarimetric imaging microscopy for advanced inspection of vegetal tissues », *in: Scientific reports* 11.1 (2021), p. 3913, DOI: [10.1038/s41598-021-83421-8](https://doi.org/10.1038/s41598-021-83421-8).
- [461] Ilse M. Van Meerbeek, Benjamin C. Mac Murray, Jae Woo Kim, Sanlin S. Robinson, Perry X. Zou, Meredith N. Silberstein, and Robert F. Shepherd, « Morphing Metal and Elastomer Bicontinuous Foams for Reversible Stiffness, Shape Memory, and Self-Healing Soft Machines », *in: Advanced Materials* 28.14 (2016), pp. 2801–2806, DOI: <https://doi.org/10.1002/adma.201505991>, eprint: <https://onlinelibrary.wiley.com/doi/pdf/10.1002/adma.201505991>, URL: <https://onlinelibrary.wiley.com/doi/abs/10.1002/adma.201505991>.
- [462] Marynel Vázquez, Eric Brockmeyer, Ruta Desai, Chris Harrison, and Scott E. Hudson, « 3D Printing Pneumatic Device Controls with Variable Activation Force Capabilities », *in: Proceedings of the 33rd Annual ACM Conference on Human*

- Factors in Computing Systems*, CHI '15, Seoul, Republic of Korea: Association for Computing Machinery, 2015, pp. 1295–1304, ISBN: 9781450331456, DOI: 10.1145/2702123.2702569, URL: <https://doi.org/10.1145/2702123.2702569>.
- [463] V. Vechev, J. Zarate, B. Thomaszewski, and O. Hilliges, « Computational Design of Kinesthetic Garments », *in: Computer Graphics Forum* 41.2 (2022), pp. 535–546, DOI: <https://doi.org/10.1111/cgf.14492>, eprint: <https://onlinelibrary.wiley.com/doi/pdf/10.1111/cgf.14492>, URL: <https://onlinelibrary.wiley.com/doi/abs/10.1111/cgf.14492>.
- [464] Velko Vechev, Ronan Hinchet, Stelian Coros, Bernhard Thomaszewski, and Otmar Hilliges, « Computational Design of Active Kinesthetic Garments », *in: Proceedings of the 35th Annual ACM Symposium on User Interface Software and Technology*, UIST '22, Bend, OR, USA: Association for Computing Machinery, 2022, ISBN: 9781450393201, DOI: 10.1145/3526113.3545674, URL: <https://doi.org/10.1145/3526113.3545674>.
- [465] Ramiro Velázquez and Edwige E Pissaloux, « Modelling and temperature control of shape memory alloys with fast electrical heating », *in: Int. J. Mech. Control* 13.2 (2012), pp. 1–8, URL: <https://www.robotica-up.org/PDF/JoMaC12B04.pdf>.
- [466] Fernando Vidal-Verdú and Rafael Navas-González, « A Thermopneumatic Approach for Tactile Displays », *in:* URL: <https://api.semanticscholar.org/CorpusID:6125709>.
- [467] Kathleen Villaluz, *Crunchy Engineering of Pringles' Hyperbolic Paraboloid Shape*, (last retrieved January 2, 2024), 2020, URL: <https://interestingengineering.com/culture/geometry-of-pringles-crunchy-hyperbolic-paraboloid>.
- [468] P. Vink, R. Porcar-Seder, Álvaro Page de Pozo, and F. Krause, « Office chairs are often not adjusted by end-users », *in: Proceedings of the Human Factors and Ergonomics Society Annual Meeting* 51.17 (2007), pp. 1015–1019, DOI: 10.1177/154193120705101704, eprint: <https://doi.org/10.1177/154193120705101704>, URL: <https://doi.org/10.1177/154193120705101704>.
- [469] Ingrid M L C Vogels, Astrid M L Kappers, and Jan J Koenderink, « Haptic After-effect of Curved Surfaces », *in: Perception* 25.1 (1996), PMID: 8861174, pp. 109–119, DOI: 10.1068/p250109, eprint: <https://doi.org/10.1068/p250109>, URL: <https://doi.org/10.1068/p250109>.

- [470] Ingrid M.L.C. Vogels, Astrid M.L. Kappers, and Jan J. Koenderink, « Influence of shape on haptic curvature perception », *in: Acta Psychologica* 100.3 (1999), pp. 267–289, ISSN: 0001-6918, DOI: [https://doi.org/10.1016/S0001-6918\(98\)00041-9](https://doi.org/10.1016/S0001-6918(98)00041-9), URL: <https://www.sciencedirect.com/science/article/pii/S0001691898000419>.
- [471] Vincent Wall, Raphael Deimel, and Oliver Brock, « Selective stiffening of soft actuators based on jamming », *in: 2015 IEEE International Conference on Robotics and Automation (ICRA)*, 2015, pp. 252–257, DOI: 10.1109/ICRA.2015.7139008.
- [472] Dangxiao WANG, Yuan GUO, Shiyi LIU, Yuru ZHANG, Weiliang XU, and Jing XIAO, « Haptic display for virtual reality: progress and challenges », *in: Virtual Reality & Intelligent Hardware* 1.2 (2019), pp. 136–162, ISSN: 2096-5796, DOI: <https://doi.org/10.3724/SP.J.2096-5796.2019.0008>, URL: <https://www.sciencedirect.com/science/article/pii/S2096579619300130>.
- [473] Guanyun Wang, Humphrey Yang, Zeyu Yan, Nurcan Gecer Ulu, Ye Tao, Jianzhe Gu, Levent Burak Kara, and Lining Yao, « 4DMesh: 4D Printing Morphing Non-Developable Mesh Surfaces », *in: Proceedings of the 31st Annual ACM Symposium on User Interface Software and Technology*, UIST '18, Berlin, Germany: Association for Computing Machinery, 2018, pp. 623–635, ISBN: 9781450359481, DOI: 10.1145/3242587.3242625, URL: <https://doi.org/10.1145/3242587.3242625>.
- [474] Guanyun Wang, Lining Yao, Wen Wang, Jifei Ou, Chin-Yi Cheng, and Hiroshi Ishii, « XPrint: A Modularized Liquid Printer for Smart Materials Deposition », *in: Proceedings of the 2016 CHI Conference on Human Factors in Computing Systems*, CHI '16, San Jose, California, USA: Association for Computing Machinery, 2016, pp. 5743–5752, ISBN: 9781450333627, DOI: 10.1145/2858036.2858281, URL: <https://doi.org/10.1145/2858036.2858281>.
- [475] Wen Wang, Lining Yao, Chin-Yi Cheng, Teng Zhang, Hiroshi Atsumi, Luda Wang, Guanyun Wang, Oksana Anilionyte, Helene Steiner, Jifei Ou, Kang Zhou, Chris Wawrousek, Katherine Petrecca, Angela M. Belcher, Rohit Karnik, Xuanhe Zhao, Daniel I. C. Wang, and Hiroshi Ishii, « Harnessing the hygroscopic and biofluorescent behaviors of genetically tractable microbial cells to design biohybrid wearables », *in: Science Advances* 3.5 (2017), e1601984, DOI: 10.1126/sciadv.1601984, eprint: <https://www.science.org/doi/pdf/10.1126/sciadv.1601984>, URL: <https://www.science.org/doi/abs/10.1126/sciadv.1601984>.

- [476] Wen Wang, Lining Yao, Teng Zhang, Chin-Yi Cheng, Daniel Levine, and Hiroshi Ishii, « Transformative Appetite: Shape-Changing Food Transforms from 2D to 3D by Water Interaction through Cooking », *in: Proceedings of the 2017 CHI Conference on Human Factors in Computing Systems*, CHI '17, Denver, Colorado, USA: Association for Computing Machinery, 2017, pp. 6123–6132, ISBN: 9781450346559, DOI: 10.1145/3025453.3026019, URL: <https://doi.org/10.1145/3025453.3026019>.
- [477] Thomas R. Waters, « The National Occupational Research Agenda for Musculoskeletal Disorders: An Overview », *in: Proceedings of the Human Factors and Ergonomics Society Annual Meeting 45.14* (2001), pp. 1070–1073, DOI: 10.1177/154193120104501417, eprint: <https://doi.org/10.1177/154193120104501417>, URL: <https://doi.org/10.1177/154193120104501417>.
- [478] Michael Wehner, Ryan L Truby, Daniel J Fitzgerald, Bobak Mosadegh, George M Whitesides, Jennifer A Lewis, and Robert J Wood, « An integrated design and fabrication strategy for entirely soft, autonomous robots », *in: nature 536.7617* (2016), pp. 451–455, DOI: 10.1038/nature19100.
- [479] Christian Weidner, Martin Schmelz, Roland Schmidt, Björn Hammarberg, Kristin Ørstavik, Marita Hilliges, H. Erik Torebjörk, and Hermann O. Handwerker, « Neural Signal Processing: The Underestimated Contribution of Peripheral Human C-Fibers », *in: Journal of Neuroscience 22.15* (2002), pp. 6704–6712, ISSN: 0270-6474, DOI: 10.1523/JNEUROSCI.22-15-06704.2002, eprint: <https://www.jneurosci.org/content/22/15/6704.full.pdf>, URL: <https://www.jneurosci.org/content/22/15/6704>.
- [480] Martin Weigel, Tong Lu, Gilles Bailly, Antti Oulasvirta, Carmel Majidi, and Jürgen Steimle, « ISkin: Flexible, Stretchable and Visually Customizable On-Body Touch Sensors for Mobile Computing », *in: Proceedings of the 33rd Annual ACM Conference on Human Factors in Computing Systems*, CHI '15, Seoul, Republic of Korea: Association for Computing Machinery, 2015, pp. 2991–3000, ISBN: 9781450331456, DOI: 10.1145/2702123.2702391.
- [481] Martin Weigel and Jürgen Steimle, « DeformWear: Deformation Input on Tiny Wearable Devices », *in: Proc. ACM Interact. Mob. Wearable Ubiquitous Technol. 1.2* (June 2017), DOI: 10.1145/3090093, URL: <https://doi.org/10.1145/3090093>.

- [482] Malte Weiss, Julie Wagner, Yvonne Jansen, Roger Jennings, Ramsin Khoshabeh, James D. Hollan, and Jan Borchers, « SLAP Widgets: Bridging the Gap between Virtual and Physical Controls on Tabletops », *in: Proceedings of the SIGCHI Conference on Human Factors in Computing Systems*, CHI '09, Boston, MA, USA: Association for Computing Machinery, 2009, pp. 481–490, ISBN: 9781605582467, DOI: 10.1145/1518701.1518779.
- [483] Michael Wessely, Ticha Sethapakdi, Carlos Castillo, Jackson C. Snowden, Ollie Hanton, Isabel P. S. Qamar, Mike Fraser, Anne Roudaut, and Stefanie Mueller, « Sprayable User Interfaces: Prototyping Large-Scale Interactive Surfaces with Sensors and Displays », *in: Proceedings of the 2020 CHI Conference on Human Factors in Computing Systems*, CHI '20, <conf-loc>, <city>Honolulu</city>, <state>HI</state>, <country>USA</country>, </conf-loc>: Association for Computing Machinery, 2020, pp. 1–12, ISBN: 9781450367080, DOI: 10.1145/3313831.3376249, URL: <https://doi.org/10.1145/3313831.3376249>.
- [484] Michael Wessely, Theophanis Tsandilas, and Wendy E. Mackay, « Stretchis: Fabricating Highly Stretchable User Interfaces », *in: Proceedings of the 29th Annual Symposium on User Interface Software and Technology*, UIST '16, Tokyo, Japan: Association for Computing Machinery, 2016, pp. 697–704, ISBN: 9781450341899, DOI: 10.1145/2984511.2984521, URL: <https://doi.org/10.1145/2984511.2984521>.
- [485] George M Whitesides, « The origins and the future of microfluidics », *in: nature* 442.7101 (2006), pp. 368–373, DOI: 10.1038/nature05058.
- [486] Mario Wiesendanger and Deborah J. Serrien, « Toward a Physiological Understanding of Human Dexterity », *in: Physiology* 16.5 (2001), pp. 228–233, DOI: 10.1152/physiologyonline.2001.16.5.228, eprint: <https://doi.org/10.1152/physiologyonline.2001.16.5.228>, URL: <https://doi.org/10.1152/physiologyonline.2001.16.5.228>.
- [487] wikipedia, *AirPods*, (last retrieved January 23, 2024), URL: <https://en.wikipedia.org/wiki/AirPods>.
- [488] wikipedia, *Apple Vision Pro*, Last retrieved January 25, 2024, URL: https://en.wikipedia.org/wiki/Apple_Vision_Pro.
- [489] wikipedia, *Apple Watch*, (last retrieved January 23, 2024), URL: https://en.wikipedia.org/wiki/Apple_Watch.

BIBLIOGRAPHY

- [490] wikipedia, *History of clothing and textiles*, Last retrieved January 25, 2024, URL: https://en.wikipedia.org/wiki/History_of_clothing_and_textiles.
- [491] wikipedia, *iMac G3*, (last retrieved January 2, 2024), URL: https://en.wikipedia.org/wiki/IMac_G3.
- [492] wikipedia, *iPhone 4s*, (last retrieved January 2, 2024), URL: https://en.wikipedia.org/wiki/IPhone_4s.
- [493] wikipedia, *Meta*, Last retrieved January 25, 2024, URL: <https://about.meta.com/metaverse/>.
- [494] wikipedia, *Panton Chair*, (last retrieved January 2, 2024), URL: https://en.wikipedia.org/wiki/Panton_Chair.
- [495] wikipedia, *Stanford bunny*, Last retrieved January 4, 2024, URL: https://en.wikipedia.org/wiki/Stanford_bunny.
- [496] wikipedia, *Xiaomi Mi Band*, (last retrieved January 23, 2024), URL: https://en.wikipedia.org/wiki/Xiaomi_Mi_Band.
- [497] wikipedia, *Zero crossing*, Last retrieved January 4, 2024, URL: https://en.wikipedia.org/wiki/Zero_crossing.
- [498] Anouk Wipprecht, *Proximity Dress*, Last retrieved January 24, 2024, URL: <https://www.youtube.com/watch?v=QkzD8oQa9qc>.
- [499] Anouk Wipprecht, *Spider Dress*, Last retrieved January 24, 2024, URL: https://www.youtube.com/watch?v=cK02id_3aS8.
- [500] Dennis Wittchen, Bruno Fruchard, Paul Strohmeier, and Georg Freitag, « Tact-Jam: A Collaborative Playground for Composing Spatial Tactons », in: *Proceedings of the Fifteenth International Conference on Tangible, Embedded, and Embodied Interaction*, TEI '21, Salzburg, Austria: Association for Computing Machinery, 2021, ISBN: 9781450382137, DOI: 10.1145/3430524.3442699.
- [501] Timothy H. Parker Wolfgang Forstmeier Eric-Jan Wagenmakers, « Detecting and avoiding likely false-positive findings – a practical guide », in: *Biological Reviews* 92 (4 Nov. 2017), pp. 1941–1968, DOI: 10.1111/brv.12315, URL: <https://doi.org/10.1111/brv.12315>.
- [502] Christopher Woo, *Roland S. Johansson's experiment of mach's striking with anesthetized fingers*, video, 2011, URL: <https://www.youtube.com/watch?v=0LfJ3M3Kn80>.

- [503] Matheus S. Xavier, Charbel D. Tawk, Ali Zolfagharian, Joshua Pinski, David Howard, Taylor Young, Jiewen Lai, Simon M. Harrison, Yuen K. Yong, Mahdi Bodaghi, and Andrew J. Fleming, « Soft Pneumatic Actuators: A Review of Design, Fabrication, Modeling, Sensing, Control and Applications », *in: IEEE Access* 10 (2022), pp. 59442–59485, DOI: 10.1109/ACCESS.2022.3179589.
- [504] Xiaomi, *Two notifications for single application*, Last retrieved January 25, 2024, URL: https://help.mibandtools.com/knowledge_base/topics/two-notifications-for-single-application.
- [505] Jiushu Xie, Zhi Lu, Ruiming Wang, and Zhenguang G Cai, « Remember hard but think softly: Metaphorical effects of hardness/softness on cognitive functions », *in: Frontiers in Psychology* 7 (2016), p. 1343, DOI: 10.3389/fpsyg.2016.01343.
- [506] Humphrey Yang, Kuanren Qian, Haolin Liu, Yuxuan Yu, Jianzhe Gu, Matthew McGehee, Yongjie Jessica Zhang, and Lining Yao, « SimuLearn: Fast and Accurate Simulator to Support Morphing Materials Design and Workflows », *in: Proceedings of the 33rd Annual ACM Symposium on User Interface Software and Technology*, UIST '20, Virtual Event, USA: Association for Computing Machinery, 2020, pp. 71–84, ISBN: 9781450375146, DOI: 10.1145/3379337.3415867, URL: <https://doi.org/10.1145/3379337.3415867>.
- [507] Munseok Yang and Junichi Yamaoka, « MultiJam: Fabricating Jamming User Interface Using Multi-Material 3D Printing », *in: Sixteenth International Conference on Tangible, Embedded, and Embodied Interaction*, TEI '22, Daejeon, Republic of Korea: Association for Computing Machinery, 2022, ISBN: 9781450391474, DOI: 10.1145/3490149.3505565.
- [508] Tae-Heon Yang, Hyunki Son, Sangkyu Byeon, Hyunjae Gil, Inwook Hwang, Gwanghyun Jo, Seungmoon Choi, Sang-Youn Kim, and Jin Ryong Kim, « Magnetorheological Fluid Haptic Shoes for Walking in VR », *in: IEEE Transactions on Haptics* 14.1 (2021), pp. 83–94, DOI: 10.1109/TOH.2020.3017099.
- [509] Lining Yao, Ryuma Niiyama, Jifei Ou, Sean Follmer, Clark Della Silva, and Hiroshi Ishii, « PneuUI: Pneumatically Actuated Soft Composite Materials for Shape Changing Interfaces », *in: Proceedings of the 26th Annual ACM Symposium on User Interface Software and Technology*, UIST '13, St. Andrews, Scotland, United Kingdom: Association for Computing Machinery, 2013, pp. 13–22, ISBN: 9781450322683,

- DOI: 10.1145/2501988.2502037, URL: <https://doi.org/10.1145/2501988.2502037>.
- [510] Lining Yao, Jifei Ou, Chin-Yi Cheng, Helene Steiner, Wen Wang, Guanyun Wang, and Hiroshi Ishii, « BioLogic: Natto Cells as Nanoactuators for Shape Changing Interfaces », in: *Proceedings of the 33rd Annual ACM Conference on Human Factors in Computing Systems, CHI '15*, Seoul, Republic of Korea: Association for Computing Machinery, 2015, pp. 1–10, ISBN: 9781450331456, DOI: 10.1145/2702123.2702611, URL: <https://doi.org/10.1145/2702123.2702611>.
- [511] Huizhong Ye, Charlaïne Janssen, Daan Noordman, and Rong-Hao Liang, « Understanding How to Support Remote Co-Design with a Conceptual Modular Shape-Changing Interface Toolkit », in: *Sixteenth International Conference on Tangible, Embedded, and Embodied Interaction, TEI '22*, Daejeon, Republic of Korea: Association for Computing Machinery, 2022, ISBN: 9781450391474, DOI: 10.1145/3490149.3505563, URL: <https://doi.org/10.1145/3490149.3505563>.
- [512] Hui-Shyong Yeo, Juyoung Lee, Hyung-il Kim, Aakar Gupta, Andrea Bianchi, Daniel Vogel, Hideki Koike, Woontack Woo, and Aaron Quigley, « WRIST: Watch-Ring Interaction and Sensing Technique for Wrist Gestures and Macro-Micro Pointing », in: *Proceedings of the 21st International Conference on Human-Computer Interaction with Mobile Devices and Services, MobileHCI '19*, Taipei, Taiwan: Association for Computing Machinery, 2019, ISBN: 9781450368254, DOI: 10.1145/3338286.3340130, URL: <https://doi.org/10.1145/3338286.3340130>.
- [513] Jessica Yin, Ronan Hinchet, Herbert Shea, and Carmel Majidi, « Wearable Soft Technologies for Haptic Sensing and Feedback », in: *Advanced Functional Materials* 31.39 (2021), p. 2007428, DOI: <https://doi.org/10.1002/adfm.202007428>, eprint: <https://onlinelibrary.wiley.com/doi/pdf/10.1002/adfm.202007428>, URL: <https://onlinelibrary.wiley.com/doi/abs/10.1002/adfm.202007428>.
- [514] Gao Ying, *Flowing water, Standing time*, Last retrieved January 24, 2024, URL: <http://yinggao.ca/interactifs/flowing-water-standing-time/>.
- [515] Gao Ying, *Possible tomorrows*, Last retrieved January 24, 2024, URL: <http://yinggao.ca/fr/possible-tomorrows/>.

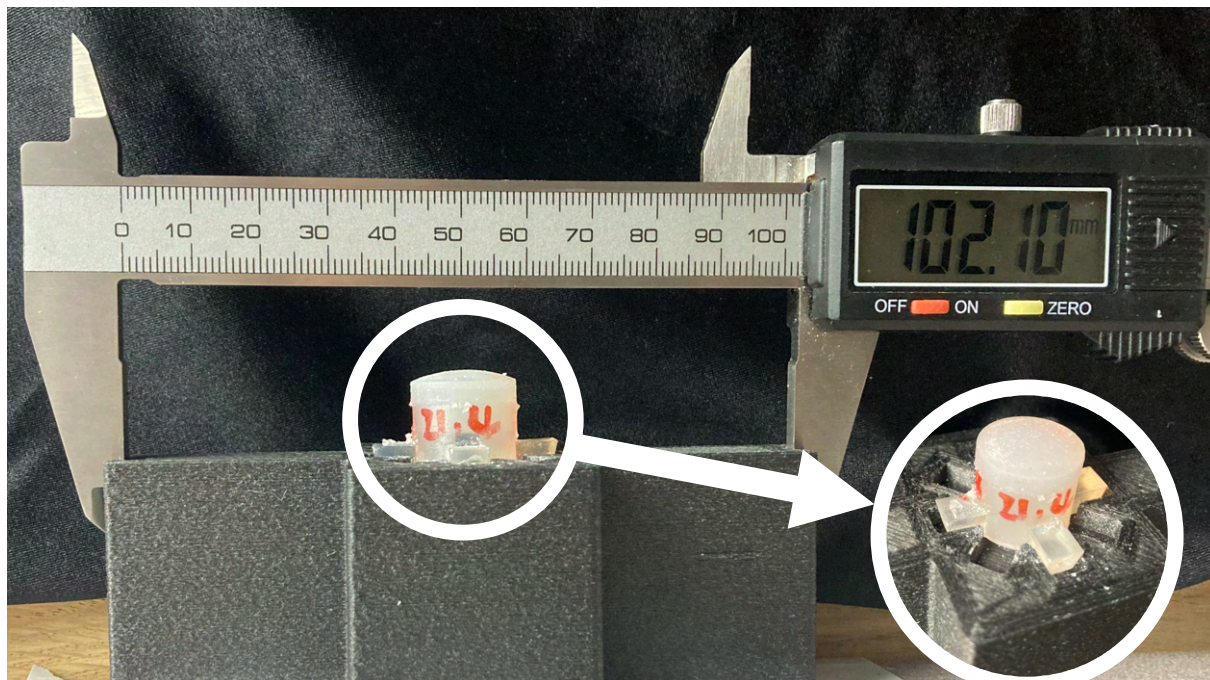
-
- [516] Sang Ho Yoon, Ke Huo, and Karthik Ramani, « Wearable textile input device with multimodal sensing for eyes-free mobile interaction during daily activities », *in: Pervasive and Mobile Computing* 33 (2016), pp. 17–31, ISSN: 1574-1192, DOI: <https://doi.org/10.1016/j.pmcj.2016.04.008>, URL: <https://www.sciencedirect.com/science/article/pii/S1574119216300311>.
- [517] Sang Ho Yoon, Luis Paredes, Ke Huo, and Karthik Ramani, « MultiSoft: Soft Sensor Enabling Real-Time Multimodal Sensing with Contact Localization and Deformation Classification », *in: Proc. ACM Interact. Mob. Wearable Ubiquitous Technol.* 2.3 (Sept. 2018), DOI: 10.1145/3264955, URL: <https://doi.org/10.1145/3264955>.
- [518] Hye Jun Youn and Ali Shtarbanov, « PneuBots: Modular Inflatables for Playful Exploration of Soft Robotics », *in: Extended Abstracts of the 2022 CHI Conference on Human Factors in Computing Systems*, CHI EA '22, New Orleans, LA, USA: Association for Computing Machinery, 2022, ISBN: 9781450391566, DOI: 10.1145/3491101.3514490, URL: <https://doi.org/10.1145/3491101.3514490>.
- [519] Bin Yu, Nienke Bongers, Alissa van Asseldonk, Jun Hu, Mathias Funk, and Loe Feijs, « LivingSurface: Biofeedback through Shape-Changing Display », *in: Proceedings of the TEI '16: Tenth International Conference on Tangible, Embedded, and Embodied Interaction*, TEI '16, Eindhoven, Netherlands: Association for Computing Machinery, 2016, pp. 168–175, ISBN: 9781450335829, DOI: 10.1145/2839462.2839469, URL: <https://doi.org/10.1145/2839462.2839469>.
- [520] Michelle C. Yuen, R. Adam Bilodeau, and Rebecca K. Kramer, « Active Variable Stiffness Fibers for Multifunctional Robotic Fabrics », *in: IEEE Robotics and Automation Letters* 1.2 (2016), pp. 708–715, DOI: 10.1109/LRA.2016.2519609.
- [521] Hyunwoo Yuk, Shaoting Lin, Chu Ma, Mahdi Takaffoli, Nicolas X Fang, and Xuanhe Zhao, « Hydraulic hydrogel actuators and robots optically and sonically camouflaged in water », *in: Nature communications* 8.1 (2017), p. 14230, DOI: 10.1038/ncomms14230.
- [522] Clint Zeagler, « Where to Wear It: Functional, Technical, and Social Considerations in on-Body Location for Wearable Technology 20 Years of Designing for Wearability », *in: Proceedings of the 2017 ACM International Symposium on Wearable Computers*, ISWC '17, Maui, Hawaii: Association for Computing Machinery, 2017, pp. 150–157, ISBN: 9781450351881, DOI: 10.1145/3123021.3123042.

- [523] Huichan Zhao, Jonathan Jalving, Rukang Huang, Ross Knepper, Andy Ruina, and Robert Shepherd, « A Helping Hand: Soft Orthosis with Integrated Optical Strain Sensors and EMG Control », *in: IEEE Robotics & Automation Magazine* 23.3 (2016), pp. 55–64, DOI: 10.1109/MRA.2016.2582216.
- [524] Huichan Zhao, Yan Li, Ahmed Elsamadisi, and Robert Shepherd, « Scalable manufacturing of high force wearable soft actuators », *in: Extreme Mechanics Letters* 3 (2015), pp. 89–104, ISSN: 2352-4316, DOI: <https://doi.org/10.1016/j.eml.2015.02.006>, URL: <https://www.sciencedirect.com/science/article/pii/S2352431615000450>.
- [525] Jianwen Zhao, Junming Zhang, David McCoul, Zhaogang Hao, Shu Wang, Xinbo Wang, Bo Huang, and Lining Sun, « Soft and Fast Hopping–Running Robot with Speed of Six Times Its Body Length Per Second », *in: Soft Robotics* 6.6 (2019), PMID: 31553262, pp. 713–721, DOI: 10.1089/soro.2018.0098, eprint: <https://doi.org/10.1089/soro.2018.0098>, URL: <https://doi.org/10.1089/soro.2018.0098>.
- [526] Qin Gao Zhaoyi Ma and Mei Yang, « Adoption of Wearable Devices by Older People: Changes in Use Behaviors and User Experiences », *in: International Journal of Human–Computer Interaction* 39.5 (2023), pp. 964–987, DOI: 10.1080/10447318.2022.2083573, eprint: <https://doi.org/10.1080/10447318.2022.2083573>, URL: <https://doi.org/10.1080/10447318.2022.2083573>.
- [527] Ying Zheng and John B. Morrell, « A vibrotactile feedback approach to posture guidance », *in: 2010 IEEE Haptics Symposium*, 2010, pp. 351–358, DOI: 10.1109/HAPTIC.2010.5444633.
- [528] Zhermack, *Elite Double 32*, Last retrieved January 4, 2024, URL: <https://www.zhermack.com/en/product/elite-double-32/>.
- [529] Kening Zhu, Morten Fjeld, and Ayça Ünlüer, « WristOrigami: Exploring Foldable Design for Multi-Display Smartwatch », *in: Proceedings of the 2018 Designing Interactive Systems Conference, DIS '18*, Hong Kong, China: Association for Computing Machinery, 2018, pp. 1207–1218, ISBN: 9781450351980, DOI: 10.1145/3196709.3196713.

- [530] Mengjia Zhu, Thanh Nho Do, Elliot Hawkes, and Yon Visell, « Fluidic Fabric Muscle Sheets for Wearable and Soft Robotics », *in: Soft Robotics 7.2* (2020), PMID: 31905325, pp. 179–197, DOI: [10.1089/soro.2019.0033](https://doi.org/10.1089/soro.2019.0033), eprint: <https://doi.org/10.1089/soro.2019.0033>, URL: <https://doi.org/10.1089/soro.2019.0033>.
- [531] Mengjia Zhu, Amirhossein H. Memar, Aakar Gupta, Majed Samad, Priyanshu Agarwal, Yon Visell, Sean J. Keller, and Nicholas Colonnese, « PneuSleeve: In-Fabric Multimodal Actuation and Sensing in a Soft, Compact, and Expressive Haptic Sleeve », *in: Proceedings of the 2020 CHI Conference on Human Factors in Computing Systems, CHI '20*, Honolulu, HI, USA: Association for Computing Machinery, 2020, pp. 1–12, ISBN: 9781450367080, DOI: [10.1145/3313831.3376333](https://doi.org/10.1145/3313831.3376333), URL: <https://doi.org/10.1145/3313831.3376333>.
- [532] G. Zulauf, J. Zulauf, and H. Maul, « Quantification of the geometrical parameters of non-cylindrical folds », *in: Journal of Structural Geology 100* (2017), pp. 120–129, ISSN: 0191-8141, DOI: <https://doi.org/10.1016/j.jsg.2017.06.001>, URL: <https://www.sciencedirect.com/science/article/pii/S019181411730113X>.

APPENDIX

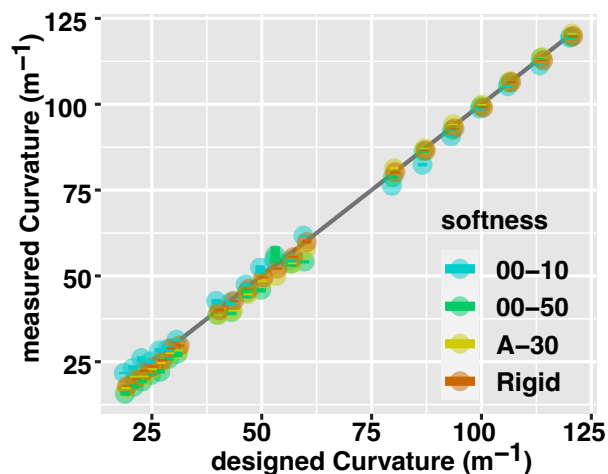
A.1 Stimuli curvature measurements



(a) A stimulus (Shore 00-10 $R=21.4$ mm) installed on 3D-printed support for the curvature measurement. A vernier scale is fixed on the support to ensure the precision of conversion of our measurement on pixels to mm.



(b) A stimulus (Shore 00-10 $R=21.4$ mm) with edge detected, bolded, and highlighted in red color for visualization.



(c) The measured curvature of our stimuli vs. the designed curvature of our stimuli. Data points were slightly jittered horizontally to avoid total overlap. The gray line indicates where the measured curvature equals the designed curvature.

Figure A.1 – Validation of the curvature of our stimuli.

Post-hoc test on JND				
Rref(mm)	Softness Pair	W	Z	p
	Shore 00-10 vs. Shore 00-50	37	-0.16	1
	Shore 00-10 vs. Shore A-30	54	1.18	1

We verified the curvature of our stimuli as in [416]. We first took pictures of our stimuli (Figure A.1(a)) with a Panasonic Lumix G Hybrides camera with a LUMIX G VARIO 14-140 lens (Focal length $f=135$ mm, resolution 1096×2160). Pictures were calibrated to remove the distortion of the camera lens with OpenCV 4.6.0. To ensure measurement accuracy, we took pictures of each stimulus from 8 angles (Figure A.1(a) (bottom right)) by turning the stimulus around its axis in the placeholders, 3D printed support of the stimulus.

We then detected the contour of the curved surface of each stimulus with OpenCV. We fitted points to this contour (Figure A.1(b)) using the circle-fit 0.1.3 [214] python package, to finally find its curvature (Figure A.1(c)). To convert curvature from pixels (px) to mm as shown in the y-axis of Figure A.1(c), we fixed a vernier scale on the support (Figure A.1(a)) to ensure the precision of the conversion. We found that 102.10 mm on the scale equals 1945 px in the pictures. We, therefore, convert our measurements of the curvature with 0.053 mm/px. Figure A.1(c) presents on the y-axis the results of our measurements with the average curvature of each stimulus and respective 95% CI. The exact values of this graph and the code to compute the curvature are available in the supplementary material [100].

A.2 Stimulus height change computation

Figure A.2 presents the profile of a curved surface with three parameters: the radius of the curve surface R , the width D , and the total height change Δh . The total height change Δh depends on the width D :

$$\Delta h = R - \sqrt{R^2 - \frac{D^2}{4}} \quad (R \geq \frac{D}{2}) \quad (\text{A.1})$$

Pont, Kappers, and Koenderink [348] found that the total height change over the surface $\frac{\Delta h}{D}$ is an effective kinesthetic cue that humans used for curvature perception. With Equation A.1, we have:

$$\frac{\Delta h}{D} = \frac{(R - \sqrt{R^2 - \frac{D^2}{4}})}{D} \quad (R \geq \frac{D}{2}) \quad (\text{A.2})$$

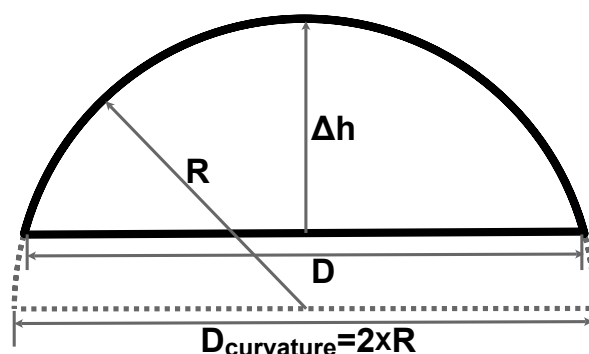


Figure A.2 – Parameters of the profile of the experimental apparatus (stimulus). The gray dotted line presents a semicircle. The larger black solid line presents the part of the semicircle that makes the stimulus.

To analyze the impact of the surface D on the ratio $\frac{\Delta h}{D}$, we compute the derivative of $\frac{\Delta h}{D}$ over D :

$$\frac{\partial(\frac{\Delta h}{D})}{\partial D} = \frac{1}{D^2} \left(\frac{R^2}{\sqrt{R^2 - \frac{D^2}{4}}} - R \right) \quad (R \geq \frac{D}{2}) \quad (\text{A.3})$$

In Equation A.3, as $D > 0$, $\sqrt{R^2 - \frac{D^2}{4}} < R$ is always true. We can deduce that $\frac{R^2}{\sqrt{R^2 - \frac{D^2}{4}}} - R$ is always greater than 0 and $\frac{\partial(\frac{\Delta h}{D})}{\partial D}$ is always positive. As a consequence, the ratio $(\frac{\Delta h}{D})$ increases with a larger D .

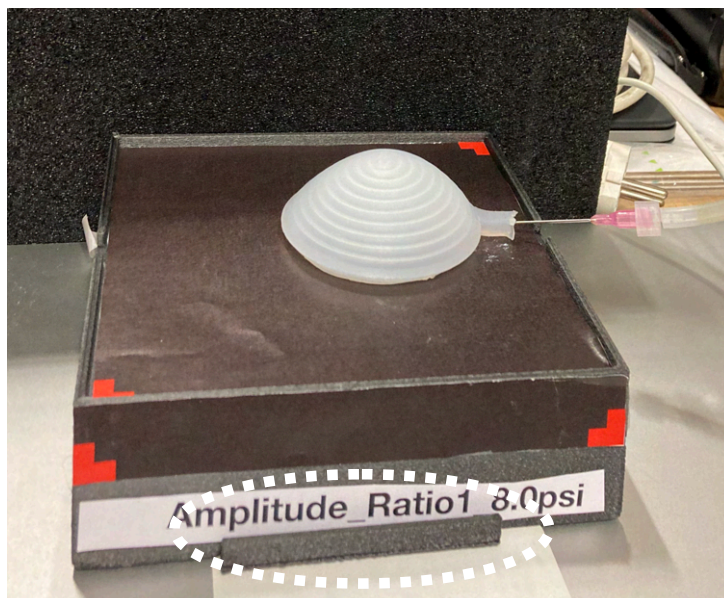
When two stimuli have the same curvature but are of different base diameters, the larger stimulus has the larger total height change over the surface, i.e. the larger $(\frac{\Delta h}{D})$. Therefore, a larger base diameter can improve participants' curvature perception precision with better kinesthetic cues [348].

In our experiment, the stimulus width D is constant with $D = 16$ mm. The stimulus width D is smaller than the smallest diameters of our curved surfaces ($D_{curvature}$ in Figure A.1). I.e., 16.6 mm in the case of the curviest stimuli whose radius is 8.3 mm. In contrast, in the Provancher et al.'s experiment [351, 352], the stimulus width D becomes larger with a flatter stimulus, i.e., a larger stimulus radius R . The data provided in [351, 352] does not allow to precisely compute their stimuli width D and radius R . However, from the schematic representation of their stimuli in Figure 4-6 from [352], we can easily speculate that their stimuli width is larger than ours. As a consequence, we suppose that their stimuli provide participants with more kinesthetic cues thanks to a larger ratio of $(\frac{\Delta h}{D})$ in their flatter conditions compared to our flatter conditions.

On the contrary to Provancher et al. [351, 352], we wanted to prevent any confounding cues from the contact area [137]. In addition, curvature and size are two independent dimensions of shape-changing UIs [226], and curvature-changing UIs do not necessarily change their size (e.g., [132]).

We chose our base diameter D in order to prepare guidelines for the design of soft curvature-changing UIs, such as buttons. A 16 mm button lies within the common range of physical buttons [9]. Additionally, once the UIs are created and worn on the body, it might be troublesome to enlarge too much because of geometrical constraints from the body or the surrounding environment [10]. Further comparison of our experiment and Provancher et al.'s experiment [351, 352] can be found in the discussion section of Chapter 3.

A.3 SoftMorphees shape measurements



(a) Setup for SoftMorphees shape measurement. In the front of the 3D printed support, there is a 3D printed label holder (indicated in the dashed white circle). Label in this holder can help to get prototype information when processing photos. For example, in this figure, the label “ Amplitude Ratio 1 8.0Psi ” indicates photos of an Amplitude changing prototype with a Wall-AirChannels width ratio of 1 under the pressure of 8.0 Psi. Markers in red colors are used for facilitating the photo cropping during photo processing.



(b) A vernier scale measuring the label holder's length to ensure the precision of the conversion between pixels and mm.

Figure A.3 – SoftMorphees shape measurements setup

Figure A.3(a) presents our setup for measuring Softmorphees prototype shape. We first took pictures of our prototypes (Figure A.16(a)) with a Panasonic Lumix G Hybrides

camera with a LUMIX G VARIO 14-140 lens (Focal length $f=135$ mm, resolution 1096×2160). Figure A.3(b) present using a vernier scale measuring the label holder's length to ensure the precision of the conversion between pixels and mm. For example, when measuring the *Amplitude* changing of the prototype shown in Figure A.3(a), the two jaws of the vernier scale measure as 70.64 mm as distance and 1245 pixels in photos. We, therefore, convert our measurements of the curvature with 0.057 mm/px. Each time we change the setup, e.g. measuring a new feature, we take a new photo with a vernier scale to ensure precision.

Pictures were calibrated to remove the distortion of the camera lens and processed with OpenCV 4.6.0 [315]. Shape features of *Curvature* and *Amplitude* are measured with photos taken from a side view. *Length*, *Area*, *Closure* and *Porosity* are measures with photos taken from a side view.

We introduce the following calculation of each shape's feature.

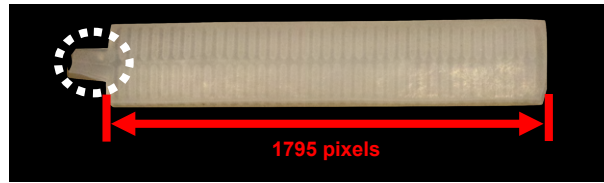


Figure A.4 – *Length* changing *SoftMorpheus* Measurement. The dashed white circle indicates the supplementary part for inserting the needle, which is not included in *Length* measurement.

Length Figure A.4 presents a *Length* measurement of a *Length* changing prototype under 3.0 Psi. Its *Length* is measured from the left end to the right end; the supplementary part (indicated in the dashed white circle) for inserting the needle is not included. In this photo, the prototype's length is measured as 1795 pixels, which can be converted to 105 mm with a conversion ratio of 0.058 mm/px.

Area Figure A.5 presents a *Area* measurement of a *Area* changing prototype under 1.5 Psi. Its *Area* is measured by counting the number of pixels in white colors. For example, the prototype in Figure A.5 is measured with 636002 pixels in white colors, which can be converted to 2194 mm^2 with a conversion ratio of 0.059 mm/px.

Curvature The Curvature calculation is calculated by fitting the prototype's top surface with a circle A.6. For example, Figure A.6 presents an R20 prototype under 4.8 psi.



Figure A.5 – Area changing *SoftMorphees* Measurement.

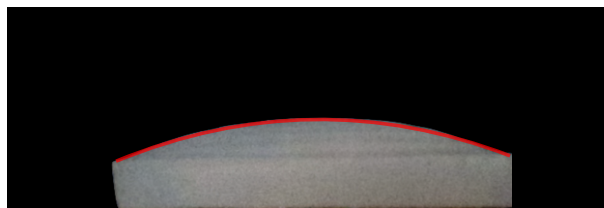


Figure A.6 – A R20 *Curvature* changing *SoftMorphees* under the pressure of 4.8 psi. The red curved line indicated the circular fitting edge using the circle-fit 0.1.3 [214] python package.

A circle with a radius of 569.21 mm can fit well with $R^2 > 0.99$, which can be converted to 32.27 mm with a conversion ratio of 0.057 mm/px.

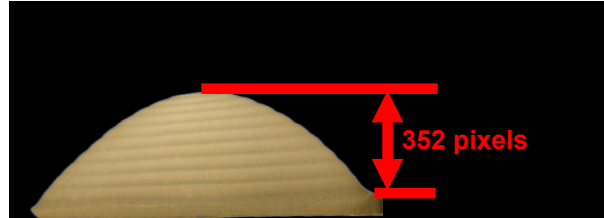


Figure A.7 – An *Amplitude* changing *SoftMorphees* with a Wall-AirChannels width ratio of 1 under the pressure of 8 psi.

Amplitude Figure A.7 presents a *Amplitude* measurement of a *Amplitude* changing prototype with a Wall-AirChannels width ratio of 1 under the pressure of 8.0 Psi Its *Amplitude* is measured height difference between the center and the border. For example, the height difference in Figure A.7 is measured as 352 pixels, which can be converted to 19.95 mm with a conversion ratio of 0.057 mm/px.

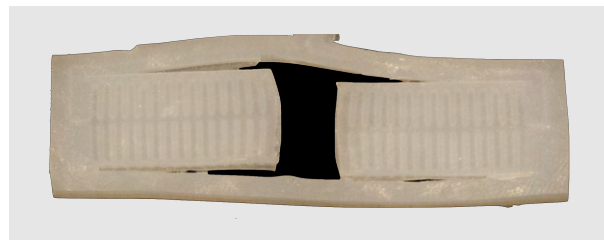


Figure A.8 – A *Porosity* changing via length-changing *SoftMorphees* under the pressure of 6.0 psi.

Porosity The *Porosity* is measured by calculating the area ratio between the hole and the total surface of the prototype. Figure A.8 presents a photo of *Porosity*-changing via length-changing prototype under a pressure of 6.0 psi. The hole area is calculated by counting the number of pixels in black colors. The total prototype area is calculated by counting the number of pixels both in black colors and white colors. Porosity can be calculated as $Porosity = 100 \times \frac{Area_{hole}}{Area_{prototype}} = 100 \times \frac{Area_{black}}{Area_{black} + Area_{white}}$. For example, with Figure A.8, 1034659 white pixels are counted, and 96408 black pixels are counted, which leads to a *Porosity* value as 8.5%.

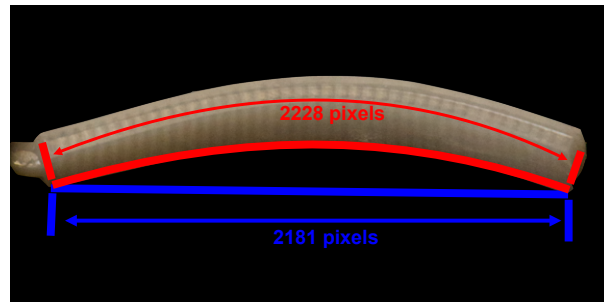


Figure A.9 – A *Closure* changing *SoftMorphees* under the pressure of 3.4 psi.

Closure Figure A.9 presents photos of *Closure* changing prototype under the pressure of 3.4 Psi. We measured the prototype's *Length* (the red curve in Figure A.9) and the boundary *Length* (the blue line in Figure A.9) to calculate the *Closure*, with $Closure = 100 \times \frac{Length_{prototype} - Length_{boundary}}{Length_{boundary}}$. The prototype *Length* $Length_{prototype}$ is measured as 2228 pixels and the boundary *Length* $Length_{boundary}$ is measured as 2181 pixels. Respective *Closure* value is 2.1%.

A.4 Details of design parameters of prototypes

We report detailed parameters of our prototypes in Table A.1 and A.2. Values in bold blue were values of respective controlled parameter that we studied. Table A.1 presents values of prototypes tested in section 5.3 and Table A.2 for section 5.4 respectively. We decide these parameters based on the parameters of the first prototype that we succeeded fabricated and controlled its curvature and strength, i.e., $\mathbf{h}_{\text{Prism}} = 5$ mm, $\mathbf{h}_{\text{Tooth}} = 4$ mm, $\Delta_{\text{Thickness}} = 1$ mm, $\alpha = 120^\circ$, $\beta = 40^\circ$, $\Delta_{\text{Angle}} = 80^\circ$, $\mathbf{h}_{\text{Membrane}} = 0.5$ mm, $\mathbf{N}_{\text{JammingLayers}} = 7$ mm.

Table A.1 – Parameters of prototypes for curvature and strength measurement

Parameter controlled	Parameters of prototype								
	h_{Prism} (mm)	h_{Root} (mm)	$\Delta_{Thickness}$ (mm)	α ($^{\circ}$)	β ($^{\circ}$)	Δ_{Angle} ($^{\circ}$)	$h_{Membrane}$ (mm)	$N_{JammingLayers}$	P_{Vacuum} (bar)
$\Delta_{Thickness}$	5	4,3,2,1	1,2,3,4	120	40	80	0.5	7	0.9
Δ_{Angle}	5	4	1	90,100, 110,120, 130	70,60, 50,40, 30	20,40, 60,80, 100	0.5	7	0.9
h_{Prism}	2,3,4, 5,7	1,2,3, 4,6	1	120	40	80	0.5	7	0.9
$h_{Membrane}$	5	4	1	120	40	80	0.1,0.2, 0.3,0.4, 0.5	7	0.9
P_{Vacuum}	5	4	1	120	40	80	0.5	7	0.2,0.4, 0.6,0.8, 0.9
Whether Jamming	5	4	1	120	40	80	0.5	0,7	0.9

Table A.2 – Parameters of prototypes for supplementary strength measurement

Parameter controlled	Parameters of prototype									
	h_{Prism} (mm)	h_{Tooth} (mm)	$\Delta_{\text{Thickness}}$ (mm)	α ($^{\circ}$)	β ($^{\circ}$)	Δ_{Angle} ($^{\circ}$)	h_{Membrane} (mm)	$N_{\text{JammingLayers}}$	P_{Vacuum} (bar)	
P_{Vacuum}	5	4	1	120	40	80	0.5	7	0.2,0.3,0.4,0.5,0.6,0.7,0.8,0.9	
$N_{\text{JammingLayers}}$	5	4	1	120	40	80	0.5	0,3,7,11	0.9	

A.5 Force-displacement curves with different design parameters

Plot here are result of compression test with the setup as shown in Figure 5.5(b).

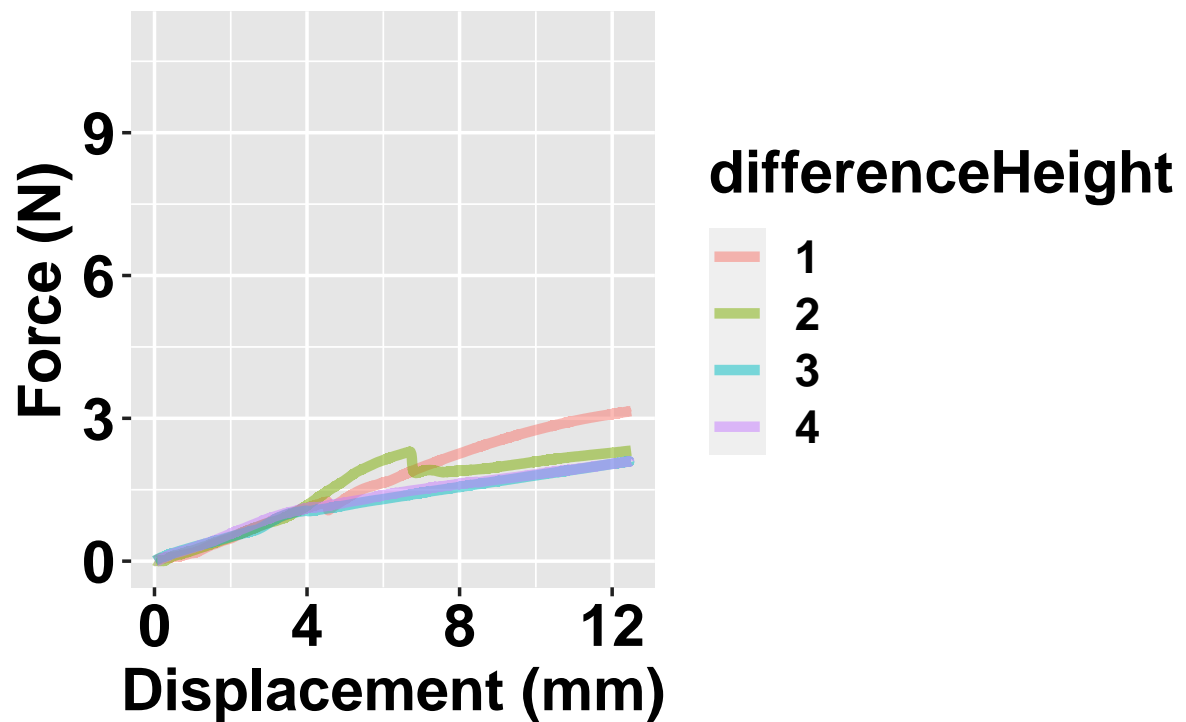


Figure A.10 – Force-displacement curves in conditions of different thickness between two gear layers

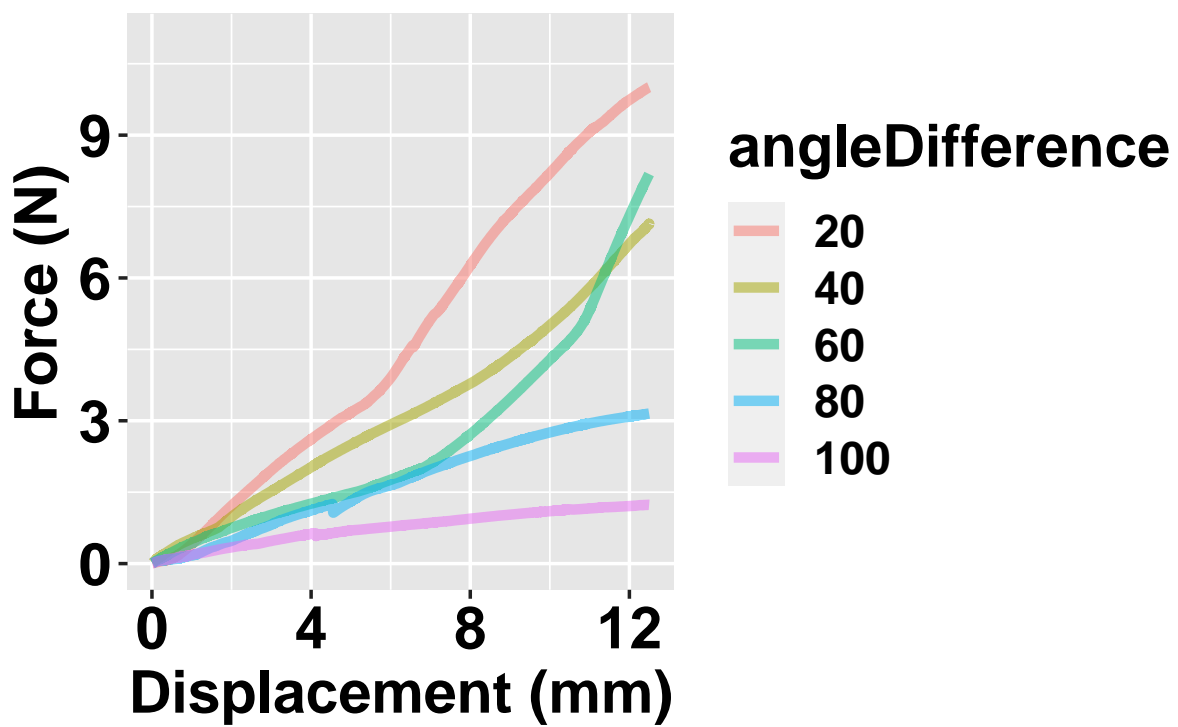


Figure A.11 – Force-displacement curves in conditions of different angles between two gear layers

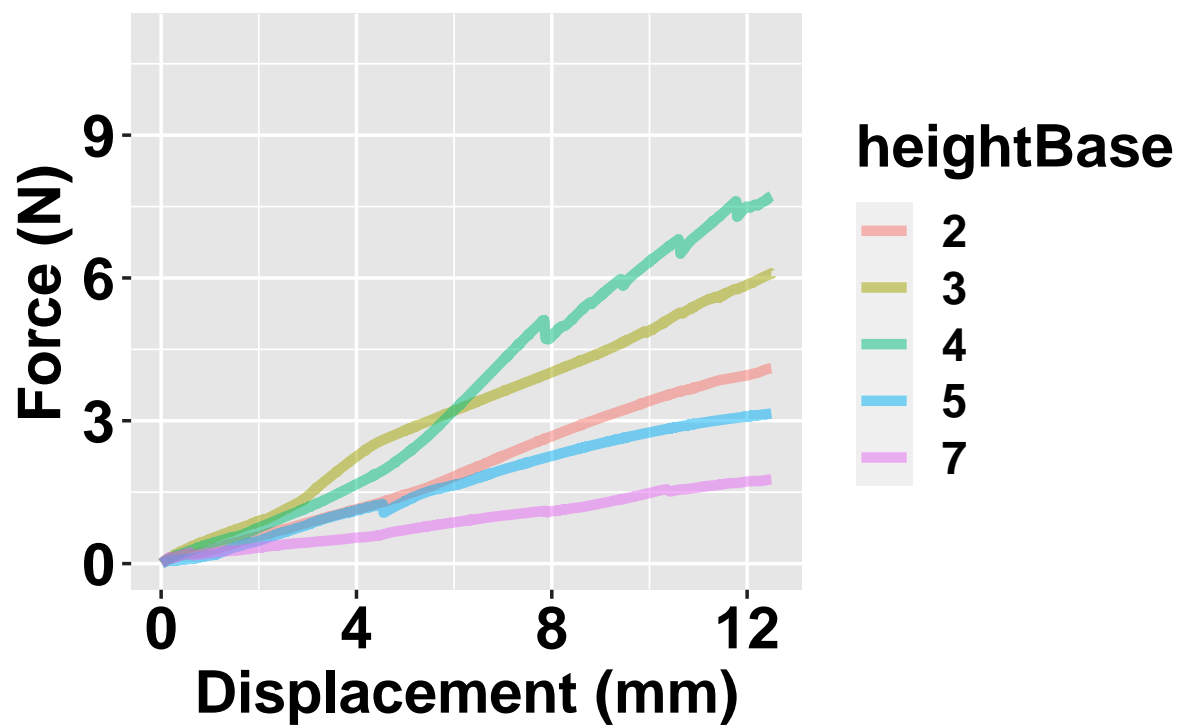


Figure A.12 – Force-displacement curves in conditions of different thickness of the thicker gears

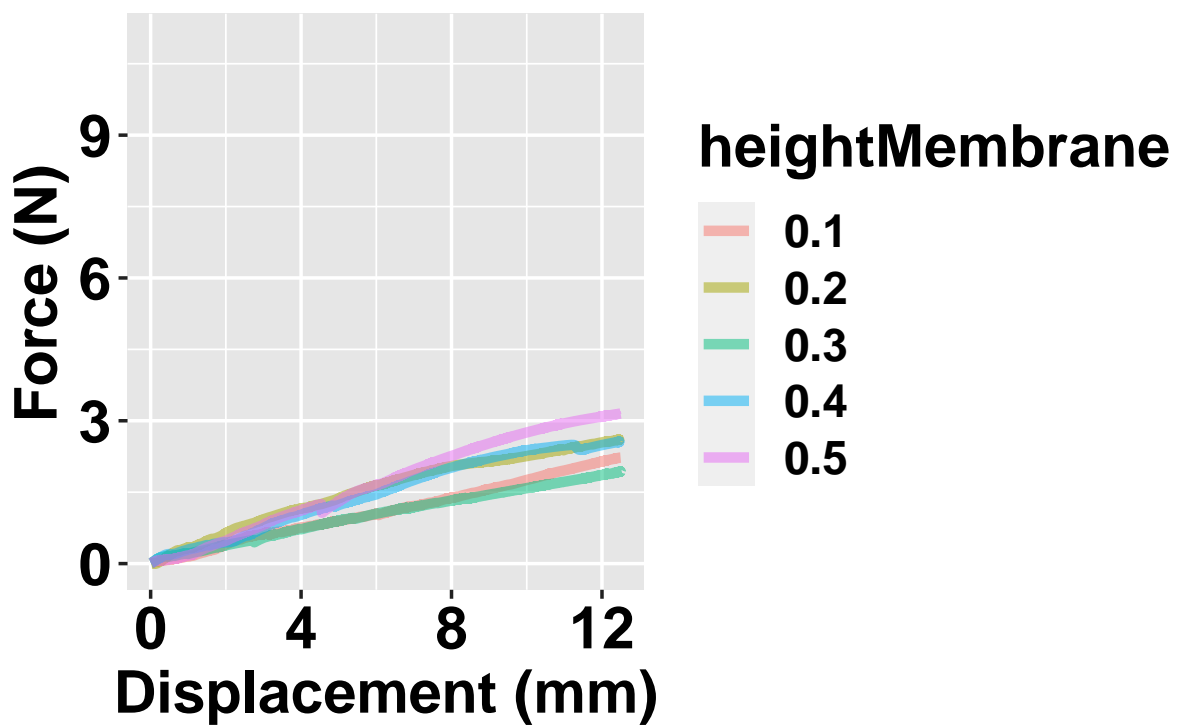


Figure A.13 – Force-displacement curves in conditions of different thickness of membranes connecting gears

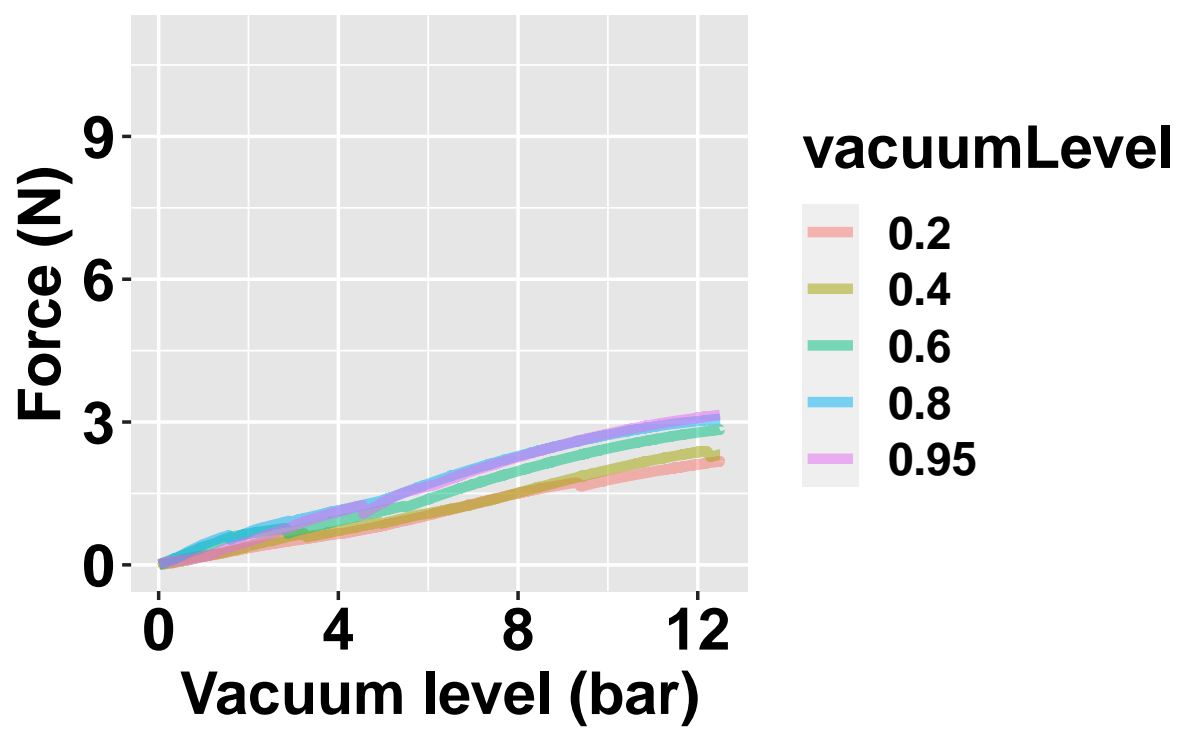


Figure A.14 – Force-displacement curves in conditions of different vacuum levels

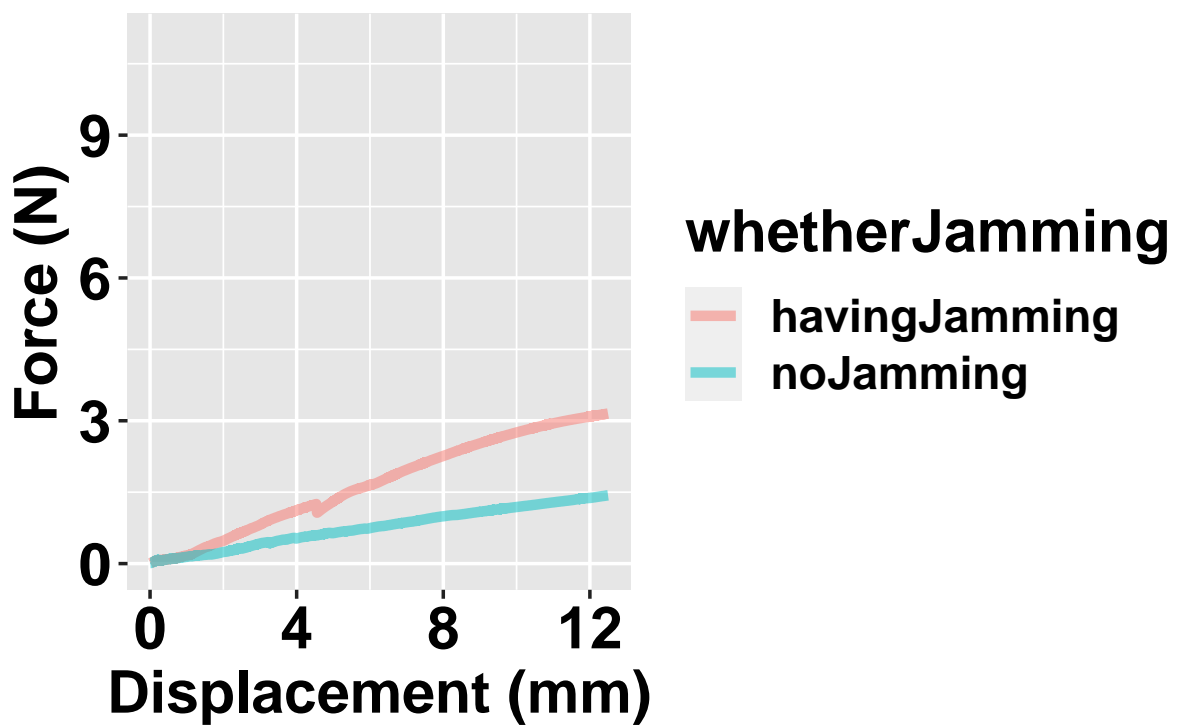
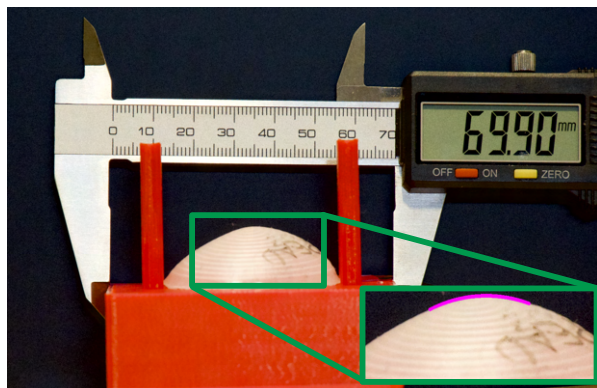
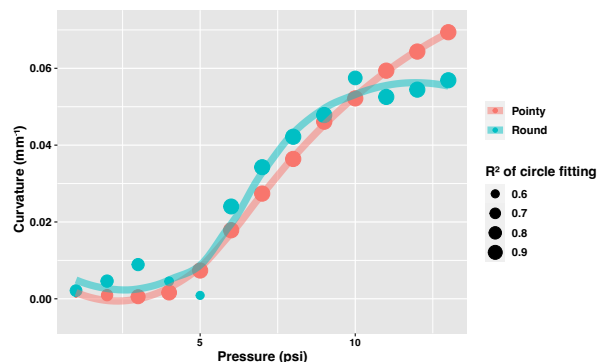


Figure A.15 – Force-displacement curves in conditions of whether having origami layers between gears

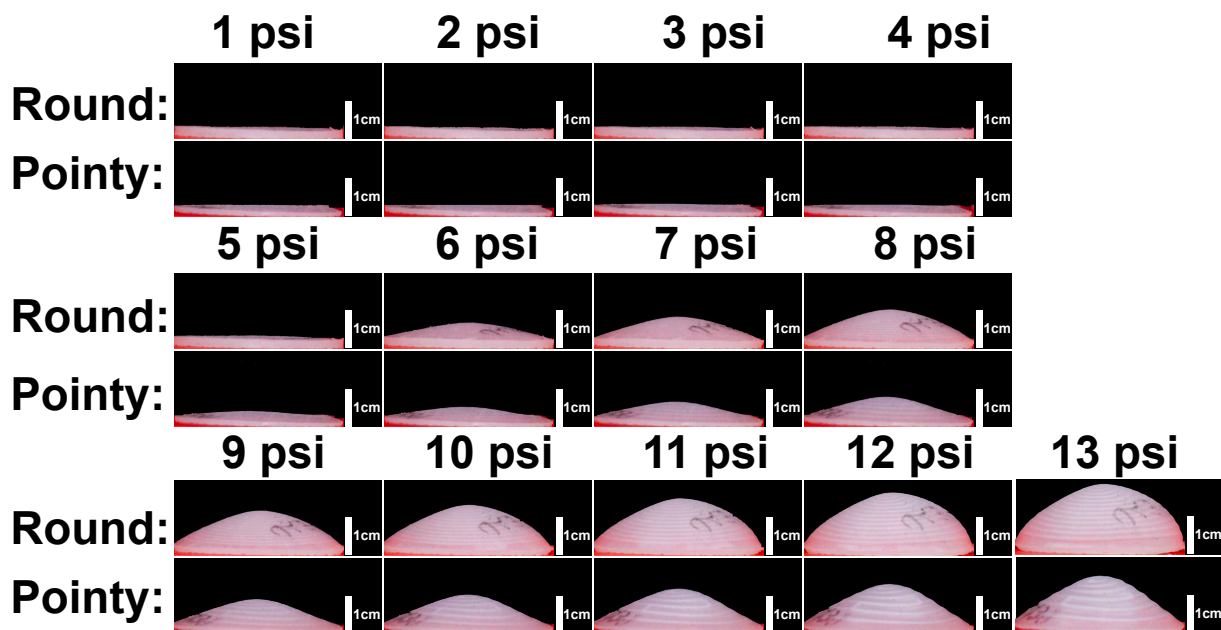
A.6 Curvature measurements for Morphing watch



(a) Setup for curvature measurement. The fitted arc is shown in purple.



(b) curvature measurements of each prototype inflated at different air pressures.



(c) Prototypes at different air pressures.

Figure A.16 – curvature measurement setup and results.

We verified the curvature of our prototypes as in [417]. We first took pictures of our prototypes (Figure A.16(a)) with a Panasonic Lumix G Hybrides camera with a LUMIX G VARIO 14-140 lens (Focal length $f=135$ mm, resolution 1096×2160). Pictures were calibrated to remove the distortion of the camera lens with OpenCV 4.6.0 [315]. To ensure measurement accuracy, we took pictures of each prototype with each air pressure three times, by inflating them from 0 psi to objective pressure each time.

We then detected the contour of the curved surface of each stimulus with OpenCV. We fitted points to this contour (Figure A.16(a)) using the circle-fit 0.1.3 [215] python package, to finally find its curvature as presented in the green square in Figure A.16(a). As shown in Figure A.16(c), the curvatures of our prototypes are not constant across the whole surface, so we fitted the central part where the prototype firstly contact with participants' skin for curvature calculation. We take the central $\varnothing 15$ mm part, as cropping images with smaller size leads to failed circle fitting because of too little pixels of prototypes among noise. To convert to curvature from pixels (px) to mm as shown in the y axis of Figure A.16(b), we fixed a vernier scale on the 3D printed support (Figure A.16(a)) to ensure the precision of the conversion. We found that 69.9 mm on the scale equals 1213 px in the pictures. We therefore convert our measurements of the curvature with 0.058 mm/px. Figure A.16(b) presents on the y-axis the results of our measurements with the average curvature of each prototype in each pressure condition. With Figure A.16(c), we can see that when air pressure is low (i.e., R prototype under 6 psi and P prototype under 5 psi), our prototypes barely inflates and stays nearly flat. This is coherent with the poor circle fitting result shown in Figure A.16(b), i.e, low R^2 value in low pressure conditions. The exact values in the Figure A.16(b) and the code to compute the curvature are available in the supplementary material [101].